

RADIATION CHEMISTRY OF DIMETHYLSULFOXIDE

BY

TERRY KENNETH COOPER

B.Sc., University of British Columbia, 1968

A THESIS SUBMITTED IN PARTIAL FULFILMENT OF
THE REQUIREMENTS FOR THE DEGREE OF
DOCTOR OF PHILOSOPHY

in the Department

of

CHEMISTRY

We accept this thesis as conforming to the
required standard

THE UNIVERSITY OF BRITISH COLUMBIA

July, 1972

In presenting this thesis in partial fulfilment of the requirements for an advanced degree at the University of British Columbia, I agree that the Library shall make it freely available for reference and study.

I further agree that permission for extensive copying of this thesis for scholarly purposes may be granted by the Head of my Department or by his representatives. It is understood that copying or publication of this thesis for financial gain shall not be allowed without my written permission.

Department of Chemistry

The University of British Columbia
Vancouver 8, Canada

Date July 7, 1972

ABSTRACT

A comprehensive study of the radiation chemistry of dimethylsulfoxide (DMSO), and DMSO-H₂O mixtures, by steady-state γ -radiolysis, pulse radiolysis and low temperature matrix isolation techniques has revealed several significant features about the transient ionic products of the radiolysis. Very short-lived ($\tau_{1/2} < 25$ nsec), weakly bound solvated electrons are formed in quite high yields in these liquids at room temperature. Solvated electrons in the binary DMSO-H₂O mixtures exhibit single optical absorption bands with maxima which vary smoothly with composition from pure water ($\lambda_{\max} = 720$ nm) to pure DMSO ($\lambda_{\max} > 1500$ nm). The electron stability varies with composition, showing a minimum lifetime coinciding with DMSO-H₂O mixtures which exhibit maximum inter-molecular structure. In glassy mixtures at 77°K, electrons generated radiolytically or photochemically are not trapped and stabilized. The positive ions formed from irradiated DMSO are longer lived ($\tau_{1/2} \sim 2$ μ sec) than the solvated electrons and have a strong absorption band centered at $\lambda_{\max} \sim 550$ nm. In DMSO-H₂O mixtures this same absorption band is formed. The cationic yield is directly proportional to the fraction of the total dose absorbed initially by DMSO which suggests there is no charge transfer, proton exchange or positive ion scavenging in these mixtures. The yield of both e_s^- and cations was $\sim 30\%$ higher in the fully deuterated DMSO than in the hydrogenated material indicating some alteration in the electron escape probability due to isotopic substitution.

Most of the above observations are interpreted in terms of the physical properties of DMSO and its aqueous mixtures. The radiation

yield of free ions is measured to be 1.30 ± 0.15 which is in reasonably good accord with a liquid having a dielectric constant of 48. The yield of solvated electrons was ascertained by observing the formation of anthracene anions in solutions of anthracene and corresponded very closely to the yield of positive ions determined from the formation of Br_2^- in KBr solutions. The near infrared absorption band of solvated electrons in DMSO indicates a weakly stabilized species which is consistent with the very poor solvating power for negative ions afforded by DMSO due to the aprotic nature of the solvent. On the other hand the lack of charge transfer or proton exchange with H_2O shown by the DMSO cation is consistent with the dipolar character of DMSO and its strong solvation of positive ions.

A variety of free radicals have been observed by electron spin resonance in γ -irradiated polycrystalline DMSO at 77°K amongst which the $\cdot\text{CH}_3$ and a sulfur containing radical are distinguished. Under γ -radiolysis liquid DMSO produces H_2 , CH_4 , C_2H_6 , and $(\text{CH}_3)_2\text{S}$ with G values of 0.20 ± 0.01 , 3.3 ± 0.1 , 0.49 ± 0.03 and 1.2 ± 0.2 respectively.

TABLE OF CONTENTS

<u>Chapter</u>		<u>Page</u>
I.	INTRODUCTION	1
	A. Interaction of High-Energy Radiation with Matter	2
	1. Electromagnetic radiation	2
	2. High-energy electrons	8
	3. Range of electrons	13
	4. Track entities: spurs, blobs and short tracks	14
	B. Chemical Consequences Following Absorption of High-Energy Radiation	17
	1. Time scale of events	18
	2. Phase-dependent phenomena	21
	3. Studies on the chemical events in condensed phases	22
	4. Chemical yields	24
	C. Stabilized Electrons	26
	1. Stabilization	26
	2. Properties	27
	2.1 Optical spectrum	28
	2.2 Electron spin resonance	32
	2.3 Conductivity	34
	3. Models	35
	4. Free ion yields	43
	D. Binary Mixtures	48
	E. Scope of Study	53

<u>Chapter</u>		<u>Page</u>
II.	EXPERIMENTAL	58
A.	⁶⁰ Co γ -Radiolysis	58
	1. Materials	58
	2. Radiation source	59
	3. Dosimetry	59
	4. Sample preparation	65
	5. Product analysis	71
B.	Pulse Radiolysis	77
	1. Outline of the technique	77
	2. Radiation source	79
	3. Irradiation cell and optical detection system	79
	4. Oscilloscope measurements	82
	5. Cerenkov emission	84
	6. Dosimetry	88
	7. Materials and purification	91
C.	Electron Spin Resonance	92
	1. Materials and purification	92
	2. Radiation source	92
	3. Sample preparation	92
	4. Electron spin resonance spectra	93
	5. Photolysis apparatus	94

<u>Chapter</u>		<u>Page</u>
III.	STUDIES ON LIQUID DMSO	95
A.	^{60}Co γ -Radiolysis	95
	1. Gaseous products	95
	2. Liquid products	98
	3. Scavenger studies	100
	4. Discussion	113
B.	Pulse Radiolysis	122
	1. Absorption spectra in DMSO and DMSO_{d_6}	122
	2. Free ion yields	132
	3. Geminate ion scavenging	148
	4. Dielectric constant and electron stabilization	154
IV.	PULSE RADIOLYSIS OF DMSO-WATER BINARY MIXTURES	156
	1. Solvated electrons	157
	2. DMSO positive ions.....	169
	3. Transient intermediates at 77°K	173
V.	ELECTRON SPIN RESONANCE STUDIES ON DMSO AND DMSO- H_2O MIXTURES AT 77°K	177
A.	Introduction	177
	1. Basic principles of esr	177
	2. Amorphous and polycrystalline media	183
B.	Results and Discussion	187
	1. Pure DMSO	187
	1.1 Ultraviolet irradiated	187
	1.2 γ -Irradiated	190

<u>Chapter</u>	<u>Page</u>
V (continued)	
2. DMSO-water matrices	193
2.1 γ -irradiated polycrystalline H_2O	193
2.2 γ -irradiated DMSO- H_2O mixtures	195
2.3 photoionization of $K_4Fe(CN)_6$ in aqueous glasses	205
REFERENCES	211

LIST OF TABLES

<u>Table</u>		<u>Page</u>
I.	Optical data for electrons stabilized in liquid media at room temperature	56
II.	Radiation yields from irradiated DMSO containing 0.05 M N ₂ O plus the second scavenger indicated in column 1 at concentration given in column 2	105
III.	Ratio of k_S/k_{N_2O} obtained for the precursor of N ₂ in DMSO with various second scavengers (S) added to a 0.05 M solution of N ₂ O. Column headed water refers to the published rate constant ratio for the hydrated electron	110
IV.	Summary of data obtained from studies on pulse irradiated DMSO-water mixtures at room temperature.	160
V.	Summary of data obtained from studies on γ -irradiated DMSO-water matrices at 77°K	196

LIST OF FIGURES

<u>Figure</u>		<u>Page</u>
1	Atomic absorption coefficients for water. Curve A, Total absorption coefficient (with coherent scattering); B, photoelectric absorption coefficient; C, Compton coefficient (with coherent scattering); D, Compton coefficient (without coherent scattering); E, pair-production coefficient. 1 barn = 10^{-24} cm ² ..	6
2	Huygens construction of electron trajectory and resulting Cerenkov waveform	11
3	Schematic plot of percentage of energy split between spurs, blobs and short tracks for electrons in water.	16
4	Theoretical time scale for the initial processes in radiation chemistry. The numbers are the negative logarithm of time (pt = -log t (sec)).....	20
5	Schematic representation of electron localization (shaded region) produced by polarization of the medium. The dotted area represents the void or cavity in which the electron is centered	30
6	Correlation curve of the transition energy of the electron in DMSO and its cavity radius using the continuous dielectric model with an adiabatic approximation	39
7	Plot of G (free ion) as a function of the static dielectric constant of the medium. Data taken from references 32, 33, 34, 46, 101.....	46

<u>Figure</u>		<u>Page</u>
8	Fricke dosimeter results obtained from the radiolysis of the solutions in the irradiation cell used in this study	63
9	Pyrex irradiation cells used for deoxygenation of the liquid samples	66
10	Schematic diagram of vacuum line used for degassing the liquid samples and adding nitrous oxide to the samples	68
11	Plot showing the relationship of the partial pressure of nitrous oxide to its solubility in DMSO at 23°C for the two bubbler cells containing a medium (cell A) and fine (cell B) porosity sintered disk.....	70
12	Schematic diagram of apparatus used for flushing the volatile gaseous products into the gas chromatograph.	72
13	Typical chromatograph obtained for 20 ml DMSO sample containing 0.05 M nitrous oxide and receiving an absorbed dose of 8×10^4 rads	75
14	Typical chromatograph obtained after injection of 25 μ l of irradiated DMSO sample. Total absorbed dose was 6 Mrad.....	76
15	Lay-out of the pulse radiolysis equipment at the National Research Council radiation laboratory in Ottawa, Ontario	78

<u>Figure</u>		<u>Page</u>
16	Schematic diagram of irradiation cell used for deoxy- genation of liquid samples used in the pulse radiolysis study. The spectroscopic cell was filled by tipping the cell horizontally after flushing with high purity argon	80
17	Hypothetical oscilloscope trace showing the build up and decay of transient absorbing species. The time profile of the electron pulse is shown as the dotted curve	83
18	Typical oscilloscope traces showing the response time of the detection apparatus to Cerenkov light genera- ted using a 40 nsec wide electron pulse	85
19	Effect of Cerenkov emission on the absorption of the transients absorbing at 500 nm in pure DMSO. (a) pure Cerenkov (analyzing light off); (b) observed absorption; (c) absorption that would have been observed had there been no Cerenkov emission. The detector was a Si photodiode with a 93 ohm load resistor. The pulse width was 40 nsec.....	87
20	Typical oscilloscope traces for the formation and decay of $(\text{CNS})_2^-$ at 500 nm obtained by using a 40 nsec pulse of 35 MeV electrons on a nitrous oxide saturated solution of 5×10^{-3} M thiocyanate in water. (a) Si photodiode, 93 ohm load resistor; (b) photo- multiplier, 470 ohm load resistor	90

<u>Figure</u>		<u>Page</u>
21	Radiation yields as a function of absorbed dose: □, C ₂ H ₆ and ○, H ₂ . The methane curve was obtained by taking the slope at various portions of the curve shown in Figure 22.....	96
22	Accumulated gas yields as a function of accumulated dose: ●, △, ▲, ▲, CH ₄ at various doses: □, C ₂ H ₆ ; ○, H ₂	97
23	Accumulated dimethyl sulfide yield as a function of accumulated dose. The extrapolated portion of the curve corresponds to G(DMS) = 1.2 ± 0.2	99
24	Radiation yields of CH ₄ (△), C ₂ H ₆ (□) and H ₂ (○) as a function of the N ₂ O concentration. In the case of CH ₄ , all doses were < 1.8 × 10 ⁵ rads	101
25	Radiation yield of nitrogen as a function of N ₂ O concentration	102
26	Accumulated nitrogen yield as a function of accumulated dose	103
27	Plot of 1/G(N ₂) as a function of [Scavenger]/[N ₂ O]. The N ₂ O concentration was 0.05 M and the second scavenger concentration was varied. The data was taken from Table II. ●, CCl ₄ ; △, I ₂ ; ■, CHCl ₃ ; ○, Ag ⁺ and □, acetone.....	108
28	Plot of 1/G(N ₂) as a function of [H ⁺]/[N ₂ O] in which ○, ▲, and □ correspond to different N ₂ O concentra- tions: ○, 0.05 M N ₂ O; ▲, 0.04 M N ₂ O and □, 0.07 M N ₂ O. ● Corresponds to 0.5 M methanol added to the acid solution	109

<u>Figure</u>		<u>Page</u>
29	Radiation yields of CH ₄ (△), C ₂ H ₆ (□), and H ₂ (○) as a function of I ₂ concentration. The doses were < 5 x 10 ⁴ rads	111
30	Radiation yields of CH ₄ (△), C ₂ H ₆ (□) and H ₂ (○) as a function of H ⁺ concentration. ▲ corresponds to the yield of CH ₄ when 0.05 M N ₂ O was added to the corresponding acid solution of DMSO. In the case of CH ₄ , all doses were < 1.8 x 10 ⁵ rads	112
31	Transient spectra observed in (CH ₃) ₂ SO and (CD ₃) ₂ SO. The circles refer to the solvated electron band corrected for the detector response time and the triangles refer to the DMSO positive ion, or oxidizing species. ○ and △ are for (CH ₃) ₂ SO; ● and ▲ are for (CD ₃) ₂ SO. Almost all data points are the mean of at least two measurements. The λ _{max} for the △ spectrum was established to be at 550 nm from a previous set of experiments	123
32	Typical oscilloscope traces showing the decay of the solvated electron in DMSO. Both traces were obtained using a Ge photodiode with a 50 ohm load resistance. (a) pulse width 10 nsec; (b) pulse width 40 nsec.....	125
33	Typical oscilloscope traces showing the decay of the DMSO positive ion or oxidizing species at 550 nm. The fast initial decay in (a) is due to the solvated electron. Both traces were obtained using a pulse width of 40 nsec. (a) Si photodiode with 93 ohm load resistor; (b) photomultiplier with 470 ohm load resistor.....	126

<u>Figure</u>		<u>Page</u>
34	First-order decay plot of the solvated electron in DMSO taken at 1300 nm. The pulse width was 10 nsec, giving an absorbed dose of 900 rads per pulse. The decay was measured using a Ge photodiode with a 50 ohm load resistor	130
35	First-order plot of the decay of the DMSO positive ion. The decay was measured at 550 nm using the photo-multiplier with a 470 ohm load resistor. The pulse was 40 nsec, giving an absorbed dose of 2200 rads per pulse	131
36	End of pulse absorption spectrum of the anthracene radical anion obtained from a DMSO solution 0.02 M in anthracene after absorbances due to the electron and oxidizing species had been subtracted.....	134
37	Typical oscilloscope traces showing the decay of the electron and build up of the anthracene radical anion at 750 nm. (a) no anthracene added; (b) 0.001 M anthracene in DMSO; (c) 0.005 M anthracene in DMSO.	135
38	Typical oscilloscope traces showing the build up and decay of the anthracene radical anion at 750 nm. (a) 0.01 M anthracene in DMSO; (b) 0.02 M anthracene in DMSO	136

<u>Figure</u>		<u>Page</u>
39	Graph showing the scavenging of solvated electrons in pure DMSO by anthracene and the formation of anthracene radical anions. \odot , absorbance at 750 nm due to A^- immediately at the end of the pulse; \circ , maximum in the absorbance at 750 nm due to A^- after the pulse; \triangle , absorbance due to the positive ions at 550 nm; \blacksquare , absorbance due to solvated electrons at 1275 nm (not corrected for decay during the pulse nor for the detector response time)	138
40	Absorption spectra for KBr solutions in DMSO. Solid curve refers to Br_2^- spectra; the dotted curve refers to the transient precursor of Br_2^- . \blacktriangle , Br_2^- from 0.1 M KBr solution; \bullet , Br_2^- from 0.01 M KBr solution; \blacksquare , transient precursor of Br_2^- at 0.01 M KBr. The inset is a plot of G_E at 375 nm for Br_2^- against $\log ([Br^-]/M)$	142
41	Typical oscilloscope traces showing the build up and decay of Br_2^- at 365 nm in pure DMSO. Detection made using the photomultiplier with a 470 ohm load resistor. (a) 0.1 M KBr; (b) 0.01 M KBr; (c) 0.001 M KBr	143
42	Plot showing first-order build up of Br_2^- (Figure 41(c)) for DMSO solution 0.001 M in KBr	145

<u>Figure</u>		<u>Page</u>
43	Typical oscilloscope traces showing the decay of Br_2^- and its transient precursor. The fast initial decay in (b) and (c) is attributed to the transient complex. Detection was made using the photomultiplier with a 470 ohm load resistor	146
44	End of pulse absorption spectrum of the DMSO positive ion in 0.2 M H_2SO_4 . The dotted line refers to the absorbance of the positive ion in pure DMSO. X refers to the long-lived SO_4^- intermediate produced in the acid solution	149
45	First-order decay plot of the DMSO positive ion in the presence of 0.2 M H_2SO_4 . Decay measured at 550 nm using the photomultiplier with a 470 ohm load resistance	151
46	Typical oscilloscope traces showing the decay of the DMSO positive ion in the presence of 0.2 M H_2SO_4 at 650 nm and 450 nm. The longer-lived SO_4^- transient is readily observed at 450 nm.....	152
47	End of pulse spectrum of transients produced in a DMSO solution 0.5 M in Ag^+	153
48	Absorption spectra of solvated electrons in DMSO- H_2O mixtures; 0, 0.20, 0.28, 0.43, 0.72, 0.93 and 1.0 mole fraction DMSO. Data points were obtained at 50 nm intervals. The data for pure water have been multiplied by a factor of 0.3 relative to the others.	159

<u>Figure</u>		<u>Page</u>
49	Plot of the values of $G\epsilon_{\max}$ for the solvated electron absorption bands presented in Figure 48 as a function of the mole fraction DMSO for the DMSO-H ₂ O mixtures. The non-linear axis showing the change as a function of static dielectric constant of the bulk mixture is shown on the top abscissa. ○, actual observed absorbance peak heights. ●, corrected for decay during the pulse and response time of the detector	162
50	Plot of the photon energy of the absorption band maximum for the solvated electron in the DMSO-H ₂ O mixtures against the bulk static dielectric constant of the mixtures (at 25°C). The non-linear axis showing the corresponding mole fraction DMSO is shown in the upper abscissa	167
51	Plot of the photon energy of the absorption band maximum for the solvated electron in the DMSO-H ₂ O mixtures against the mole fraction of water. The non-linear axis showing the corresponding bulk dielectric constants of the mixtures is shown in the upper abscissa	168
52	(a) Absorption spectra attributed to the DMSO positive ion produced in DMSO-H ₂ O mixtures. Curve 6 is pure DMSO; 5, 0.93; 4, 0.72; 3, 0.43; 2, 0.28; and 1, 0.20 mole fraction DMSO. (b) Peak absorbance (at 550 nm) of the bands shown in (a) plotted against the fraction of dose absorbed initially by DMSO	170

<u>Figure</u>		<u>Page</u>
53	Absorption spectrum of transients produced by the pulse radiolysis of a DMSO-H ₂ O glass (39 mole % DMSO) at 77°K. The pulse width was 500 nsec, the dose per pulse being ~ 10 krad. The dotted curve is that of the DMSO positive ion in pure DMSO normalized at 600 nm..	175
54	Theoretical esr line shapes for (a) axially symmetric and (b) completely asymmetric g tensors. The upper curves refer to absorption spectra of the paramagnetic species. The lower curves refer to the experimentally observed first derivative spectra....	185
55	Theoretical first derivative esr spectrum for a paramagnetic species with S = 1/2, I = 1/2 and with axially asymmetric g and A tensors. The central dotted portion is the theoretical spectrum in the absence of the hyperfine interactions	186
56	Electron spin resonance spectrum obtained after the ultraviolet photolysis of polycrystalline DMSO at 77°K. The arrows correspond to the asymmetric g-factors of the sulfur radical CH ₃ ·S ^o . The methyl radical quartet is indicated by the stick plot.....	189
57	Electron spin resonance spectra of γ-irradiated DMSO. The sample was irradiated in the dark at 77°K to a total absorbed dose of 0.72 Mrad. (a) microwave power 0.44 mW; (b) microwave power 10 mW. g _{DPPH} = 2.0036..	191

<u>Figure</u>		<u>Page</u>
58	Electron spin resonance spectra of γ -irradiated DMSO after bleaching irradiated sample with ultraviolet light for forty minutes (in spectrometer cavity). Sample γ -irradiated at 77°K in the dark to a total absorbed dose of 0.72 Mrad. (a) microwave power 0.52 mW; (b) microwave power 10 mW.....	192
59	Electron spin resonance spectrum of γ -irradiated polycrystalline ice at 77°K. Resonance pattern corresponds to that of the $\cdot\text{OH}$ radical	194
60	Resonance pattern showing behaviour of $\cdot\text{X}$ with (a) increasing water composition (microwave power 0.42 mW) and (b) increasing microwave power (pure DMSO). Numbers corresponding to spectra on left refer to mole fraction DMSO. The arrows refer to ξ_{DPPH}	198
61	Electron spin resonance spectra of polycrystalline γ -irradiated DMSO-water mixture (0.80 mole fraction DMSO) at 77°K. (a) microwave power 0.42 mW; (b) after bleaching with ultraviolet light for 20 minutes, microwave power 0.42 mW; (c) same as (b), microwave power 10 mW	199
62	Electron spin resonance spectra of γ -irradiated DMSO-water glass (0.20 mole fraction DMSO) at 77°K. The "sulfur pattern" and methyl radical quartet are readily observed. (a) microwave power 0.42 mW; (b) microwave power 10 mW	200

<u>Figure</u>		<u>Page</u>
63	Electron spin resonance spectra of γ -irradiated polycrystalline DMSO-water mixture (0.01 mole fraction DMSO) at 77°K. (a) microwave power 0.42 mW; (b) microwave power 10 mW. The low field "hump" and doublet of the $\cdot\text{OH}$ radicals are evident at 10 mW power (see Figure 59)	202
64	Electron spin resonance spectrum obtained after photoionization at 77°K of 0.01 M $\text{K}_4\text{Fe}(\text{CN})_6$ in 0.20 mole fraction DMSO-water glass (compare to Figure 62(a)).	207
65	Electron spin resonance spectra obtained for the photoionization of 0.01 M $\text{K}_4\text{Fe}(\text{CN})_6$ in 8 M NaOH glass at 77°K. (a) no DMSO added; (b) 1.0 M DMSO present in glass	208
66	Electron spin resonance spectra obtained for γ -irradiated (0.24 Mrad) of 8 M NaOH glass at 77°K. (a) no DMSO added; (b) 1.0 M DMSO added; (c) after photobleaching (b) with ultraviolet light for 20 minutes	209

ACKNOWLEDGEMENTS

The author would like to sincerely thank Dr. D.C. Walker for his encouragement and guidance during the course of this study as well as for introducing him to Radiation Chemistry.

It is the author's pleasure to acknowledge the cooperation of the National Research Council for use of the pulse radiation facilities in Ottawa. The author is especially grateful to Dr. Hugh A. Gillis, Dr. Norman V. Klassen and Mr. George G. Teather for their invaluable assistance in performing the pulse radiolysis experiments.

Special thanks are due to the National Research Council and the F.J. Nicholson Family for financial support in the form of post graduate scholarships.

Finally, the author would like to thank his wife Carol, who has shown great understanding and forbearance during the preparation and writing of this thesis.

CHAPTER I

INTRODUCTION

Radiation chemistry encompasses the study of the chemical effects induced in a system by high-energy radiations such as those made available by radioactive substances, particle accelerators and nuclear reactors. In carrying out such a study an attempt is made to identify the products formed, decide how they were formed and what their precursors were with the hope of elucidating and understanding the chemical and physical processes involved. This dissertation is concerned with the effect of ionizing radiation on dimethyl sulfoxide (DMSO) and binary mixtures of DMSO and water. Particular emphasis is placed on one of the early processes in radiation chemistry, namely electron stabilization, and how this process is related to the physical and chemical properties of the medium.

In order to unravel the many complexities involved in studying radiation-chemical phenomena, it is necessary to know how high-energy radiation interacts with matter to produce the ultimate chemical effect.

A. INTERACTION OF HIGH-ENERGY RADIATION WITH MATTER

In the study of the radiation chemistry of dimethyl sulfoxide, two sources of high-energy radiation were used: (1) electromagnetic radiation in the form of ^{60}Co γ -rays and (2) short pulses of high-energy electrons from a linear accelerator.

1. Electromagnetic Radiation

There are four principal processes by which electromagnetic radiation may be absorbed by matter¹: (i) photoelectric, (ii) Compton, (iii) pair-production, and (iv) photonuclear reactions. Each of these processes depends primarily on the energy of the incident radiation but does depend upon the atomic number (Z) of the absorbing medium to some extent. Furthermore, the incident electromagnetic beam may be scattered by the electrons of the medium with little or no loss in energy and is termed coherent scattering. This scattering becomes important only for high- Z materials and low photon energies (< 0.1 MeV). Whenever electromagnetic radiation passes through matter, its intensity is governed by the relationship

$$I = I_0 e^{-\mu_a x} \tag{1.1}$$

where I is the intensity of the radiation transmitted through a thickness, x , of absorber and I_0 is the intensity of the incident radiation. The linear absorption coefficient, μ_a , is the sum of all the partial coefficients representing the various processes of absorption mentioned above.

In the photoelectric effect, the entire energy of the photon, E_p , is transferred to a single atomic electron. This electron is then ejected from the atom with an energy, E_e , equal to the difference between the photon energy and the binding energy, B , of the electron in the atom.

$$E_e = E_p - B \quad (1.2)$$

Photoelectrons may be ejected from any of the K, L, M,... shells of an atom. However a free electron cannot absorb a photon to become a photoelectron because a third body, in this case the nucleus, is necessary in order to conserve momentum. The probability of photoelectron absorption increases with the tightness of the binding electron so that at photon energies greater than the binding energies of the K- and L-shells, ejection from the outer shells is negligible. The vacancy created by the loss of an electron from the inner shell will be filled by an electron from the outer shell and the excess energy is dissipated by the emission of low-energy Auger electrons or X-rays. Photoelectric absorption is predominant at low photon energies (< 0.1 MeV). In materials of high atomic number the absorption cross section, τ_a , is given approximately by²

$$\tau_a \approx kZ^4/E_p^3 \quad (1.3)$$

where k is a constant.

At energies > 0.1 MeV, the photon interacts with loosely bound or free electrons resulting in a reflection of the photon with reduced energy.

The electron is ejected with energy, E_e , equal to the difference between the incident and scattered photon energy (the binding energy is neglected).

$$E_e = E_p - E_\gamma \quad (1.4)$$

The energy of the scattered photon is given by¹

$$E_\gamma = \frac{E_p}{1 + (E_p/m_o c^2)(1 - \cos\theta)} \quad (1.5)$$

where θ is the scattering angle and $m_o c^2$ is the rest mass energy of the electron (0.51 MeV). These recoil electrons are called Compton electrons and have their maximum energy when the scattering angle is 180° . In general, however, Compton electrons have a fairly uniform distribution in energy, the average being about half the incident photon energy. Compton interactions are the predominant absorption process for photon energies between 1 and 5 MeV in high atomic number materials such as lead. In low-Z materials such as water and DMSO, Compton interactions are dominant over a much wider range; that is, from about 30 keV to 20 MeV (see Figure 1).

The complete absorption of a photon in the vicinity of an atomic nucleus resulting in the production of two particles, an electron and a positron, is called pair-production. Because part of the photon energy is used to create the positron and electron, pair-production cannot occur at photon energies less than the sum of their rest mass energies, namely 1.02 MeV. The remaining photon energy is divided between the kinetic energies of the electron and positron since energy

transfer to the nucleus and its subsequent recoil is considered negligible. The positron, either before or after losing its kinetic energy, is annihilated by combining with an electron with the subsequent emission, in opposite directions, of two 0.51 MeV γ -rays. Pair production is of major importance only with high atomic number materials and photon energies > 10 MeV.

In the photoelectric, Compton and pair-production processes, the photons either eject or create high-energy electrons. However, at energies above about 8 MeV for high-Z materials and in the region of 10 to 20 MeV for low-Z materials, the photons may have sufficient energy to eject a proton or neutron from the nucleus of an atom. However photonuclear cross sections are generally smaller than Compton and pair-production cross sections at the same energy so that the photonuclear process generally makes a negligible contribution to the total energy absorption.

The three main processes then in which high-energy photons may be absorbed by matter are the photoelectric, Compton and pair-production processes. Figure 1 shows the variation of the total and partial molecular absorption coefficients for water as a function of photon energy. The atomic absorption coefficient, μ_a , is related to the linear absorption coefficient by the relationship¹

$$\mu_a = \mu_a A / \rho N_0 \text{ cm}^2 \text{ atom}^{-1} \quad (1.6)$$

where ρ is the density and A the atomic weight of the stopping material, N_0 being Avogadro's number. Since the probability of a photon

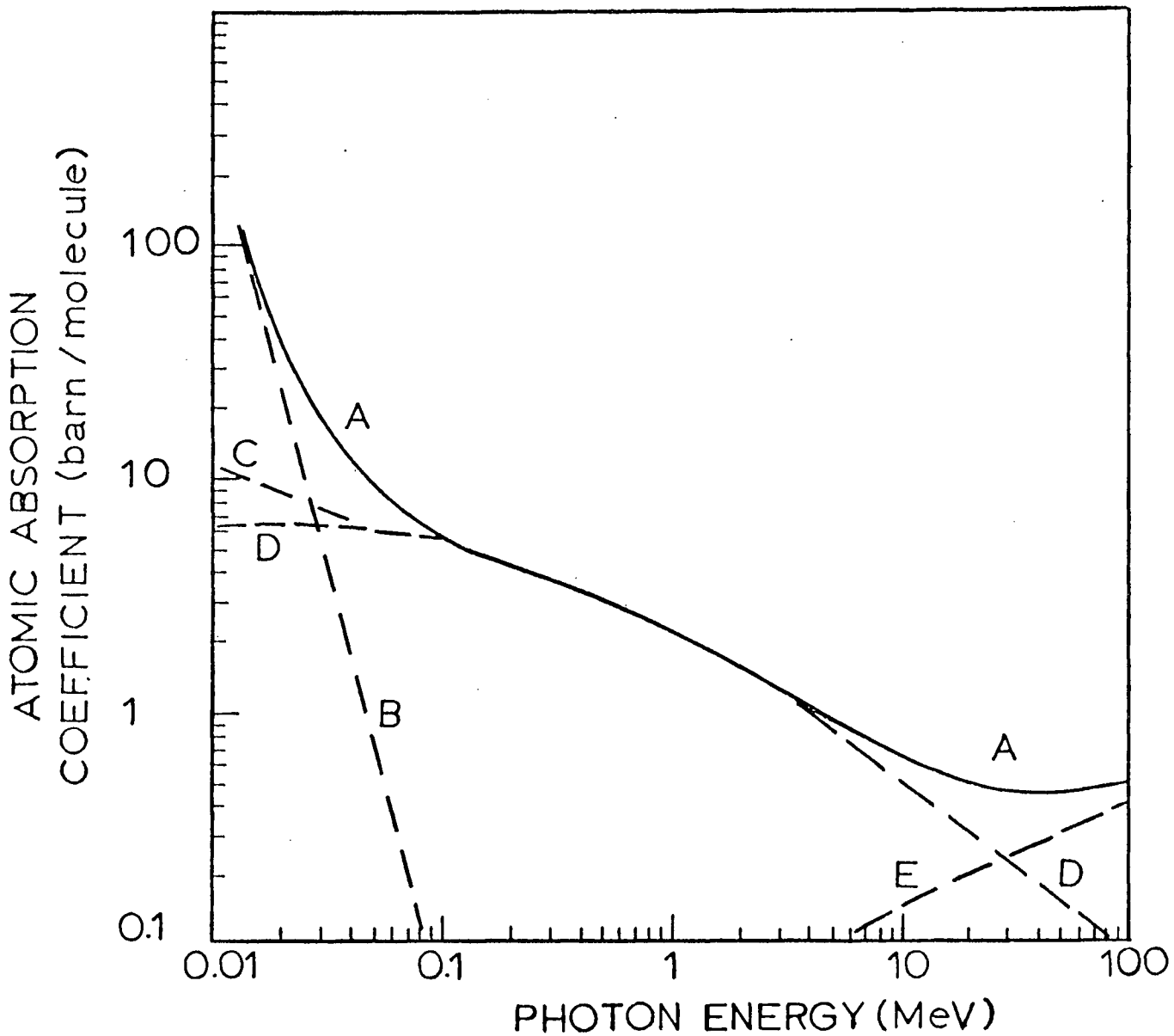


Figure 1. Atomic absorption coefficients for water. Curve A, total absorption coefficient (with coherent scattering); B, photoelectric absorption coefficient; C, Compton coefficient (with coherent scattering); D, Compton coefficient (without coherent scattering); E, pair-production coefficient. 1 barn = 10^{-24} cm². (Adapted from Figure 3.6, page 54, reference 1).

interacting with an atom is independent of its environment, the molecular absorption coefficient is simply the sum of the atomic absorption coefficients. Thus the molecular absorption coefficient for water is:

$$(\mu_a)_{H_2O} = 2(\mu_a)_H + (\mu_a)_O \quad (1.7)$$

As indicated previously, the absorption coefficients for the various processes mentioned above may be added to give the total absorption coefficient,

$$\mu_a = \tau_a + \sigma_a + \kappa_a \quad (1.8)$$

where τ_a , σ_a and κ_a are the linear absorption coefficients for the photoelectric, Compton and pair-production processes respectively. The small contributions from coherent scattering and photonuclear reactions are neglected. Since the two γ -rays emitted by ^{60}Co are 1.33 MeV and 1.17 MeV in energy, the absorption in water and other low-Z materials (such as DMSO) will be predominantly by the Compton process for the primary γ -ray so that $\mu_a \approx \sigma_a$. However Compton photons of lower energy will have a much more important photoelectric contribution.

The Compton electronic absorption coefficient, ${}_e\sigma_a$, is related to the linear absorption coefficient in the following manner,

$$(\sigma_a/\rho) = {}_e\sigma_a (Z/A) N_o \text{ cm}^2 \text{ gm}^{-1} \quad (1.9)$$

where ρ is the density, A is the atomic weight (molecular weight) and Z is

the atomic number (or sum of atomic numbers if a compound) of the stopping medium. For radiation of a given energy the Compton electron energy coefficient is the same for all materials¹ so that $(\sigma_a/\rho) \propto (Z/A)$.

Thus for radiation energies for which materials absorb energy predominantly by the Compton process, energy absorption is proportional to the electron density (the number of electrons per gram). Most of the γ -ray energy is transferred to the kinetic energy of one or two high-energy electrons. Since these Compton electrons are responsible for the chemical effects observed, it is necessary to know how high-energy electrons subsequently interact with the chemical constituents of matter.

2. High-Energy Electrons

High-energy electrons interact with matter through inelastic and elastic collisions and by the emission of electromagnetic radiation called bremsstrahlung emission.

When a high-energy electron passes close to the nucleus of an atom, it is decelerated by the electric field and radiates electromagnetic radiation (bremsstrahlung) with a rate, $-dE/dx$, proportional to $e^2 Z^2 / m^2$ where e and Z are the charge on the electron and nucleus respectively and m is the electron mass. As a result, bremsstrahlung emission will be greatest for stopping materials of high atomic number. Thus lead and tungsten are generally used for efficient X-ray production from electron beams. The X-radiation emitted may then be partially

absorbed in the medium by the processes described earlier. Bremsstrahlung emission is unimportant below 100 keV but predominates above 100 MeV. For 10 MeV electrons bombarding tungsten ~ 50% of the energy is dissipated by bremsstrahlung emission.

At low energies where bremsstrahlung emission is unimportant, electron deceleration is predominantly through coulombic interaction with the electrons of the stopping material. The linear rate of energy loss, called linear energy transfer (LET) and expressed as $-dE/dx$, for an electron having relativistic velocity v is given by the Bethe expression³.

$$\begin{aligned} \frac{-dE}{dx} = & \frac{2\pi N e^4 Z}{m_0 v^2} \left[\ln \frac{m_0 v^2 E}{2I^2 (1-\beta^2)} - (2\sqrt{1-\beta^2} - 1 + \beta^2) \ln 2 + 1 - \beta^2 \right. \\ & \left. + 1/8(1 - \sqrt{1 - \beta^2})^2 \right] \text{ergs cm}^{-1} \end{aligned} \quad (1.10)$$

Here, N is the number of atoms per cubic centimeter,
 e is the electron charge,
 Z is the atomic number of the stopping material,
 m_0 is the electron mass,
 E is the kinetic energy of the electron, ergs,
 v is the velocity of the electron,
 β equals v/c , where c is the velocity of light,
 I is the average excitation potential of the stopping medium.

As these electrons are slowed down by these inelastic collisions, sufficient energy is transferred to the medium or stopping material to cause ionizations and excitations. From expression (1.10), it can be seen that the LET for this process increases with the atomic number of the medium (Z) and decreases with increasing kinetic energy of the electron. In water, the LET is ~ 0.02 eV/A $^\circ$ for electrons having approximately 1 MeV of energy but increases to about 0.22 eV/A $^\circ$ as the kinetic energy falls to 10 keV.¹

The ratio of energy loss per unit path length by bremsstrahlung emission to that by inelastic collisions is given by¹

$$\frac{(-dE/dx)_{\text{brem}}}{(-dE/dx)_{\text{coll}}} \approx \frac{EZ}{1600 m_0 c^2} \quad (1.11)$$

where the terms have already been defined. For Compton electrons of up to 1.3 MeV from ^{60}Co γ -rays traversing DMSO, less than 1% of the energy will be emitted as bremsstrahlung radiation. However, in the case of 35 MeV electrons from the linear accelerator, approximately 25% of the energy is lost as bremsstrahlung emission.

In addition to bremsstrahlung radiation, there is another form of radiative emission which occurs when high-energy electrons pass through matter, namely Cerenkov radiation. This occurs whenever a charged particle passes through any medium with a velocity greater than the phase velocity of light in the material. As the electrons traverse the dielectric medium, the molecules become temporarily polarized. When

the electron passes, they relax and emit an electromagnetic wave which is in the visible and ultraviolet region of the spectrum. Only those photons emitted at an angle θ with respect to the electron's trajectory will constructively interfere as shown in the simple Huygens construction in Figure 2.

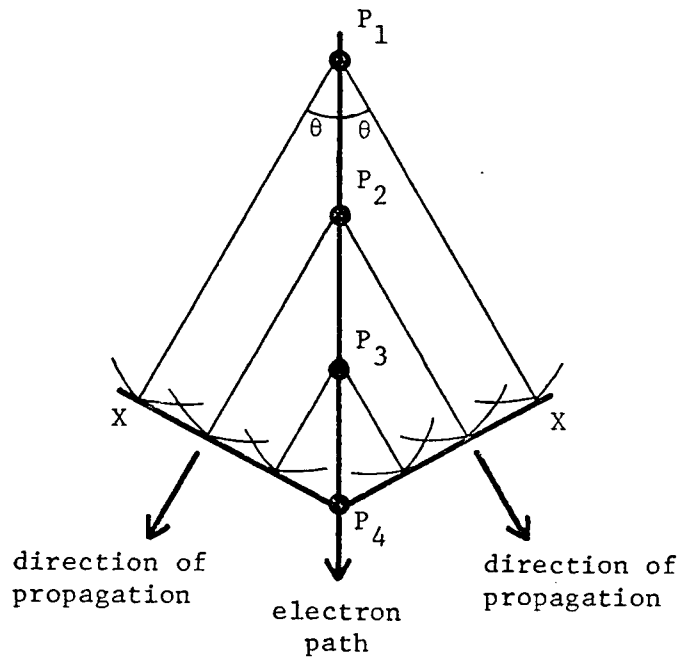


Figure 2. Huygens construction of electron trajectory and resulting Cerenkov waveform.

If the electron travels a distance P_1 to P_4 in the time the light wave travels from P_1 to X , then the wavelets from P_1 , P_2 and P_3 will constructively interfere. From Figure 2, the "Cerenkov relation"⁴

$$\cos\theta = 1/\beta n \quad (1.12)$$

is established where β is the velocity of the particle relative to the

velocity of light in vacuo, v/c , and n is the refractive index of the medium. Since $\cos\theta < 1$, Cerenkov emission will occur only if $\beta > 1/n$; that is, if the velocity of the electron is greater than the phase velocity of light in the medium. According to the Frank-Tamm theory⁵ the rate of energy loss per unit distance in the form of Cerenkov radiation is given by⁴

$$-\frac{dE}{dx} = \frac{e^2}{c} \int_{\beta n > 1} \left(1 - \frac{1}{\beta^2 n^2}\right) \omega d\omega \quad (1.13)$$

where $\omega = 2\pi\nu$. Since the light intensity of frequency ω is $E = N\hbar\omega$, where N is the number of photons, it can be shown that equation (1.13) may be written as equation (1.14) for all frequencies where $n > 1$.⁴

$$\frac{d^2N}{d\ell d\lambda} \propto \frac{1}{\lambda^2} \quad (1.14)$$

According to equation (1.14) the number of photons emitted per unit path length, ℓ , of the electron's track per unit wavelength interval follows a $1/\lambda^2$ spectral distribution in the visible and ultraviolet regions.

Although energy loss by Cerenkov emission is negligible compared to that by inelastic collisions and bremsstrahlung radiation, its intensity exceeds the bremsstrahlung by a very large factor in the visible region. For this reason, and the fact that the emission is "instantaneous", Cerenkov emission is often used to monitor the pulse shape of an electron accelerator. This will be discussed more fully later.

3. Range of Electrons

Unlike electromagnetic radiation, high-energy electrons have a finite range in an absorbing medium. As electrons traverse the medium they are constantly deflected and slowed down by elastic and inelastic collisions with the medium electrons or by interactions with the atomic nuclei (bremsstrahlung). Because of these deflections their total path length will exceed their depth of penetration. Therefore the path length is defined as the distance travelled by the impinging electron along its path before it is brought to rest whereas the range or penetration is the distance travelled in the direction of original momentum. In theory, the range may be obtained by numerical integration of a suitable stopping-power formula similar to equation (1.10). If one neglects the velocity dependence of LET then the range would be proportional to the square of the electron energy. For high-energy electrons this approximation is reasonable since the range is roughly proportional to E^m , m being only slightly less than 2 but decreasing as E decreases.⁶ Empirical formulæ have been developed to relate the range and energy of electrons in aluminum absorbers. For electrons of energy 0.01 to 2.5 MeV, the range in mg cm^{-2} is given by¹

$$\text{Range} = 412^{1.265-0.0954 \ln E} \quad (1.15)$$

where E is the kinetic energy of the electrons (MeV). For electron energies greater than 2.5 MeV, the range is given by (1.16).¹

$$\text{Range} = 530E - 106 \quad (1.16)$$

These formulae can be applied to other light elements since the range (mg cm^{-2}) varies only slightly with atomic number. Thus for a 1 MeV electron in DMSO, the range, calculated using (1.15), corresponds to 1.41 gm cm^{-2} or to a thickness of 1.28 cm. Using 35 MeV electrons, an approximate range, calculated using (1.16), is found to be 17 cm. This is only a rough estimate since equation (1.16) is good only up to about 20 MeV.

4. Track Entities: Spurs, Blobs, and Short Tracks

In radiation chemistry the primary chemical events arise from the ionizations and excitations of the molecules produced by the secondary high-energy electrons or other charged particles. The distribution of these active species in the irradiated material is not homogeneous or random. Instead the active species are produced only along the track of the incident particle and it is only after these species have diffused throughout the reaction volume that the system can be considered homogeneous. In addition, the actual yields of active species and their specific distribution in space depend upon the LET of the particular incident particle. Consequently, different overall chemical changes can arise from different ionizing radiations simply because of the various spatial distributions of the primary species formed.

As the primary electrons (or Compton electrons) are slowed down by interactions with the medium, they produce a trail of excited and ionized species along their tracks. The electrons which are ejected

as a consequence of the ionizations may themselves be sufficiently energetic to produce further ionizations and excitations. If the energy of these secondary electrons is small (< 100 eV), their range in a liquid or solid will be short. Consequently any further ionizations or excitations produced will be localized in a small region (perhaps roughly approximated to a sphere) with a mean diameter of $\sim 20 \text{ \AA}$. These small clusters of excited and/or ionized species are called spurs. For a 1 MeV electron, whose LET is $\sim 10^{-2} \text{ eV/\AA}$, the spurs will be separated, on the average, by several thousand Angstrom units.

However there will be a continuous distribution of ejected electron energies and therefore a distribution in inter-spur distances. In some cases the secondary electrons may have sufficient energy to form branch tracks of their own. These electrons are called δ -rays. In other cases the spurs may overlap so that there is essentially a continuous cylindrical region of activated species. Mozumder and Magee⁶ considered this distribution of species for the case of water in the following way. Those electrons which have energies in excess of 100 eV but insufficient energy to allow them to escape the coulombic attraction of their positive "hole" are called super spurs or "blobs". If the electrons are energetic enough to escape the "hole" but not energetic enough to prevent spur overlap, they form "short tracks". In the case of water, these energies are divided as follows: spur, $\sim 6-100$ eV; blob, $\sim 100-500$ eV; short track, ~ 500 eV-5 keV. Mozumder and Magee⁶ estimated the partition of the primary energy of the electron into these various track entities and the results of their calculations are shown in Figure 3. ⁶⁰Co γ -rays

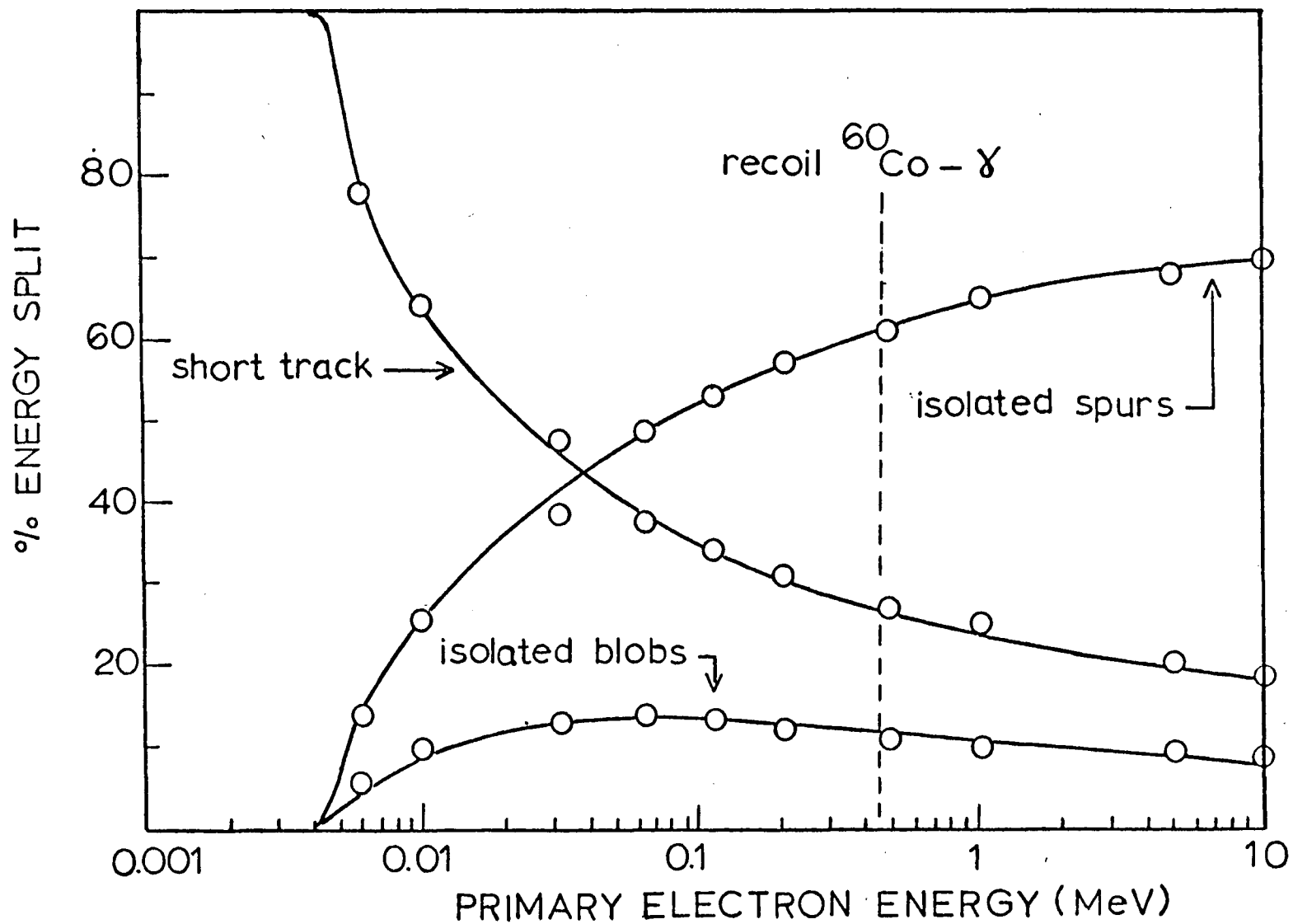


Figure 3. Schematic plot of percentage of energy split between spurs, blobs and short tracks for electrons in water. (Adapted from Figure 5, page 211, reference 6).

in water give rise to electrons having a mean energy of 440 keV. About 64% of this energy is deposited in the form of isolated spurs, about 25% in the form of short tracks, and about 11% as "blobs". From Figure 3, it can be seen that as the primary electron energy increases, the fraction of energy deposited in isolated spurs increases. Knowledge of this approximate distribution is useful in describing spur diffusion processes since reactions in isolated spurs are expected to be different from those in "blobs" and "short tracks" where ion and radical recombination reactions will be more highly favoured.

B. CHEMICAL CONSEQUENCES FOLLOWING ABSORPTION OF HIGH-ENERGY RADIATION

The overall process of producing chemical changes in a medium with ionizing radiation begins with the bombardment and production of ionized and excited species and terminates with the reestablishment of chemical equilibrium. However there are several orders of magnitude in time between these two stages. The chemical events observed before or after the attainment of chemical equilibrium may not necessarily arise directly from the primary processes but rather from the intermediates so produced. For this reason it is necessary to know the types of processes which may occur and their relative time scale in order to correctly interpret the chemical events observed.

1. Time Scale of Events

In radiation chemistry one usually recognizes three stages following the absorption of high-energy radiation and lasting up to the time of the production of the ultimate chemical effect. These are referred to, in order of increasing time, as the physical stage, the physico-chemical stage and the chemical stage.

In the physical stage, energy is transferred to the system by the processes mentioned earlier. This involves the primary process and its duration is of the order of 10^{-16} to 10^{-14} sec, the upper limit being fixed by the Heisenberg Uncertainty Principle ($\Delta E \cdot \Delta t \sim \hbar$) for an electron depositing 20 eV to 30 eV of energy. As the primary, secondary and higher-order electrons are slowed down by inelastic collisions with the medium, they lose their excess energy by molecular excitations or ionizations. When their energy has dropped below the lowest electronic excitation level (usually 1 to 10 eV), the electrons are called "subexcitation electrons" and they subsequently lose their energy by excitation of molecular vibrations and rotations. Since the period of a molecular vibration or rotation is of the order 10^{-14} to 10^{-12} sec, energy transfer by these processes occurs over this time range. These interactions are the germane initial events and thus the primary reactive species are the positive ions, nearly thermalized electrons, vibrationally and electronically excited molecules, all of which are the precursors of the observed chemical consequences of the radiation absorption.

The next stage is called the physico-chemical stage and lasts up to about 10^{-11} sec. It is during this period that the unstable primary

species undergo secondary reactions, either spontaneously or by collisions with adjacent ions or molecules. The positive ions may be involved in charge neutralization, proton transfer or they may decompose into other fragments whereas the highly excited molecules may decompose into radical species or lose energy by internal conversion. The electron reaches thermal equilibrium with its environment, with $E \sim kT$ (0.025 eV), at which time it faces several different possibilities. It may be (i) recaptured by its parent ion, (ii) captured by a solvent molecule to produce a negative ion, (iii) captured by a radiation-produced ion or product other than its parent, (iv) captured by a scavenger molecule or ion initially present in the system, or it may (v) become trapped or stabilized among the molecules of the medium. The formation and properties of these temporarily stabilized, or solvated electrons will be discussed later. Ultimately the system attains thermal equilibrium and the chemical stage begins.

In the chemical stage the newly formed reactive species which have escaped geminate recombination in the spurs diffuse out into the bulk of the medium and eventually they become homogeneously distributed. These primary or secondary species undergo thermal chemical reactions with each other, with scavengers or with the medium itself. Excited molecules, formed either in the primary process or from ion recombination, can undergo various luminescent processes. These events continue until the system once again attains chemical equilibrium.

The above is a rather general description of the types of chemical processes possible when a system is bombarded by ionizing radiation. These processes and their time scales are indicated schematically in Figure 4. The time scale refers to the liquid phase and would be

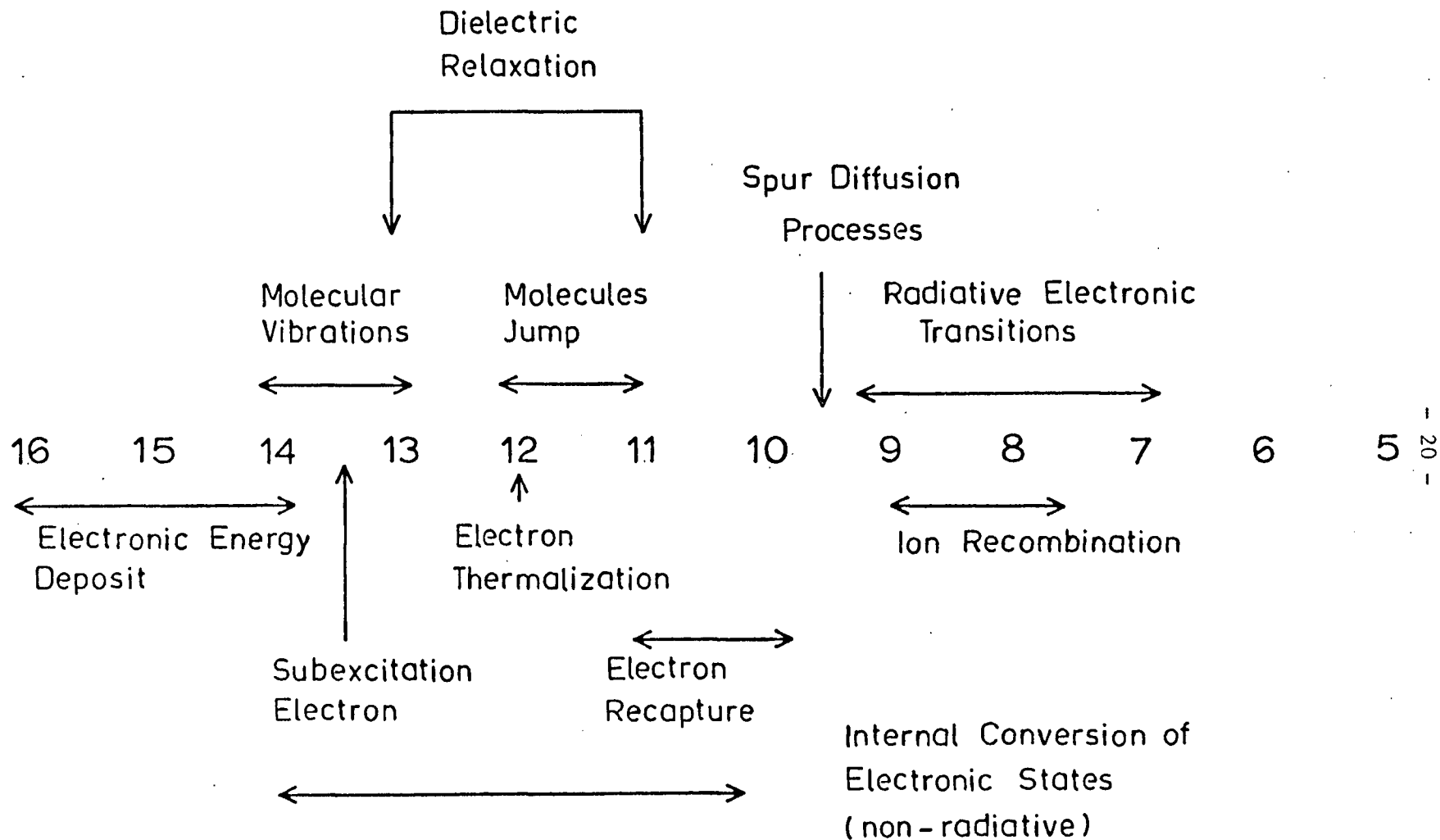


Figure 4. Theoretical time scale for the initial processes in radiation chemistry. The numbers are the negative logarithm of time ($pt = -\log t$ (sec)). The time scale refers to the liquid state.

different in several respects when this description is applied to the solid or gas phase.

2. Phase-Dependent Phenomena

Whenever a compound is exposed to a source of ionizing radiation the primary processes are largely independent of the phase of the medium. However the subsequent chemical processes will depend markedly on the phase. For instance, there are no track effects or spur-controlled reactions of consequence in the gas phase. The ion-pairs formed in the gas phase have a negligible probability of undergoing geminate recombination because the mean free path of the electron is too long. Consequently the positive ion may experience several collisions with neutral molecules before neutralization occurs and thus has the opportunity to decompose or undergo ion-molecule reactions. The electron, on the other hand, may attach itself to a neutral molecule and the resulting negative ion may disproportionate before undergoing neutralization with a positive ion. However, in an identical ionization event in the liquid or solid phase, the ionized and excited molecules and molecular fragments formed by decomposition of excited molecules are produced at high local concentrations in the tracks and spurs. Consequently the probability of their reaction with each other is increased relative to their reaction with the medium or added scavengers. Furthermore, concomitant partners formed by the rupture of a given molecule will be trapped within the same solvent cage thereby increasing the probability of geminate recombination. Because of this difference in spatial distribution of the reactive intermediates, the radiation chemistry of a gaseous system is often different from its

liquid or solid phase counterpart. Since only studies on the liquid and solid phase were undertaken in this work, further discussions will be limited to the condensed phase.

3. Studies on the Chemical Events in Condensed Phases

Radiation chemical studies are not just concerned with the net chemical effect but with an understanding of the detailed mechanism leading to the change. The ionized and excited molecules initially formed subsequently give rise to a series of ionic or radical intermediates which then produce the stable chemical products. By identifying these products and studying the effects on their yields caused by the addition of various radical, ionic or electron scavengers, it is possible, by inference, to speculate on the identity of the intermediates and thereby propose a reaction scheme. The lifetime of the transient species which have escaped the intra-spur reactions is often of the order 10^{-9} seconds to 10^{-6} seconds, and assuming the scavengers react at diffusion-controlled rates, $10^{10} \text{ M}^{-1} \text{ sec}^{-1}$, scavenger concentrations of the order 10^{-1} M to 10^{-4} M are required to compete effectively with their alternative decay processes. Those species which decay by intra-spur reactions and hence cannot be scavenged at these concentrations give rise to products which are referred to as "molecular products". By the method of pulse radiolysis,⁷⁻⁹ it is possible to observe the formation and decay of many of these transient intermediates. In this technique short pulses (typically 10^{-9} to 10^{-6} sec) of high energy electrons are used as the radiation source at intensities sufficiently high to produce "instantaneous" concentrations of transient species which may be detected

and identified by various fast physical methods, particularly by optical absorption spectroscopy. From the absorption spectra, it is often possible to identify free radicals, molecular ions, solvated electrons or excited molecules. Sometimes this identification comes from comparison to other systems where the species have been well characterized but in many cases they have to be assigned on the basis of their chemical behaviour to various scavengers.

In the liquid phase these active species will usually react with each other or with the solvent or scavengers in times of microseconds or less. As a result, they can only be observed, if at all, by using very fast pulse radiolysis techniques. However, if the medium is in the solid state, and at sufficiently low temperatures (usually 77°K or lower), the rate of reaction of these transient intermediates may be slowed down so that they can be observed over periods of minutes or even years. This approach is often referred to as the "isolation technique". If these species are paramagnetic, such as radicals and trapped electrons, they can then be studied by electron spin resonance spectroscopy. They may also be observed by optical spectroscopy if the sample is sufficiently transparent. The formation and decay of the various intermediates, in particular the electron, depend to a great extent upon whether or not the medium is glassy (amorphous) or polycrystalline. Often studies on the solid state give a valuable insight into the processes occurring in the liquid state, especially since not all transients can be positively identified through their optical and chemical behaviour alone.

The techniques of optical spectroscopy, electron spin resonance

(esr) spectroscopy and pulse radiolysis will be described more fully in the next chapter. However, it must be stressed that the transient intermediates observed using these techniques are those active species reacting during the chemical stage only. The earliest events which have been resolved experimentally using pulse radiolysis occur later than 10 picoseconds after energy deposition; consequently any extrapolation to the events occurring from 10^{-16} to 10^{-11} seconds can only be speculative.

4. Chemical Yields

Any successful description of the effect of radiation on matter must involve the yields of the radiolytic products. In radiation chemistry chemical yields are expressed as G values, the number of events of a specific kind induced in a medium per 100 eV of energy absorbed. The unit energy, 100 eV, is an entirely arbitrary magnitude and, as such, G values have no intrinsic or stoichiometric significance. In general the yields are written as G(X) where X refers to the atoms, ions, radicals, excited species or molecules used up or produced by the energy deposition. Often correlations are drawn between the G value for ionization in the gas phase and the W value, which is the mean energy required in ion-pair formation. Typical W values for gases are in the region of 30 eV. Since ionization potentials are typically ~ 10 eV it follows that only 30-40% of the energy is dissipated in ionizing processes. The relationship may be expressed as follows:

$$G(\text{ion-pairs}) = 100/W \quad (1.17)$$

If one assumes that the W value for the condensed phase is the same as its gas phase counterpart, then G(ion-pairs) in the condensed phases should be 3-4. Scavenging studies at very high concentrations have indicated ionic yields not just between 3 and 4 but even up to 5, to indicate that W values may be somewhat smaller in the condensed phase than in the gas phase.

Another parameter which is often used to characterize radiation effects is the ion-pair yield, M/N, where M is the number of species X produced and N is the number of ion-pairs. This parameter was widely used in the earlier years of radiation chemistry when it was believed that virtually all induced chemical changes arose from ionic precursors. It is related to the G value by equation (1.18).

$$G(X) = \frac{M}{N} \cdot \frac{100}{W} \quad (1.18)$$

However, expression (1.18) is not useful when applied to condensed systems since N and W cannot be measured directly. For this reason, G values are used to express radiation chemical yields since they can be obtained directly and do not imply, as does the ion-pair yield, that the chemical action is controlled by the number of ions formed. All that is required is a knowledge of the number of species produced and the dose absorbed by the medium. The latter is obtained by dosimetry and will be described later.

Generally the G values of species produced by ionizing radiation range from 0 to 5. Yields greater than 5 usually signify chain reactions. However it must be emphasized that the G values measured

represent average values. They are averaged over the range of LET involved and therefore small yields can arise, for instance, exclusively from the specific chemistry peculiar to short tracks or "blobs" and may not be at all representative of isolated spurs.

C. STABILIZED ELECTRONS

In many systems stabilized electrons are the principal chemically-reducing species produced by the interaction of ionizing radiation with matter. Although the existence of stabilized electrons in solutions of alkali metals in ammonia has been known for over fifty years, it was only with the advent of pulse radiolysis that they were directly observed as intermediates in the radiation chemistry of water.¹⁰ This was because the electrons have a high reduction potential and as such are extremely reactive and very short-lived. In the last decade stabilized electrons have been identified and studied in many other systems; indeed, no other species studied in radiation chemistry has likely commanded as much attention.¹¹

1. Stabilization

In gaseous media the thermalized electrons collide elastically or inelastically with unreactive molecules until they are eventually captured by reactive molecules or ions, undergoing electron attachment or dissociative reactions. However, in condensed media electrons may become confined to a cavity, either by the thermalized electron

polarizing the medium through repulsive forces followed by reorientation of the molecules to produce a better trap, or by the electron "falling into" a pre-existing, suitably oriented void. The lifetime of these localized or stabilized electrons will depend upon the thermal motion of the molecules forming the cavity walls. In the liquid phase the lifetime of these electrons, which will be called solvated electrons and denoted by e_s^- , is often less than 10^{-6} sec due to their mobility and high reactivity towards the medium, other radicals, positive ions, radiation products or scavengers. In the solid phase, however, and at low enough temperatures, the cavities may be "frozen in" and the electron lifetime may be extended by several orders of magnitude. Such electrons are called trapped electrons and are designated by e_t^- . The similarity between the chemical and physical properties of electrons solvated in liquids and those trapped in the solid phase suggest that the two species are identical except for mobility. By studying these properties information regarding the stabilization process can hopefully be obtained, for, despite the amount of work being carried out on the stabilized electron, no satisfactory theory regarding the nature of the trapping sites nor the mechanism of solvation has yet been proposed.

2. Properties

The stabilized electron is regarded as the simplest and most reactive chemical entity. It is highly characterized by its intense absorption spectrum in the visible and near infra-red region, its paramagnetism and its high mobility.

2.1 Optical Spectrum

The most prominent feature of stabilized electrons is their intense absorption spectra in the visible and near infrared region. The spectra are characterized by their broadness and lack of structure, their asymmetry on the high-energy side and by their intensity, with typical molar extinction coefficients $> 10^4 \text{ M}^{-1} \text{ cm}^{-1}$ at the maximum. All current theories regard the stabilized electron as being confined to a type of potential well, or cavity, the depth of which depends upon the polarization energy acting back on the electron. Like any localized system, there will be quantized energy levels associated with each cavity. The absorption spectrum may then be attributed to transitions between these levels and thus the transition energy may be taken as representative of the well depth or the solvation energy of the electron.

In nonpolar media, such as the hydrocarbons, stabilization can only occur through short-range repulsions or induced electronic polarization of the surrounding molecules, so that the cavity depth will be rather shallow. On the other hand, with polar molecules such as water, alcohols and amines, orientation (atomic and dipole) polarization can also occur thereby increasing stabilization. Since the absorption spectra of e_t^- in vitreous, glassy solids are virtually the same as those of their liquid counterpart, this suggests that these cavities, with the optimum dipole arrangement, existed before the arrival of the electron. This is particularly true of polar media which owe their strong solvation to orientation polarization. In the liquid state this dipole relaxation may follow the initial electronic polarization by the electron but may take several orders of magnitude longer at lower temperatures. However dielectric relaxation times are measured on a macroscopic scale whereas rotational

oscillations by the polar molecules forming the cavity walls may be possible under the electron's field at all temperatures. Recently Richards and Thomas¹² observed a shift in the absorption spectra of trapped electrons in glassy ethanol at 77°K towards the blue on a microsecond time scale. Similar observations in binary mixtures of alcohols and water were made by Kevan.¹³ This blue shift was attributed to initial trapping of the thermal electrons in less than optimum traps followed by microscopic relaxation to produce deeper, more stable traps. Thus the stabilization of electrons is probably facilitated by the pre-existence in the medium of suitably oriented voids, but reorganization of the cavities occurs after electron capture. Unfortunately the time scale of current apparatus is limited to the 20 picosecond range,¹⁴ by which time electrons in liquid media at room temperature have already been solvated. Extension of these studies to low temperature liquid systems is also possible.

In polycrystalline media, the spectra are similar to the liquid phase but the yield of trapped electrons is much lower. Because of the long-range order in crystals, there are less suitably oriented voids for initially trapping the electron compared to the glassy state. As a result, the electrons can only be trapped at defect sites in the crystal lattice.

Besides the medium polarizability, the cavity or void radius is also a factor in governing the solvation energy of the electron. All theories concerning the localized electron predict that the energy level separations should diminish with increasing cavity radius. That is, the self-induced energy acting on the electron falls off with the

distance from the cavity center. However, it should be noted that the cavity radius is not to be confused with the effective ionic radius. The stabilized electron has a small mass and low momentum and is therefore "smeared out" over a large volume in accordance with the uncertainty principle. This is represented in Figure 5 where the electron, represented by the shaded portion, is spread over several molecules. The arrows represent the induced or permanent dipole moments. The tips of the dipole vectors represent the cavity, or void, in the medium.

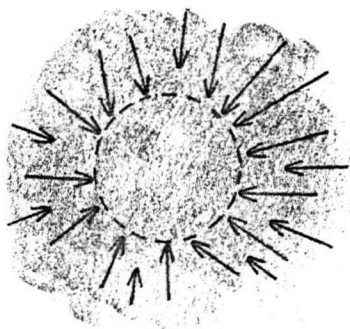


Figure 5. Schematic representation of electron localization (shaded region) produced by polarization of the medium. The dotted area represents the void or cavity in which the electron is centered.

As the cavity radius is decreased, the self-energy increases, and the solvation energy is increased. This has been demonstrated in studies on systems at low temperatures and high pressures where the shift in the electron absorption band towards the blue has been attributed to a decrease in the cavity radius caused by these external effects.

The shape and position of the absorption band will depend upon the

manner in which the energies of the ground and excited states vary with the shape of the cavity due to the various arrangements of the molecules forming the cavity walls as well as any distribution in cavity sizes. This would suggest a reasonable explanation for the exceptional width (~ 1 eV) of the optical spectra of stabilized electrons and why they show no structure. Each electron will be stabilized in a particular environment and will exhibit a characteristic absorption. The observed spectrum is then simply the envelope of the individual spectra in which the maximum represents the most probable cavity or potential well. The asymmetric tail of the absorption band on the high-energy side of the absorption maximum may be interpreted, perhaps, in terms of transitions of the stabilized electrons to higher excited states or an energy continuum (conduction band).

In the discussion so far it has been assumed that the excited state of the electron is a bound state. If one treats the cavity as a spherically symmetric potential well and the electronic wave functions as hydrogenic in nature, then the separation between successive quantized energy levels will converge, the first transition, ($2p \leftarrow 1s$), being three quarters of the well depth. However the first excited state may be very close to, or perhaps overlap, with either the conduction band or an auto-ionization state. This is in keeping with the observations obtained when the electrons are photobleached in low temperature glasses. By illuminating γ -irradiated n-propanol¹⁵ and alkaline aqueous glasses¹⁶ at 77°K alternately with red ($\lambda > 640$ nm) and blue ($\lambda < 500$ nm) light it was possible to "photoshuttle" the trapped electrons between shallow and deep traps without causing any loss of

electrons. All that changed was the shape of the absorption band. Furthermore, by using near-monochromatic light, it was possible to show that photoconductivity could be induced in γ -irradiated aqueous alkaline glasses¹⁷ and methyltetrahydrofuran glasses¹⁸ by light which matches the absorption spectrum.

2.2 Electron spin resonance

In contrast to the optical absorption spectrum of the stabilized electron, electron spin resonance (esr) can be used to give a more sensitive indication of the electron's immediate environment. The esr signal consists of a single, narrow line with a g-factor near that of the free electron, $g = 2.0023$. In liquids the line width is typically less than 0.1 gauss whereas in solid media the line width is much broader, generally 5-15 gauss, due to the magnetic interaction of the electron spin with the nuclear magnetic moments of the nuclei surrounding it. The narrowness of the line in the liquid state is due to the extensive time averaging of the nuclear dipolar interactions. The absence of any resolvable hyperfine splitting indicates that the electron is not strongly localized on any particular molecule but rather interacts weakly with the molecules forming the cavity. Furthermore, the signals are easily power saturated at low temperatures. In nonpolar hydrocarbon matrices, the esr signal becomes saturated at only 0.02 mW, whereas in polar media, saturation becomes appreciable if the microwave power saturation exceeds 0.2 mW.^{11h}

One interesting feature of esr studies on stabilized electrons is that the line widths of trapped electrons in polar media are considerably

broader than those in nonpolar systems. The cavity radii for nonpolar media are larger, consequently there is a diminished interaction of the electron with the nuclei of the cavity walls as compared to those of polar media.

In the majority of studies to date, trapped electrons have shown no resolvable hyperfine structure suggesting that the electron is not strongly localized. However a few cases of observable hyperfine structure have been reported, in particular that by Bennett, Milne and Thomas¹⁹ in which trapped electrons at 77°K were prepared by the co-deposition of sodium and water vapour on a rotating cryostat. Upon slowly warming the sample to 140°K, the single esr line was split into seven equally spaced lines and was attributed to the interaction of the electron with six equivalent protons arranged octahedrally around the electron. It has been suggested that this observation may be due to a phase transition of ice from the amorphous to the cubic state which leads to the preferred orientation of the solvation shell.^{11e}

Other examples of hyperfine interaction were found in the case of deuterated pyrrolidine²⁰ and crystalline deuterated acetonitrile²¹ at 77°K. In the former case a seven line spectrum was observed, indicating interaction of the electron with three or four equivalent nitrogen atoms. In the latter case, a five line spectrum was observed and it was suggested that the electron was trapped between the dipoles and interacting with the two nitrogen nuclei. However this observation has since been attributed to a dimer radical anion of acetonitrile.^{22,23} To date, no other experiments have been reported regarding hyperfine structure of stabilized electrons.

A more detailed description of esr spectroscopy and its application to this study on dimethyl sulfoxide is given in Chapter V.

2.3 Conductivity

A third important property of stabilized electrons is their high conductivity. The stabilized electron is associated with several molecules of its cavity. Therefore, if the classical picture of ionic mobility, in which the ion moves carrying its solvation sheath with it, holds for stabilized electrons, then the electron's mobility should be comparable to other ionic species. However, its mobility is significantly greater than most other negative ions, suggesting that the electron moves from trap-to-trap by quantum mechanical tunnelling or through voids formed in the cavity wall by the rotation of one of the cavity molecules. In the solid state at low temperatures such rotation is inhibited and the electrons can only be mobilized by the absorption of light (photoconductivity) or by thermal release. Measurements of electron conductivities are helpful in determining the extent of electron solvation. Those electrons which are strongly solvated, as in polar alcohols and water, exhibit a much lower mobility than those in hydrocarbons where the polarization forces are very weak. However, because of the high background conductance in polar and partially ionic solvents, experiments dealing with radiation-induced conductances are usually restricted to materials of low dielectric constant, such as the saturated hydrocarbons and ethers. Studies on electron conductivity in DMSO were not undertaken.

3. Models

In order to account for the observed physical and chemical properties of stabilized electrons in various media, several theoretical models have been proposed. Such models are essential if one is to understand all features of the experimental results, in particular the variation in properties between different systems.

Probably the most widely accepted theory is Jortner's^{24,25} continuum model in which the electron is regarded as being stabilized by the induced polarization field of the medium. The electron initially polarizes the medium by electronic polarization which is followed, in the liquid phase, by orientation (atomic and dipole) polarization if the molecules of the medium have a permanent dipole. In the case of low temperature glasses these traps are considered as being preformed with the dipoles suitably oriented before the arrival of the electron. In this way one can explain the similar spectral properties of stabilized electrons in the liquid and glassy phases. Once stabilized, the electron is regarded as being largely confined to a spherical cavity of radius R in which the electrostatic potential function is constant. Outside the cavity the function is continuous. The stabilization is attributed to long-range polarization interactions, the short-range attractions being offset by short-range repulsions. The self-energy, E_i , of the electron may be represented by

$$E_i = T + V(r) \quad (1.19)$$

where T is the inherent kinetic energy ($< kT$) and $V(r)$ is the potential

energy acting on the electron produced by the polarization. The Landau orientation potential energy function, $P(r)$, is given as follows:

$$\begin{aligned} P(r) &= -\beta e^2/r && \text{for } r > R \\ &= -\beta e^2/R && \text{for } r < R \end{aligned} \quad (1.20)$$

where $\beta = (1/D_{op} - 1/D_s)$. D_{op} and D_s are the optical and static dielectric constants and r is the distance from the centre of the electron cavity. The ground and first excited state (presumed to be bound) of the electron are considered as being similar to one-parameter hydrogenic-type 1s and 2p wave functions, which take the following form:

$$\begin{aligned} \psi_{1s} &= (\gamma^3/\pi)^{1/2} e^{-\gamma r} \\ \psi_{2p} &= (\alpha^5/\pi)^{1/2} r \cos\theta e^{-\alpha r} \end{aligned} \quad (1.21)$$

where γ and α are the variational parameters.

The energy of the ground state can be represented by the expression

$$W_{1s} = \int_r \psi_{1s} \left[-\frac{h^2}{8\pi^2 m} \nabla^2 + P(r) \right] \psi_{1s} d\tau \quad (1.22)$$

where ∇^2 is the Laplacian operator, $P(r)$ is the potential energy operator, h is Planck's constant and m is the electron mass. For a given value of R and β , W_{1s} is then obtained as a function of γ . Using the variation procedure

$$\frac{\partial W_{1s}}{\partial \gamma} = 0 \quad (1.23)$$

the best value of γ is obtained which, when substituted into (1.21) and (1.22) yields the wave function and energy for the ground state of the stabilized electron. The first excited state is treated in a similar manner. However, according to the Frank-Condon principle, the value of R and the form of the potential selected for the ground state must be the same for the 2p-type state since the molecules cannot reorient themselves fast enough to follow the excitation.

The electronic polarization energy is represented, approximately, by the expression

$$S_i = \frac{-e^2}{2\bar{r}_i} (1 - 1/D_{op}) \quad (1.24)$$

where \bar{r}_i is the mean radius of the charge distribution in the i state, being $\frac{3}{2\gamma}$ and $\frac{5}{2\alpha}$ for the ground and first excited state respectively.

Thus the total energy of the ground and first excited state of the electron may be represented as:

$$E_{1s} = W_{1s} + S_{1s} \quad (1.25)$$

$$E_{2p} = W_{2p} + S_{2p}$$

The energy for the (2p \leftarrow 1s) transition is then given by:

$$h\nu = E_{2p} - E_{1s} \quad (1.26)$$

which is regarded to correspond to the excitation energy at the absorption maximum.

It should be stressed, however, that this model is semi-empirical because the cavity radius is introduced as an adjustable parameter and does not provide any real physical information regarding the short-range structural modifications and interactions. Furthermore, because D_s is fairly large for most polar media, and D_{op} is ~ 1 to 2 for all media, the terms $(1/D_{op} - 1/D_s)$ and $(1 - 1/D_{op})$ in the energy expressions are fairly constant so that the spectral and thermodynamic properties of stabilized electrons are often attributed to changes in the cavity radius. Assuming a constant value of 2 for D_{op} , Noda, Fueki and Kuri²⁶ have drawn up a contour map of the optical transition energy in 0.1 eV steps as a function of R and D_s . From this map it is possible to draw a correlation curve of the transition energy and cavity radius for any solvent knowing its static dielectric constant. The curve for DMSO is shown in Figure 6, taking $D_s = 48$.

Using Jortner's model, experimental data can be fitted for any solvent (using empirical values of R) and has been done for several polar media, in particular ammonia, water and the alcohols, with reasonable success. However, in spite of the apparent success of this qualitative approach, there exist very serious theoretical arguments against its application, especially for strongly solvated electrons. The treatment is really an electronic adiabatic approximation since it assumes that the extra electron is much more loosely bound and therefore of lower mean velocity than the valence or core electrons of the medium. In polar media the binding or solvation energy is ~ 1 to 2 eV so that the electron is not appreciably more weakly bound than the valence electrons. The extra electron should be considered on an equal basis with the

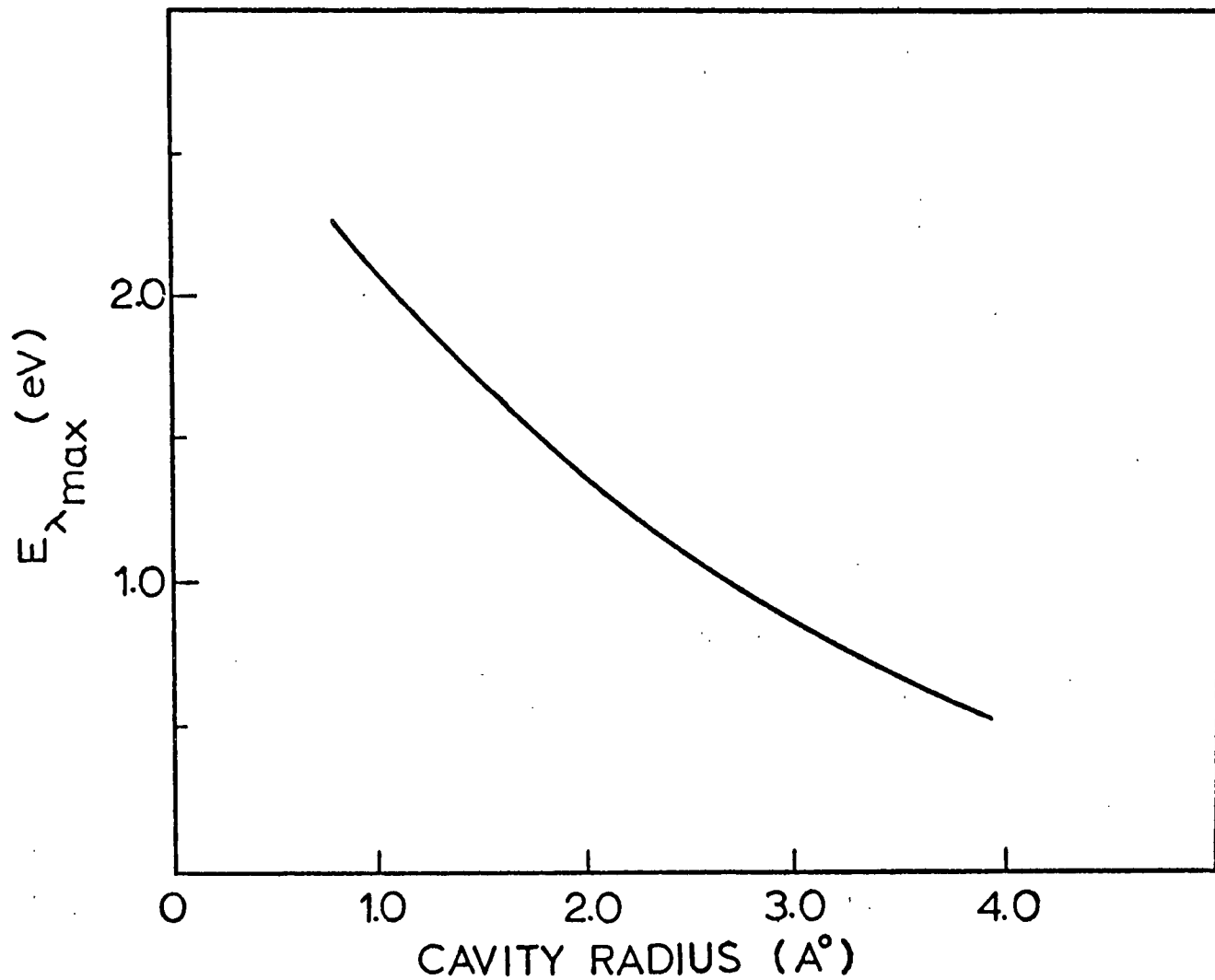


Figure 6. Correlation curve of the transition energy of the electron in DMSO and its cavity radius using the continuous dielectric model with an adiabatic approximation.

medium electrons by including the electronic polarization potential in the eigenvalue equation for determining the wavefunction parameters and energies of the electronic states. Treating the total polarization energy in this way thus constitutes an independent particle or self-consistent field (Hartree-Fock) type approximation. When this approximation is applied to the hydrated electron, the cavity radius must be made vanishingly small ($R \sim 0$) for the theoretical optical transition energy to agree reasonably with the experimental results.²⁴ However short-range overlap interactions are not accounted for by this continuum model and is really only applicable provided that the cavity radius is taken to be equal or larger than a molecular or atomic radius. Moreover, the shift in the absorption spectrum with temperature and pressure cannot be adequately explained assuming a near zero cavity radius. For these reasons both the semi-empirical adiabatic and self-consistent field approximation to the continuous dielectric model are too limited to provide a proper interpretation of the properties of stabilized electrons in polar solvents.

Whereas the continuous dielectric model accounts for electron stabilization through long-range polarization forces, other models attribute these forces to short-range electron-solvent interactions. Natori and Watanabe²⁷ proposed a structural model for the hydrated electron which involves a trapping center consisting of four water molecules with one OH bond of each water molecule tetrahedrally oriented around the electron. The theoretical transition energy was fitted to the experimental value by varying the oxygen-oxygen distance and by stretching the bond distances and angles. However, the calculated value

was much lower than the experimentally observed value (0.8 eV versus 1.7 eV). This was undoubtedly due to the fact the dominant long-range polarization interactions were neglected.

A second model, called an oriented dipole model, has been suggested by Iguchi.²⁸ In this model the potential field arises from the molecular dipoles oriented in a spherical manner about the excess electron. The approximations used are essentially the same as for the electronic adiabatic continuum model in which the electronic polarization energy is added as a correction term to the computed energy. The thermal dependence of the absorption spectra are attributed to the degree of orientation of the dipoles as well as by the thermal expansion of the liquid rather than a simple change in cavity radius.

The success of any of these treatments for electron solvation and trapping are judged essentially in terms of their ability to produce "agreement" between theory and experiment. However, in view of the crude approximations used, such as the neglect of either the short- or long-range interactions, none of these models can be considered as giving a true picture of electron stabilization. Furthermore, either the cavity radius (continuum model) or a specific dipole orientation (atomic models) are varied until theory and experiment agree, implying these are the only factors involved.

Recently a semicontinuum model for the stabilized electron in ammonia,²⁹ water³⁰ and methanol³¹ was developed which included both long- and short-range interactions. In this treatment the excess electron interacts with the induced and permanent dipole moments of the molecules in the first solvation shell by a short-range charge-dipole

attractive potential, similar to that proposed by Iguchi,²⁸ whereas the solvent molecules beyond the first solvation sheath are treated as a continuous dielectric medium with which the electron interacts by a long-range polarization potential (continuum model). By performing variational calculations similar to those described previously for various cavity radii, the authors were able to construct configurational coordinate diagrams for the ground and excited states. In this manner a minimum in the total energy of the system could be established, which could not be obtained at a finite radius by only including long-range polarization interactions, and a unique cavity radius could be predicted. In the case of ammonia, a self-consistent field treatment was used for short-range interactions and a Landau-type potential for long-range interactions (adiabatic approximation) whereas both short- and long-range interactions were treated self-consistently in the case of the electron in methanol and water. Using such a treatment, the observed optical absorption of both the solvated electron in ammonia and methanol and the hydrated electron in water (using $D_s = 78$) and in polycrystalline ice at 77°K (using $D_s = 3$) could be satisfactorily explained. Moreover, the energy levels were moved toward the continuum so that the excited states are less strongly bound. This is in keeping with the photobleaching and conductivity studies on low temperature glasses mentioned earlier. Thermodynamic and structural data, such as the heat of solution and charge distribution of the stabilized electron, were in good agreement with the experimental results.

Although the semicontinuum model is only approximate in nature, it does show that both short- and long-range interactions must be

considered when describing the trapping and stabilizing of electrons and when anticipating their inherent chemical and physical properties. Such considerations are essential if one is to understand all the features of the experimental results, especially the variation in properties between different solvents. Studies of other systems, in particular polar aprotic solvents such as DMSO, should provide a rigorous test to these models and a better insight into the structural, thermodynamic and optical properties of the stabilized electron.

4. Free Ion Yields

In the preceding section it was suggested that the solvation energy of the electron depends to a great extent on the polarizability of the medium. Similarly, the radiation yield of stabilized electrons depends on the bulk dielectric constant of the medium.

The primary, secondary and higher-order electrons produced by the incident radiation are reduced to thermal energies by the processes mentioned earlier. Because of the random nature of the collisions and scattering, there will be a distribution of the thermalization distances resulting in a range of initial separation distances between the thermalized electrons and their parent positive ion. Once thermalized, the electrons are doomed either to geminate recombination with their concomitant partner or to diffusion outwards into the milieu to undergo reaction there. Those that escape are referred to as "free ions", those undergoing geminate combinations as "geminate ions". Since the coulombic energy of attraction, E_{att} , is given as follows,

$$E_{\text{att}} = q^2/Dr \quad (1.27)$$

where q is the electron charge, D is the dielectric constant of the medium and r is the separation distance, it follows that for a given initial separation distribution the free ion yield will increase with dielectric constant.

The distance y at which the thermal kinetic energy, kT , of the electron equals that of the coulombic attractive potential is given as follows:

$$y = q^2/DkT \quad (1.28)$$

The probability of escaping geminate recombination, $\phi(\text{esc})$, is given by equation (1.29)

$$\phi(\text{esc}) = e^{-E_{\text{att}}/kT} \quad (1.29)$$

which, when combined with (1.27) and (1.28), yields the celebrated Onsager relationship (1.30).

$$\phi(\text{esc}) = e^{-y/r} \quad (1.30)$$

If one were to make the crude approximations that (i) the distribution of separation distances and (ii) the initial ionization yield were the same for all media, then the yield of free ions should vary exponentially with the dielectric constant of the medium. The dependence of the

free ion yield on the static dielectric constant of the liquids is shown in Figure 7. The empirical curve appears to follow the exponential behavior predicted although there are some significant exceptions such as liquid ammonia.

Apart from the approximations stated earlier there are other factors which must be included when considering this electrostatic model. If electron solvation is to be attributed to the relaxation of the medium around the thermal electron, then the solvation time will have to be comparable to the macroscopic dielectric relaxation time of the medium. However if the solvation time is in the vicinity or smaller than the dielectric relaxation time, τ , of the liquid, then a time-averaged dielectric constant must be used. For nonpolar liquids, $D_{op} = D_s$, and the dielectric constant is time independent. In polar media the permanent molecular dipoles require a certain time to rotate and line up with the electric field of the electron so that D in equation (1.27) will be less than D_s . This is supported by the fact that recent studies on the pulse radiolysis of water indicate that the solvation time of the hydrated electron is shorter than its bulk dielectric relaxation time.¹⁴ Therefore, as suggested by Mozumder,³⁵ the dielectric constant should be treated as a time-dependent variable, given as follows,

$$D(t) = \frac{D_{op}}{1 - (1 - D_{op}/D_s)(1 - e^{-t/\phi})} \quad (1.31)$$

where $\phi = (D_{op}/D_s)\tau$ and t is the time after the start of the polarization of the medium by the electron. Unfortunately the time resolution of present optical detection equipment is limited to 20 picoseconds, by which

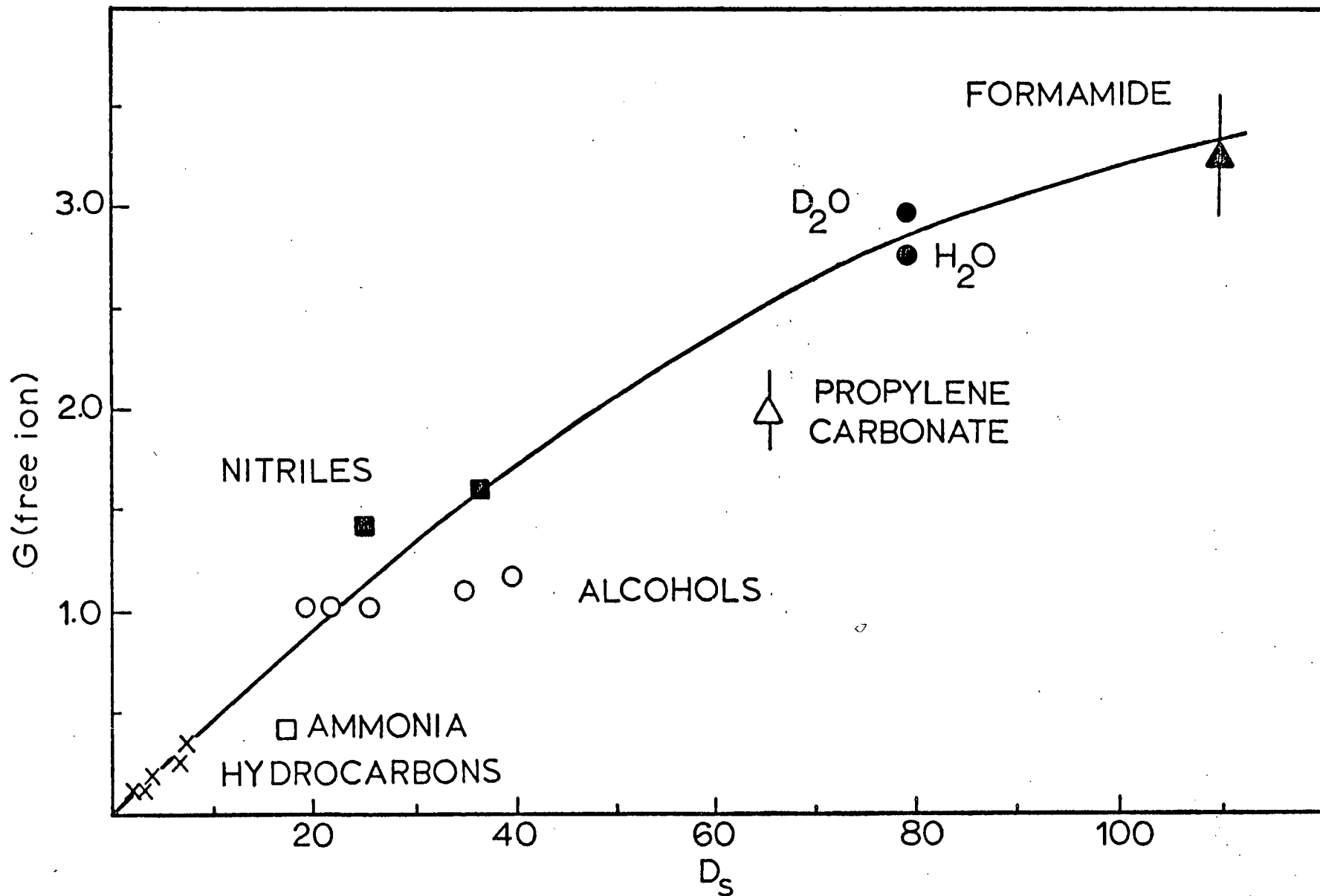


Figure 7. Plot of G (free ion) as a function of the static dielectric constant of the medium. Data taken from references 32, 33, 34, 46, 101.

time the electrons are already solvated, so that application of this relationship is not yet possible.

Another parameter which has not received the attention it deserves is the initial distribution of thermalization distances. The low energy electrons lose their excess energy mainly by electronically exciting the molecules they encounter. As their kinetic energy drops below the lowest excited level, further energy degradation proceeds by exciting intramolecular and intermolecular vibrations and molecular rotations. The distance travelled by the electron during this second part of its thermalization, the so-called subexcitation range, makes the greatest contribution to the total electron range. According to Lassettre and Silverman,³⁶ the Born approximation, upon which the Bethe stopping power formula given in equation (1.10) is based, is only good above about 120 eV so that theoretical thermalization distances cannot be calculated using this formula. Unfortunately no successful treatment has been proposed to account for thermalization distances for electrons having energies below 100 eV. It would appear that electrons have shorter thermalization paths in media in which the molecules have several internal degrees of freedom. However, the ionic mobility of the electron before, during and after the medium begins to relax will also contribute to the thermalization length.

Although the free ion yield is dependent on several variables, the static dielectric constant is the only parameter with which yields in various media have been compared. From the empirical relationship shown in Figure 7, it appears that this parameter does indeed play the dominant role in most media; but this relationship needs to be much more widely tested, particularly in media such as the aprotic polar solvents.

D. BINARY MIXTURES

The chemical yields of solvated electrons and their optical absorption spectra in binary solvent systems are of interest because they offer a test of the theoretical models described previously. If the continuum or semi-continuum models are applicable, then the electrons should be delocalized, thereby sampling the average environment of the mixture and thus the optical properties and yields should be determined by the macroscopic properties of the medium. On the other hand, if the electrons are strongly localized through short-range interactions, then the yields and optical characteristics should be governed by the solvation due to a small number of solvent molecules, perhaps 4 to 6. Thus an examination of electron yields, absorption band maxima and the width-at-half-height, ΔW , of the absorption bands as a function of binary solvent composition should provide a better insight into the nature of electron solvation. Perhaps for these reasons several investigations have been undertaken very recently on binary mixtures of widely different polarity.

Arai and Sauer³⁷ have studied binary mixtures of water and alcohols at various concentrations. In all the mixtures examined the electron absorption had only one peak and the absorption maxima and half-width were intermediate to those of the pure components. If the absorption spectra were a mere superposition of the bands arising from the individual components, a much broader band (enhanced ΔW) with well-defined shoulders at intermediate concentrations would be expected. Furthermore, in the case of the ethanol-water mixture, $G(e_s^-)$ increased linearly with the

dielectric constant of the mixture. These results were taken as suggesting that the solvation of the electron depends on the aggregate properties of the mixture, such as the macroscopic dielectric constant, in which it interacts with a large number of molecules. Similar conclusions were arrived at by Dorfman et al.³⁸ from their investigations on binary mixtures of water with ammonia and ethylenediamine. Whereas the λ_{\max} of the pure components in the water-alcohol binary mixtures are very close (see Table 1), so that any changes would be small, those of water (720 nm), ethylenediamine (1350 nm) and ammonia (1550 nm) are sufficiently widely separated so that any broadening effects would be readily observed.

Binary mixtures of protic polar media with nonpolar hydrocarbons or slightly polar ethers have also been studied but the results are different from the mixtures mentioned above. Kemp et al.³⁹ pulse irradiated binary mixtures of methanol in tetrahydrofuran (67 mole % methanol) and cyclohexane (4% methanol). In both mixtures the lifetime of the solvated electron was unchanged with respect to that in pure methanol. Although the absorption maximum was shifted slightly (~ 80 nm), the band was not broadened. The maximum absorbances, expressed as $G(e_s^-)\epsilon_{\max}$, were 13,900 (pure methanol), 14,000 (33% tetrahydrofuran, 67% methanol) and 3500 (96% cyclohexane-4% methanol) ions $(100 \text{ eV})^{-1} M^{-1} \text{ cm}^{-1}$. If one assumes that the extinction coefficients of e_s^- are not drastically changed in these mixtures from that in methanol, then the latter value suggests that aggregates of methanol molecules must exist in the mixture and that these aggregates are capable of trapping and solvating electrons formed in the hydrocarbon component. This conclusion arises because the yield of solvated electrons

was approximately six times greater than that expected simply from the mole fraction of methanol in the mixture. Once trapped in the methanol cluster, the electron decays by the same processes of electron decay in pure methanol, hence its lifetime is unchanged. A similar result was observed for solvated electrons in mixtures of 3-methylhexane in ethanol and methanol.⁴⁰ Analogous investigations in ethanol/n-hexane mixtures over a concentration range of 2-100 mole % ethanol have also been reported.⁴¹ No shift in the position of the absorption spectrum maximum of the solvated electron from that in ethanol was observed. This, together with the fact that the electron had a constant half-life, was interpreted to mean that the electron was trapped in basically the same type of potential well, regardless of the n-hexane concentration. The electron yields in the ethanol/n-hexane mixtures were observed to be greater than those free ion yields predicted (using Figure 7) for pure liquids which have dielectric constants equal to the bulk dielectric constants of the mixtures. However this comparison was criticized by Freeman⁴² on two points. Firstly, the bulk dielectric constant of the ethanol/n-hexane mixture is lower than the average microscopic dielectric constant. Secondly, some of the electrons and ions generated by the ionization of the hydrocarbon are probably scavenged by clusters of ethanol molecules resulting in an increase in the average dielectric constant in the vicinity of the geminate ion pairs, thereby decreasing the probability of geminate recombination.

Recently Dorfman et al.,⁴³ using fast infrared optical techniques, were able to investigate the optical properties of tetrahydrofuran-water mixtures over the complete range of compositions. They observed that

both the peak position and half-width, although intermediate between the two pure components, were dominated by the water despite the fact that the value of the macroscopic dielectric constant of the mixtures was dominated by tetrahydrofuran. A similar observation was observed for water-1,4 dioxane mixtures.⁴⁴ In the latter study there was a gradual shift of the electron band with increasing water content until at 34 mole % water the peak absorption corresponded to that of the hydrated electron. A possible explanation is that these slightly polar organic molecules are able to disrupt the water aggregates somewhat through weak dipole interactions thereby causing a variety of traps of different polarity to be formed at low water concentrations. At higher water concentrations, there is presumably a predominance of suitable "pure water" traps in which the electrons are more stable and therefore the optical spectrum is governed by the water aggregates.

When ethylenediamine was added to tetrahydrofuran in various concentrations, both the peak position and half-width showed an almost linear dependence upon composition analogous to the mixtures of protic polar media.⁴³ Magnusson et al.⁴⁰ investigated mixtures of 3-methyl hexane and diethylether and observed an almost linear dependence of the electron yield on the ether concentration. The spectrum showed no shift with concentration, being the same as that of the pure ether. However, the detection apparatus was too slow to observe the pure hydrocarbon spectrum so the question of whether or not there was a shift at low ether concentrations is uncertain. Because of the linearity of yield with ether concentration, the authors suggest that the electron stabilization is by an electron-ether molecule complex with the electron being bound by a charge-dipole interaction.

Recently a study on binary mixtures of a highly polar aprotic solvent, formamide ($D_s = 109$ at 20°C), with water was reported⁴⁵ in which only the hydrated electron band was observed, its position and shape being unaltered by changes in composition. Since no absorption band that could be attributed to the solvated electron in formamide was observed, it was suggested that the high free ion yield ($G(\text{free ion}) = 3.3$) reported earlier⁴⁶ was due to reactive radical anions produced by electron reaction with the solvent molecules. The diminished intensity of the absorption band of the hydrated electron in these mixtures was rationalized on the basis that water aggregates were competing with the formamide molecules for the thermalized electron. Kinetic data showed that the hydrated electron formed then decayed by reaction with the formamide milieu.

Thus, from the studies to date on binary mixtures, it appears that the macroscopic dielectric constant is not the major factor in determining the electron yields and solvation properties; but rather it is the binary solvent structure that controls these properties. Mixtures in which the pure components do not interact strongly, such as the protic polar solvents and nonpolar media, the electron yield and optical properties are determined by the ability of the polar aggregates to scavenge and stabilize the electrons. On the other hand, components which may interact strongly so that the medium becomes a homogeneous mixture, the electron yield and optical characteristics appear to depend upon the macroscopic properties.

It should be noted that the binary mixtures mentioned above were for studies on the liquid state. Binary mixtures of glassy alcohols⁴⁷

and water-alcohols⁴⁸ have been investigated. They showed similar characteristics to their liquid counterparts; that is, electron absorption maxima vary continuously with change in composition, shifting towards the shorter wavelengths with increasing concentration of the more polar component. Support for the formation of polar aggregates in nonpolar media comes from the observation that γ -irradiated glassy mixtures of n-propanol with 3-methylpentane⁴⁷ yield two absorption bands attributable to trapped electrons, one characteristic of each pure component. Similarly, γ -irradiated glassy mixtures of methyltetrahydrofuran and ethanol show two absorption peaks, one attributable to methyltetrahydrofuran and the other to ethanol.⁴⁹

E. SCOPE OF STUDY

The dielectric constant has been used extensively in attempts at explanations of various types of solvent effects. In the field of radiation chemistry both the yield of free ions and the stabilization of electrons are considered as being dominated by the dielectric constant. However this parameter is a macroscopic property of the medium and the electrostatic situation in the vicinity of any particular solvent molecule or "cluster" may be quite different from this average value. In general there is a direct correspondence between the solvation energy of stabilized electrons, as characterized by their optical absorption band maxima, and the static dielectric constant of the medium. Dorfman showed that for a homologous series of aliphatic

alcohols, the energy corresponding to the absorption maximum increases smoothly with an increase in dielectric constant.⁵⁰ A similar correlation was found by Ekstrom and Willard for a series of organic glasses at 77°K, ranging from 3-methylpentane ($D_s = 2.0$) to glycerol ($D_s = 42.5$).⁴⁷ However, neither water nor ammonia obey this empirical relationship (see Table I) suggesting that other factors may be involved. One such property is the "solvating power" of the medium. For the systems studied to date, those media with high dielectric constants are also protic solvents and hence readily solvate ionic species by hydrogen bonding. These solvents, such as water and the alcohols, are characterized by high dielectric constants, excellent ionic solvating ability, high free ion yields and absorption maxima in the visible region of the spectrum. On the other hand, aprotic nonpolar hydrocarbons and slightly polar ethers are characterized by low static dielectric constants, poor ionic solvating ability, low free ion yields and absorption maxima in the infrared region of the spectrum. As a result, studies on these media are not indicative of whether or not the medium's solvating power is a determining factor in electron stabilization. The dielectric constant influences the stability of an ion, but the influence is only important when the dielectric constant is small. In media of dielectric constant less than 10 or so the effect of the dielectric constant should be at least comparable to that of its specific solvating power. However, in media of dielectric constants greater than 30 or so the effect of the dielectric constant is of minor importance compared with the specific solvating action.^{51,52} For this reason DMSO seemed particularly suited to such a study. DMSO is a

polar aprotic solvent which is widely used in organic and inorganic chemistry because of its inability to solvate negative ions; indeed bases appear exceptionally strong in this medium. However DMSO has a fairly high static dielectric constant ($D_s = 48$ at 20°C) and large dipole moment (4.3 D).⁵¹ Therefore, if the static dielectric constant of the continuum is the important criterium in determining electron stability, then one would expect the solvation energy to be intermediate between that of the polar alcohols and water; that is, the electron absorption band maximum should be in the visible region of the spectrum. On the other hand, if the solvating power of the medium is the dominant factor, as given by its specific interactions, then the stabilized electron in DMSO should resemble the aprotic hydrocarbons. In addition, comparison of the free ion yield with the empirical correlation shown in Figure 7 should similarly indicate whether or not the static dielectric has a commanding influence on the yield in DMSO.

Mixtures of DMSO and water were also investigated in order to determine whether or not the free ion yield and optical properties of the stabilized electrons are dependent upon the bulk or local properties of the dielectric medium. DMSO and water are completely miscible in all proportions, consequently aggregate effects which hinder studies on other protic-aprotic mixtures should be absent in this system.

In addition, studies were made on trapped electrons and other species in the solid state at 77°K on γ -irradiated polycrystalline DMSO as well as polycrystalline and glassy solids of DMSO-water mixtures. Such studies were of interest in their own right but also for correlation with the liquid phase work.

TABLE I. Optical data for electrons stabilized in liquid media at room temperature.

Medium	λ_{\max} (nm)	$E_{\lambda_{\max}}$ (eV)	$G(e_s^-)$	f^a	ϵ_{\max} ($M^{-1}cm^{-1}$)	$\Delta W_{1/2}$ (eV)	D_s^b
water	720	1.72	2.7	0.65	18,500	0.92	78
glycerol	528	2.35	--	--	--	1.5	43
ethylene glycol	580	2.16	1.2	0.68	14,000	1.35	39
methanol	630	1.97	1.1	0.78	17,000	1.29	33
ethanol	700	1.77	1.0	0.87	15,000	1.55	25
n-propanol	740	1.67	1.0	0.59	13,000		21
isopropanol	820	1.51	1.0	0.67	14,000	1.22	19
n-butanol	680	1.82	--	--	--	1.47	18
ethylenediamine	1350	0.92	--	--	20,000	0.88	--
ammonia	1550	0.80	0.45	0.77	49,000	0.46	22 ^c
tetrahydrofuran	2100+50	0.59	--	--	14,000 ^d	--	7.4
dimethoxyethane	1900+150	0.65	--	--	--	--	7.2
diethylether	2050+150	0.60	0.19	--	7,500 ^d	--	4.3
diethylamine	1900+80	0.65	--	--	10,000	--	3.6
dioxane	>1100	<1.1	0.04,0.10	--	--	--	2.2

TABLE I (continued)

Medium	λ_{\max} (nm)	$E_{\lambda_{\max}}$ (eV)	$G(e_s^-)$	f^a	ϵ_{\max} ($M^{-1}cm^{-1}$)	$\Delta W_{1/2}$ (eV)	D_s^b
n-hexane	>1500	<0.80	0.10	--	>10,000	--	1.9
methylcyclohexane	>1500	<0.80	--	--	>10,000	--	2.0

Data taken from references 11e, 29, 37, 38, 43, 44, 102, 103

^a Oscillator strength of the solvated electron band.

^b Static dielectric constant at 20°C.

^c -33°C.

^d Uncertainty may be as much as 50%.

CHAPTER II

EXPERIMENTAL

A. ^{60}Co γ -RADIOLYSIS

1. Materials

DMSO (Matheson, Coleman and Bell, spectroscopic grade) was stirred in a closed vessel over calcium hydride for at least two days in a nitrogen dry box. It was then distilled under reduced pressure (~ 1 torr at $48-50^\circ\text{C}$). Only the middle 50% was collected and stored over a layer of Linde 4A molecular sieves and sealed in an atmosphere of pure nitrogen. Prior to use, a portion of it was redistilled and the samples immediately prepared. Analysis by gas chromatography showed that the water content was less than 0.001% by volume. The only other impurity detected was a trace ($\sim 0.005\%$ by volume) of dimethyl sulfide.

Triply distilled water was prepared by firstly refluxing an acidic dichromate solution made with singly distilled water. The distillate was γ -irradiated with a dose of ~ 0.5 Mrad to remove any trace impurities. It was then placed under continuous reflux distillation from alkaline permanganate until required.

Nitrous oxide, obtained from Matheson, was purified by "trap-to-trap" distillation in a high vacuum system to remove any traces of nitrogen

and oxygen. It was subsequently stored in a five litre flask on the vacuum line until required. The argon and helium used for degassing the liquid samples and as a carrier gas for the gas chromatographs were obtained from Canada Liquid Air.

All other chemicals used in this study were analytical grade or better and were not purified further.

All glassware used in the experiments was scrupulously cleaned by washing in permanganic acid followed by rinsing with distilled water and a solution of concentrated hydrogen peroxide and nitric acid to remove any residual MnO_2 on the glass surface. Finally the glassware was thoroughly rinsed with singly distilled and then triply distilled water before drying in the oven at $250^\circ C$. In the case of the irradiation sample cells, the excess grease from the stopcocks and stoppers was first removed with hexane and the cell was then rinsed with hexane and water before putting them in the acid bath. Generally, however, the sample cells were annealed in the glassblowers' oven prior to washing in the acid because some of the radiation products could not be removed using the above procedure.

2. Radiation Source

The radiation source was a 4000 curie ^{60}Co Atomic Energy of Canada Gammacell 220.

3. Dosimetry

In order to calculate G values it is necessary to know the absorbed radiation dose. The unit of absorbed dose is called the rad and is equal

to 100 ergs per gram or 6.24×10^{13} eV gm⁻¹. Often one refers to the absorbed dose rate of the source which is the absorbed dose per unit time.

Since the primary energy absorption by the Compton process depends only on the electron density of the medium, the energy absorbed by a sample can be determined from a standard simply by comparing the electron densities of the two samples as given by the relationship (2.1)

$$R_{\text{sample}} = R_{\text{std.}} \times \frac{(Z/A)_{\text{sample}}}{(Z/A)_{\text{std.}}} \quad (2.1)$$

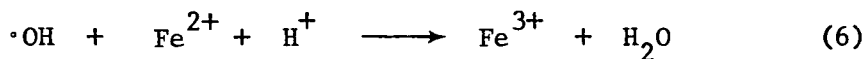
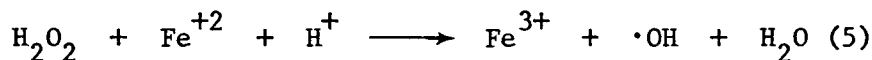
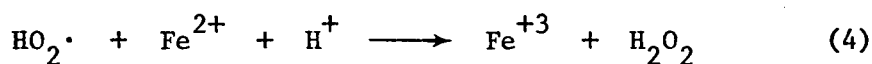
where R is the absorbed dose rate, Z the atomic number and A the gram atomic weight of the medium considered. The chemical standard, or dosimeter, most commonly used, and the one used in this study, is the Fricke dosimeter which measures the oxidation of ferrous ions to ferric ions.

The Fricke solution was prepared by dissolving 0.4 grams of $\text{Fe}(\text{NH}_4)_2(\text{SO}_4)_2 \cdot 6\text{H}_2\text{O}$, 0.060 grams NaCl and 22 ml concentrated (95-98%) H_2SO_4 in sufficient triply distilled water to make 1 litre of solution. The solution was then 0.001 M with respect to ferrous ammonium sulfate, 0.001 M with respect to sodium chloride and 0.4 M with respect to sulfuric acid. All the reagents used were analytical grade or better. Since the radiation field in the Gammacell 220 chamber is not uniform, irradiations of the Fricke solutions were done in the same cells and placed in the same position in the cavity as the DMSO samples.

When water is irradiated, the following process occurs:



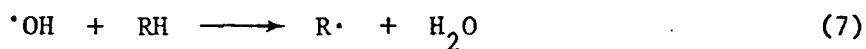
In the presence of 0.8 N acid, air (oxygen) and ferrous ions



so that $G(\text{Fe}^{3+}) = 3[G(e_{\text{aq}}^-) + G(\text{H}\cdot)] + G(\cdot\text{OH}) + 2G(\text{H}_2\text{O}_2)$ (2.2)

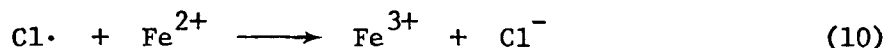
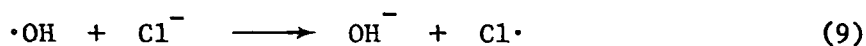
which equals 15.5. This value has been determined on an absolute basis by measuring by calorimetry the energy absorbed by the Fricke solution.⁵³

Any factor which alters the molecular or radical yield in water will alter the yield of Fe^{3+} as seen by equation (2.2). The Fricke dosimeter is very sensitive to organic impurities. Oxidation of the organic impurity by $\cdot\text{OH}$ radicals and subsequent reaction of the organic radical with oxygen via reactions (7) and (8) produces an organic peroxide, $\text{RO}_2\cdot$.



The organic peroxide then reacts with the ferrous ion in an analogous manner to $\text{HO}_2\cdot$, thus increasing the yield of the ferric ion.

As a result, $G(\text{Fe}^{3+}) > 15.5$ in the presence of some oxidizable organic impurities. To suppress reaction (7) the chloride ion was added to the dosimeter solution. In its presence, the hydroxyl radical is readily reduced and the chlorine atom then oxidizes the ferrous ion so that the overall yield of $G(\text{Fe}^{3+})$ is the same.



The concentration of ferric ions produced was measured spectrophotometrically on a Cary 14 spectrophotometer using an unirradiated Fricke sample as the blank and reading the absorbance at 304 nm. The linearity of the absorbance of Fe^{3+} versus the irradiation time is shown in Figure 8. The irradiation time is that of the automatic timer on the Gammacell. The positive intercept is due to the fact that the micro-switch which activates the automatic timer is engaged only when the Gammacell drawer reaches its fully lowered position. Consequently, the samples were exposed to the radiation field for a short period during the raising and lowering of the drawer which was not

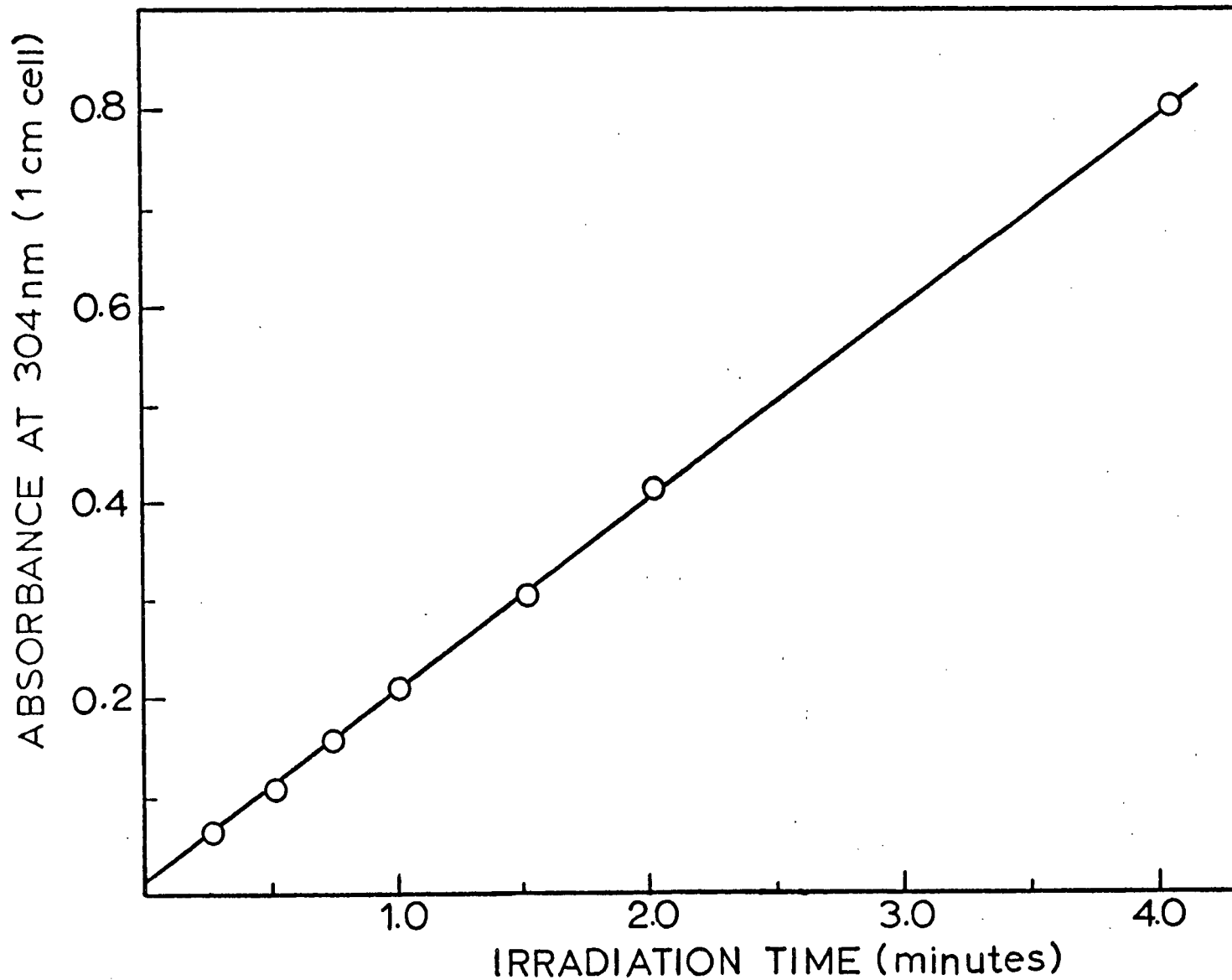


Figure 8. Fricke dosimeter results obtained from the radiolysis of the solutions in the irradiation cell used in this study.

accounted for by the timer. This small correction factor was taken into account in subsequent dose calculations and is equivalent to a 5 sec exposure with the timer operating.

From the slope of the graph, the absorbed dose rate, R , of the Fricke solution was calculated from the following relationship⁵³

$$R_{\text{Fricke}} = \frac{0.965 \times 10^9 \times (\Delta\text{O.D.}/\Delta t)}{\epsilon_{304} \times \ell \times \rho \times G(\text{Fe}^{3+})} \text{ rads min}^{-1} \quad (2.3)$$

where ϵ_{304} is the molar extinction coefficient of Fe^{3+} at 304 nm ($2174 \text{ M}^{-1} \text{ cm}^{-1}$), ℓ is the path length of the cell (1 cm), ρ is the density of the Fricke solution (1.024 ± 0.001 between 15 and 25°C) and $G(\text{Fe}^{3+}) = 15.5$. All irradiations on the dosimetry solutions and subsequent DMSO samples were conducted at $23 \pm 2^\circ\text{C}$. The dose rate corresponding to Figure 8 was found to be $5500 \text{ rads minute}^{-1}$. Since (Z/A) for the Fricke solution is 0.553 and (Z/A) for DMSO is 0.538, the dose rate for DMSO is 0.971 that of the Fricke solution for DMSO in the same cell and in the same position in the Gammacell chamber.

A further correction must be made for the radioactive decay of the ^{60}Co . The activity, A_t , after a period of decay, t , is related to the original activity A_0 by the expression⁵³

$$A_t = A_0 e^{-\lambda t} \quad (2.4)$$

where λ is the decay constant ($\lambda = 0.693/\tau_{1/2}$) and $\tau_{1/2}$ is the half-life of ^{60}Co , 5.27 years. As a result, the dose rate, R_t , at day t after the dosimetry was performed, R_0 , was obtained from relationship (2.5).

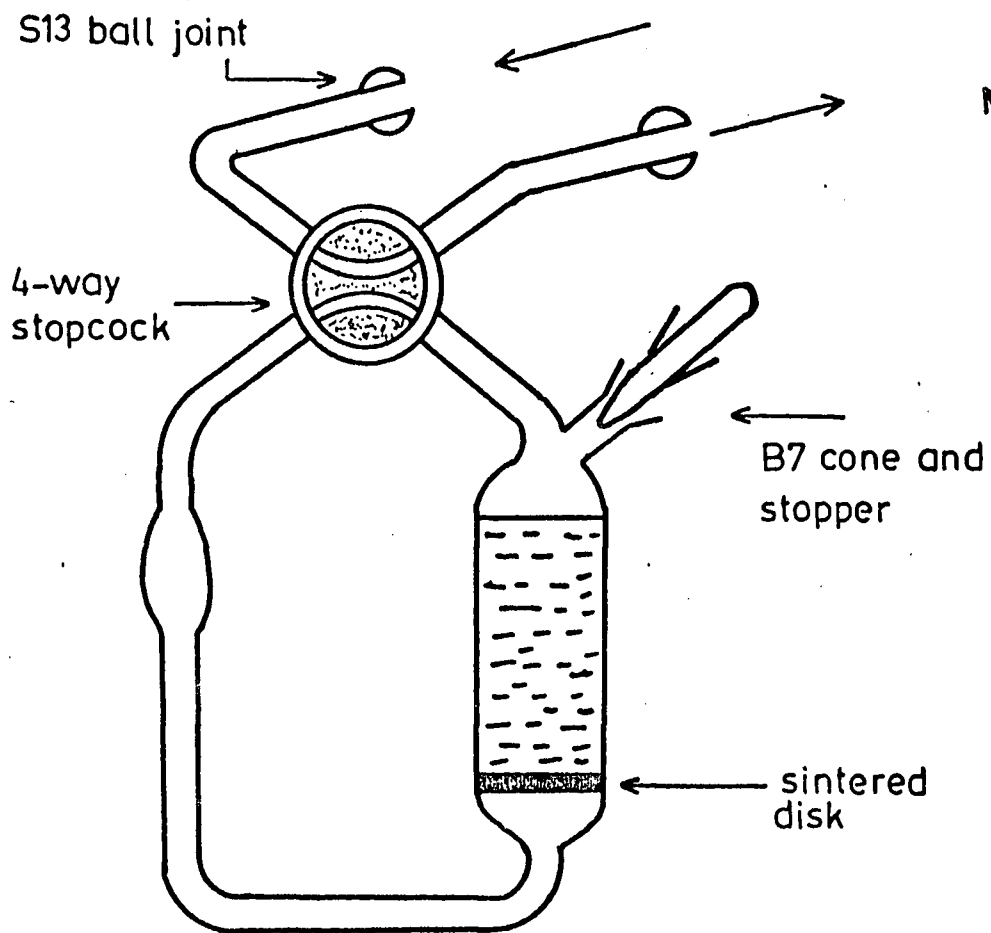
$$R_t = R_o e^{-(0.693 \times t/1925 \text{ days})} \quad (2.5)$$

A computer program was written⁵⁴ to give the dose rate and the absorbed dose for a given irradiation time for a particular liquid on any given day.

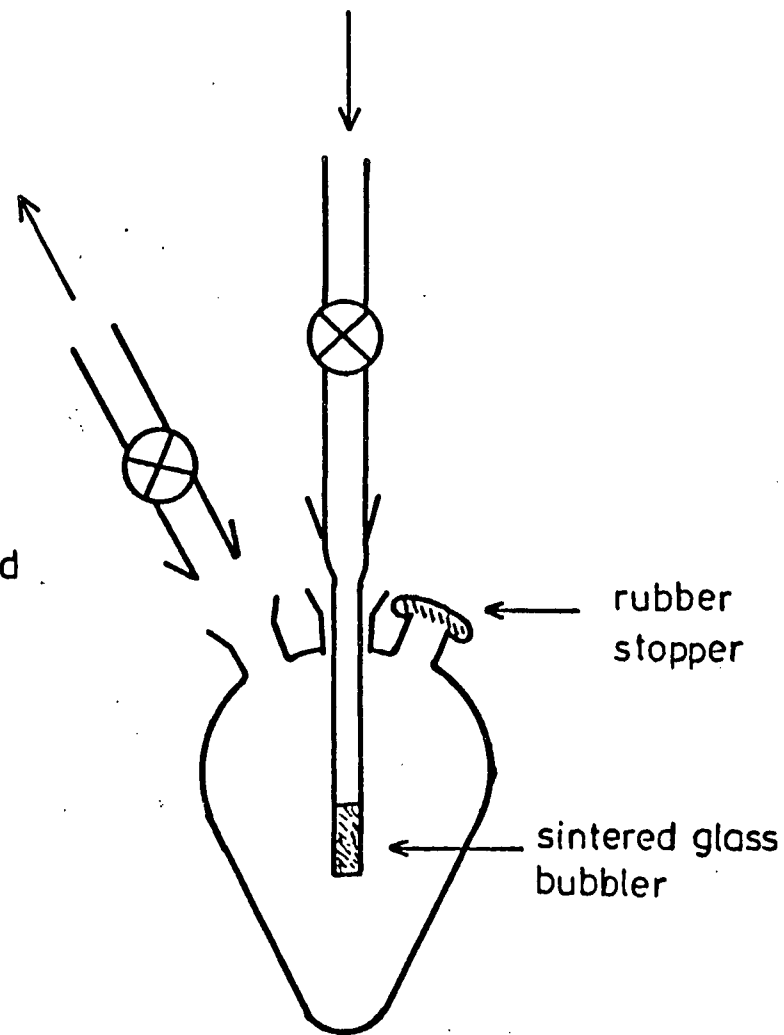
4. Sample Preparation

Two different types of pyrex glass sample cells were used, depending upon whether liquid or gaseous products were to be analyzed. Schematic diagrams of the sample cells are shown in Figure 9.

For gas analysis, the DMSO was distilled directly into the pre-weighed sample cell (Figure 9(a)) through the B7 socket using a modified Perkin triangle. After about 20-25 ml of DMSO had been collected, the cell was quickly removed and stoppered. The B7 cone and socket joint were greased sparingly with high vacuum Apiezon N grease and held together with two stainless steel springs. The four-way stopcock was similarly greased with Apiezon N and was held in place with an aluminum stopcock retainer. The stopcock retainer and springs were required because the cell was pressurized during the analysis procedure. The cell was then reweighed on a beam balance to the nearest 0.01 gram and the sample weight determined. This was necessary in order to calculate the total absorbed dose and hence G values. Following this weighing and greasing, the sample was deoxygenated by flushing with argon for 30 minutes after which the cell stopcock was turned about 45°, thereby sealing the cell under an argon atmosphere. The stopcock was only turned 45° so that the sample



(a) Irradiation cell for gas products



(b) Irradiation cell for liquid products

Figure 9. Pyrex irradiation cells used for deoxygenation of the liquid samples.

would remain above the fritted glass disk. If it was turned 90°, the sample tended to flow through the sintered disk and fill the opposite sidearm of the cell. Since the dosimetry had been done with the solution above the disk, the actual absorbed dose would be different. After deoxygenation, the sample was irradiated immediately or else attached to the vacuum line for degassing and addition of nitrous oxide prior to irradiation. DMSO samples containing solid and liquid scavengers were prepared by weighing a given quantity of the scavenger into a volumetric flask and immediately made up to the required volume with freshly distilled DMSO. The sample was then added to the pre-weighed cell through the B7 cone, after which the cell was greased, reweighed and degassed.

For nitrous oxide studies, the deoxygenated DMSO samples were attached to the vacuum line illustrated in Figure 10 and degassed. The S13 ball joints of the cell were greased and then connected to the two S13 sockets of the vacuum line. The ball and sockets were held together by metal clips in order to produce a hard vacuum. Each of the connections was isolated from the vacuum line by small stopcocks, S_1 and S_2 . A third stopcock, S_3 , further separated the cell and these external connections from the main vacuum manifold. With the four-way stopcock turned initially at 45°, the vacuum line up to cell bore was pumped to a hard vacuum, typically 10^{-6} torr, using a three-stage mercury diffusion pump backed by a rotary oil pump. Then, with stopcock S_2 closed and S_1 partially closed, the four-way stopcock of the cell was gradually rotated until the argon inside the cell started to bubble out through S_1 . It was necessary to turn the stopcock slowly because opening the sample to the vacuum line too quickly resulted in excessive

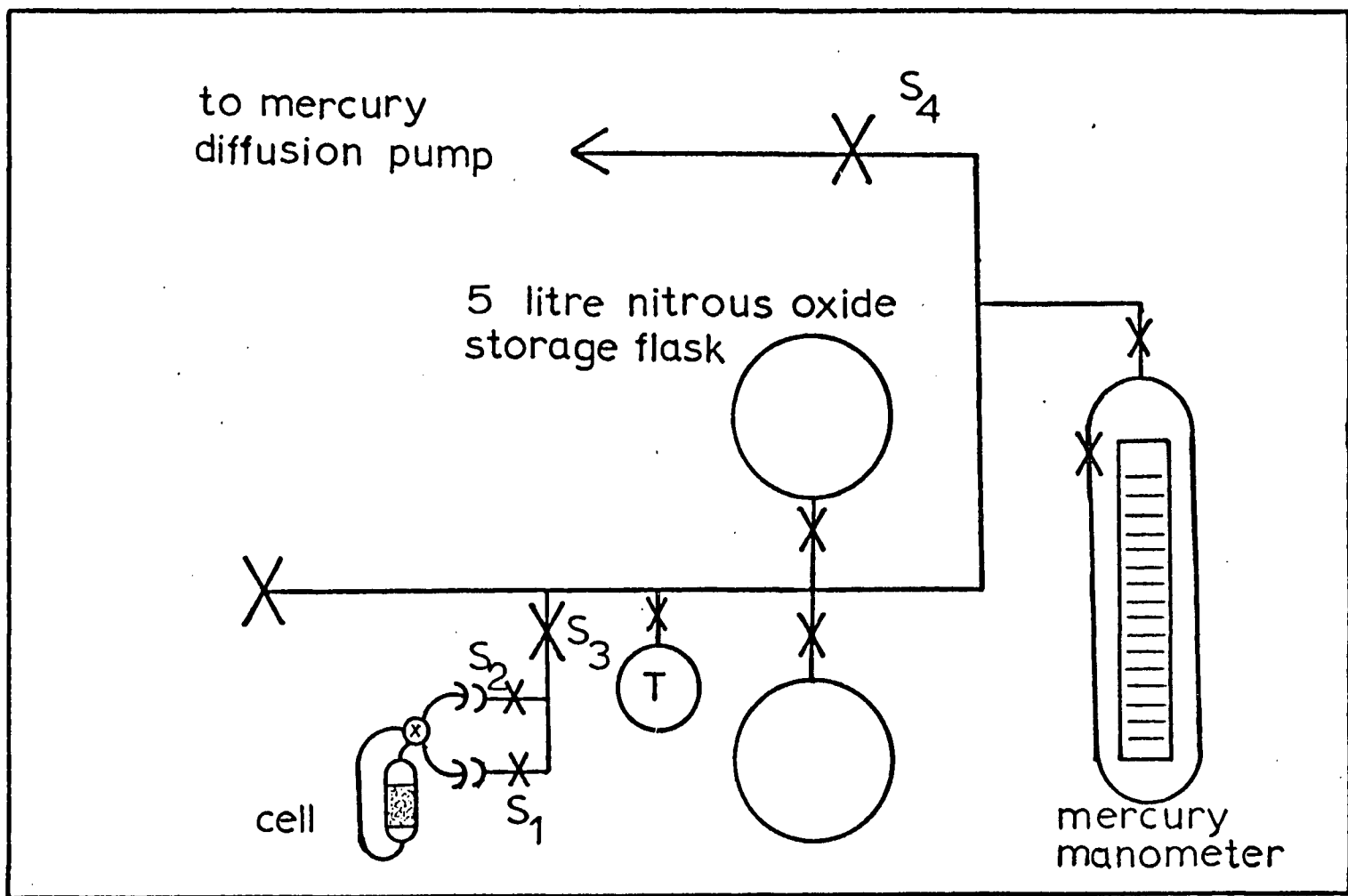


Figure 10. Schematic diagram of vacuum line used for degassing the liquid samples and adding nitrous oxide to the samples.

bubbling and loss of sample by splashing into the connectors. Once the bubbling had subsided, S_2 was slowly opened and traces of gas remaining on that side of the sintered disk were removed. After pumping down to a good vacuum, stopcocks S_1 , S_2 and S_4 were closed.

Nitrous oxide, which had been previously degassed and trapped out in bulb T using liquid nitrogen, was slowly vapourized into the evacuated line between stopcocks S_4 , S_1 and S_2 . From the initial nitrous oxide pressure, as read from the mercury manometer, and from the previously determined volume of the line between the stopcocks S_1 , S_2 and S_4 , the initial number of moles of nitrous oxide could be obtained from the ideal gas law, $n = PV/RT$. Then S_2 was slowly opened and the nitrous oxide allowed to bubble until equilibrium was established, usually about 30 minutes. S_1 was then opened, the four-way stopcock turned 45° and the final pressure read. Knowing the volume of the DMSO sample in the cell, the volume of the unfilled cell and the volume between the bore and stopcocks S_1 and S_2 , one could calculate the amount of nitrous oxide dissolved in the sample. The variation of nitrous oxide concentration with the equilibrium partial pressure is shown in Figure 11 for two similar cells. One cell (A) had a medium porosity sintered disk whereas the second cell (B) had a fine porosity disk. It can be seen that neither cell gives a "zero" intercept although both have the same slope. The "non-zero" intercept is believed to be an empirical artifact of the system, probably arising because of an "effective" back-pressure due to the presence of the sintered disk. From the inverse of the slope, the solubility factor for nitrous oxide in DMSO was found to be $1.10 \pm 0.05 \times 10^{-4} \text{ M torr}^{-1}$ at 23°C .

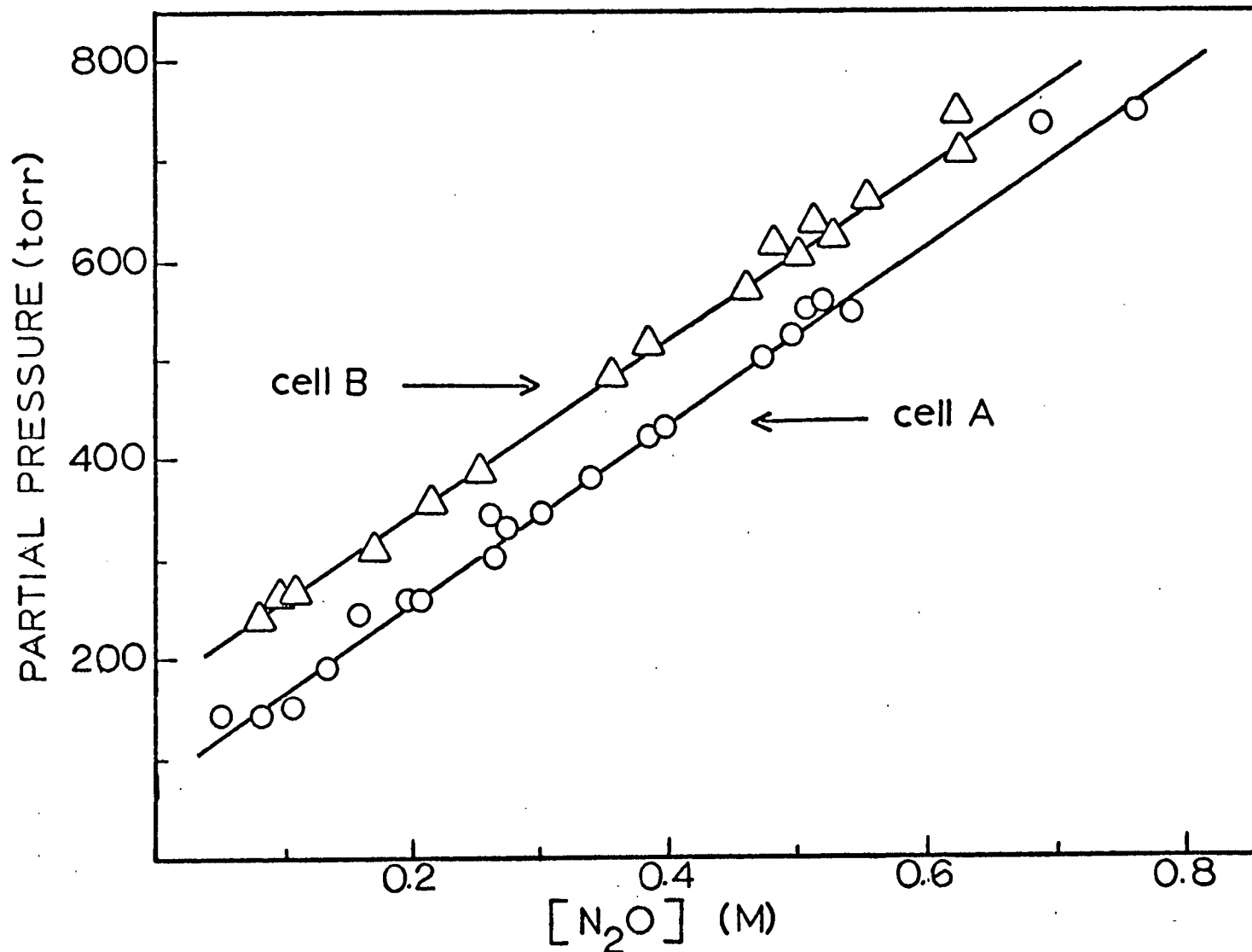


Figure 11. Plot showing the relationship of the partial pressure of nitrous oxide to its solubility in DMSO at 23°C for the two bubbler cells containing a medium (cell A) and fine (cell B) porosity sintered disk.

The sample cell used for liquid product analysis is shown in Figure 9(b). This cell consisted of a three-necked, 50 ml flask with B10 sockets. A sintered glass bubbler was attached to the centre neck by means of a B10 cone. The 25 ml sample was pipetted into the flask through a side arm which was then sealed with a rubber septum. The sample was deoxygenated by flushing with helium and then sealed under a small excess pressure of helium.

5. Product Analysis

Following irradiation the sample cell for gaseous analysis was attached to the external loop of the gas chromatograph via S13 sockets. A schematic diagram of the experimental setup is shown in Figure 12. Attached to the external loop were the sample cell, an 18 x 1/8 inch Porapak Q "pre-column" and an "on-line" sample loop. The Porapak Q "pre-column" was used to prevent DMSO vapours from entering the gas chromatograph system. After each experiment, the "pre-column" was back-flushed for about 30 minutes to remove the collected vapour. The "on-line" sample loop contained a four-way stopcock so that the loop could be bypassed.

Initially, the four-way stopcock of the sample cell was turned so that the exterior loop of the gas chromatograph and its attachments, including the outside bore of the sample cell, could be flushed of air. Once the air had eluted, the stopcock was rotated by 90° and the gases were flushed into the chromatograph. The chromatograph used was a Varian Aerograph Series 1700 containing dual 20 ft. x 1/4 inch stainless steel 13X molecular sieve columns. Detection was made using WX thermal conductivity detectors maintained at 125°C at a filament current of

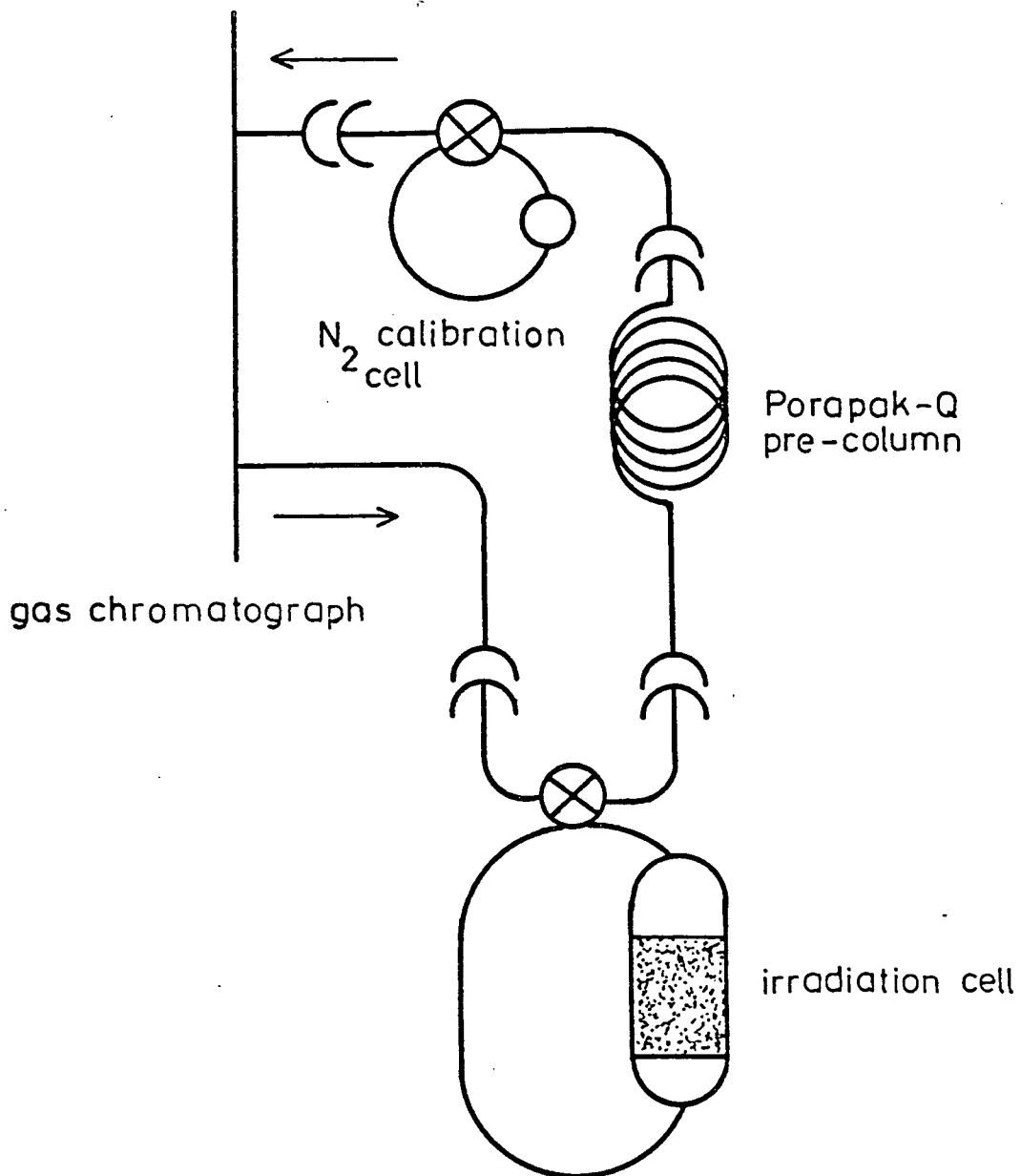


Figure 12. Schematic diagram of apparatus used for flushing the volatile gaseous products into the gas chromatograph.

100 ma and the signal registered on a Westronics, variable speed chart recorder. Using a column temperature of 55°C and an argon flow rate of 30 ml a minute, H₂, O₂, N₂ and CH₄ were eluted within 30 minutes after the start of flushing. Ethane took much longer, consequently it was measured by temperature programming. After the other gas products were detected the column was heated to 130°C at a rate of 20°C per minute. With a flow rate of 30 ml a minute, it was found that over 95% of these volatile gases were extracted in the first 3 minutes so that tailing of the peaks was very small. However, the bubbling was continued throughout the analysis (except for ethane) to avoid a pressure change and resulting base line drift on terminating the bubbling. At the start of the temperature programming the four-way stopcock of the sample cell was rotated by 45°, the exterior loop of the gas chromatograph bypassed, and the Porapak Q "pre-column" back-flushed. This allowed another sample to be prepared while C₂H₆ was being eluted (~ 45 minutes).

The "on-line" sample loop was used for monitoring the variation of the detector sensitivity from day to day. During the elution of the sample gases the sample loop was in the bypass position. After CH₄ had been detected the four-way stopcock of the sample loop was rotated by 90° and the standard gas sample, which was N₂, was flushed into the column. After the N₂ standard had been detected, the chromatograph was temperature programmed for ethane as previously described. The linearity of the detector response and sensitivity towards the various gases were established by injecting known quantities of sample gases using a second sample loop in place of the irradiation cell. This

secondary loop was filled with the required amount of gas on the vacuum line, its amount being measured using a McLeod gauge. The response of the detector was linear for all the gases over the range studied. Under the conditions used, the sensitivity or response factors ($\text{cm}^2/\mu\text{mole gas}$) for H_2 , N_2 , CH_4 and C_2H_6 were 59.5, 4.85, 15.2, and 12.7, respectively. The peak areas were measured by manual triangulation. A typical chromatogram is shown in Figure 13.

The liquid products were analyzed by firstly inserting the needle of a liquid syringe through the rubber septum of the sample cell to extract a known volume of irradiated liquid ($25 \mu\text{l}$) and then injecting this sample into a Varian Aerograph A-90-P2 gas chromatograph. This chromatograph used a Porapak Q column maintained at 215°C . Detection was made using WX thermal conductivity detectors at 215°C coupled to a Leeds and Northrup Speedomax chart recorder. The filament current was maintained at 170 ma and the helium carrier gas had a flow rate of 50 ml per minute. The sensitivity factors ($\text{cm}^2/\mu\text{mole}$) for water and dimethyl sulfide were 17 and 8 respectively. A representative chromatogram is shown in Figure 14. Products eluting at retention times greater than that for DMSO were not observed. No thermal decomposition of DMSO occurred despite the high column and detector temperatures used.

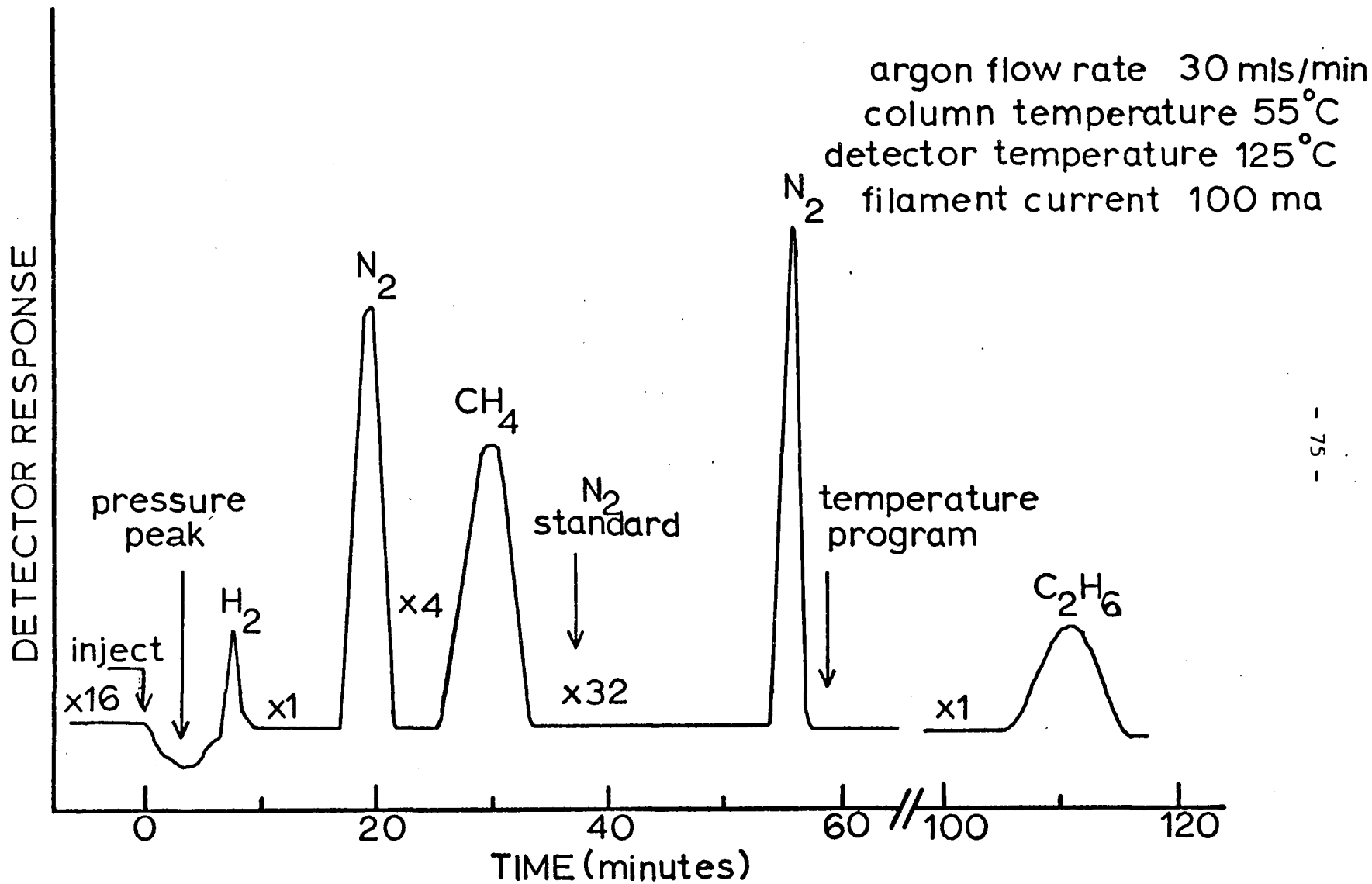


Figure 13. Typical chromatograph obtained for 20 ml DMSO sample containing 0.05 M nitrous oxide and receiving an absorbed dose of 8×10^4 rads.

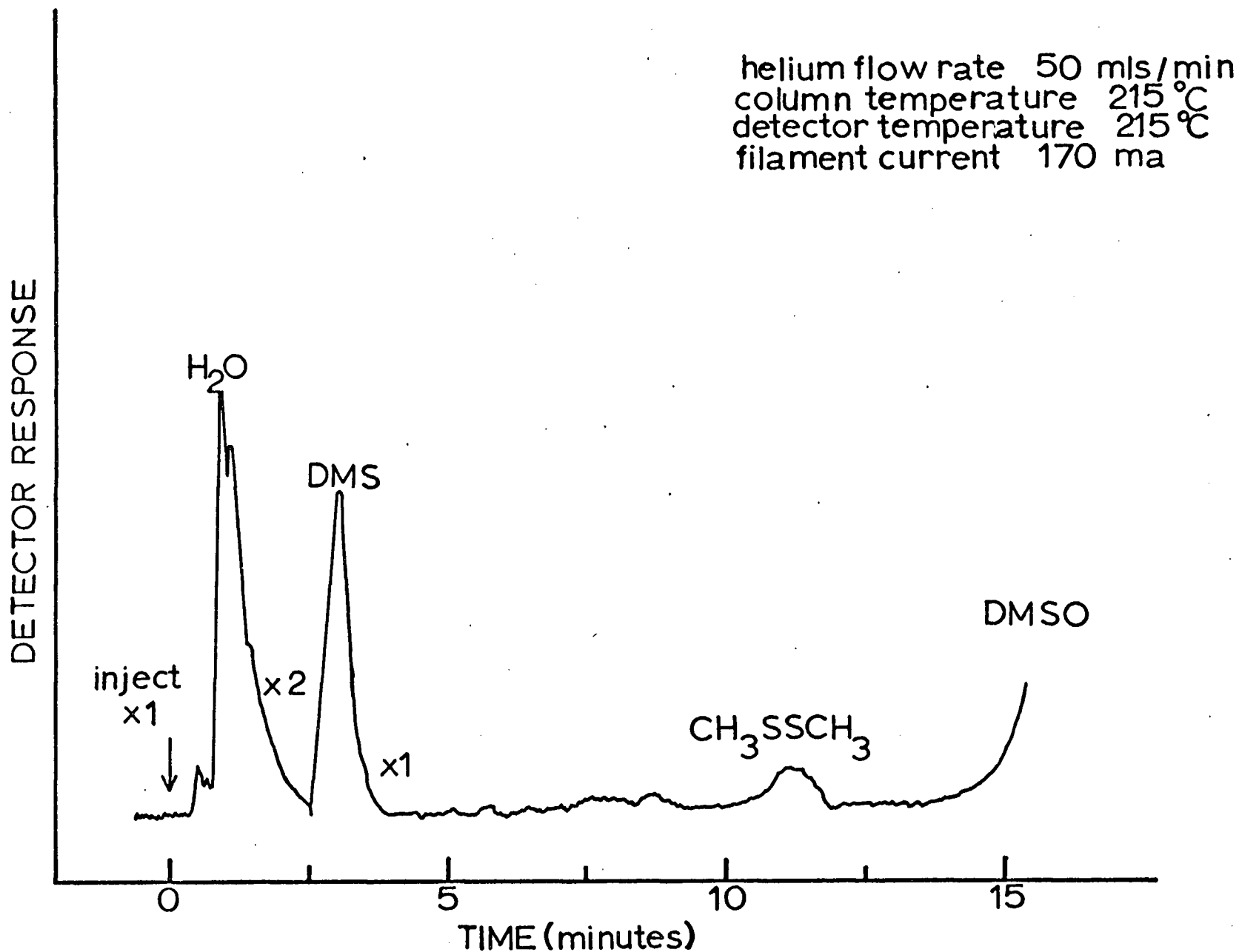


Figure 14. Typical chromatograph obtained after injection of 25 μ l of irradiated DMSO sample. Total absorbed dose was 6 Mrad.

B. PULSE RADIOLYSIS

1. Outline of the Technique

Pulse radiolysis studies of DMSO and DMSO-H₂O mixtures were performed during a series of field trips to the Physics Division of the National Research Council in Ottawa. As mentioned in the Introduction, pulse radiolysis enables one to detect and observe the formation and decay of the reactive intermediate species. The studies reported are all concerned with absorption spectroscopic measurements. These were done spectrophotometrically with a limit of ~ 10 nsec on the time resolution.

A schematic plan of the layout of the apparatus which was used is shown in Figure 15. The electron beam was partially absorbed in a small irradiation cell through which the light beam passed in a direction at right angles to the electron beam. The transmitted light was then directed, by means of a series of lenses and mirrors, out of the irradiation area through a small aperture in the concrete wall where it was split into two beams by a partially reflecting mirror. After splitting the beam, the resultant light beams were passed through suitable filters and focussed onto the entrance slits of the monochromators, the outputs of which were observed by photodiodes or photomultipliers coupled to a dual-beam oscilloscope. The oscilloscope traces corresponding to various oscilloscope sweep speeds and monochromator wavelengths were obtained for a permanent record by photographing the oscilloscope screen. In this way absorption spectra could be constructed and decay rates at selected wavelengths could be assessed.

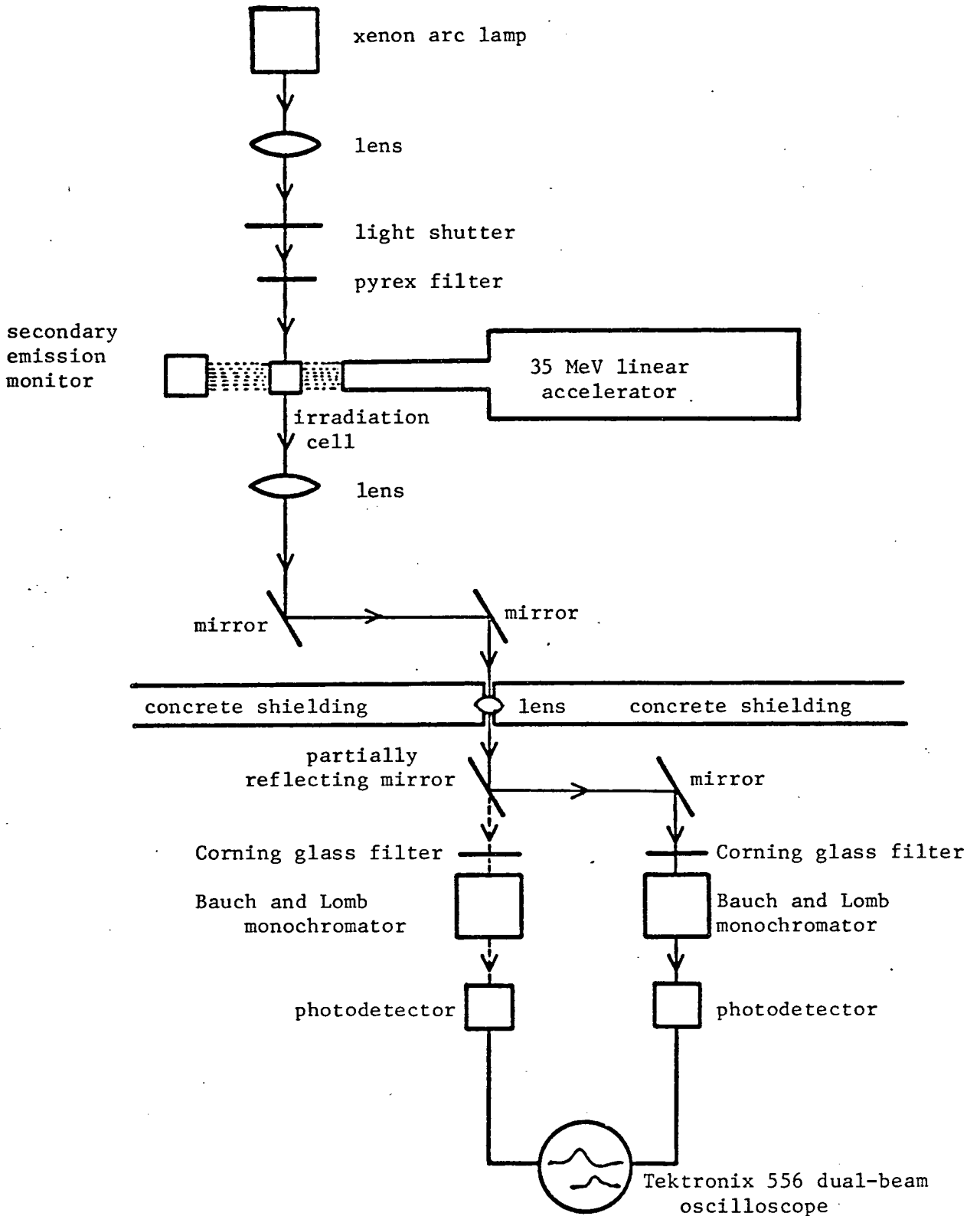


Figure 15. Lay-out of the pulse radiolysis equipment at the National Research Council radiation laboratory in Ottawa, Ontario

2. Radiation Source

The source of high-energy electrons was a 35 MeV electron microwave linear accelerator (linac) operated by the National Research Council in Ottawa. Electron pulse widths of 10 nsec and 40 nsec were used which deposited about 900 rads and 2200 rads per pulse respectively. Pulse-to-pulse variations were monitored with a secondary emission monitor (SEM) behind the irradiation cell as shown in Figure 15. The monitor consisted of a series of thin aluminum foils which collect the secondary electrons emitted by the impinging primary electrons. The total charge collected was measured by a charge integrator, the reading being proportional to the beam current or the number of high-energy electrons traversing the irradiation cell. The monitor was calibrated daily using an aqueous potassium thiocyanate dosimeter solution saturated with nitrous oxide. For a 10 nsec pulse, the peak beam current was ~ 1 Amp.

3. Irradiation Cell and Optical Detection System

The irradiation cell used is shown in Figure 16. The cell was placed in a rigid holder so that the light beam passed through the optically flat end windows. The windows were made of high purity silica so that they were resistant to radiation coloration. The optical path length was 1 cm. The white light source was a 900-watt xenon arc lamp. In order to prevent photochemical changes in the solution by continuous illumination from the high intensity lamp, a pyrex filter was placed between the cell and light source to cut out the ultraviolet light. Effects of this kind were further reduced by using

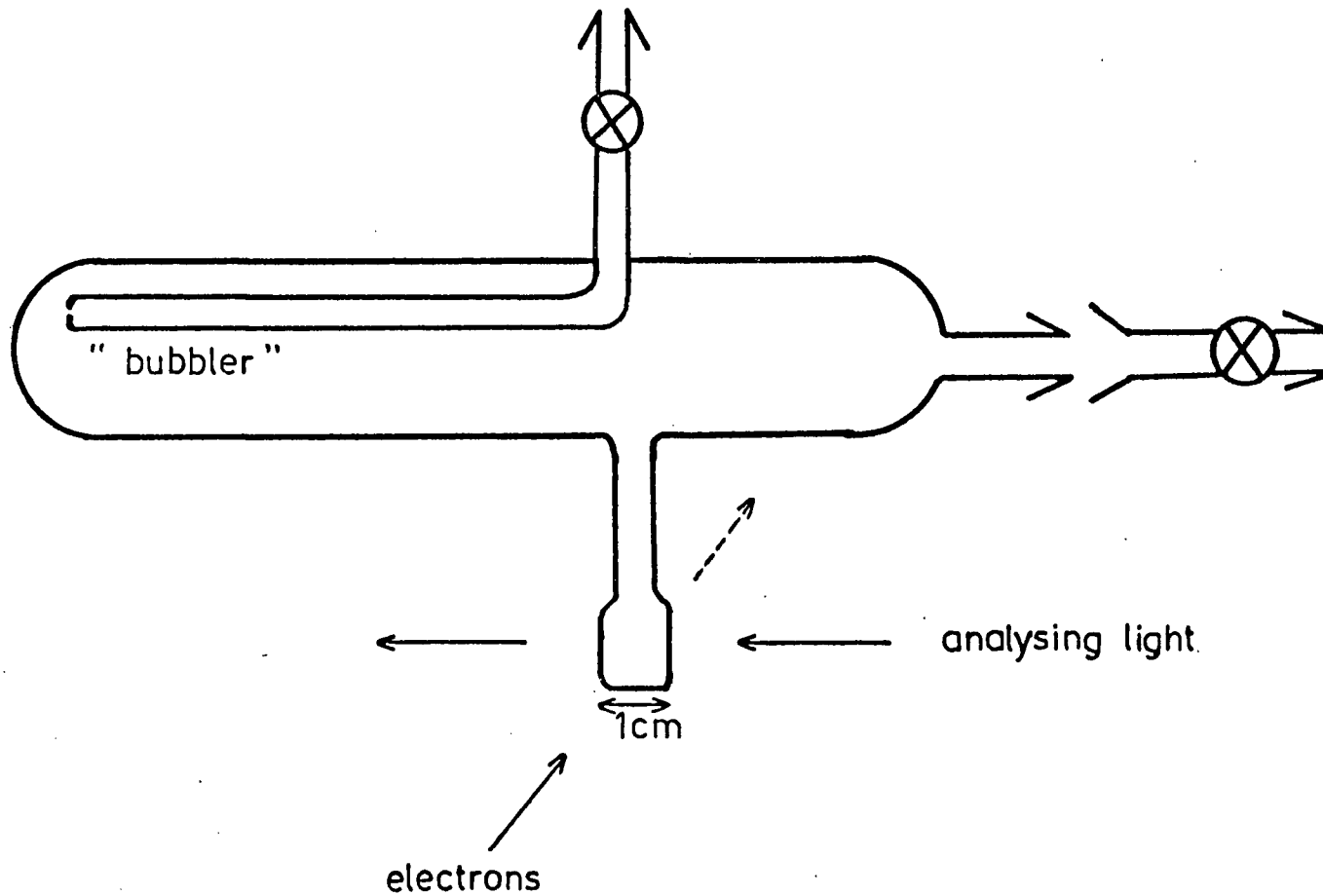


Figure 16. Schematic diagram of irradiation cell used for deoxygenation of liquid samples used in the pulse radiolysis study. The spectroscopic cell was filled by tipping the cell horizontally after flushing with high purity argon.

a remotely operated shutter between the lamp and irradiation cell which was kept closed until just before the electron pulse. Although the lamp was usually used in the continuous mode, a few experiments used the lamp under pulsed operation in which the current was increased briefly ($\sim 10^{-3}$ sec) to produce a higher light intensity.

The transmitted light beam was split using either partially aluminized mirrors or mirrors which transmitted only selected wavelengths, reflecting all others. The desired wavelengths were isolated using either narrow band pass interference filters or Bauch and Lomb grating monochromators. Appropriate Corning colour glass filters placed before the monochromator entrance slit were used to eliminate second- and higher-order diffracted light from the gratings. For the wavelength range below 450 nm a Phillips XP1003 photomultiplier was used. Above 450 nm two different photodiodes were used, a Si photodiode (HP 5082-4207) for the range 450-750 nm and a Ge photodiode (Philco-Ford L 4521) for the range 750-1500 nm. In most cases either a 93 ohm or a 50 ohm load resistor was used in the photodetector anode circuit. The voltage signals from the photomultiplier or photodiode were amplified and displayed on a dual-beam oscilloscope (Tektronix 556) and photographed using high speed film (Polaroid type 410). The horizontal sweep of the oscilloscope trace was normally triggered off the electron pulse although it was occasionally initiated by an electron pick-up placed close to the SEM chamber.

Because of the dual-beam oscilloscope and split beam arrangement, it was possible to follow concurrently the absorption and decay of two different transients. This was also useful when measuring their

absorption spectra. By splitting the light beam and using one beam as a variable wavelength and the other at a fixed (reference) wavelength, the spectra could be properly normalized to compensate directly for variations in the pulse to pulse amplitude or any slight wandering of the electron beam.

4. Oscilloscope Measurements

The photodetectors used produce an anode current which is proportional to the light intensity striking the photocathode. This current creates a voltage drop across the anode load and consequently the voltage measured by the oscilloscope is directly proportional to the light intensity. Changes in voltage are then proportional to changes in light intensity.

Figure 17 shows a hypothetical oscilloscope trace in which I_o is the 100% light transmission before the pulse, I_t the light transmitted at the end of the pulse (ΔI the light absorbed). The absorbance, D , of a solution is given by:

$$\begin{aligned} D &= \log_{10} I_o / I_t \\ &= -\log_{10} (1 - \Delta I / I_o) \end{aligned} \tag{2.6}$$

In the experiments reported the absorbances measured were generally very small such that $I_o \gg \Delta I$ so that $\Delta I / I_o$, the fraction absorption, was determined from the oscilloscope trace. This was normally achieved by using the differential comparator to offset the d.c. level so that I_o appeared on the lower part of the screen and ΔI filled the screen.

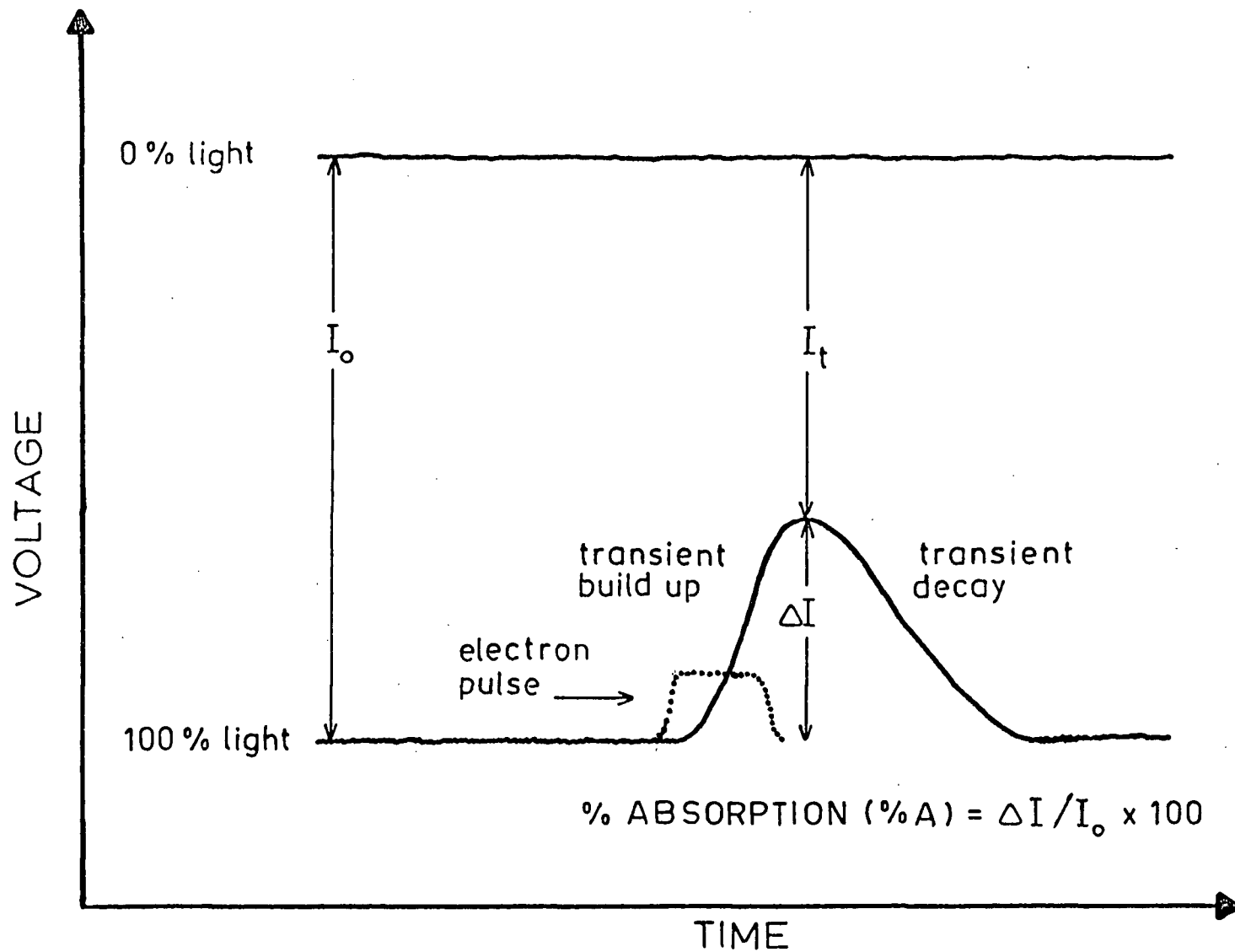


Figure 17. Hypothetical oscilloscope trace showing the build up and decay of transient absorbing species. The time profile of the electron pulse is shown as the dotted curve.

When $\Delta I/I_0$ is very small then it is simply proportional to D. In the oscilloscope traces shown, %A refers to the % absorption or $\Delta I/I_0 \times 100$.

5. Cerenkov Emission

As mentioned previously, Cerenkov radiation is emitted whenever high-energy electrons pass through matter with a velocity greater than the phase velocity of light in the medium. Although the emission interfered with the absorbance measurements, it was useful in determining the time response of the detection system. Since the emission coincides with the time profile of the electron pulse and assuming the electron pulse is square, then the risetime of the detection system may be observed from the oscilloscope trace. The risetime is defined as the time interval between the 10% and 90% amplitude points for a step voltage change. For the Tetronix 556 dual-beam oscilloscope the inherent risetime of the amplifier is 9 nsec, consequently the total risetime of the optical detection apparatus was greater than this.

The Cerenkov light used for measuring the speed of the detection systems was generated in a piece of Suprasil fused silica backed by a mirror. The mirror was rotated so that the emitted light was picked up by the optical system. Figure 18 shows typical oscilloscope traces obtained for the Ge and Si photodiodes. It can be seen that the response times were all < 20 nsec. However, because the pulse is not really square, the actual response times are undoubtedly shorter, probably about 15 nsec. Larger load resistors increased the signal-to-noise ratio but lengthened the response time of the detection system.

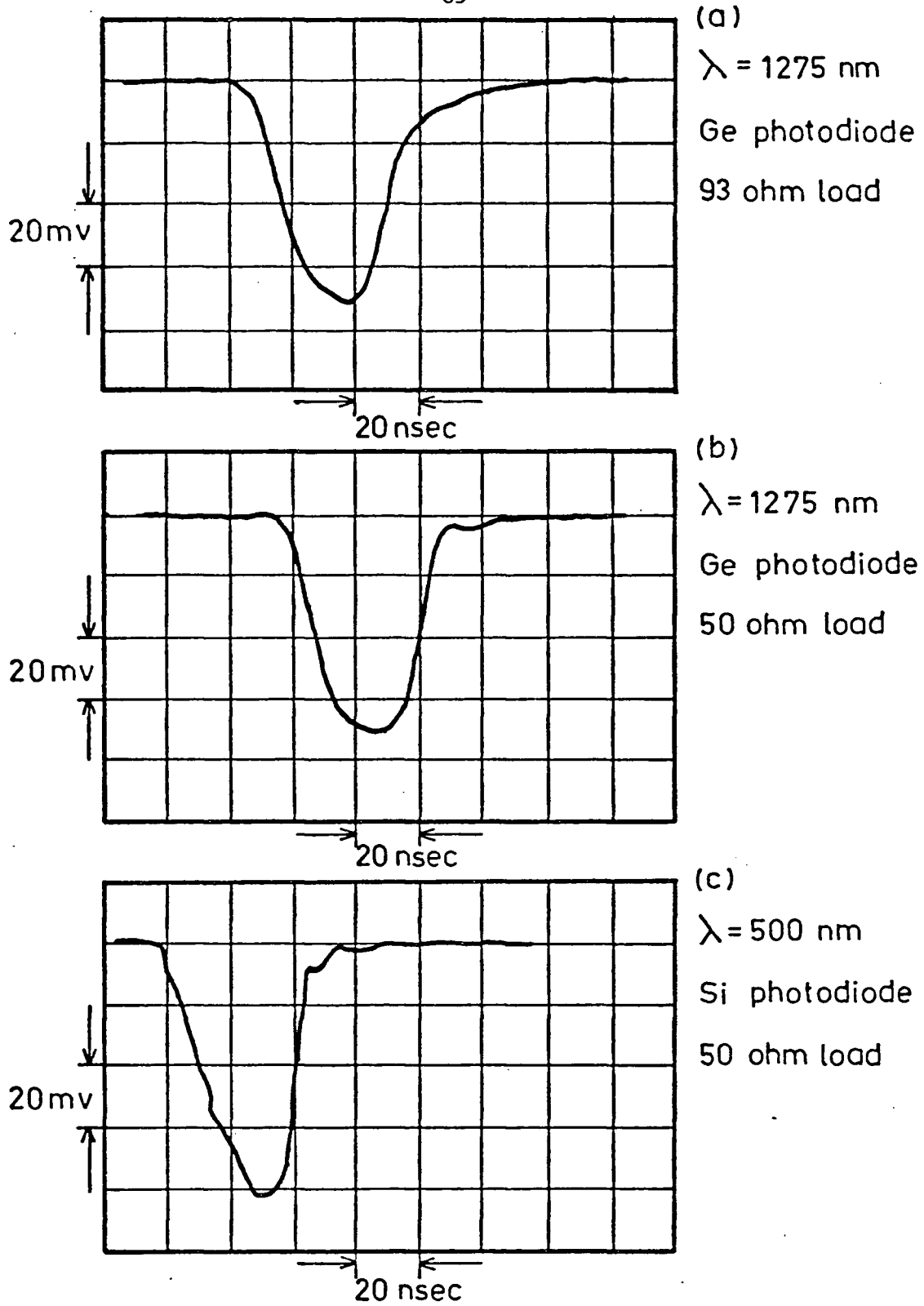


Figure 18. Typical oscilloscope traces showing the response time of the detection apparatus to Cerenkov light generated using a 40 nsec wide electron pulse.

This can be seen in Figures 18(a) and 18(b) for the Ge detector using a 93 ohm and 50 ohm load resistor in which the former load resistor displays a more pronounced tail. Generally the 50 ohm or 93 ohm load resistors were used in all experiments, especially when studying the short-lived transients, such as the solvated electron, but larger load resistors were sometimes used when studying longer-lived transients when a better signal-to-noise ratio was desired.

At wavelengths greater than 1500 nm it was shown that the risetime of the Ge photodiode system increases noticeably, taking several hundred nanoseconds to respond completely to the new light level.⁵⁵ This increase in response time was attributed to the longer time required for the electrons to diffuse to the reversed-biased p-junction. At wavelengths above 1500 nm the absorption coefficient of Ge decreases rapidly thereby causing the electrons to be formed deeper in the n-junction of the photodiode.⁵⁶

The effect of Cerenkov emission on the absorption at 500 nm of the transients produced in DMSO using a 40 nsec pulse is shown in Figure 19. The pure Cerenkov emission was obtained by irradiating the solution with the analyzing light source off (Fig. 19(a)). The actual absorption that would have been observed if there was no Cerenkov emission (Fig. 19(c)) was obtained by adding the emission (Fig. 19(a)) to the observed absorption (Fig. 19(b)). As shown, the effect of Cerenkov emission on the absorption maximum is quite small. However, when the 10 nsec pulses were used, the contribution was not negligible and had to be corrected for when calculating the end of pulse absorption.

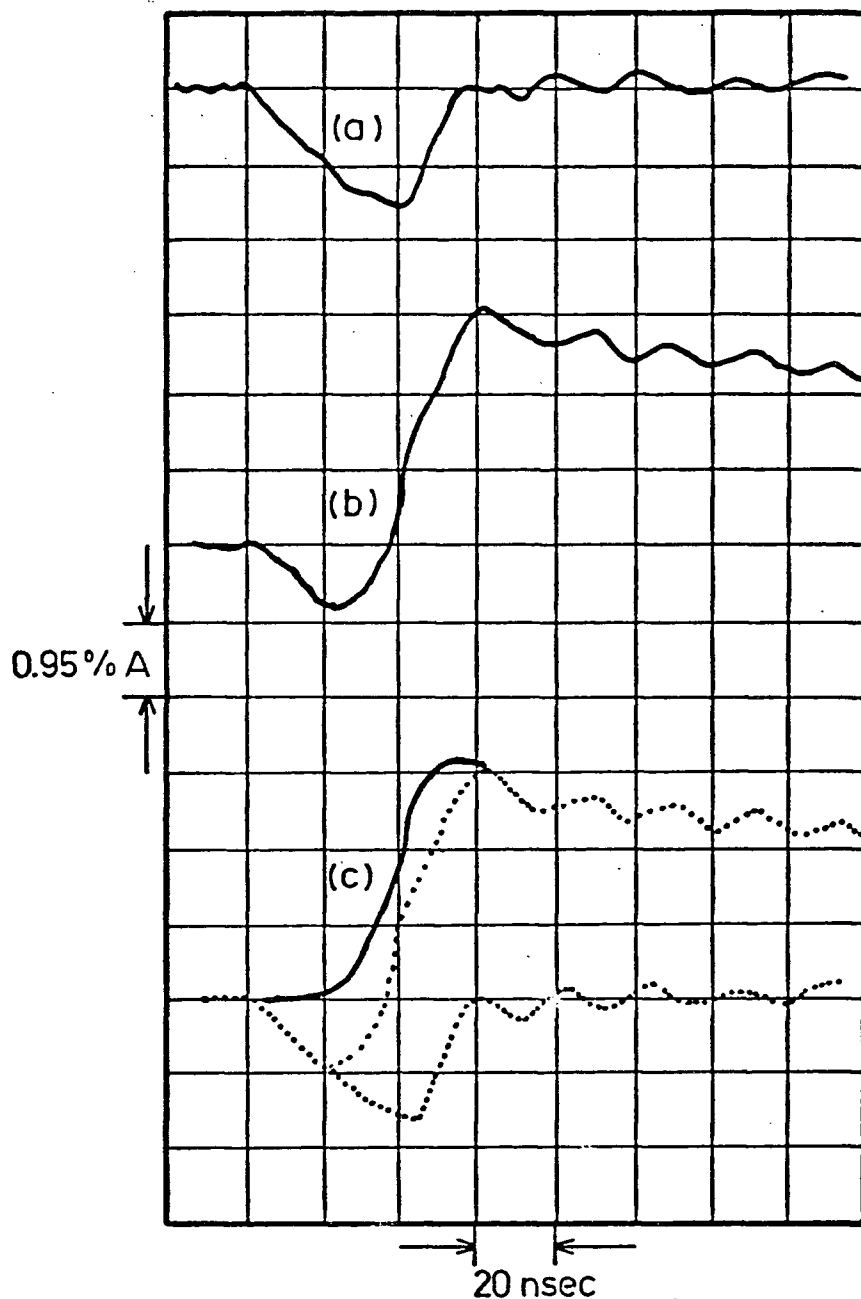
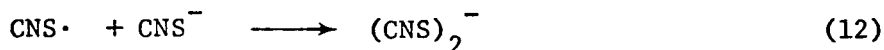


Figure 19. Effect of Cerenkov emission on the absorption of the transients absorbing at 500 nm in pure DMSO. (a) pure Cerenkov (analyzing light off); (b) observed absorption; (c) absorption that would have been observed had there been no Cerenkov emission. The detector was a Si photodiode with a 93 ohm load resistor. The pulse width was 40 nsec.

6. Dosimetry

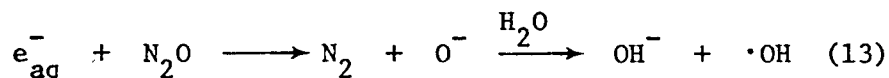
The dose per pulse absorbed by the samples was measured using an aqueous potassium thiocyanate chemical dosimeter.⁵⁷ As the absorbed dose depended very critically on the position of the cell on the optical bench, the dosimetry was carried out in the same cell in the same position with the same optical alignment as the other samples.

In the radiolysis of aqueous solutions of potassium thiocyanate the hydroxyl radical reacts rapidly with the thiocyanate ion to produce a transient absorbing radical species, $(\text{CNS})_2^-$, which has an absorption maximum at 480 nm. Reactions (11) and (12) indicate the postulated mechanism.⁵⁷



Because the molar extinction coefficient of $(\text{CNS})_2^-$ is large ($\epsilon_{500} = 7.1 \times 10^3 \text{ M}^{-1} \text{ cm}^{-1}$) and the absorption relatively long lived, it is particularly useful as a dosimeter solution. In neutral water, $G(\cdot\text{OH}) = 2.9$ so that for a concentration of CNS^- sufficient to suppress all reactions of $\cdot\text{OH}$ except (11), such as $5 \times 10^{-3} \text{ M}$, one will have $G(\cdot\text{OH}) = G((\text{CNS})_2^-) = 2.9$.

In N_2O saturated solutions one also has reaction (13)



so that the overall processes lead to relationship (2.7)

$$G((\text{CNS})_2^-) = G(\cdot\text{OH}) + G(e_{\text{aq}}^-) \quad (2.7)$$

$$= 5.7$$

where the yield of hydrated electrons scavenged is taken as 2.8.

Typical oscilloscope traces of the formation and decay of $(\text{CNS})_2^-$ at 500 nm in a nitrous oxide saturated solution of 5×10^{-3} M thiocyanate in water using 40 nsec pulses of 35 MeV electrons are shown in Figure 20. From the absorbance at the end of the pulse the dose (rads pulse⁻¹) absorbed by the dosimeter solution, for a given SEM reading, was obtained using equation 2.8 (compare to 2.3),

$$R_{(\text{CNS})_2^-} = \frac{0.965 \times 10^9 \times (\text{absorbance})_{500 \text{ nm}}}{(G\epsilon)_{500 \text{ nm}} \times \ell \times \rho} \text{ rads pulse}^{-1} \quad (2.8)$$

where ℓ is the cell path length (1 cm) and ρ the density of the dosimeter solution (1.0 gm cm^{-3}). The dose per pulse of any other system, for the same SEM reading, was obtained by multiplying by the corresponding electron density ratio. For other SEM readings it was assumed that the dose was proportional to SEM. For DMSO, the absorbed doses for 10 nsec and 40 nsec pulses were usually about 900 rads pulse⁻¹ and 2200 rads pulse⁻¹ respectively.

From equation (2.8) it can be seen that the absorbance of a given transient is related to the product of its G value and extinction coefficient; consequently once the absorbed dose of any sample is known, the absorbance can be expressed in terms of $G\epsilon$.

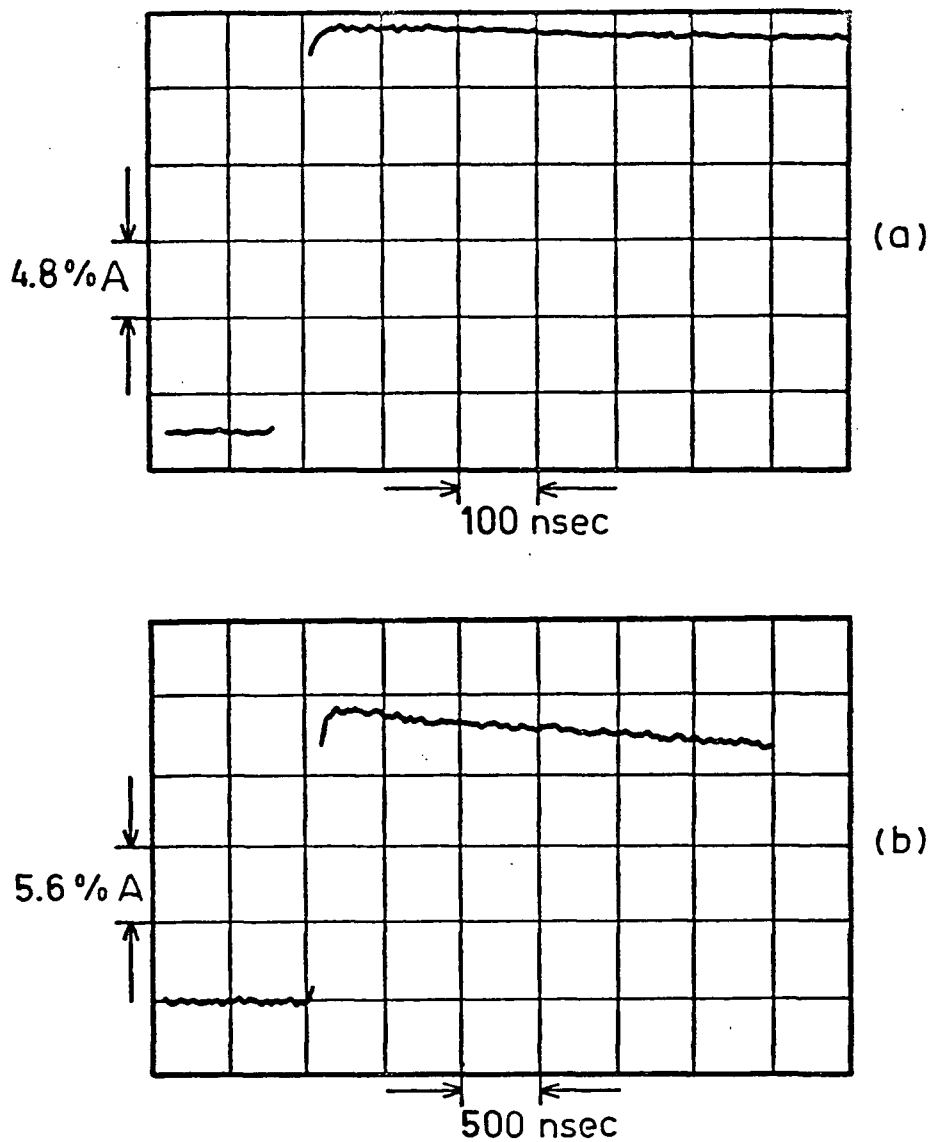


Figure 20. Typical oscilloscope traces for the formation and decay of $(\text{CNS})_2^-$ at 500 nm obtained by using a 40 nsec pulse of 35 MeV electrons on a nitrous oxide saturated solution of 5×10^{-3} M thiocyanate in water. (a) Si photodiode, 93 ohm load resistor; (b) photomultiplier, 470 ohm load resistor.

7. Materials and Purification

DMSO (Matheson, Coleman and Bell, spectroscopic grade) was used without further purification. Gas chromatography showed it to contain less than 0.01% by volume water and dimethyl sulfide. Previous pulse radiolysis studies on DMSO⁵⁸ showed that there was no difference in the optical properties or decay rates of the transients between those samples subjected to fractional distillation or fractional crystallization, followed by drying with molecular sieves and deaerated on a vacuum line and those used directly from the manufacturer (Fisher Scientific) and bubbled with high purity argon.

The deuterated DMSO (99.5%) was obtained from Matheson, Coleman and Bell and dried over Linde 4A molecular sieves. Analysis by gas chromatography showed it to have no detectable impurity.

The water was triply distilled by the methods described earlier. Potassium bromide, silver nitrate and concentrated sulfuric acid were all analytical grade or better. The blue-violet fluorescent anthracene was obtained from Eastman Organic Chemicals.

All glassware used was cleaned by the procedure described previously. After each series of experiments the irradiation cells were rinsed well with singly- followed by triply-distilled water and dried in the oven until required. At the end of the day, all the cells were placed in the annealing oven and left overnight.

The irradiation cells contained about 5 ml of sample which was added by pipette through the B10 cone shown in Figure 16. The samples were then deoxygenated by bubbling with high purity argon for at least 30 minutes after which the stopcocks were closed and the cell tipped horizontally to fill the sidearm carrying the spectroscopic cell.

C. ELECTRON SPIN RESONANCE

1. Materials and Purification

Matheson, Coleman and Bell, spectroscopic grade DMSO was purified by fractional distillation as described previously. The water was triply distilled by the method described earlier. All other chemicals used were analytical grade or better. The argon used for deoxygenation was obtained from Canada Liquid Air. All glassware used in the experiments was cleaned as outlined previously.

2. Radiation Source

The irradiation source used was the ^{60}Co Gammacell 220. The approximate dose rate was $4000 \text{ rads min}^{-1}$ as estimated by Fricke dosimetry in the other experimental apparatus. Total absorbed doses used in the ESR study ranged from 1.2×10^5 to 9.6×10^5 rads.

3. Sample Preparation

The samples for irradiation were prepared by dropping tiny spherical drops of the liquid from the capillary tip of a pipette into a dewar of liquid nitrogen. Within a few seconds the liquid drops froze into nearly spherical balls and dropped to the bottom of the dewar. Each ball was approximately 2-3 mm in diameter. Pure DMSO and DMSO_d_6 formed polycrystalline balls although several binary mixtures of DMSO and water of varying composition formed completely transparent glassy balls.

The solid balls were irradiated in a small pyrex dewar containing liquid nitrogen. After the irradiation the balls were transferred at liquid nitrogen temperature to a quartz dewar in the spectrometer cavity.

4. Electron Spin Resonance Spectra

All electron spin resonance spectra were taken using a Varian Associates E-3 spectrometer which operated at 9.1 GHz (X-band) and with a 100 kHz field modulation. The magnetic field strength and field scan linearity were calibrated with a proton-probe gaussmeter and the microwave frequency was checked with a Hewlett-Packard model 5255 A digital frequency counter. However, the microwave power levels were read directly from the power control dial of the spectrometer and were not calibrated.

The spectroscopic splitting factors, or g-values, were determined using a finely powdered sample of DPPH (diphenylpicrylhydrazyl) sealed in a thin quartz tube and placed in the quartz dewar along with the sample balls. Taking $g_{\text{DPPH}} = 2.0036$, the unknown g-values, g_x , were calculated using equation (2.9)

$$g_x = 2.0036 \left(1 - \frac{\Delta H}{H_x} \right) \quad (2.9)$$

where ΔH is the difference in magnetic field between the centre of the unknown resonance and that of the DPPH sample and H_x is the magnetic field of the unknown resonance. 59.

5. Photolysis Apparatus

An unfiltered low pressure mercury lamp (Hanovia #687A45) with a Vycor envelope was used for the ultraviolet photolysis experiments. Generally the photobleaching and photolysis experiments were carried out by removing the quartz dewar from the cavity and placing the lamp envelope directly against the portion of the dewar containing the sample balls. Surrounding the dewar and lamp with aluminum foil enhanced the photolysing light intensity. Changes in the esr spectra were followed by photolysing the sample in the cavity. The cavity grid cut down the light intensity so that the changes were not so rapid.

A 100 watt tungsten lamp was used in some photolysis experiments. These experiments were done outside the cavity but, because of the heat given off, the lamp was not placed too close to the quartz dewar.

CHAPTER III

STUDIES ON LIQUID DMSO

A. ^{60}Co γ -RADIOLYSIS

1. Gaseous Products

The gaseous products obtained under the γ -radiolysis of pure DMSO were hydrogen, methane and ethane. Hydrogen and ethane were formed with yields of $G(\text{H}_2) = 0.20 \pm 0.01$ and $G(\text{C}_2\text{H}_6) = 0.49 \pm 0.03$, which were independent of dose up to at least 1.2×10^6 rads as shown in Figure 21. Methane formation was not linear with dose and the data suggest that some non-volatile radiation product was being built up which scavenges the precursor of part of the methane. This can be seen in Figure 22 where the volatile gases were removed after each irradiation and the total accumulated yield is plotted as a function of dose. In the case of methane, three different series were carried out; one in which all the doses were the same, another in which each dose was different and a third in which a small dose was followed by a large dose and then followed by the same small dose. As can be seen in Figure 22 all the points fall on a smooth curve. From the inset of Figure 22 it is clear that the methane yield is only linear up to about 1.8×10^5 rads. Consequently, all scavenging studies with

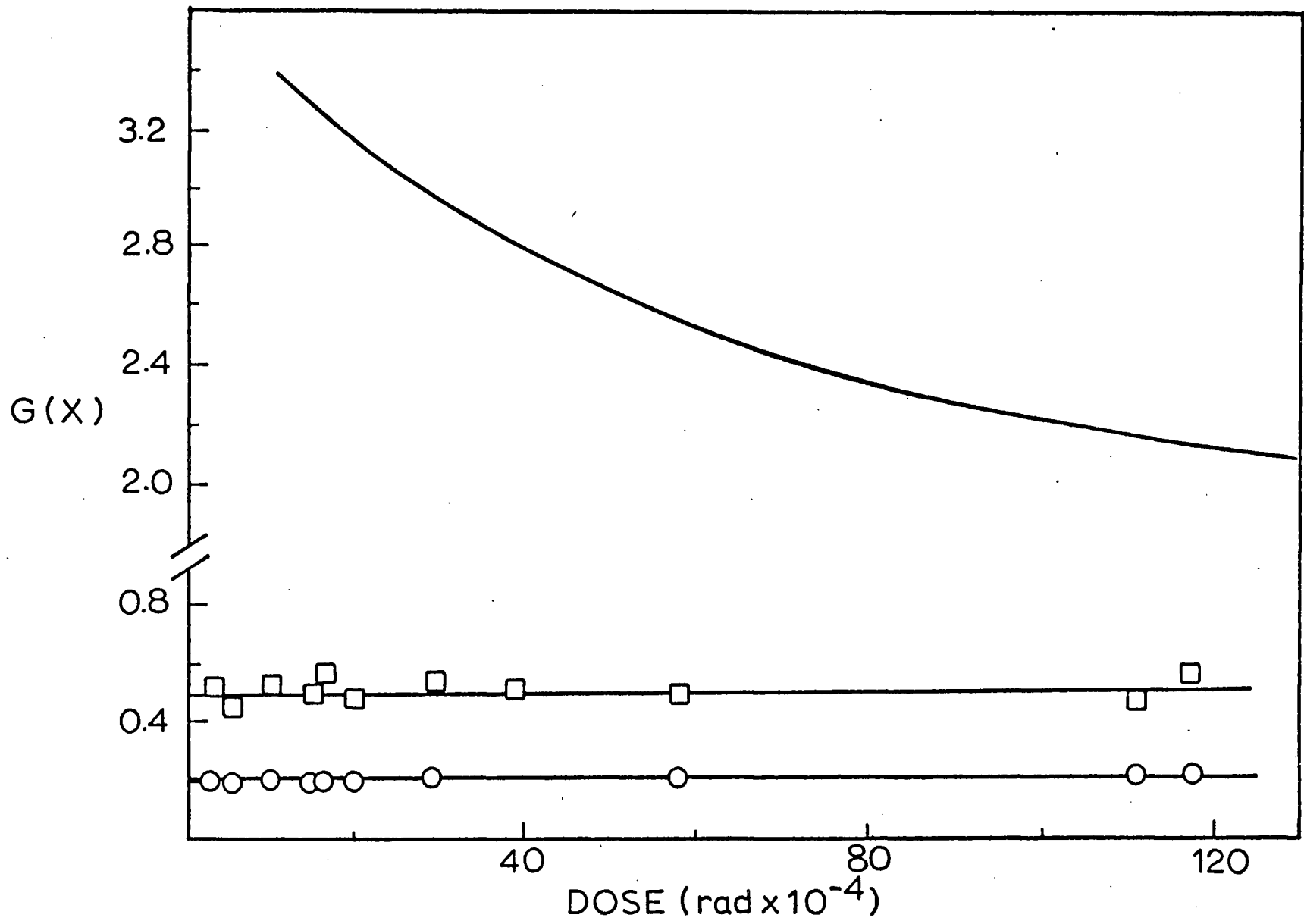


Figure 21. Radiation yields as a function of absorbed dose: \square , C_2H_6 and \circ , H_2 . The methane curve was obtained by taking the slope at various portions of the curve shown in Figure 22.

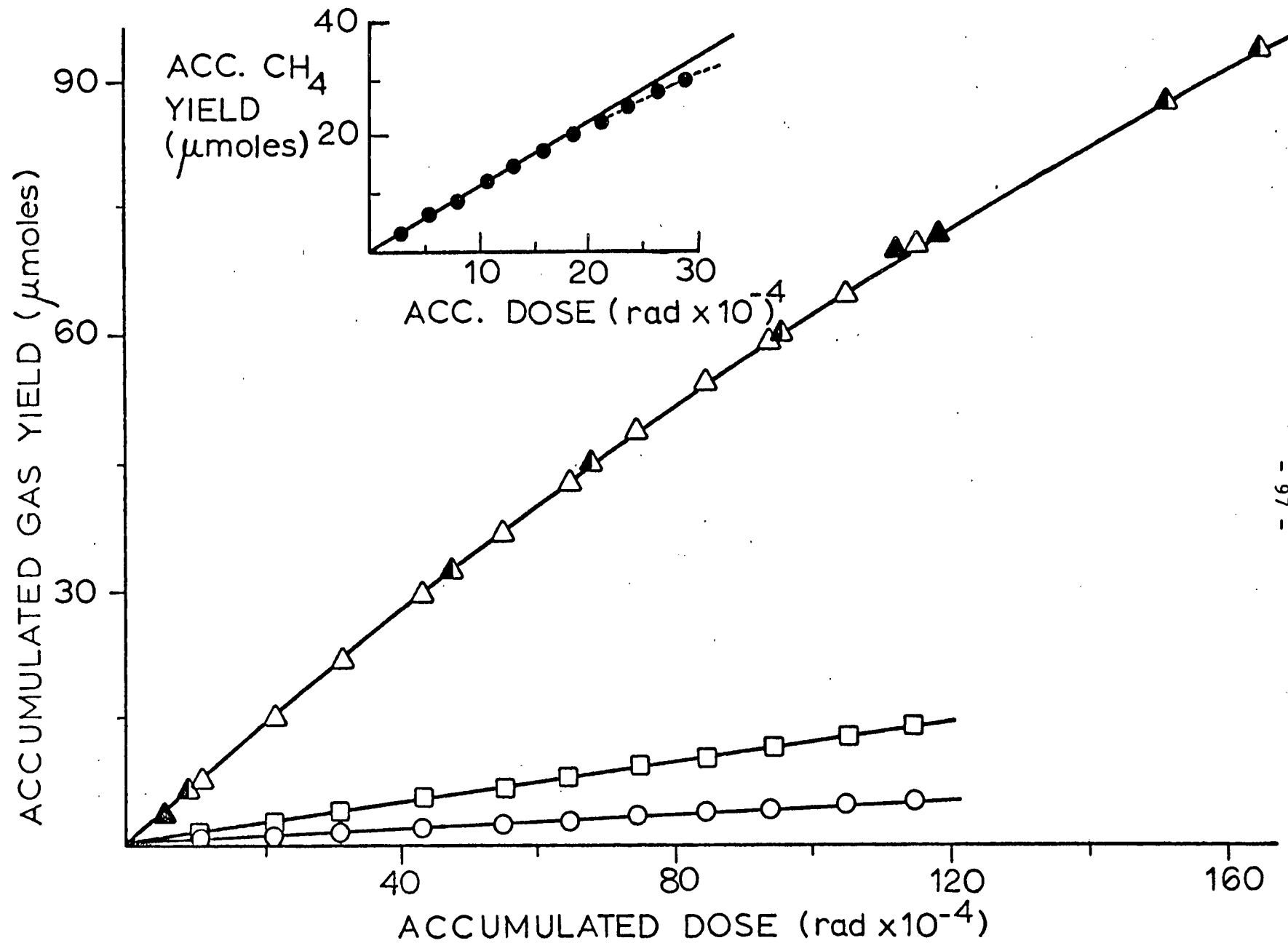


Figure 22. Accumulated gas yields as a function of accumulated dose: ●, △, ▲, ▲, CH₄ at various doses; □, C₂H₆; ○, H₂.

various added solutes were carried out with doses less than 1.8×10^5 rads so that the real effect of these scavengers on the methane yield could be observed. From the slope at various portions of the curve the change in $G(\text{CH}_4)$ with absorbed dose was obtained and this is shown in Figure 21. It can be seen that $G(\text{CH}_4)$ falls from 3.3 ± 0.1 to 2.1 ± 0.1 over the dose range studied (up to 1.3×10^6 rads).

The only other report on the radiolysis of DMSO in which the gaseous yields have been measured is by Koulkes-Pujo and Berthou⁶⁰ in which they report that the hydrogen and methane yields were both independent of dose. The yields, $G(\text{H}_2) = 0.19 \pm 0.006$ and $G(\text{CH}_4) = 3.4 \pm 0.3$, agree reasonably well with those observed in this study provided their total absorbed dose was less than 1.8×10^5 rads. Since the dose range was not stated, it is not possible to ascertain whether or not the dose independence of the methane yield is in conflict with the results obtained in this work. No mention was made of ethane being observed.

2. Liquid Products

The only liquid products identified in the γ -radiolysis of pure DMSO were dimethyl sulfide and dimethyl disulfide. Other studies on the radiolysis of DMSO have quoted dimethyl sulfide,^{60,61} methyl mercaptan⁶² and dimethyl sulfone⁶⁰ as liquid products but no yield measurements were given. Injection of methyl mercaptan as a standard showed that it did not belong to any of the unresolved peaks shown in Figure 14. In this study, only dimethyl sulfide was obtained as a measurable product; dimethyl disulfide was observed only in trace quantities. As shown in Figure 23, the yield of $(\text{CH}_3)_2\text{S}$ was dependent on dose as

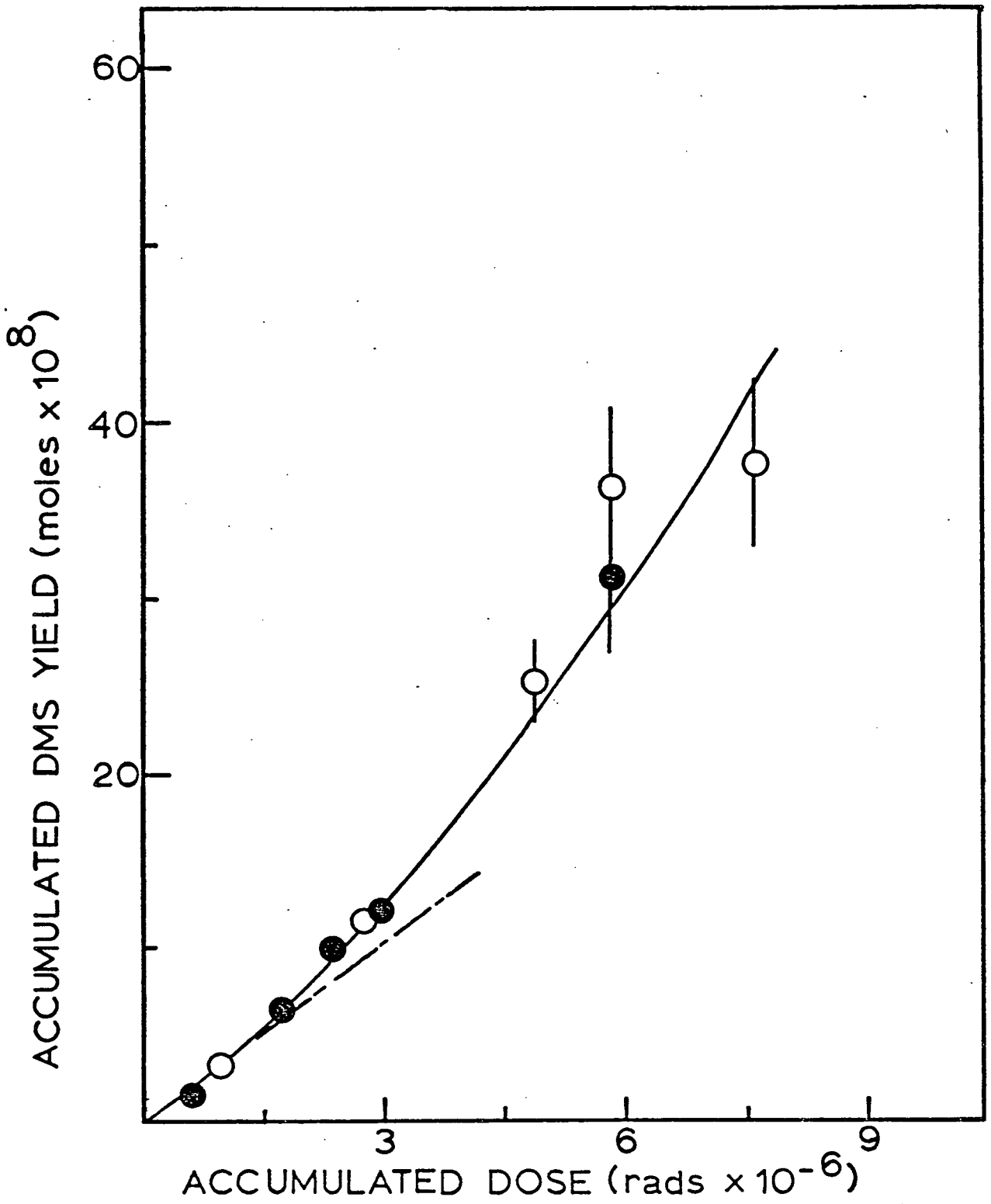


Figure 23. Accumulated dimethyl sulfide yield as a function of accumulated dose. The extrapolated portion of the curve corresponds to $G(\text{DMS}) = 1.2 \pm 0.2$.

it increased with accumulated dose. A possible explanation is that some product is being built up which yields dimethyl sulfide upon radiolysis. The extrapolated yield of dimethyl sulfide was found to be $G(\text{DMS}) = 1.2 \pm 0.2$.

3. Scavenger Studies

The gaseous and liquid products observed are the chemical consequence of the interaction of high-energy radiation with DMSO. In order to test the nature of their precursors, and in particular the primary reducing species, various electron and radical scavengers were added and the effect of these scavengers on the chemical yields observed.

Probably the most widely used scavenger for solvated electrons in liquids is nitrous oxide which yields molecular nitrogen upon reduction. The effect on the gas yields due to the addition of various concentrations of nitrous oxide to DMSO is shown in Figure 24. The methane yield was found to decrease by about 20% (from 3.3 to 2.6) while hydrogen and ethane were unaffected. As the nitrous oxide concentration was increased up to 0.09 M, $G(\text{N}_2)$ steadily increased with no simple plateau as shown in Figure 25. At $[\text{N}_2\text{O}] = 0.054 \text{ M}$, the nitrogen yield was independent of dose up to at least 7.5×10^5 rads (Figure 26) suggesting that whatever the non-volatile product is which inhibits the methane yield, it does not affect the nitrogen yield. From the slope of the line in Figure 26, $G(\text{N}_2) = 1.6 \pm 0.1$ at this concentration.

These results suggest that part of the methane yield arises from

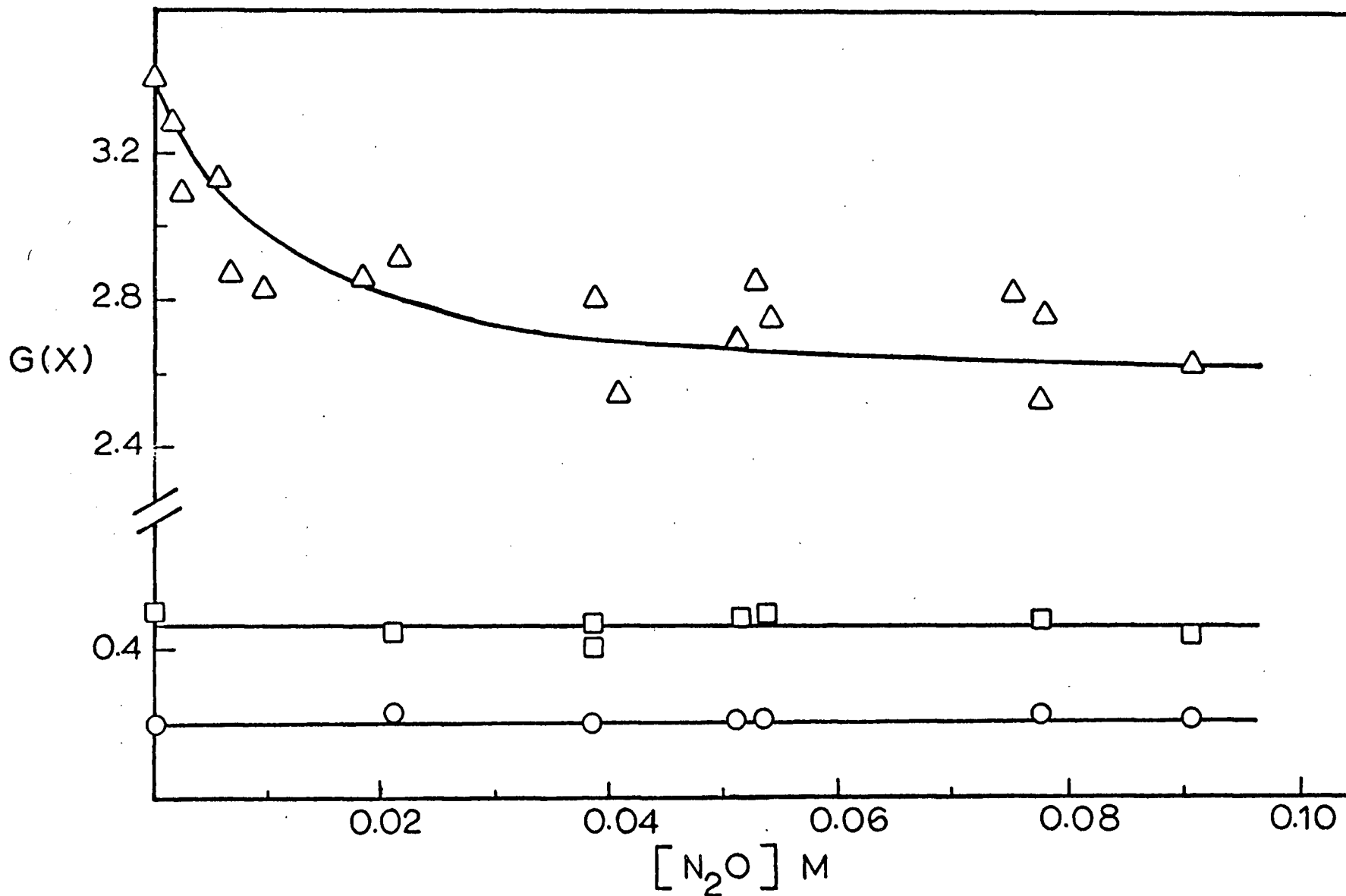


Figure 24. Radiation yields of CH₄ (Δ), C₂H₆ (□) and H₂ (○) as a function of the N₂O concentration. In the case of CH₄, all doses were < 1.8 x 10⁵ rads.

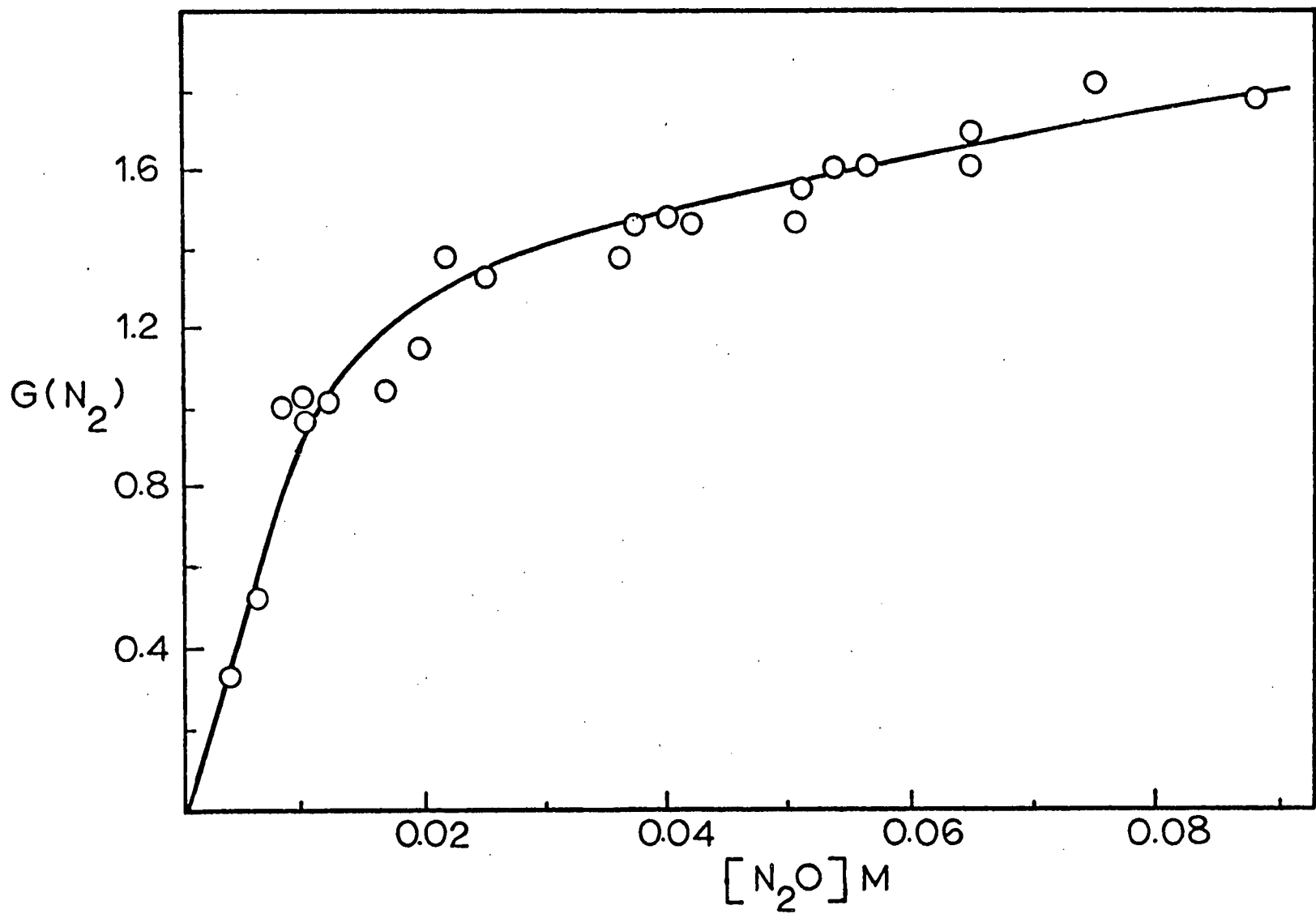


Figure 25. Radiation yield of nitrogen as a function of N_2O concentration in DMSO.

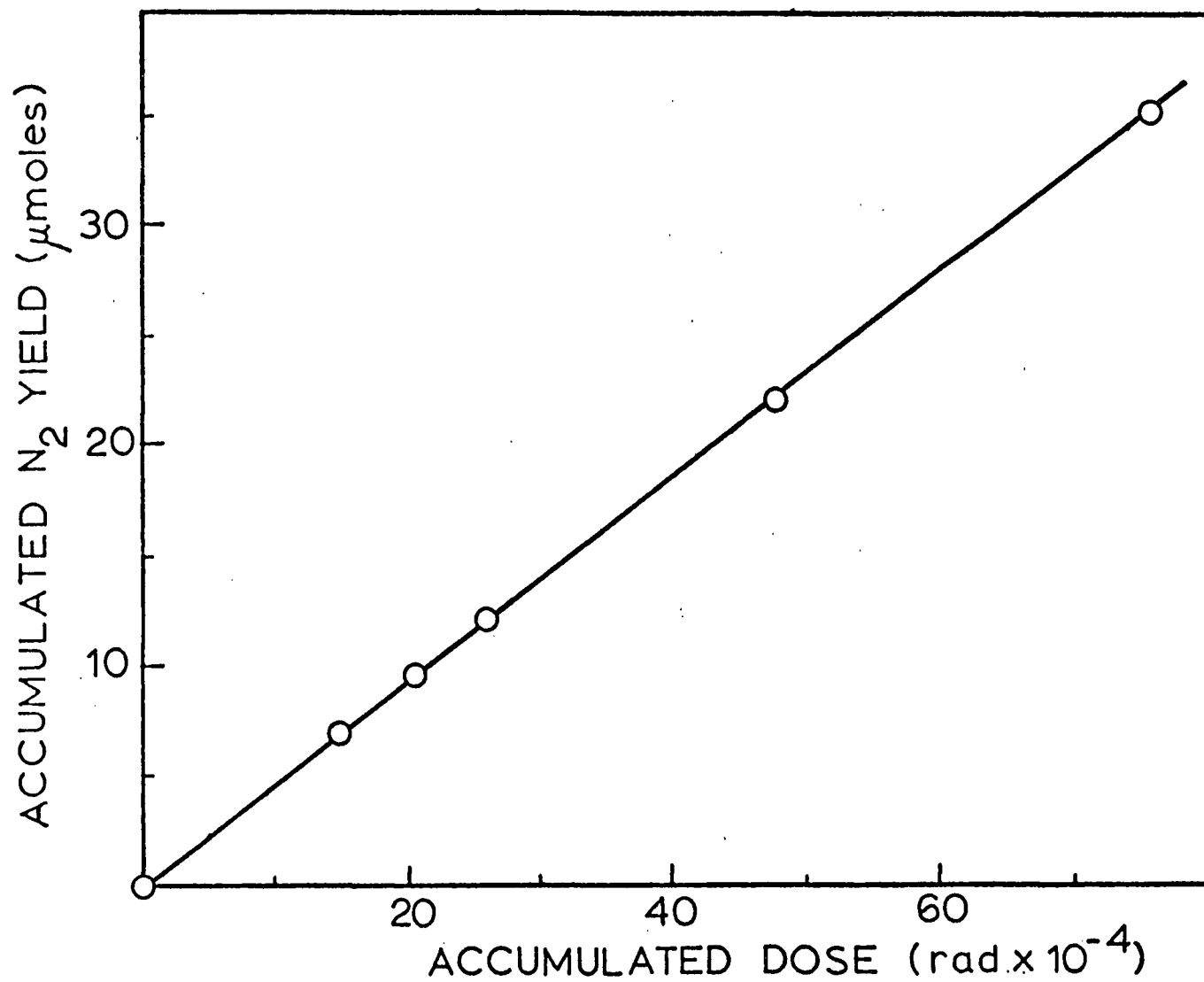
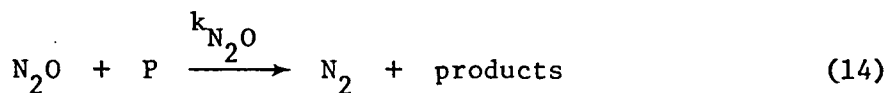


Figure 26. Accumulated nitrogen yield as a function of accumulated dose for a 0.054 M solution of N₂O in DMSO.

some strong reducing precursor. To test the nature of this chemical species with which the nitrous oxide was reacting, various second scavengers were added to 0.05 M N_2O solutions to compete with it. Data on the effect of these scavengers is shown in Table II. Methanol and isopropanol are known to react rapidly with hydrogen atoms but very slowly with solvated electrons. On the other hand, acetone, silver nitrate, chloroform, iodine, carbon tetrachloride and acid are known to react very rapidly with solvated electrons in other polar solvents. Water was added because DMSO is very hygroscopic and there could have been a trace of water in the samples despite the stringent precautions taken to eliminate it. As can be seen from Table II the added water had no appreciable effect on any of the gas yields, so that either all samples contained enough adventitious water for its effect to be fully felt or water cannot compete with the precursors of the gaseous products at this concentration (~ 0.5 % by volume).

With the assumption that nitrous oxide and the second scavenger (S) compete for the precursor (P) of nitrogen according to reactions (14) and (15)



then

$$G(N_2) = G(P) \left[\frac{k_{N_2O} [N_2O] [P]}{k_{N_2O} [N_2O] [P] + k_s [S] [P]} \right] \quad (3.1)$$

TABLE II. Radiation yields from irradiated DMSO containing 0.05 M N_2O plus the second scavenger indicated in column 1 at concentration given in column 2.

Second scavenger	Concentration (M)	G(N_2)	G(CH_4)	G(H_2)	G(C_2H_6)
Water	0.22	1.7	3.1	0.21	0.46
Methanol	0.098	1.7	3.0	0.23	0.42
	0.196	1.7	3.0	0.23	0.43
(a)	0.196	-	3.6	0.24	0.46
Isopropanol	0.103	1.8	2.8	0.26	0.45
(a)	0.103	-	3.1	0.25	0.46
Acetone	0.107	1.7	2.8	0.23	0.45
	0.264	1.8	2.6	0.23	0.44
AgNO ₃	0.00947	1.4	2.6	0.21	0.40
	0.0249	1.2	2.4	0.21	0.42
	0.0516	0.95	2.3	0.20	0.41
	0.102	0.65	2.1	0.19	0.41
	0.158	0.57	2.1	0.20	0.41
CHCl ₃	0.0124	1.2	2.3	0.20	0.36
	0.0696	0.68	2.2	0.21	0.41
	0.0990	0.63	2.2	0.19	0.39
	0.197	0.43	2.1	0.21	0.40
	0.304	0.38	1.9	0.20	0.37
Iodine	0.00652	1.5	0.32	0.22	0.42
	0.0208	1.1	0.26	0.21	0.29
	0.0300	0.99	0.25	0.22	0.28
	0.0941	0.59	0.20	0.20	0.25
	0.126	0.45	0.21	0.19	0.26

TABLE II (continued)

Second scavenger	Concentration (M)	G(N ₂)	G(CH ₄)	G(H ₂)	G(C ₂ H ₆)
CCl ₄	0.0179	1.11	2.2	0.21	0.45
	0.0490	0.74	1.8	0.21	0.38
	0.0685	0.68	1.7	0.21	0.37
	0.0740	0.65	1.7	0.20	0.36
	0.103	0.45	1.5	0.20	0.36
Anhydrous sulfuric acid	0.00918	1.4	2.4	0.20	0.41
	0.0195	1.2	2.5	0.20	0.45
	0.0295	1.1	2.7	0.21	0.45
	0.0377	1.0	2.8	0.20	0.47
	0.0559	0.80	2.7	0.19	0.47
	0.0895	0.68	3.0	0.20	0.50
	0.114	0.63	3.0	0.20	0.53
	0.137	0.55	3.2	0.20	0.50
	(b) 0.0718	0.78	2.8	0.23	

(a) No N₂O added

(b) 0.5 M methanol added

where k_s is the rate constant of P with S, k_{N_2O} is the rate constant for the reaction of P with N_2O and $G(P)$ is the yield of the precursor. Rearranging (3.1), the following relationship was obtained and applied to the competitions.

$$\frac{1}{G(N_2)} = \frac{1}{G(P)} [1 + k_s[S]/k_{N_2O}[N_2O]] \quad (3.2)$$

The data from Table II are plotted in Figures 27 and 28 and appear to follow the simple competition relationship. From the slopes of the plots the values for k_s/k_{N_2O} were obtained and are given in Table III and compared with the published values of these ratios for the corresponding reactions in water in which the precursor is the hydrated electron, e_{aq}^- .

Although the intercept of these plots all give $G(P) = 1.6 \pm 0.2$ this is not the true precursor yield. In fact $G(N_2)$ does not show a plateau value at high nitrous oxide concentrations which would correspond to complete scavenging of the precursor; thus the yield of $G(P)$ depends on the nitrous oxide concentrations used above 0.03 M (see Figure 25). This is evident from the H^+ competition shown in Figure 28 in which two different but high values (0.05 M and 0.07 M N_2O) of nitrous oxide were used. Although both lines have the same slope two different intercepts were obtained. For this reason the nitrous oxide concentration was held constant at 0.05 M while the concentration of the second scavenger was varied.

Figures 29 and 30 show the effect of iodine and hydrogen ions on the gaseous products. Acid appears to have no effect on the gas

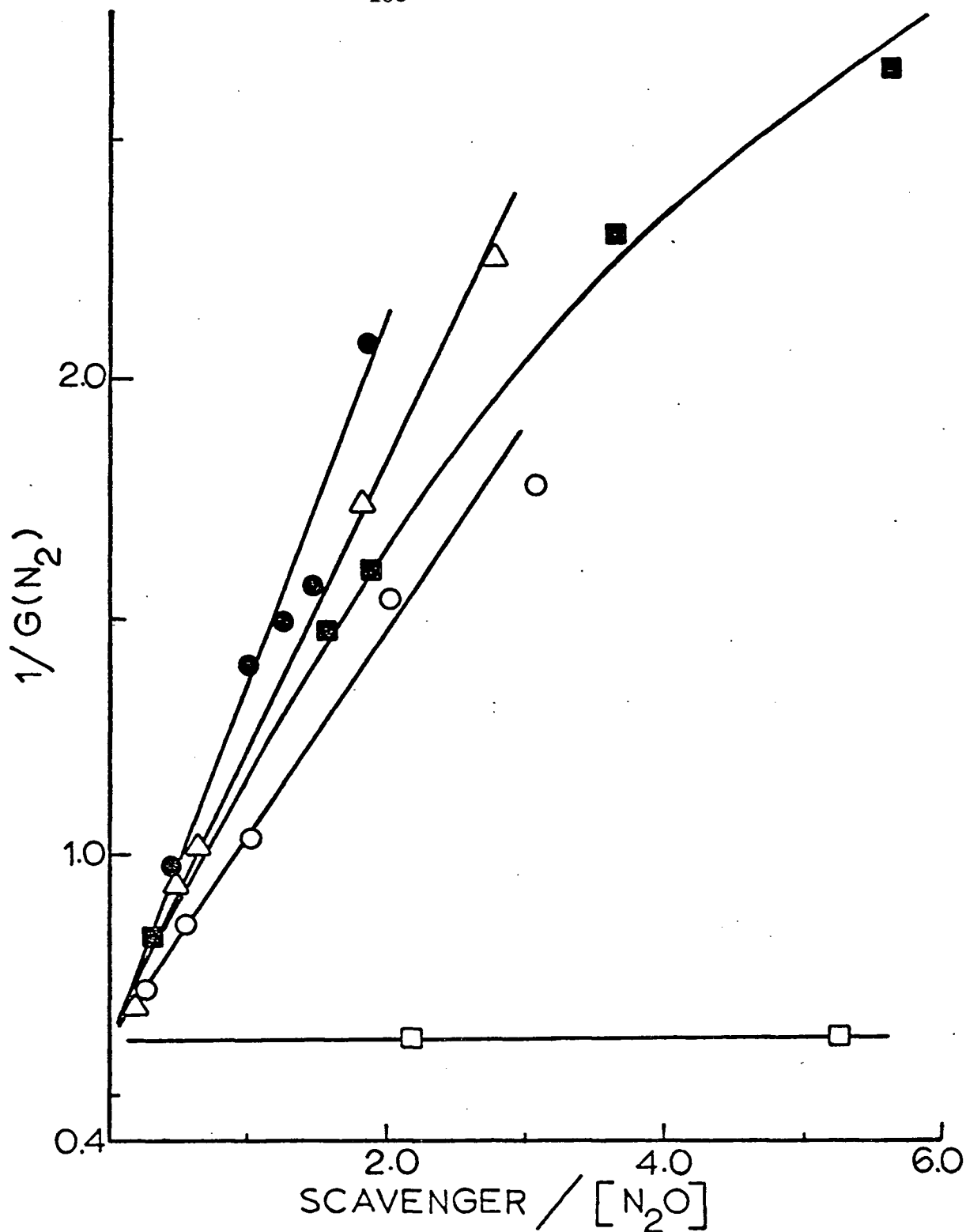


Figure 27. Plot of $1/G(N_2)$ as a function of $[\text{Scavenger}]/[\text{N}_2\text{O}]$. The N_2O concentration was 0.05 M and the second scavenger concentration was varied. The data was taken from Table 2. ●, CCl_4 ; △, I_2 ; ■, CHCl_3 ; ○, Ag^+ and □, acetone.

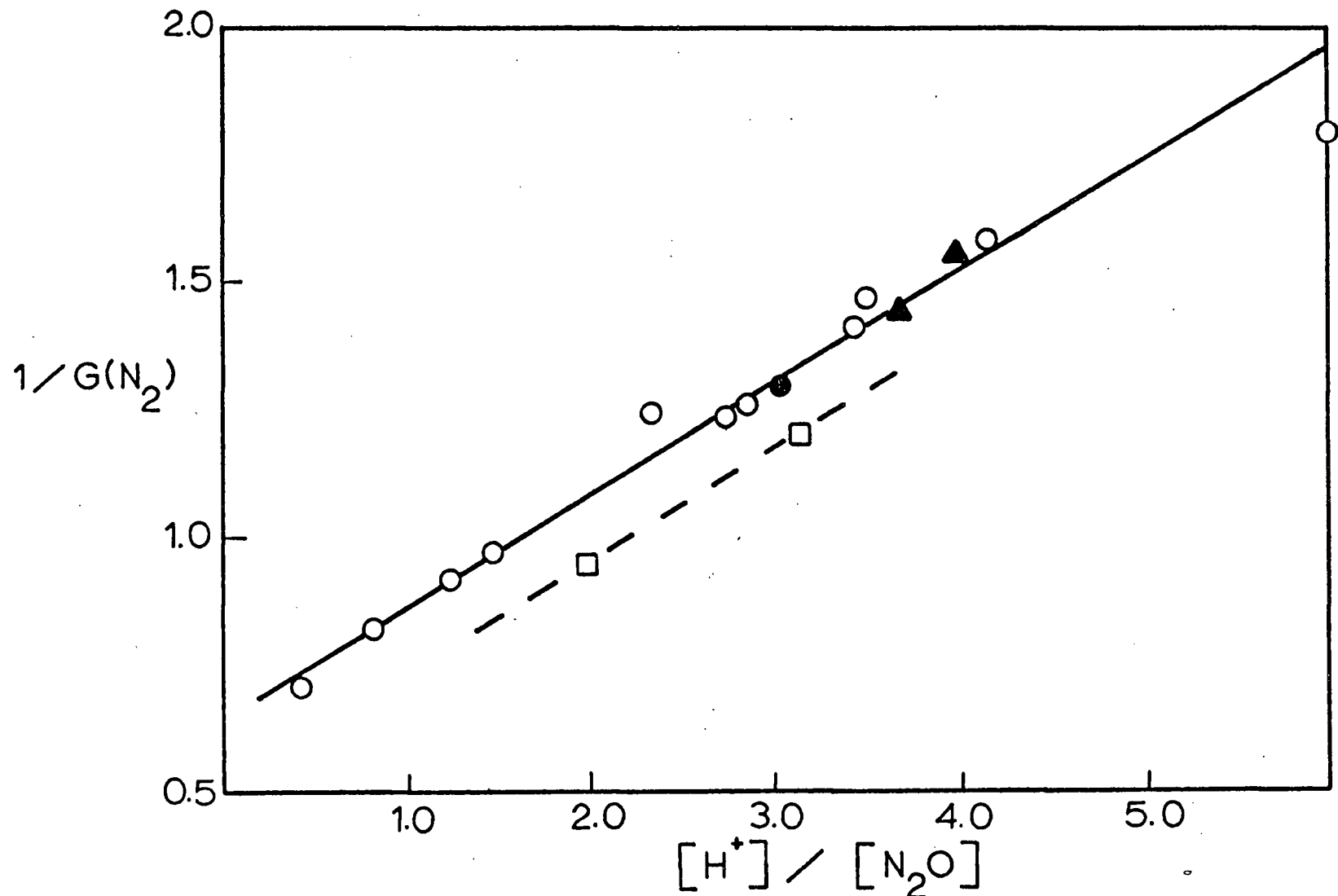


Figure 28. Plot of $1/G(N_2)$ as a function of $[H^+]/[N_2O]$ in which ○, ▲, and □ correspond to different N_2O concentrations: ○, 0.05 M N_2O ; ▲, 0.04 M N_2O and □, 0.07 M N_2O . ● corresponds to 0.5 M methanol added to the acid solution.

TABLE III. Ratio of k_S/k_{N_2O} obtained for the precursor of N_2 in DMSO with various second scavengers (S) added to a 0.05 M solution of N_2O . Column headed water refers to the published rate constant ratio for the hydrated electron.

S	k_S/k_{N_2O} (DMSO)	k_S/k_{N_2O} (water) ^a
CCl_4	0.85 ± 0.09	5.4
I_2	0.60 ± 0.06	9.1
$CHCl_3$	0.45 ± 0.05	3.6
Ag^+	0.40 ± 0.04	5.7
H^+	0.25 ± 0.03	3.9
$(CH_3)_2CO$	<0.01	1.1

^a Data taken from the compilation of rate constants by M. Anbar and P. Neta, Inter. J. Appl. Rad. Isot. 18, 493 (1967).

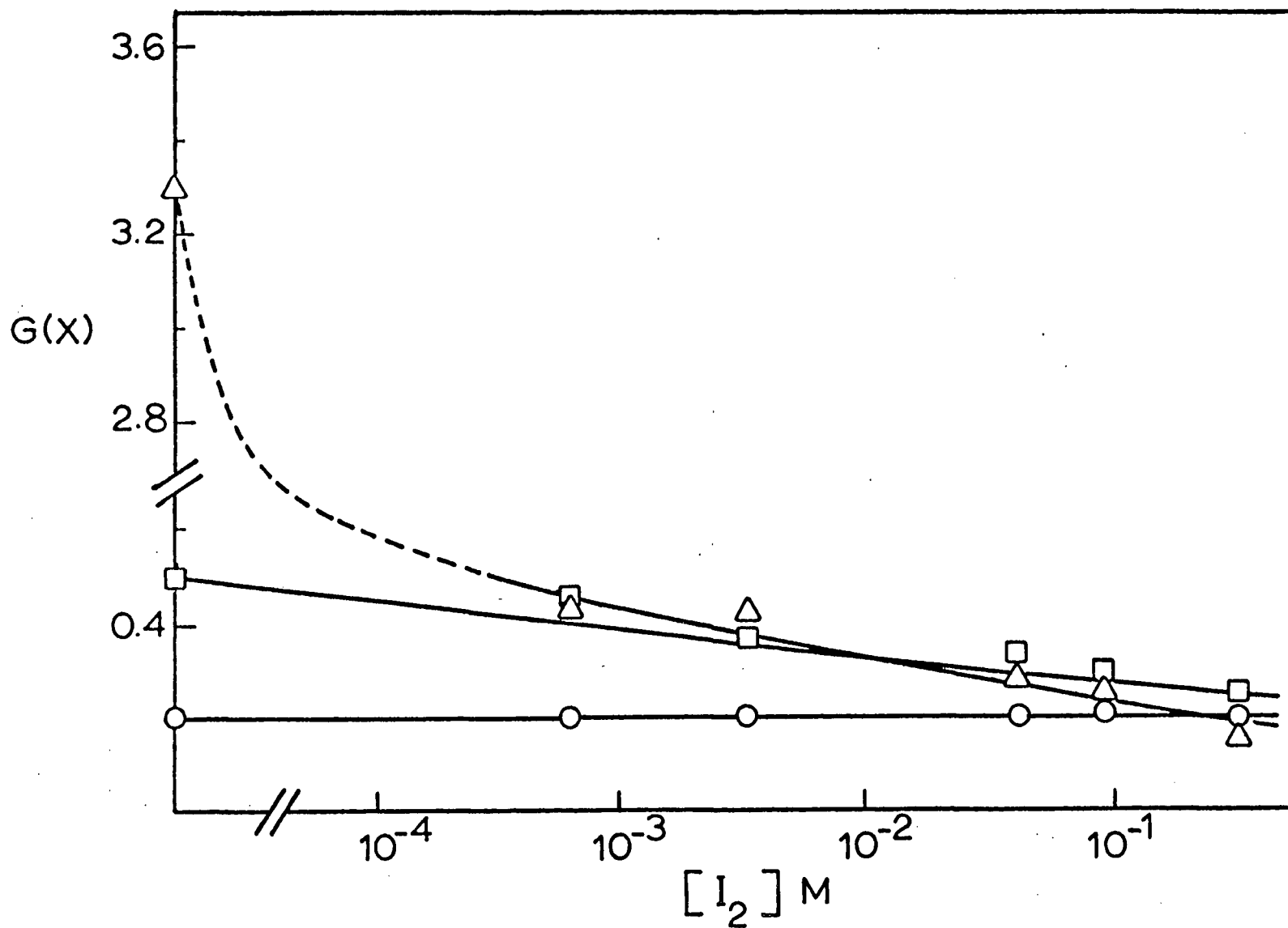


Figure 29. Radiation yields of CH_4 (Δ), C_2H_6 (\square), and H_2 (\circ) as a function of I_2 concentration. The doses were $< 5 \times 10^4$ rads.

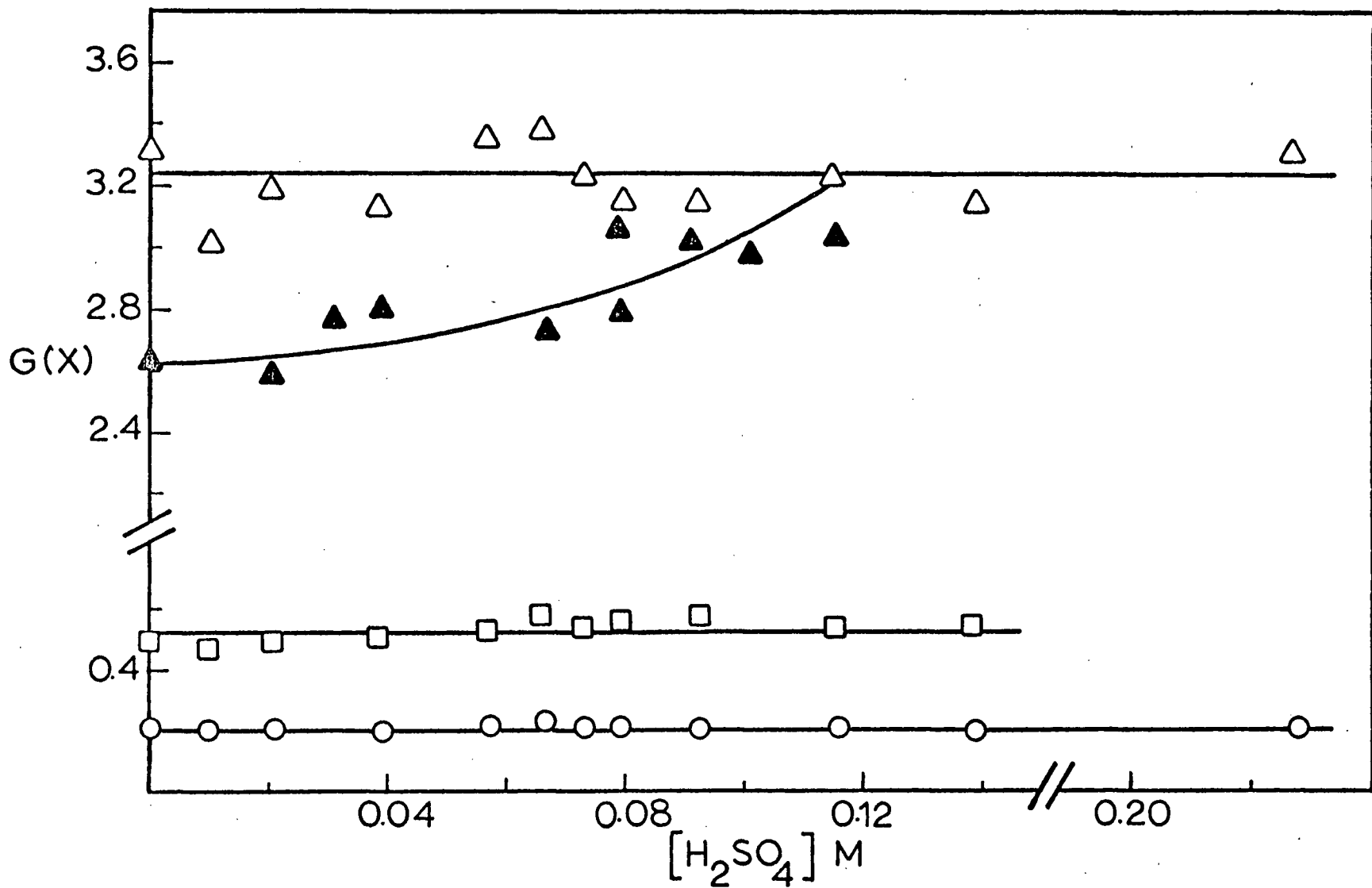
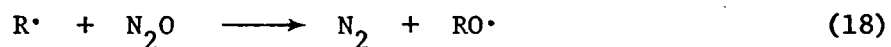
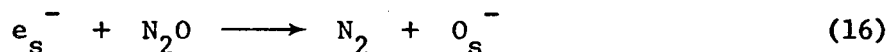


Figure 30. Radiation yields of CH₄ (Δ), C₂H₆ (□) and H₂ (○) as a function of H⁺ concentration. ▲ corresponds to the yield of CH₄ when 0.05 M N₂O was added to the corresponding acid solution of DMSO. In the case of CH₄, all doses were < 1.8 x 10⁵ rads.

yields, in contrast to nitrous oxide, whereas iodine reduces the yield of ethane and methane without affecting the hydrogen yield.

4. Discussion

Although nitrous oxide has been widely used as a specific scavenger for solvated electrons in many liquids, other strongly reducing species formed in the radiolysis may give rise to the nitrogen observed. In the case of DMSO, solvated electrons, hydrogen atoms, free radicals (R) or solvent radical anions could yield nitrogen via reactions (16), (17), (18), or (19) if their alternate fates were comparatively slow.



In this reaction scheme the solvent radical anion, $DMSO^-$, is to be regarded as an anion formed either by electron attachment of solvated or free electrons or is a decomposition product formed from it. In order to explain the observed results and to differentiate between the possible precursors of the nitrogen, strong inferences must be drawn from the competition studies with the other scavengers.

From Table II it can be seen that the addition of methanol and

isopropanol did not alter the yield of nitrogen. Since these alcohols are generally much better hydrogen atom scavengers than is nitrous oxide, this suggests that reaction (17) does not contribute to the nitrogen yield. Furthermore, the slight increase in hydrogen yield, which can be partially attributed to the yield obtained from the direct action of the radiation on the alcohols, implies that the hydrogen atoms are produced in low yield.

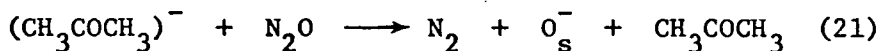
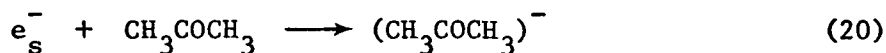
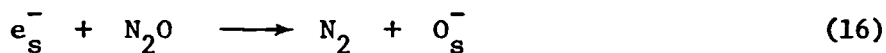
In a similar manner, reaction (18) can also be disregarded. From Table III it can be seen that iodine competes on an almost equal basis with nitrous oxide for the precursor of nitrogen despite the fact that iodine is a much better radical scavenger than nitrous oxide. If reaction (18) were the precursor of molecular nitrogen one would expect a greater reduction in the yield when iodine was added than is observed. This inference is further supported in Figure 29 where it can be seen that iodine virtually eliminates methane, even at 0.006 M. This suggests that methane arises from methyl radicals which abstract a hydrogen atom from DMSO. In this regard, it should be mentioned that methyl radicals were observed in γ -irradiated polycrystalline DMSO at 77°K (to be discussed later). From Figure 29 it can also be seen that iodine decreases the ethane yield slightly implying that part of it is similarly formed by radical reactions. On the other hand, the hydrogen yield is unaffected by iodine indicating it is formed in a "molecular process", such as molecular detachment of hydrogen or an ion-molecule or "hot" atom reaction occurring within a few collisions. Similarly about half the ethane yield and about 10% of the methane yield may be due to "molecular processes".

The inference then is that the reducing precursor of nitrogen is a solvated electron or radical anion. The reducing properties and chemical behavior of these two species may be very similar; indeed perhaps only pulse radiolysis absorption spectroscopy or esr can really differentiate between them. As mentioned earlier the absorption spectra of solvated electrons are characterized by their broadness and intensity in the visible and near infrared region of the spectrum. By contrast, radical anions would probably have weak, narrow bands in the visible. This similarity in behavior was demonstrated in a recent study on the radiolysis of liquid formamide⁴⁶ in which the pattern of reactivity of the reducing species conformed remarkably well to that of solvated electrons in other media. However later pulse radiolysis studies showed that formamide does not form solvated electrons with lifetimes $> 10^{-11}$ seconds but rather reacts rapidly with the thermalized electrons, presumably to give radical anions as their decomposition products.⁴⁵ These radical anions thus represent the "free ions" which react with the electron scavengers.

As in the case of formamide the chemical evidence for the presence or absence of solvated electrons in DMSO is not conclusive. The pulse radiolysis study which will be described later showed that solvated electrons are formed as the primary reducing species in DMSO. However, that study also showed that the electrons appear to react with the solvent quite rapidly so that radical anions are probably also involved in the reduction of N_2O and other scavengers at low concentrations in these steady state experiments.

From the data given in Tables II and III, it is evident that nitrous

oxide is a better scavenger of reducing species than the other scavengers. The relative rate constants obtained from the slopes of Figures 27 and 28 and compared with the relative rates of these scavengers with hydrated electrons show them to be markedly different. Furthermore acetone does not compete effectively with nitrous oxide although CCl_4 , I_2 , CHCl_3 , Ag^+ and H^+ do. This is at variance with the results obtained in the pulse radiolysis of DMSO containing 0.19 M acetone in which the solvated electron was completely eliminated.⁵⁸ A possible explanation is that the acetone radical anion, $(\text{CH}_3\text{COCH}_3)^-$, undergoes a charge transfer with nitrous oxide according to the following sequence:

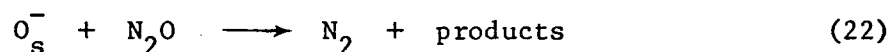
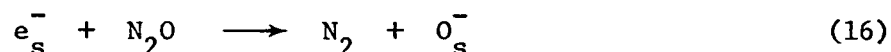


Moreover the negative ions of CCl_4 , I_2 and CHCl_3 may also undergo charge transfer with the nitrous oxide so that the actual rate constant, $k_{\text{N}_2\text{O}}$, could be actually smaller than that observed.

The curvature of $G(\text{N}_2)$ at $[\text{N}_2\text{O}] > 0.03 \text{ M}$ is difficult to interpret without knowing the alternate fates of the nitrogen precursors (solvated electrons and other reducing species, if any) and their absolute rate constants. A possible interpretation is that the nitrous oxide is scavenging electrons inside the spur. However this is

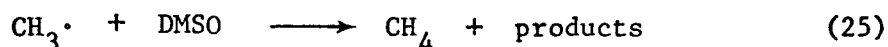
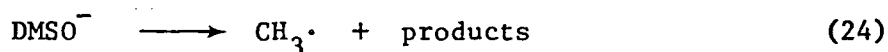
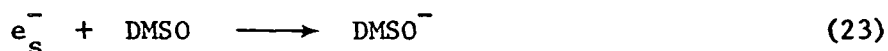
disregarded because pulse radiolysis of a solution of 0.07 M nitrous oxide in DMSO only scavenged about 80% of the solvated electrons.⁵⁸

If one equates the nitrogen yield at the high nitrous oxide concentrations with the total free ion yield, then $G(\text{free ion}) = 1.8 \pm 0.2$ (see Figure 25). However, using anthracene as a scavenger it was shown by pulse radiolysis that the yield of solvated electrons is only 1.3 (to be discussed shortly). Perhaps the higher yield in the case of nitrous oxide is due to scavenging of other highly reducing species in addition to solvated electrons. However, another possibility exists, namely that each e_s^- gives rise to more than one N_2 molecule. Studies on other systems using nitrous oxide have given higher nitrogen yields than the total free ion yield and it has been proposed that O_s^- may react further to produce more nitrogen according to reaction (22).

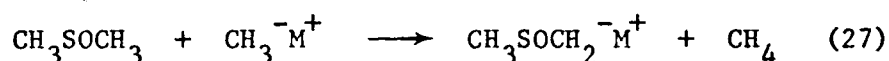
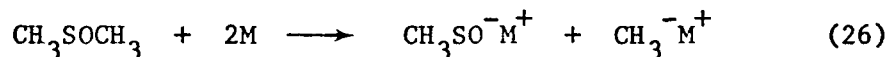


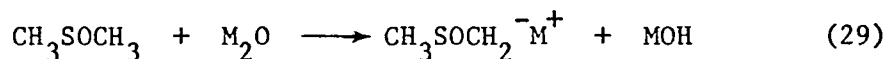
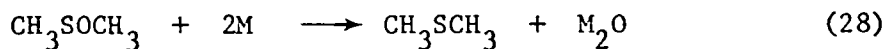
Earlier it was suggested that most of the methane arises from methyl radicals which abstract a hydrogen atom from DMSO because the methane was virtually eliminated by iodine, an excellent radical scavenger. However, the fact that nitrous oxide can decrease the methane yield by 20% suggests that it can also interfere with a minor reaction leading to CH_4 formation. Because no decrease in the methane yield was observed in the presence of methanol and isopropanol, which are better radical scavengers than nitrous oxide, the interference is

probably ionic in nature. This is still in keeping with the iodine results since I_2 is also a good electron scavenger as seen from the relative rate constants in Table III. It is suggested that part of the methane yield arises from the decomposition of the DMSO radical anion by the reaction sequence shown below.



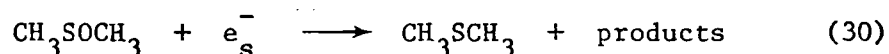
This is supported by the fact that electrons generated in DMSO-water glasses at 77°K by ultraviolet photolysis of $K_4Fe(CN)_6$ undergo reaction with the DMSO molecules to produce methyl radicals (see later). Nitrous oxide, and other electron scavengers (except H^+), could interfere with the methane formation either by scavenging the solvated electron before it reacts with the solvent molecules to produce the anion or by charge transfer with the solvent anion. Furthermore, strongly reducing metals (M) such as sodium and potassium in excess DMSO decompose the solvent yielding a mixture of methane, dimethyl sulfide and the salts of methane sulfenate and methylsulfinyl carbanion according to the reaction sequence below.⁶³



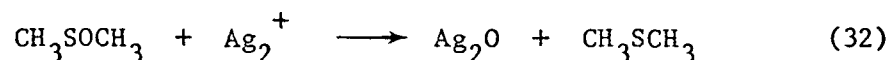
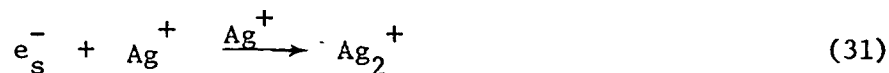


Reactions (26) and (28) were found to be about equal with sodium whereas with potassium reaction (26) greatly predominated. Reactions (26) and (27) may be considered somewhat analogous to reactions (23) to (25).

It is interesting to note that dimethyl sulfide is a major decomposition product in alkali metal solutions of DMSO. The large yield of dimethyl sulfide, $G(\text{DMS}) = 1.2 \pm 0.2$, observed in the radiolysis of DMSO may arise directly from the reduction of the solvent according to reaction (30).



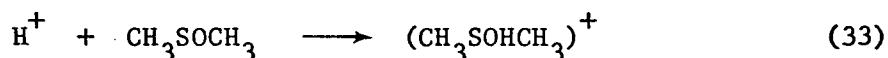
The addition of 0.5 M AgNO_3 which would readily scavenge all the solvated electrons caused no noticeable change in the dimethyl sulfide yield, which argues against reaction (30). However, it is possible that the silver atoms produced undergo charge transfer with the solvent in an analogous manner to reaction (28).



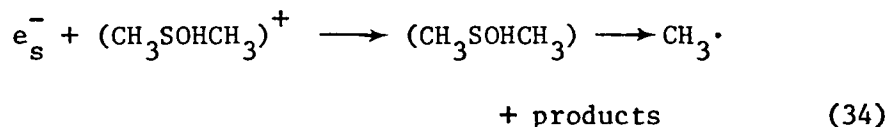
This is supported by the fact that when DMSO was allowed to remain in

contact with a freshly prepared silver mirror for several days, a strong odour of dimethyl sulfide was observed. On the other hand it is possible that DMS does not arise from e_s^- or is a molecular product whose precursor cannot be scavenged even at 0.5 M Ag^+ .

The addition of hydrogen ions at concentrations up to 0.2 M H^+ did not affect the gaseous yields from pure irradiated DMSO (see Figure 30) in marked contrast to the presence of nitrous oxide. This effect of H^+ is in agreement with the results of Pujo and Berthou.⁶⁰ The strong electron-donating power of the sulfoxide group makes DMSO a powerful Lewis base which is readily protonated by hydrogen ions in accordance with reaction (33).

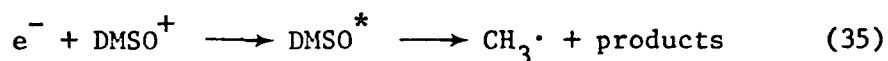


The experimental observations can be explained if the reaction of the electron with the positive ion $(\text{CH}_3\text{SOHCH}_3)^+$ has the same fate as the DMSO radical anion.



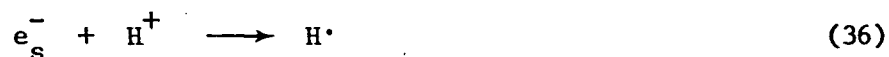
The positive ion would compete with nitrous oxide for the electron and perhaps other reducing species produced in the radiolysis. At the same time it would counteract the slight effect nitrous oxide has on the methane yield. This effect is shown in Figure 30. The electrons which are not scavenged and undergo geminate recombination would

produce a highly excited DMSO molecule which would probably dissociate according to reaction (35).



Whereas nitrous oxide at 0.07 M did not seem to be interfering with geminate recombination, sulfuric acid at 0.2 M may well be doing so, as the pulse radiolysis data indicates. Reactions (34) and (35) could therefore explain why high acid concentrations had no effect on the methane yield.

The reaction of the solvated electron with the hydrogen ion, according to reaction (36),



or with the protonated DMSO molecule to produce a hydrogen atom does not appear to occur in view of the competition between H^{+} , N_2O and methanol (see Table II). If reaction (34) produced a hydrogen atom or if reaction (36) was in competition with reaction (16), then the hydrogen yield would be increased by the presence of methanol in the acidic solution of DMSO. No such increase was observed. However, it is possible that hydrogen atoms are produced but that they react rapidly with DMSO to give non-gaseous products.

B. PULSE RADIOLYSIS

1. Absorption Spectra in DMSO and DMSO_{d₆}

Previous investigations on the pulse radiolysis of pure DMSO at room temperature^{58,64} have shown that the absorption spectra belonging to the transients fall into three main categories. From their distinct decay characteristics and behavior towards specific scavengers they were attributed to different species. The three principal branches, with their characteristic features, are given as follows: (i) a broad, structureless absorption stretching from the visible into the near infrared with a $\lambda_{\max} > 1500$ nm and having a half-life of ~ 15 nsec which was attributed to the solvated electron; (ii) a fairly broad band centered at ~ 600 nm whose half-life was ~ 1 μ sec and attributed to an oxidizing species; and (iii) absorption bands progressing from 400 nm into the near ultraviolet region belonging to at least two components possessing half-lives > 1 msec and ~ 12 μ sec. However further studies on these transients, in particular that of the oxidizing species and the solvated electron, were warranted in view of the fact that the free ion yield had not been determined nor the identity of the oxidizing species. Unless stated otherwise, the absorption spectra of these and other transients were obtained using electron pulse widths of 40 nsec depositing an average dose of 2.2 krad per pulse. The total absorbed dose which any one sample received was always less than 10^5 rads.

The absorption spectra of the oxidizing species ($\lambda_{\max} = 550$ nm) and the solvated electron ($\lambda_{\max} > 1500$ nm) obtained in pure $(\text{CH}_3)_2\text{SO}$ and $(\text{CD}_3)_2\text{SO}$ are given in Figure 31. The total absorption was

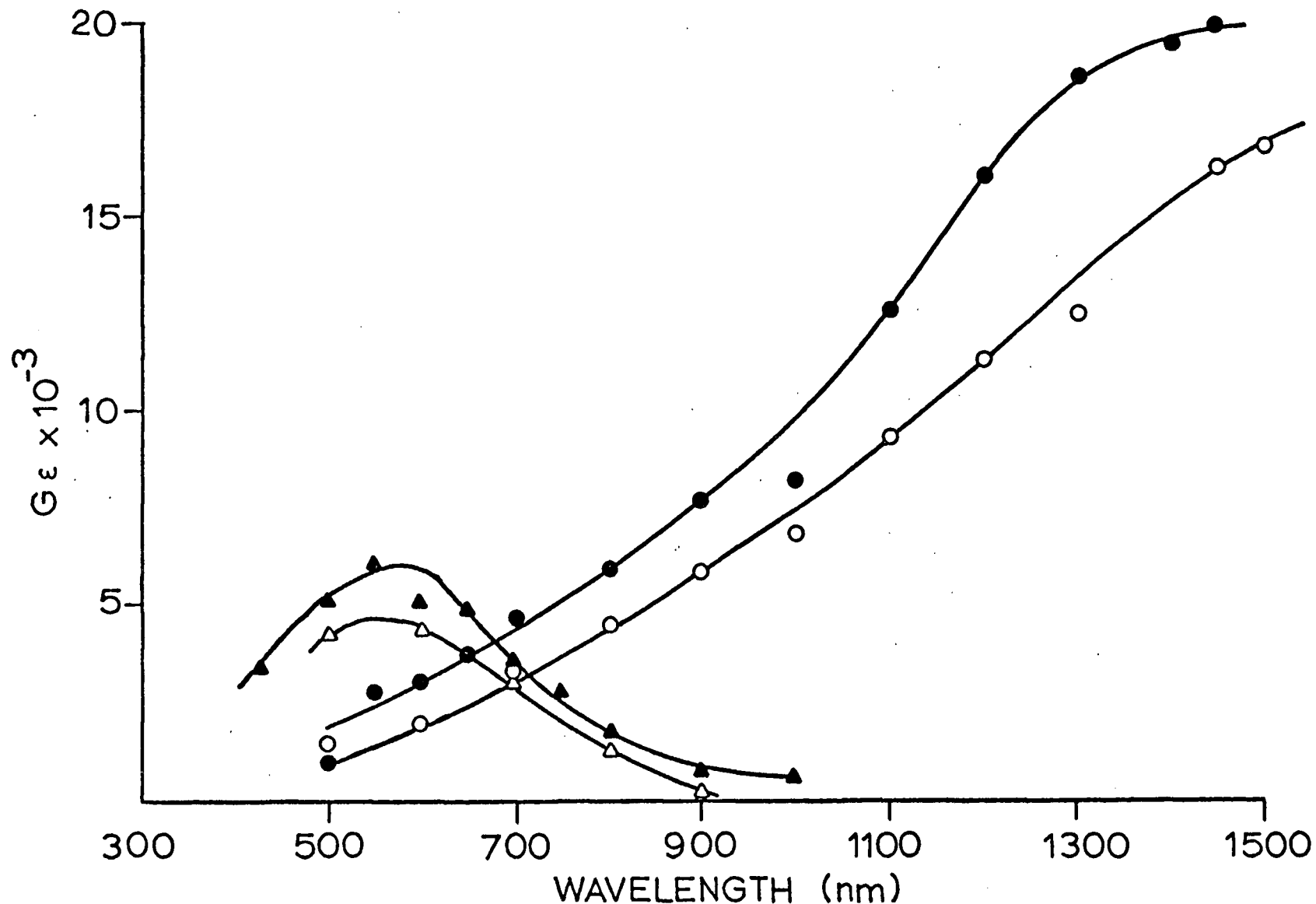


Figure 31. Transient spectra observed in $(CH_3)_2SO$ and $(CD_3)_2SO$. The circles refer to the solvated electron band corrected for the detector response time and the triangles refer to the DMSO positive ion, or oxidizing species. ○ and △ are for $(CH_3)_2SO$; ● and ▲ are for $(CD_3)_2SO$. Almost all data points are the mean of at least two measurements. The λ_{max} for the △ spectrum was established to be at 550 nm from a previous set of experiments.

obtained from the observed absorption peak heights at the end of the pulse. The bands attributed to the solvated electron in the deuterated and undeuterated DMSO had almost completely decayed within 100 nsec; consequently the maximum intensity of the bands centered at 550 nm were deduced by extrapolation to the end of the pulse from times > 100 nsec. This approximation is reasonable since the 550 nm band decays in a first-order manner with a half-life of 2.3 ± 0.2 μ sec (see Figure 35). Typical oscilloscope traces of the electron and oxidizing species are shown in Figures 32 and 33.

In order to compare the relative intensity of the bands, it was necessary to correct for the decay of the electron during the pulse. By using 10 nsec pulses it was determined that the electron decays by first-order kinetics with a half-life of 15 ± 2 nsec (see Figure 34). Therefore with a 40 nsec pulse, which was used in the determination of the absorption spectra, considerable decay of the electron would have occurred during the pulse. Furthermore, the time response of the detection system (oscilloscope and photodiodes) is comparable to the half-life of the electron so that the initial absorbance observed is not the true end of pulse absorbance. Using reasonable values for the time constants of the photodiodes and oscilloscope, the electron pulse width and the half-life of the electron, suitable correction factors were computed and applied to the observed absorbance.⁶⁵ These calculations show that under the experimental conditions, the maximum electron absorbance observed was only 43% of the absorbance which would have been observed had there been no decay. Consequently the observed absorbances for the electron band were multiplied by 2.3 relative to the 550 nm band data shown in Figure 31.

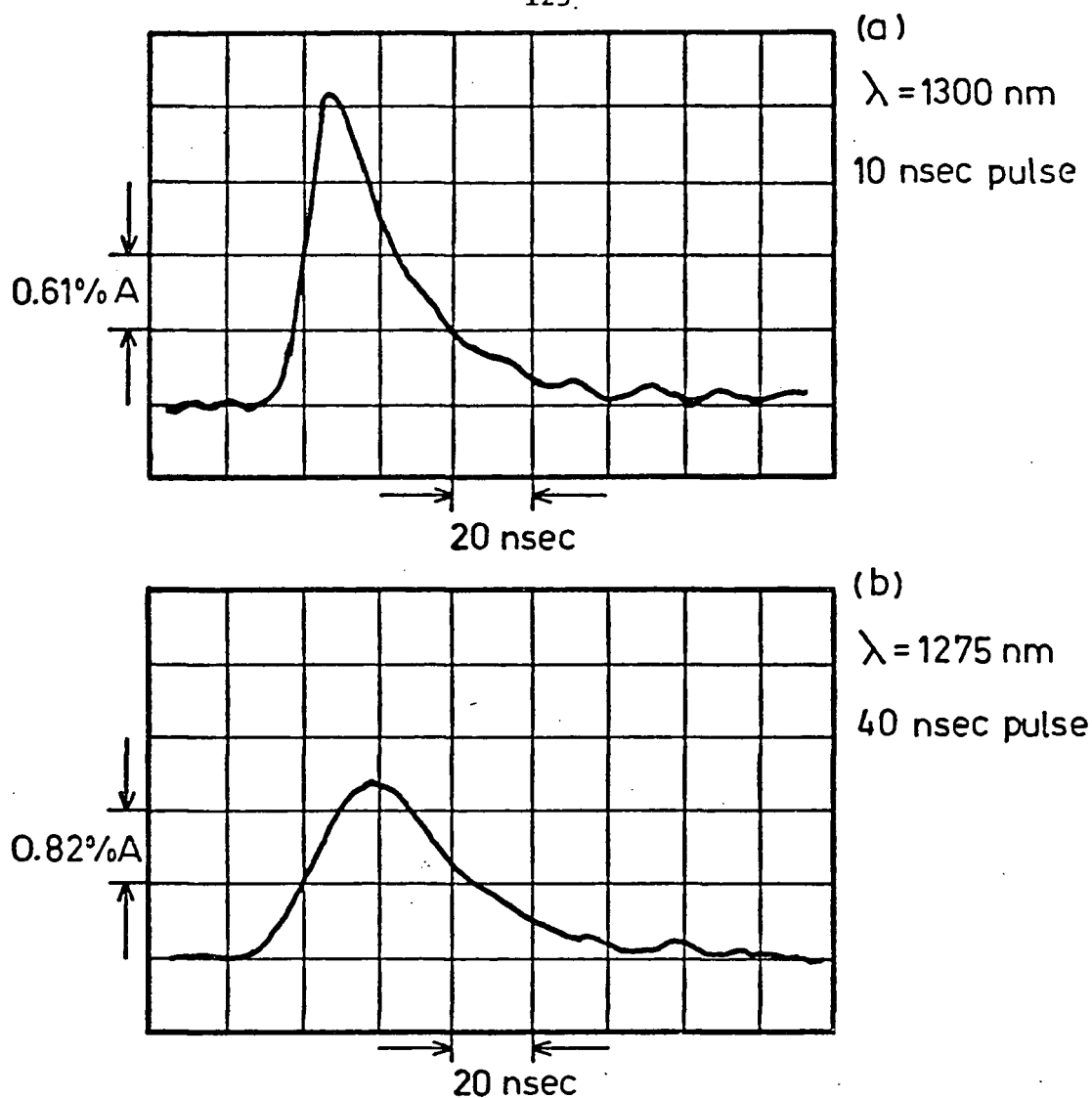


Figure 32. Typical oscilloscope traces showing the decay of the solvated electron in DMSO. Both traces were obtained using a Ge photodiode with a 50 ohm load resistance. (a) pulse width 10 nsec; (b) pulse width 40 nsec.

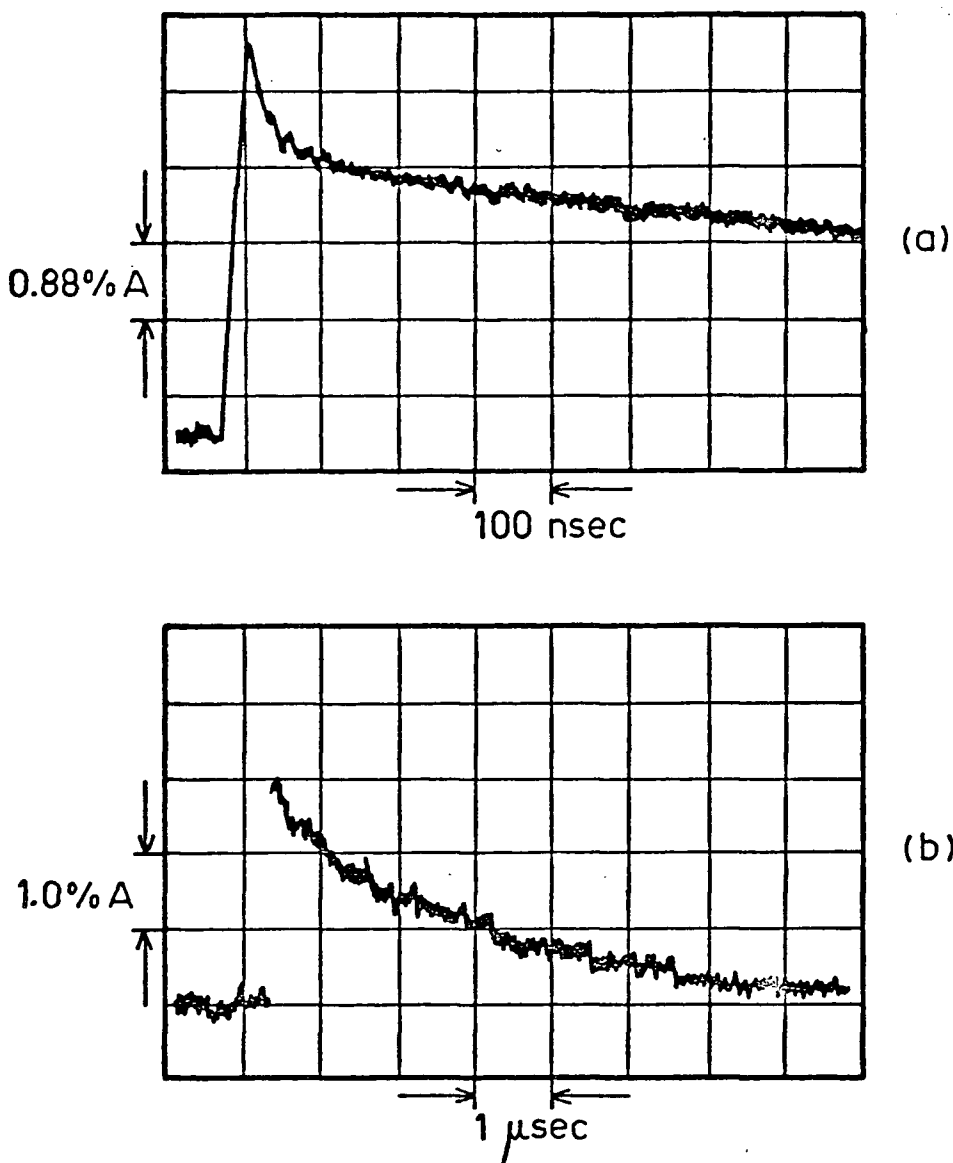


Figure 33. Typical oscilloscope traces showing the decay of the DMSO positive ion or oxidizing species at 550 nm. The fast initial decay in (a) is due to the solvated electron. Both traces were obtained using a pulse width of 40 nsec. (a) Si photodiode with 93 ohm load resistor; (b) photomultiplier with 470 ohm load resistor.

At $\lambda > 1500$ nm the Ge photodiode response is too slow to make measurements on the electron band for the reasons mentioned earlier. However, by observing the steady state absorption during long irradiation pulses (> 1 μ sec) using slow InAs (rise-time 2 μ sec)⁵⁸ and InSb (rise-time 100 nsec)⁶⁶ detectors, it appears that the maximum extinction coefficient for the electron band occurs between 1600 and 1800 nm and that $G\epsilon_{\max}$ is $< 25\%$ larger than $G\epsilon$ at 1500 nm.

There are several reasons for assigning the absorption band with $\lambda_{\max} > 1500$ nm to the solvated electron in DMSO. Firstly, it is extremely broad and intense ($\epsilon_{\max} > 10^4$ $M^{-1} \text{cm}^{-1}$), a characteristic feature of solvated electron bands. Secondly, the band is efficiently removed or reduced by known electron scavengers, such as O_2 , N_2O , anthracene, Ag^+ , acetone, CCl_4 and H^+ . Moreover, addition of known positive ion scavengers such as Br^- and water had no effect on the spectrum.

There is also evidence, which will be discussed more fully later, for the assignment of the band centered at 550 nm to the DMSO positive ion. In the presence of Br^- the 550 nm band was completely eliminated and replaced by the Br_2^- absorption. Addition of electron scavengers in sufficient concentration to just eliminate the electron band did not affect the 550 nm absorption or its decay rate, whereas addition of H^+ and Ag^+ in sufficient concentration to interfere with geminate recombination (> 0.1 M) increased its absorbance very significantly (by 90%).

The evidence for the assignment of these bands to the solvated electron and the primary oxidizing species is further substantiated by the fact that both bands show an equivalent increase upon isotopic

substitution, suggesting that the species responsible have a common origin. As shown in Figure 31, G_{ϵ} is $\sim 30\%$ larger for the deuterated DMSO than it is for the undeuterated. Since it is unlikely both bands would have exactly the same change in extinction coefficients in going from the deuterated material to the unsubstituted, it implies that the change arises from a G value effect. This suggests then that both primary species have an equal probability of surviving geminate spur reactions. A similar effect occurs in water in which the fraction of ions which escape geminate recombination and become solvated is substantially larger in the deuterated material.^{67,68} D_2O and H_2O have identical bulk dielectric constants so that the increase in yield cannot be a simple dielectric constant effect. What it does suggest is that there is a wider range of initial separation distances between the thermalized electron and its parent positive ion in D_2O than in H_2O . It is known that D_2O has a slower dielectric relaxation time than H_2O ; consequently the thermal electrons will have to travel further before they become solvated by orientational polarization and hence will have a higher probability of escaping geminate recombination. On the other hand, it is possible that the material containing the heavier isotope is less efficient in its inelastic scattering of the "subexcitation electron" so that, on the average, the electron gets further away from its concomitant partner before it becomes thermalized.

The decay rates of both the electron and positive ion were the same within experimental error in the deuterated DMSO as they were in the protonated material. In both cases the decay of the electron being

nearly 100 times faster. Both species decay by first-order kinetics, as shown in Figures 34 and 35; the pseudo first-order rate constants for the electron and positive ion are $(4.8 \pm 0.1) \times 10^7 \text{ sec}^{-1}$ and $(3.0 \pm 0.1) \times 10^5 \text{ sec}^{-1}$ respectively. This suggests both transients react with the solvent or else with some residual impurity. However addition of ~ 0.1 M dimethyl sulfide and water, which were the only detectable impurities, showed no observable increase in decay rates. It is thought that the electron decays by reacting with the solvent medium for reasons which have already been mentioned. Although the DMSO radical anion has been observed to have an absorption maximum at 350 nm in irradiated aqueous alkaline solutions (pH > 10) containing 0.7 M DMSO,⁶⁹ it was not observed in the present study. If it is formed, it is possible that it is very unstable and decays faster than the response time of the detection apparatus. It is also possible that its extinction coefficient is too small to be observed. Under the experimental conditions used in this study the limit of detectability of an absorption is given by $G\epsilon \sim 1000 \text{ mols. (100 eV)}^{-1} \text{ M}^{-1} \text{ cm}^{-1}$ providing, of course, that the mean life time of the species is long compared to the pulse length and response time of the detection apparatus. For a G value of 1.3 this imposes an upper limit of $750 \text{ M}^{-1} \text{ cm}^{-1}$ on the extinction coefficient of the solvent anion. The DMSO positive ion can presumably readily undergo ion-molecule reactions with the solvent or spontaneous unimolecular decomposition. It should be noted that Koulkes-Pujo et al.⁶⁴ found that the oxidizing species decayed by a second-order reaction which had a first half-life of 0.36 μsec . This was probably due to reaction with a negative ion

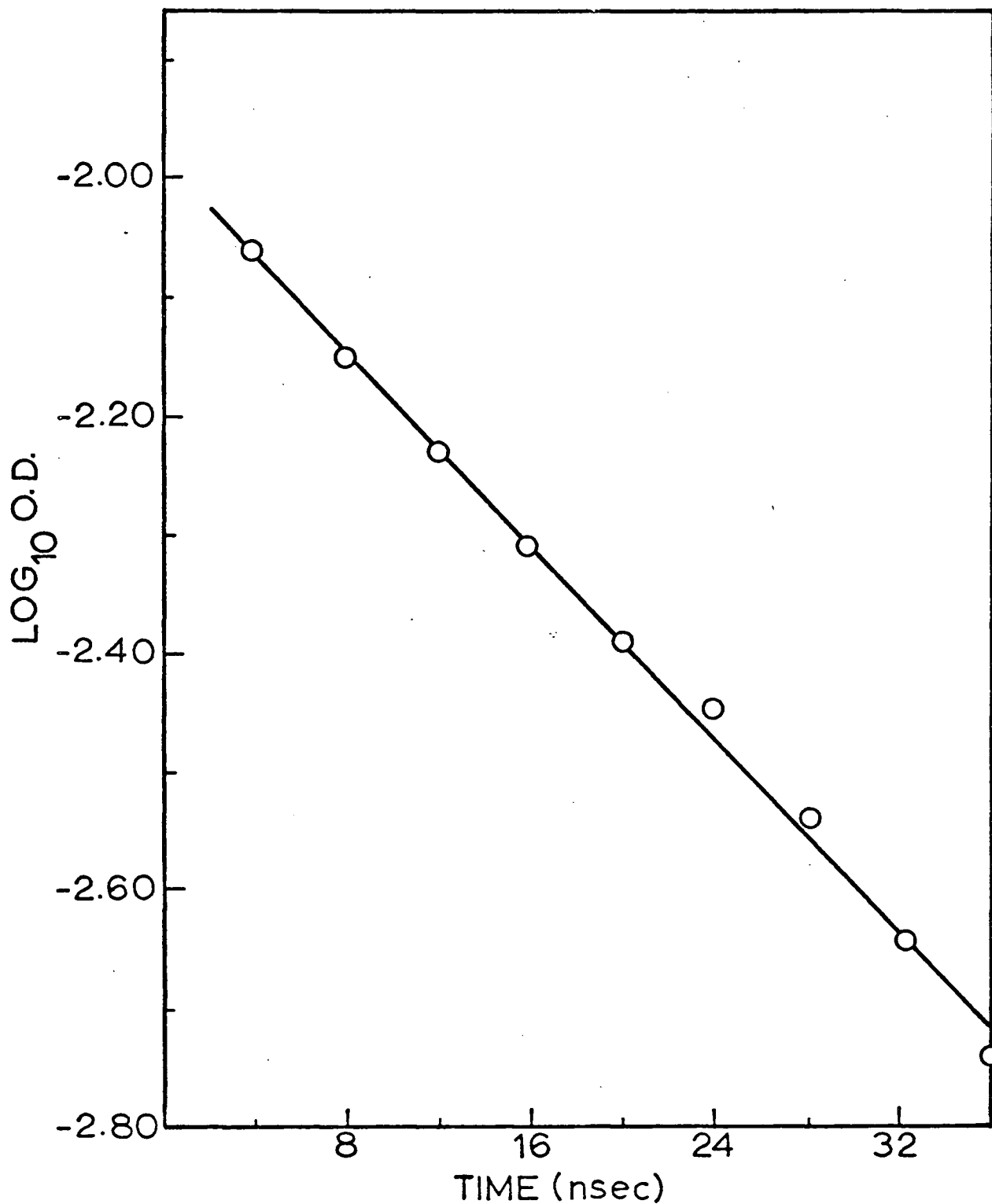


Figure 34. First-order decay plot of the solvated electron in DMSO taken at 1300 nm. The pulse width was 10 nsec, giving an absorbed dose of 900 rads per pulse. The decay was measured using a Ge photodiode with a 50 ohm load resistor.

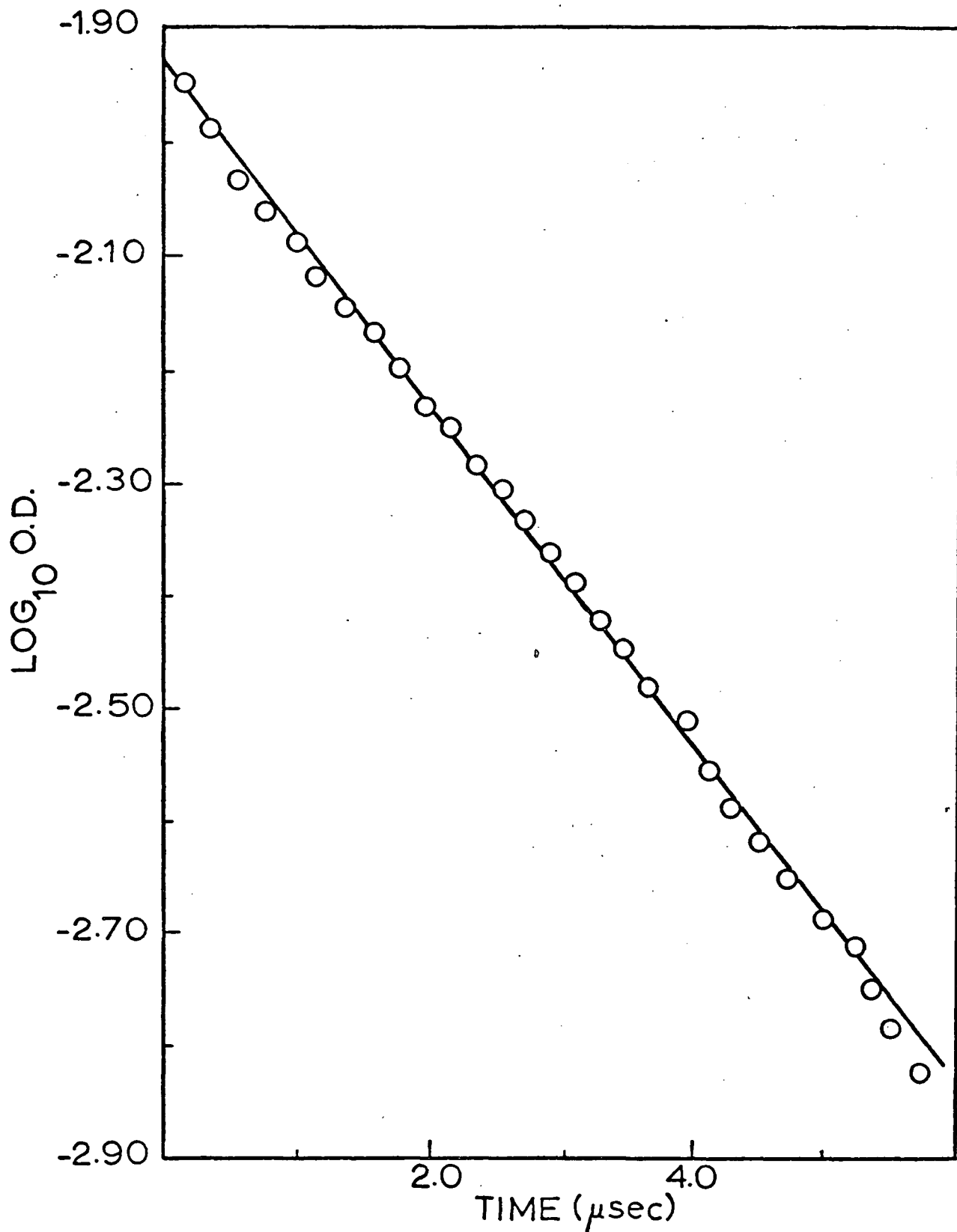


Figure 35. First-order plot of the decay of the DMSO positive ion. The decay was measured at 550 nm using the photomultiplier with a 470 ohm load resistor. The pulse width was 40 nsec, giving an absorbed dose of 2200 rads per pulse.

produced from the electron decay. Their dose rate was nearly 60 times that used in this study (3×10^{12} rads sec^{-1} compared to 5×10^{10} rads sec^{-1}) so that the "instantaneous" concentration of transient ionic species would be much higher in their study.

2. Free Ion Yields

Anthracene has been widely used as a scavenger of solvated electrons and radical anions because of its high reactivity and the intense absorption ($\epsilon_{\text{max}} = 10^4 \text{ M}^{-1} \text{ cm}^{-1}$) of its radical anion in the visible region of the spectrum ($\lambda_{\text{max}} \sim 720 \text{ nm}$). In this study anthracene was added to DMSO at various concentrations up to its solubility limit, 0.02 M. The solutions were prepared just prior to irradiation since it was observed that solutions containing anthracene "aged" on standing in the fluorescent room lighting for a day or more, probably producing the anthracene photodimer, which caused a long lived transient to be formed in the region 450-800 nm upon irradiation.

In taking the absorption spectrum of the radical anion (A^-) and evaluating its absorbance, it was necessary to make corrections for the DMSO positive ion and the solvated electron, both of which absorb to some extent in the same region. The absorption spectra of these latter two transients had already been determined and consequently the corrections were relatively easy to apply because A^- does not absorb at 550 nm (the DMSO^+ peak) nor at 1275 nm (where e_s^- absorbs strongly). The contributions of these two species at each wavelength were simply subtracted from the total observed end of pulse absorbance. The split-beam optical method was used to normalize the three spectra.

The spectrum of A^- obtained in this manner for 0.02 M anthracene in DMSO is shown in Figure 36, where it can be seen that $\lambda_{\max} = 750$ nm. Figures 37 and 38 show the oscilloscope traces at 750 nm for 0.001, 0.005, 0.01 and 0.02 M anthracene in DMSO. For all traces shown, the contribution from the positive ion decreases only slightly over the time period shown since its half-life is > 2 μ sec. At the lowest concentration, the contribution made by the short lived solvated electron can readily be observed.

From these traces it can be deduced that the absorbance due to A^- consists of two components, one of which builds up during the pulse and is larger at the higher concentrations and the other which builds in after the pulse with a rate of growth which increases with the anthracene concentration. Furthermore, it is clear from Figure 37(b) that the slow component builds in at a much slower rate than the electron decays, which strongly suggests that the anthracene is scavenging both the solvated electron and the reducing species resulting from the electron decay, either the DMSO radical anion or its decomposition product. Thus the scavenging reactions may be written as



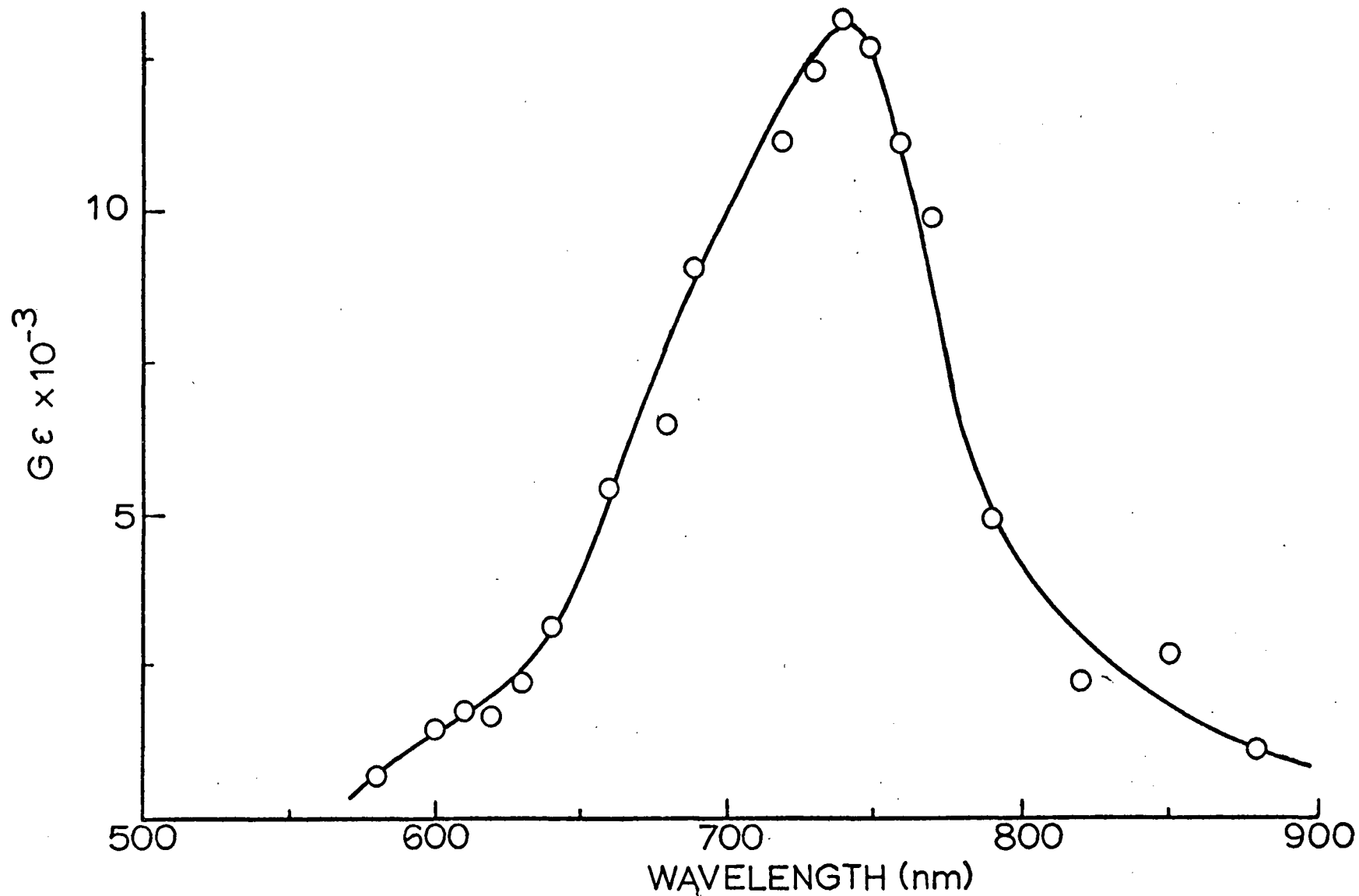


Figure 36. End of pulse absorption spectrum of the anthracene radical anion obtained from a DMSO solution 0.02 M in anthracene after absorbances due to the electron and oxidizing species had been subtracted.

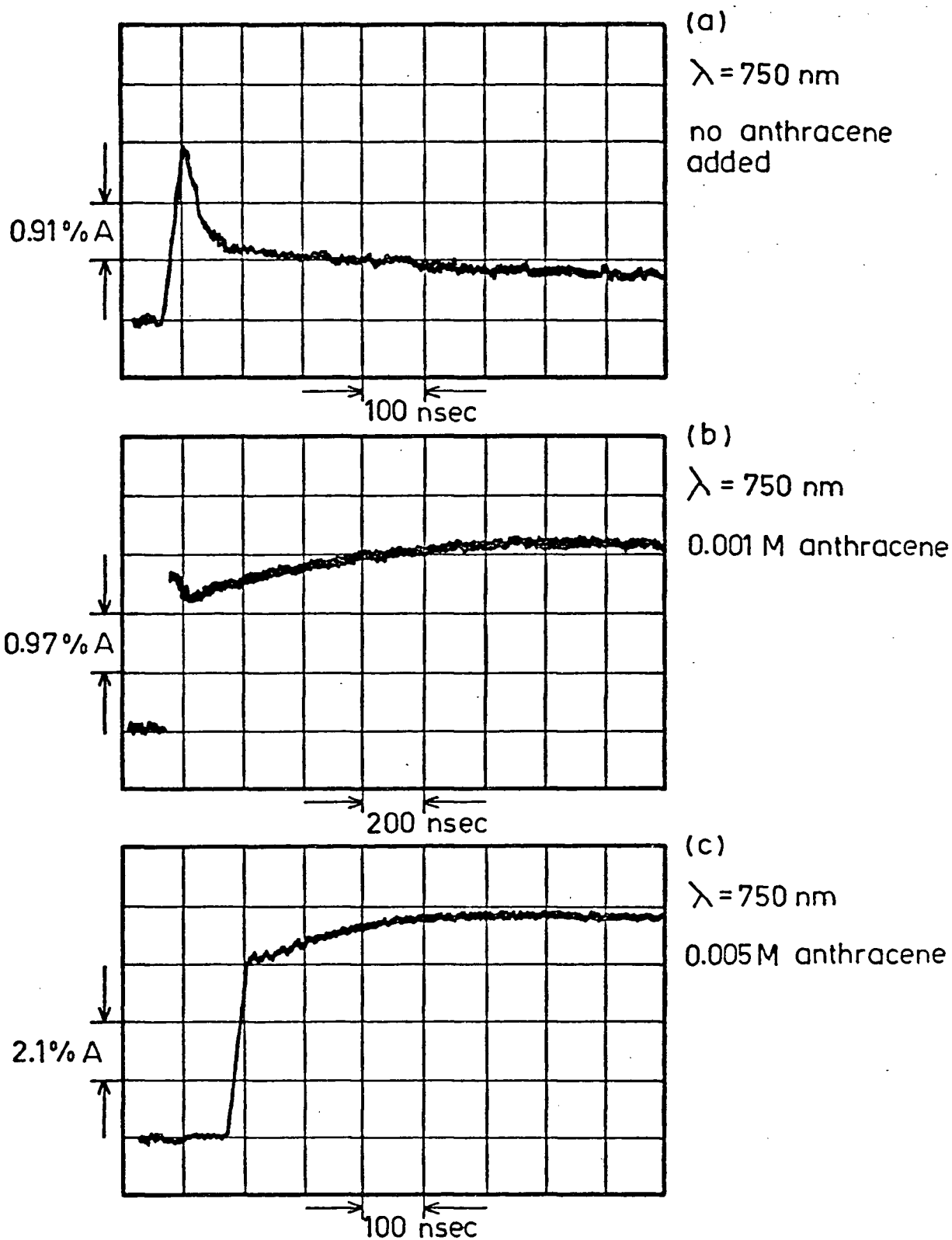


Figure 37. Typical oscilloscope traces showing the decay of the electron and build up of the anthracene radical anion at 750 nm. (a) no anthracene added; (b) 0.001 M anthracene in DMSO; (c) 0.005 M anthracene in DMSO.

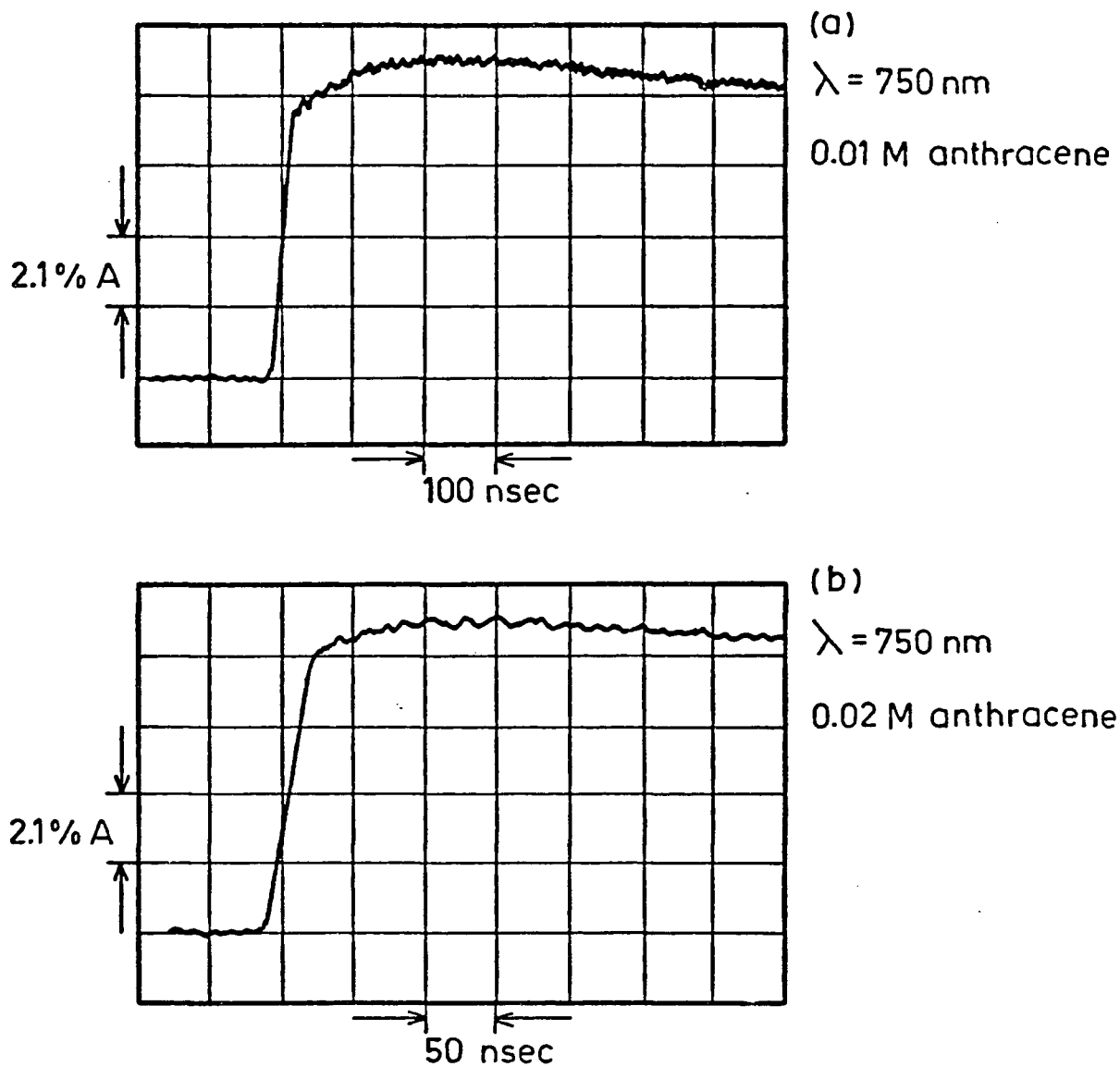


Figure 38. Typical oscilloscope traces showing the build up and decay of the anthracene radical anion at 750 nm. (a) 0.01 M anthracene in DMSO; (b) 0.02 M anthracene in DMSO.

where S is the solvent medium and S^- is the radical anion or its decomposition product.

Figure 39 shows how the absorbance observed immediately at the end of pulse (curve 2) and the maximum absorbance observed after the pulse (curve 1) of A^- at 750 nm vary with the anthracene concentration. The immediate absorbances were corrected for the positive ion and electron contributions at 750 nm by measuring their respective absorbances at 550 nm and 1275 nm and applying the appropriate correction factor according to $\epsilon_{750}/\epsilon_{550}$ and $\epsilon_{750}/\epsilon_{1275}$. The electron absorbance was monitored at 1275 nm using the split-beam optical method. The maximum absorbances were obtained by extrapolating the decaying portion of the absorbance back to the end of the pulse. The decay of the positive ion, obtained at 550 nm and using the correction procedure described above, was added to the observed decay at 750 nm so that the true A^- build up and decay could be obtained.

The effect of the anthracene on the yields of the positive ion (curve 3) and the solvated electrons (curve 4) are also shown in Figure 39. The slight increase in the positive ion yield may be due to the scavenging of electrons or other reducing species which were otherwise doomed to recombination with the cation. Nevertheless, the fact that the yield of the positive ion was not decreased nor was its decay rate appreciably increased, suggests that part of the absorbance attributed to A^- cannot be due to the presence of anthracene cations, A^+ , as has been suggested in some other systems.^{70,71} The anthracene cation is believed to have a very similar extinction coefficient and absorption spectrum as its anion counterpart and is formed through

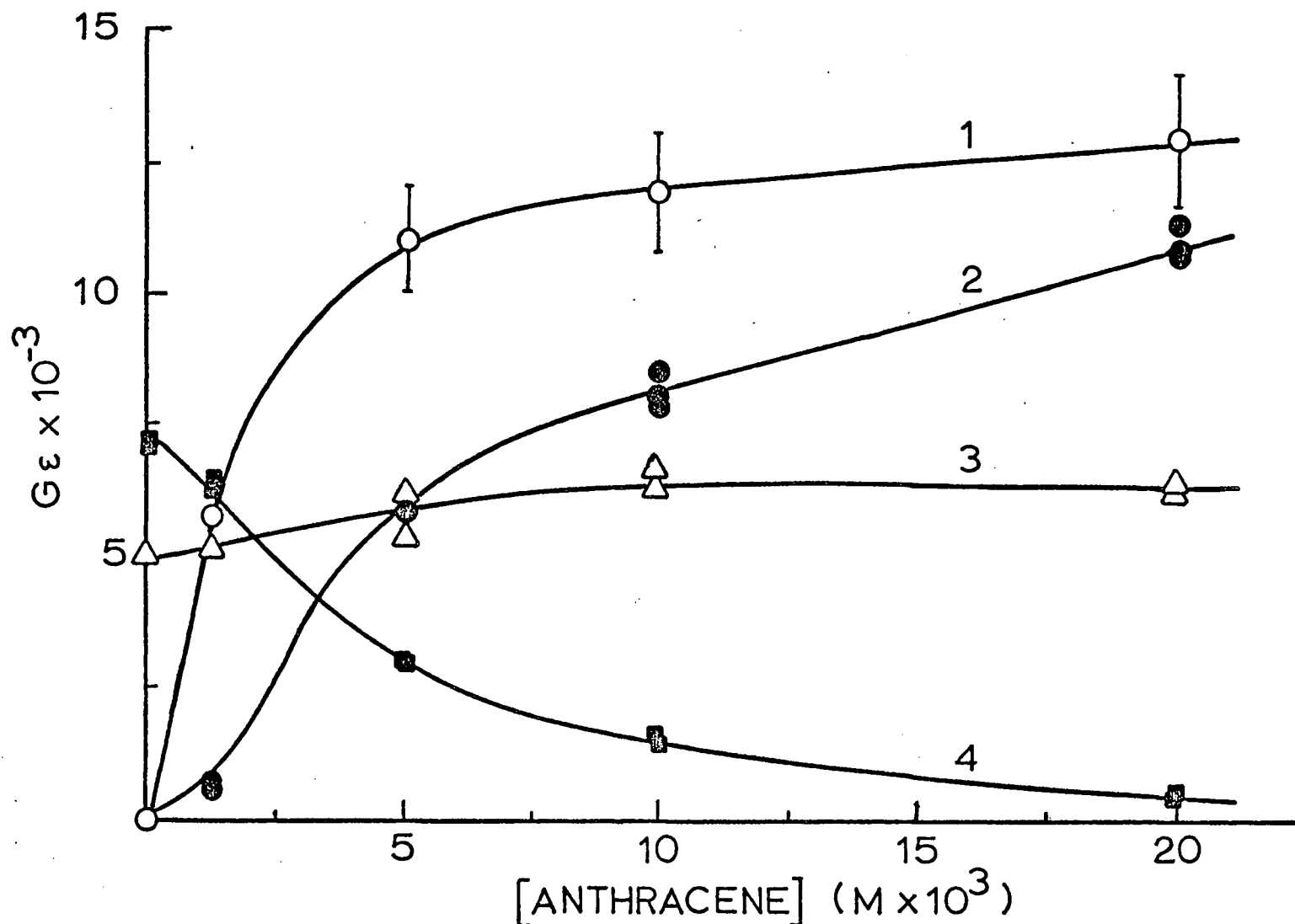


Figure 39. Graph showing the scavenging of solvated electrons in pure DMSO by anthracene and the formation of anthracene radical anions. ●, absorbance at 750 nm due to A⁻ immediately at the end of the pulse; ○, maximum in the absorbance at 750 nm due to A⁻ after the pulse; △, absorbance due to the positive ions at 550 nm; ■, absorbance due to solvated electrons at 1275 nm (not corrected for decay during the pulse nor for the detector response time).

charge transfer with the primary oxidizing species in some media.

In the previous studies on DMSO,^{34,64} anthracene was used at a concentration of 0.005 M. As can be seen from Figure 39, anthracene at 0.005 M reduced the observable yield of e_s^- to about 50% of its yield in the pure system although it then scavenged the decay product of most of these unscavenged electrons. By assuming the extinction coefficient of A^- at λ_{\max} (750 nm) to be $1.0 \times 10^4 \text{ M}^{-1} \text{ cm}^{-1}$, as used previously,^{34,64} it can be calculated that the yield immediately at the end of the pulse is $G(A^-) = 0.6$. This then increased to $G(A^-) = 1.1 \pm 0.1$ due to the slower component of the scavenging process. Hayon's³⁴ value of 1.62 is much larger than this but is probably in error because it was not corrected for the significant absorbance by the positive ions at the wavelength used (720 nm) to determine $G(A^-)$. Indeed addition of the two absorbances at this wavelength gives an "effective" G of 1.4 ± 0.1 , assuming $\epsilon_{720}/\epsilon_{550} = 0.48$ for the DMSO positive ion. On the other hand Koulkes-Pujo et al.⁶⁴ obtained a much lower yield, $G(A^-) = 0.64$, which is more difficult to reconcile with the data obtained in this study. Their yield was obtained by irradiating a solution of 0.1 M in Br^- (to scavenge the oxidizing species) and 0.005 M in anthracene. When a DMSO solution which contained 0.1 M Br^- and 0.02 M anthracene was irradiated, the anthracene anion yield was reduced by about 40%, to $G(A^-) = 0.8$, from what it was without the addition of Br^- , despite the fact that the electron was completely eliminated. However the chemistry must be rather different in this mixture because a white precipitate was produced at the end of the irradiation. For the reasons mentioned earlier, however, this decrease in absorbance at 750 nm in the presence of Br^- is thought not

to arise from the presence of A^+ contributing to the 750 nm absorption.

Thus the yield of free ions in DMSO, as obtained from $G(A^-)$ at 0.02 M, is calculated to be 1.3 ± 0.15 , assuming $\epsilon_{\max}(A^-) = 1.0 \times 10^4 \text{ M}^{-1} \text{ cm}^{-1}$. At 0.02 M anthracene, the solvated electron yield was reduced by about 90%, as shown in Figure 39, the remaining 10% being scavenged as the solvent anions or their decomposition product. However, even at this concentration the total yield of A^- is not entirely independent of the anthracene concentration, as evidenced by the lack of a good scavenging plateau. Perhaps at 0.02 M some intraspur scavenging occurs.

From $G(e_s^-) = 1.3$ one calculates that $\epsilon_{1500 \text{ nm}}$ for the solvated electron band in DMSO is about $14,000 \text{ M}^{-1} \text{ cm}^{-1}$. If $G\epsilon_{\max}$ for e_s^- in DMSO is ~25% greater than $G\epsilon_{1500 \text{ nm}}$, then ϵ_{\max} is presumably of the order of $17,000 \text{ M}^{-1} \text{ cm}^{-1}$.

In view of the difference in the free ion yield of reducing species obtained from the nitrous oxide steady state experiments and anthracene pulse radiolysis experiments, it was imperative that the yield of the positive ion (or primary oxidizing species) be determined. Br^- ions have been used in aqueous systems as a scavenger for oxidizing species such as the $\cdot\text{OH}$ radicals and possibly also H_2O^+ . It is very convenient because the transient product, the Br_2^- ion, has a strong optical absorption around 360 nm.⁷²⁻⁷⁶ Consequently KBr was selected as a positive ion scavenger in DMSO and used at various concentrations ranging from 0.001 to 0.1 M.

At $[\text{Br}^-] > 0.01 \text{ M}$ the absorption band centered at 550 nm was completely eliminated indicating complete scavenging of the free positive

ions and a new absorption band centered at 375 nm was produced. On account of its similarity to the Br_2^- spectrum in water the new band was attributed to this species. The spectrum attributed to the Br_2^- ion at two concentrations of Br^- is shown in Figure 40. The inset of Figure 40 shows the absorbance of Br_2^- at 375 nm as a function of the concentration of Br^- presented on a semi-log plot. Even at the highest concentration studied, $[\text{Br}^-] = 0.1 \text{ M}$, the electron absorption band was unaltered which suggests that the Br^- ion did not interfere with geminate recombination. The concentration independent value of $G\epsilon_{375 \text{ nm}} = 15 \times 10^3 \text{ ions (100 eV)}^{-1} \text{ M}^{-1} \text{ cm}^{-1}$ for $[\text{Br}^-] > 0.01 \text{ M}$ was identical to that reported by Koulkes-Pujo et al.⁶⁴ If one assumes that the ϵ_{max} for Br_2^- in DMSO is the same as the recently reported value for Br_2^- in water,⁷⁶ namely $1.2 \times 10^4 \text{ M}^{-1} \text{ cm}^{-1}$, then one calculates $G(\text{Br}_2^-) = 1.3 \pm 0.1$. This value should be compared to that obtained by Kemp et al.⁷⁷ in which the positive ions were scavenged using 0.01 M TMPD (N,N,N',N'-tetramethyl-p-phenylenediamine). $G(\text{DMSO}^+) = 1.7$ was calculated from the yield of TMPD^+ which is somewhat larger than the value obtained here.

Several interesting features arose from the study of the KBr solutions in DMSO. From the oscilloscope traces in Figure 41 it can be seen that at $[\text{Br}^-] = 0.01$ or 0.001 M , the absorption at 365 nm did not grow in during the 40 nsec pulse. Instead a short-lived transient absorption was observed whose spectrum is centered at 450-500 nm (see Figure 40). This transient could not be confused with the solvent cation because its absorption was almost zero at 650 nm in a 0.001 M KBr

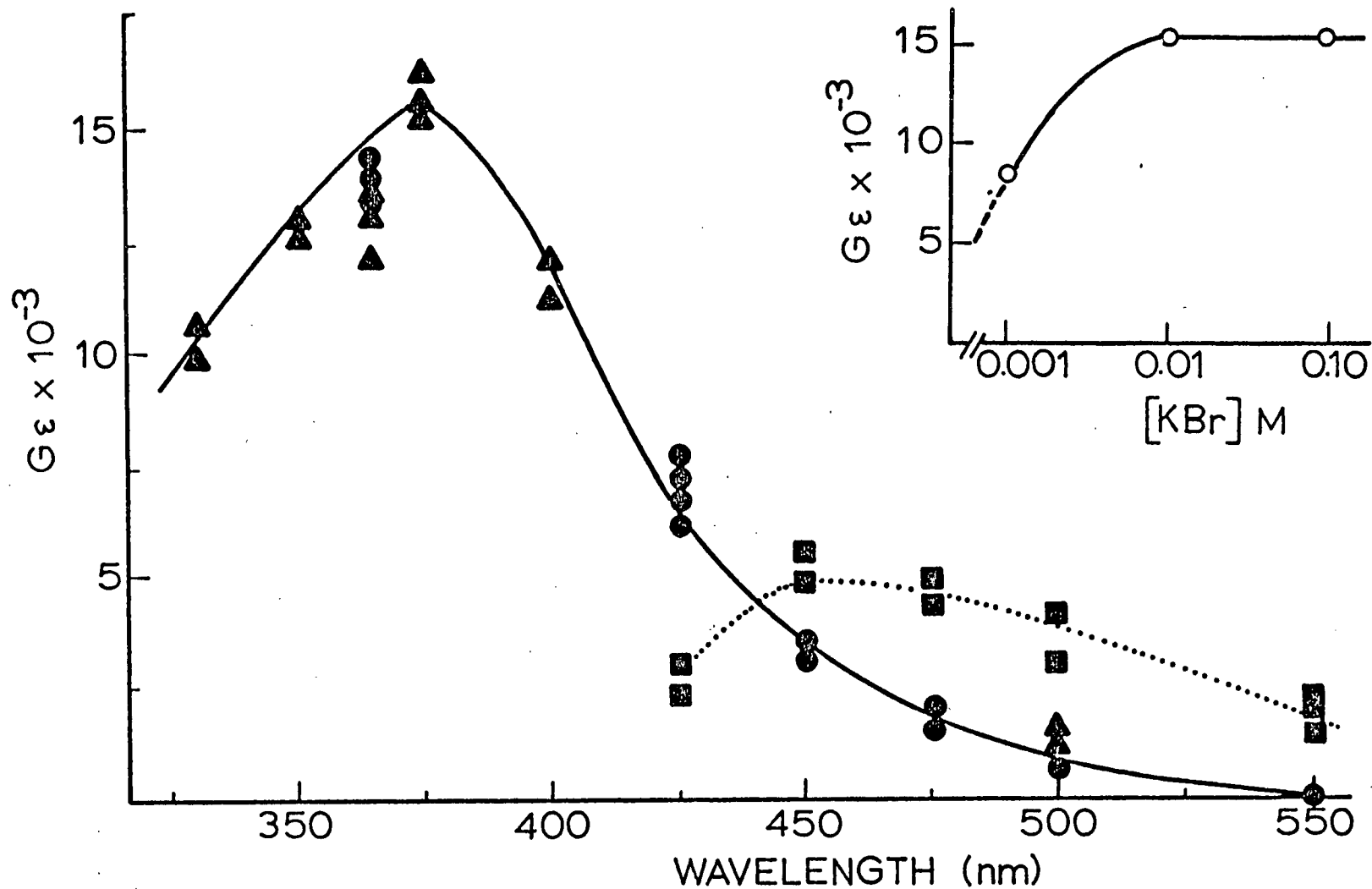


Figure 40. Absorption spectra for KBr solutions in DMSO. Solid curve refers to Br_2^- spectra; the dotted curve refers to the transient precursor of Br_2^- . \blacktriangle , Br_2^- from 0.1 M KBr solution; \bullet , Br_2^- from 0.01 M KBr solution; \blacksquare , transient precursor of Br_2^- at 0.01 M KBr. The inset is a plot of $G\epsilon$ at 375 nm for Br_2^- against $\log ([\text{Br}^-]/\text{M})$.

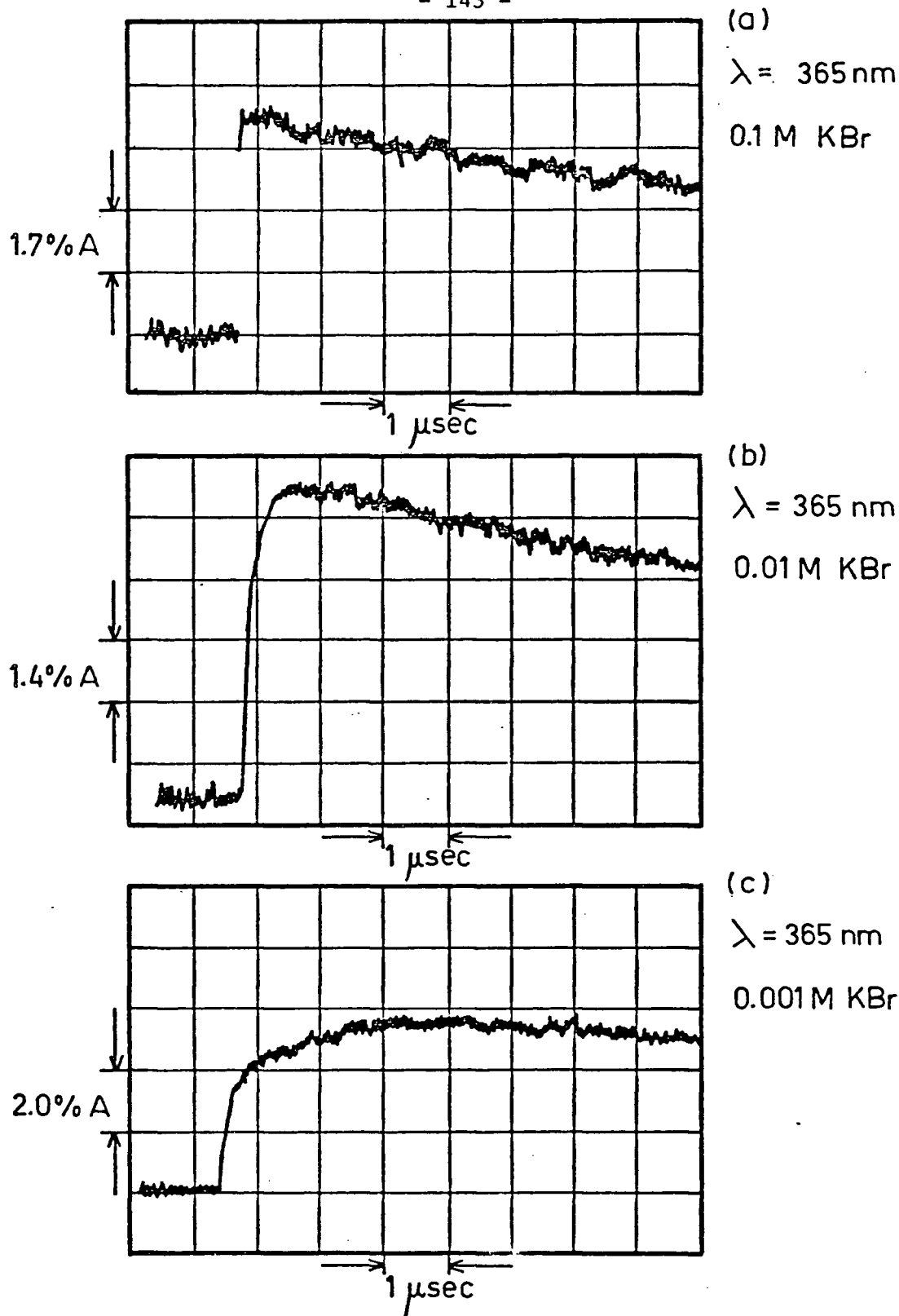
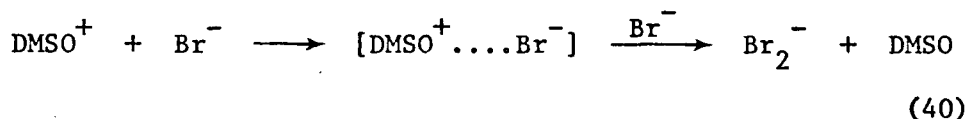


Figure 41. Typical oscilloscope traces showing the build up and decay of Br_2^- at 365 nm in pure DMSO. Detection made using the photomultiplier with a 470 ohm load resistor. (a) 0.1 M KBr; (b) 0.01 M KBr; (c) 0.001 M KBr.

solution. At this concentration, the transient decayed with a half-life of ~ 0.8 μsec , which was approximately the same rate at which the Br_2^- absorption at 365 nm grew in. This build up, shown in Figure 41(c), was observed to follow first-order kinetics as shown in Figure 42. In this plot D_t is the absorbance of Br_2^- at 365 nm at time t after the pulse and D_∞ is the maximum absorbance of Br_2^- attained after the build up. Since the build up and decay of Br_2^- at 0.001 M KBr were not well separated in time, D_∞ was obtained by extrapolating the decay curve back to the end of the pulse and taking the value of the absorbance on the extrapolation corresponding to time t . The pseudo first-order rate constant obtained from this plot, $k = (8.7 \pm 0.3) \times 10^5 \text{sec}^{-1}$, yields a second-order rate constant of $(8.7 \pm 0.3) \times 10^8 \text{M}^{-1} \text{sec}^{-1}$ for the reaction between the transient and Br^- to form the Br_2^- ion.

It is proposed that the decay of DMSO^+ and the formation of Br_2^- goes via a two step process, as shown below, with the second step being rate determining.



The transient intermediate centered at 450-500 nm is attributed to the charge transfer complex $[\text{DMSO}^+ \dots \text{Br}^-]$.

The transient complex is observed at the end of the 40 nsec pulse even in 0.001 M KBr, as shown in Figure 43, which suggests that the half-life of the DMSO positive ion is $< 10^{-11}$ seconds in 0.1 M KBr. Scavenging on this time scale should affect geminate recombination and

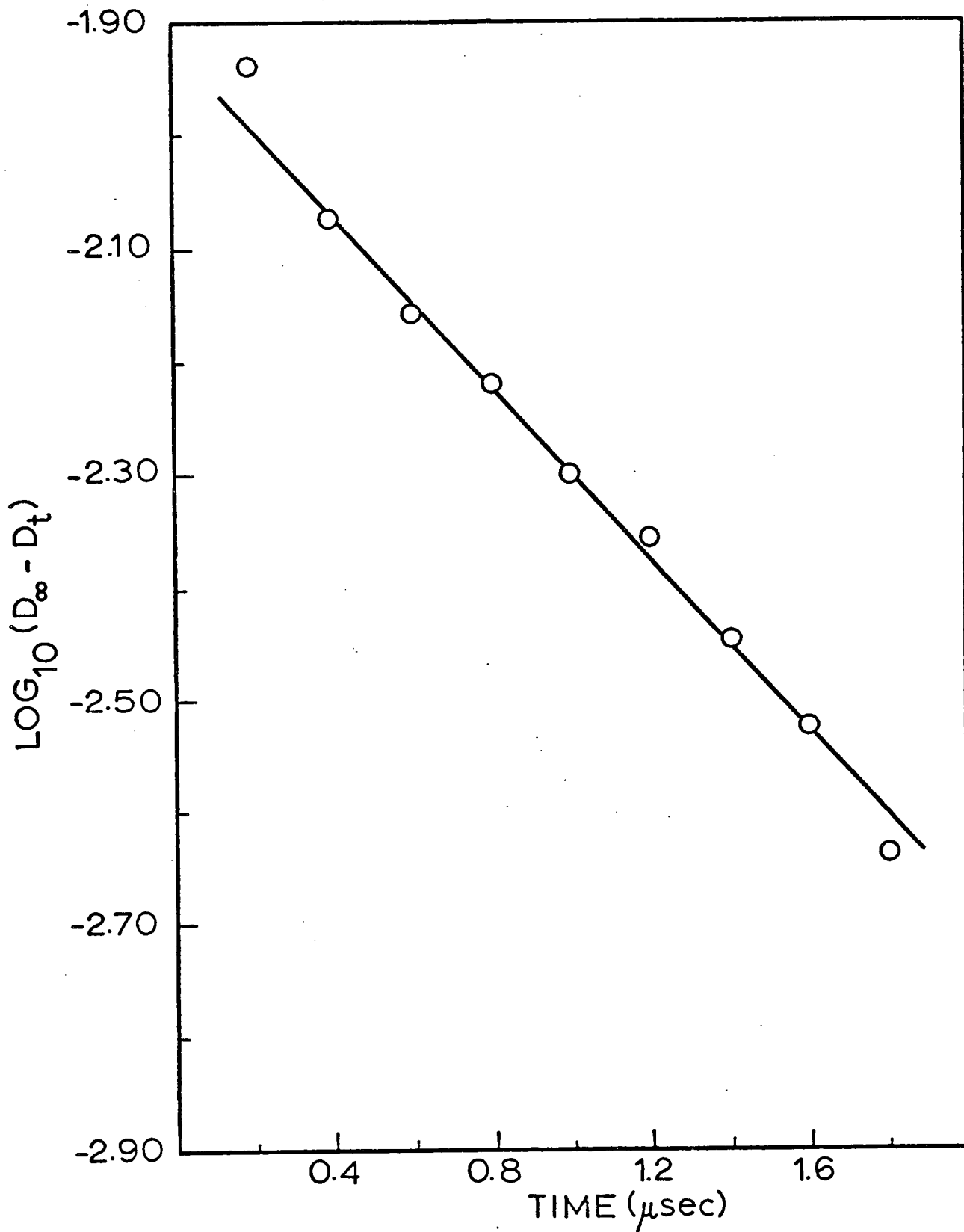


Figure 42. Plot showing first-order build up of Br_2^- (Figure 41(c)) for DMSO solution 0.001 M in KBr.

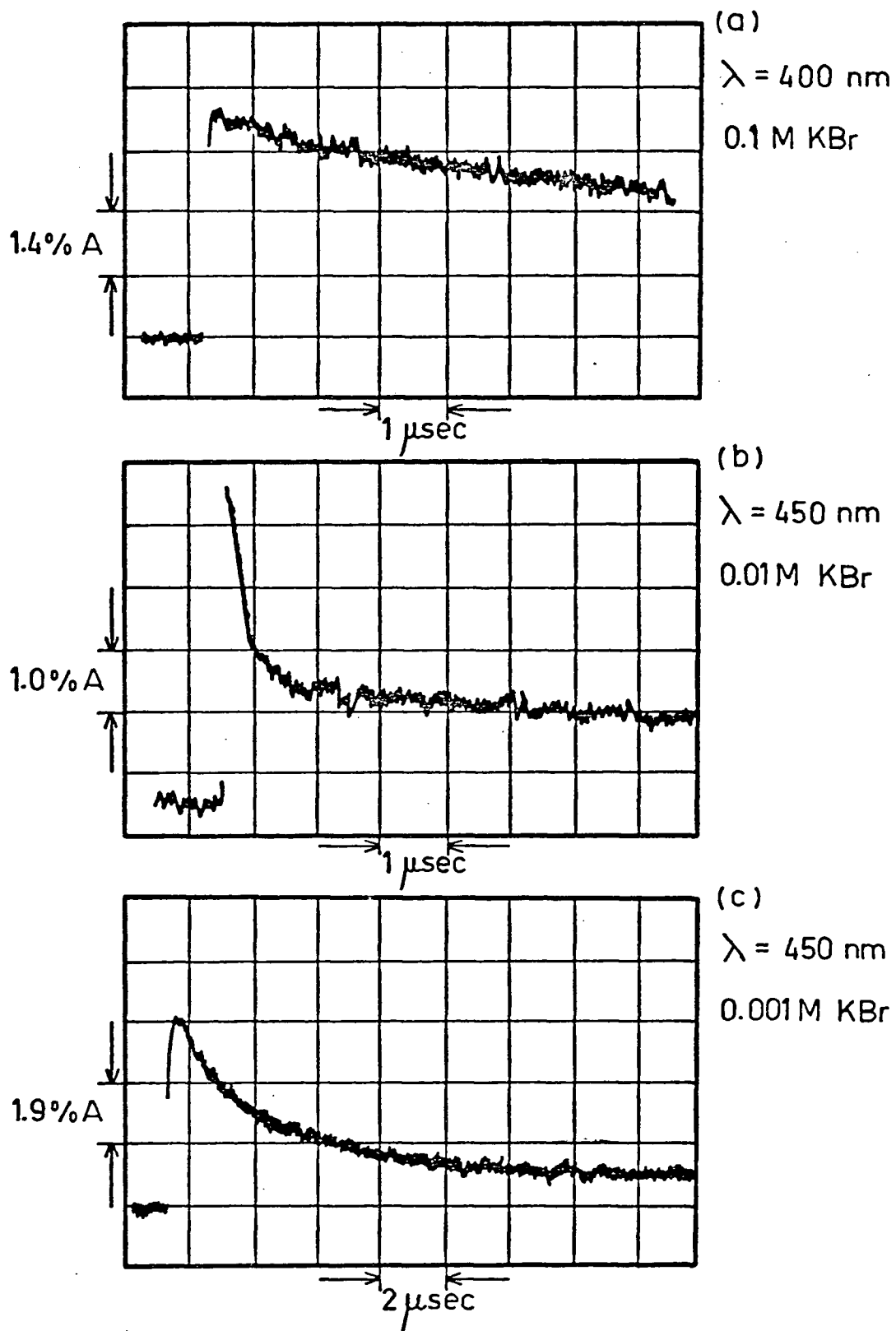


Figure 43. Typical oscilloscope traces showing the decay of Br_2^- and its transient precursor. The fast initial decay in (b) and (c) is attributed to the transient complex. Detection was made using the photomultiplier with a 470 ohm load resistor.

thereby increase the yield of e_s^- ; however no such increase was observed. This implies that the electron can react with the complex during an intra-spur decay process in the same manner as it does with the positive ion according to reaction (41),



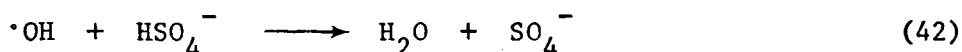
where DMSO^* is an excited DMSO molecule. From the second-order rate constant for the reaction between this complex and Br^- , $8.7 \times 10^8 \text{ M}^{-1} \text{ sec}^{-1}$, the half-life of this complex is evaluated to be $\sim 8 \text{ nsec}$ in 0.1 M KBr . This is too long to affect the recombination with the spur electron given in equation (41); consequently the yield of e_s^- is expected to be unchanged, as observed. However, the fact that the yield of Br_2^- has diminished by about 30% at 0.001 M implies that the charge transfer complex has an alternative fate, perhaps dissociation back into the Br^- ion and the positive ion. There is a trace of some transient species in the wavelength region where the positive ion absorbs which is too long-lived to be either the electron or the transient complex. This species could be the positive ion itself or else it must be attributed to yet another transient species.

So far it has been assumed that the oxidizing species observed to have an absorption band centered at 550 nm is the DMSO positive ion. However, the results are compatible with this transient being some other oxidizing species, perhaps either a free radical or other cation produced by the rapid decomposition of DMSO^+ . In any event it seems clear that $G(\text{oxidizing species}) = 1.3$, in which case ϵ_{max} for the 550 nm band is $3500 \text{ M}^{-1} \text{ cm}^{-1}$.

Thus, from the pulse radiolysis studies, it transpires that the yield of primary reducing species (e_s^-) and oxidizing species (probably DMSO^+) are identical, being 1.3 ± 0.1 . This yield can hence be equated to the free ion yield in DMSO.

3. Geminate Ion Scavenging

At high concentrations of H_2SO_4 , which is an efficient electron scavenger, the electron band was completely eliminated but the band centered at 550 nm was found to be increased markedly. This is attributed to the scavenging of electrons which were otherwise doomed to geminate recombination with their concomitant partner; consequently the positive ion yield is increased. The increase in absorbance for a DMSO solution containing 0.2 M H_2SO_4 is shown in Figure 44 and is similar to that reported previously using 0.1 M H_2SO_4 .⁶⁴ In addition, a long-lived transient having an absorption centered at 450 nm with $G\epsilon \sim 10^3$ mols. (100 eV)⁻¹ M⁻¹ cm⁻¹ at its λ_{max} was also observed. This transient is thought to be the sulfate radical anion, SO_4^- , which is known to be formed in the pulse radiolysis of aqueous sulfuric acid systems.⁷⁸⁻⁸⁰ In the aqueous system it is thought to arise from



In DMSO it may arise from the methyl radicals according to reaction (43) since the methyl radical yield is high ($G(\text{CH}_3\cdot) > 3$).



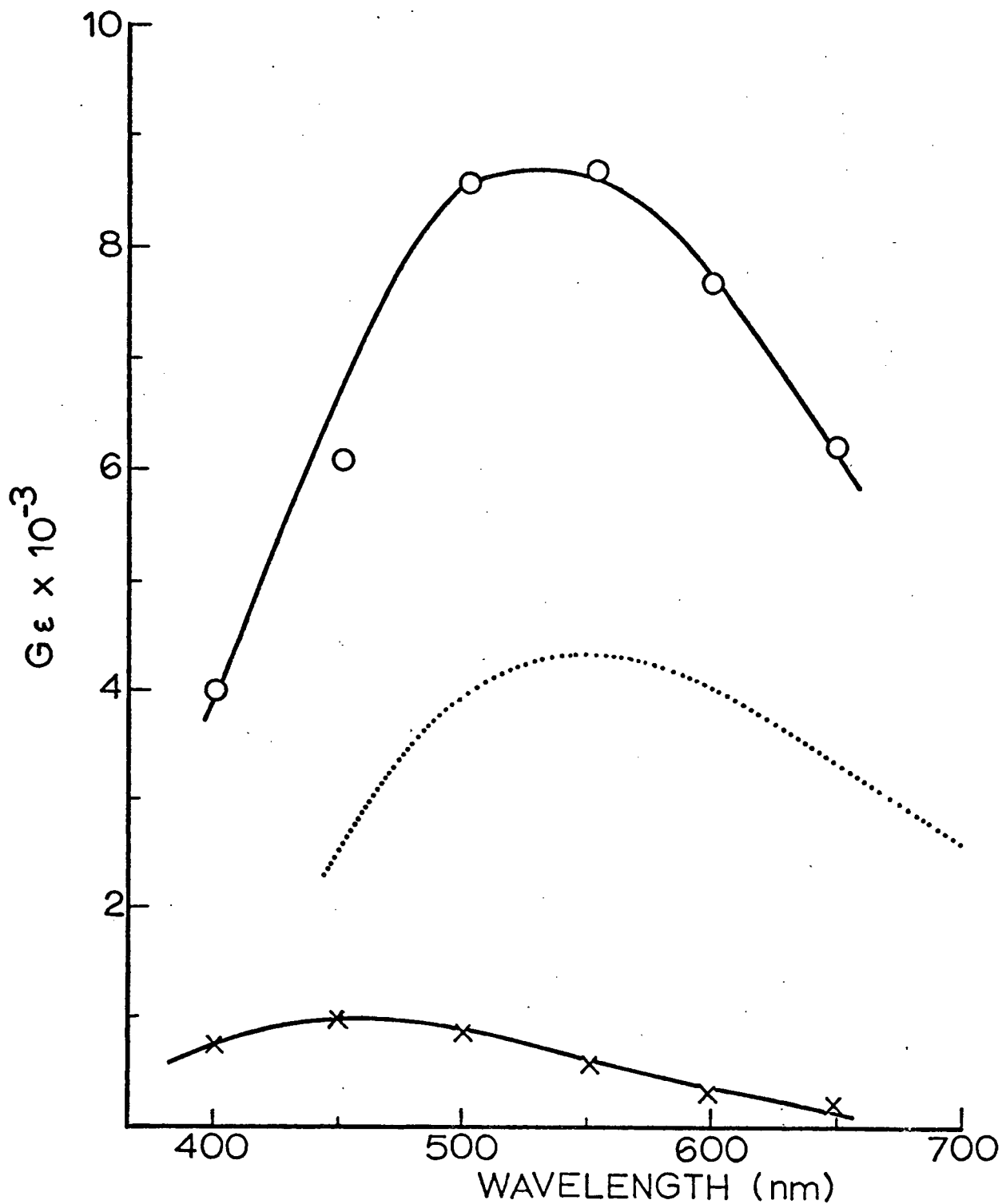


Figure 44. End of pulse absorption spectrum of the DMSO positive ion [O] in 0.2 M H_2SO_4 . The dotted line refers to the absorbance of the positive ion in pure DMSO. X refers to the long-lived SO_4^- intermediate produced in the acid solution.

When corrections for the decay of this sulfate radical anion were applied, it was noted that the DMSO positive ion decays by a first-order process with almost the same half-life (2.5 μsec) and rate constant ($2.7 \times 10^5 \text{sec}^{-1}$) as it did in pure DMSO (see Figure 45). Typical oscilloscope traces showing the decay of the positive ion and the long-lived SO_4^- radical anion are presented in Figure 46.

The absorption spectrum obtained for a DMSO solution containing 0.5 M Ag^+ is shown in Figure 47. By analogy with aqueous systems⁸¹⁻⁸³ the absorption maximum at $\lambda < 330 \text{ nm}$ is attributed to the silver atom formed by the reaction



However at $\lambda > 350 \text{ nm}$ it appears that there is absorption from other species in addition to DMSO^+ , possibly one centered at 400-500 nm. In contrast to the H^+ system discussed above, the absorbances in the range 320-700 nm were all much longer lived with first half-lives $> 100 \mu\text{sec}$. The decay kinetics were neither first-order nor second-order. Although a variety of silver ion adducts, such as Ag_2^+ and Ag_3^+ , are known to be formed in the pulse radiolysis of aqueous silver solutions, they are not known to absorb at $\lambda > 400 \text{ nm}$. It is possible that the peak centered at 400-500 nm is due to a complex of the DMSO^+ ion and a silver atom or other silver aggregates. Because the absorbances were not well separated in time, it is not possible to state whether the oxidizing species responsible for the 550 nm band in pure DMSO existed as such in these silver solutions.

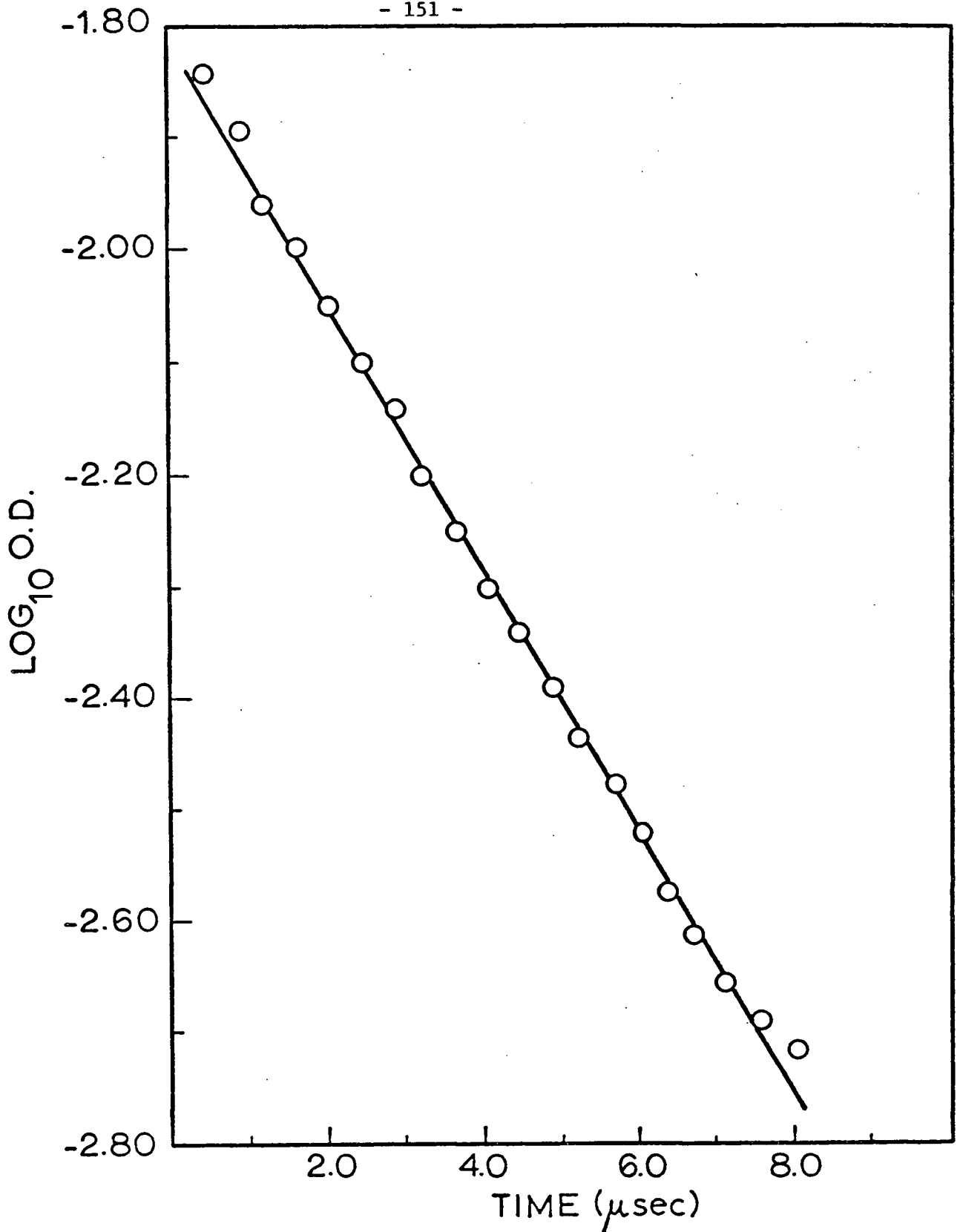


Figure 45. First-order decay plot of the DMSO positive ion in the presence of 0.2 M H₂SO₄. Decay measured at 550 nm using the photomultiplier with a 470 ohm load resistance.

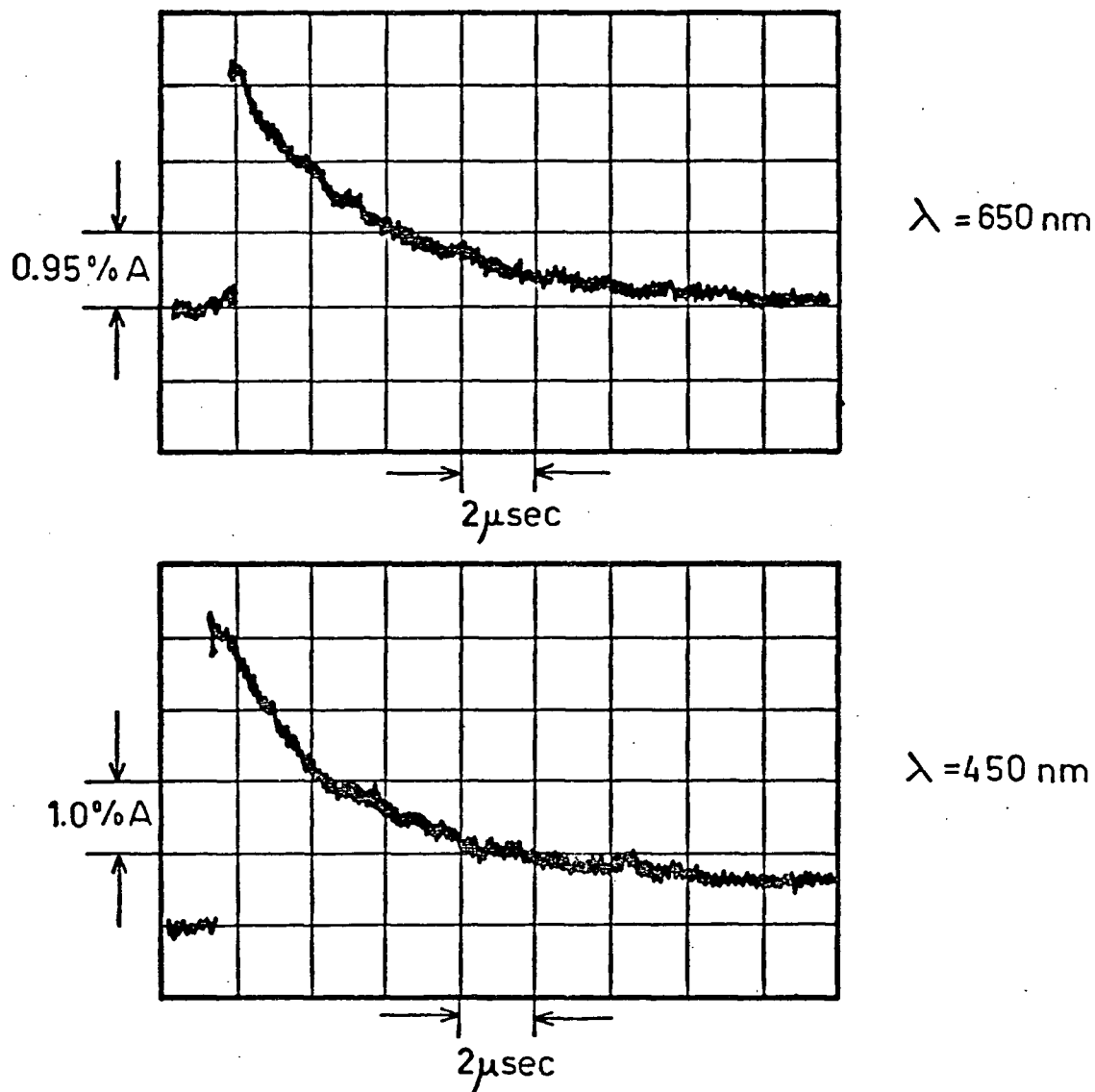


Figure 46. Typical oscilloscope traces showing the decay of the DMSO positive ion in the presence of $0.2 \text{ M H}_2\text{SO}_4$ at 650 nm and 450 nm . The longer-lived SO_4^- transient is readily observed at 450 nm .

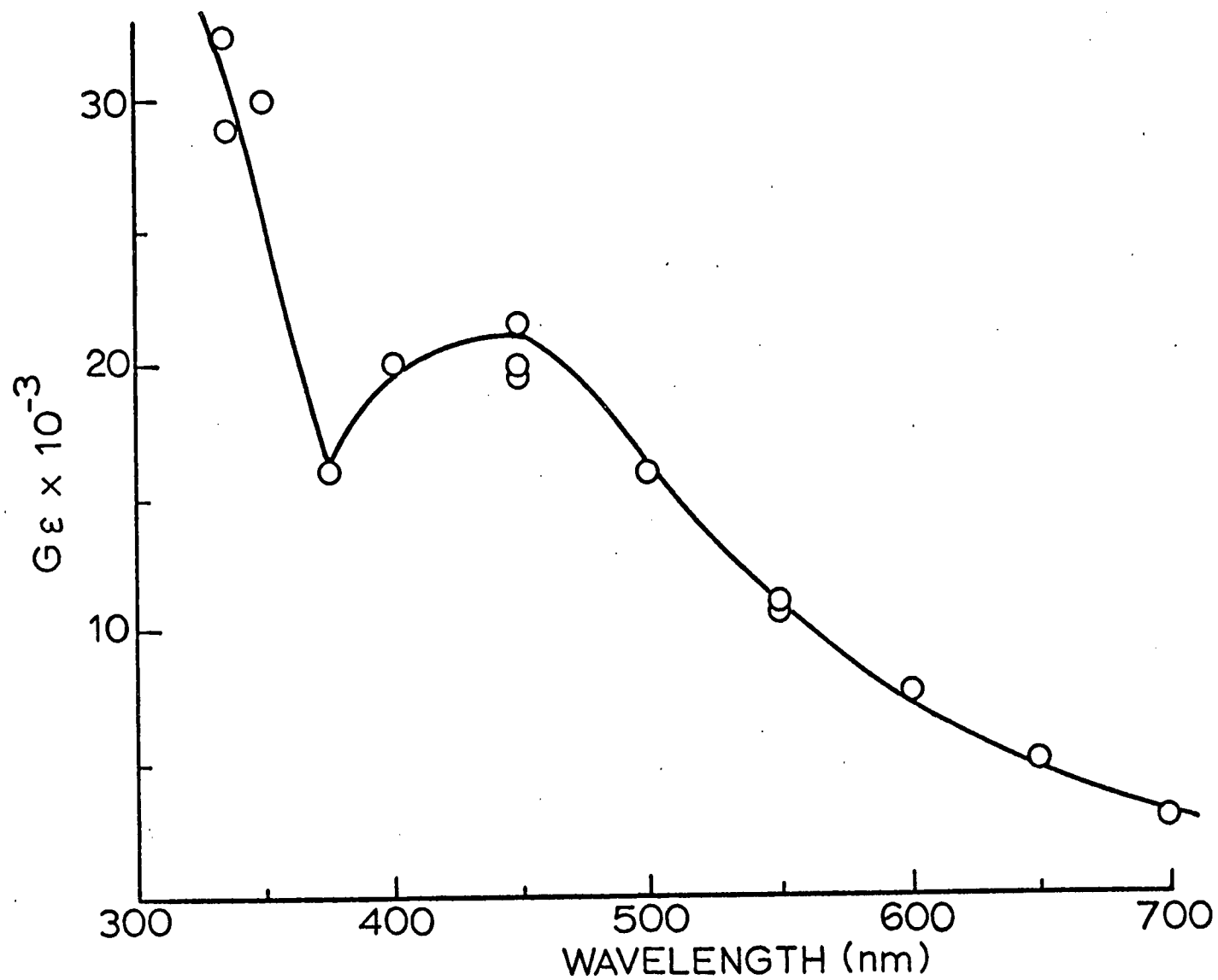


Figure 47. End of pulse spectrum of transients produced in a DMSO solution 0.5 M in Ag^+ .

4. Dielectric Constant and Electron Stabilization

The yield of free ions in DMSO, $G(\text{free ion}) = 1.3 \pm 0.1$, appears to be consistent with its relatively high dielectric constant and the empirical relationship shown in Figure 7. This would suggest that the static dielectric constant is the major factor determining the free ion yield in DMSO. On the other hand, the absorption maximum of the solvated electron is at $\lambda > 1500$ nm, corresponding to an optical transition energy < 0.8 eV. In this respect DMSO behaves like a saturated hydrocarbon towards electron solvation and suggests that the solvating power of the medium plays the dominant role in electron stabilization. The nature of these weak ion-dipole forces solvating the electron may be due to the inability of the DMSO molecules to align their dipoles for maximum interaction with the electron or due to a large cavity radius. In polar protic media, the positive charge is localized on the hydrogen atom and is able to fit more closely about the negative centre whereas in DMSO the positive charge due to the $S \rightarrow O$ dipole is shielded by the two methyl groups. Furthermore, the bulky methyl groups will prevent an optimum orientation of the dipoles around the electron, as well as producing a large void, so that the polarization potential would be considerably less than if there was no steric hinderance. It is also interesting to note that the correlation curve in Figure 6 gives a cavity radius $> 3.3 \text{ \AA}$ for the electron in DMSO based on $h\nu_{\text{max}} < 0.8$ eV.

The data suggest, therefore, that the electrostatic interactions are not the same in solvents of equivalent dielectric constant and that electron stabilization occurs through specific interactions as

governed by the microscopic properties of the medium. The electrons are still to be regarded as being stabilized by ion-dipole interactions, but the extent of this interaction is related to the intrinsic properties of the solvent, such as the molecule shape, size, type of functional groups, dipole moment and so forth, and not solely to the macroscopic dielectric constant of the continuum.

CHAPTER IV

PULSE RADIOLYSIS OF DMSO-WATER BINARY MIXTURES

In the previous chapter it was shown that the electron in DMSO is very weakly trapped as indicated by its absorption band in the near infrared with a $\lambda_{\text{max}} > 1500$ nm. On the other hand, polar protic solvents, such as water and the alcohols, are characterized by electron absorption bands in the visible region. This is in keeping with their ability to solvate negative ions through strong ion-dipole interactions and hydrogen bonding. The electron is regarded as being stabilized through interaction with several molecules so that studies on the absorption spectra, and yields, of electrons solvated in binary mixtures are of interest, particularly when the extent and manner of solvation differ markedly in the individual components. As mentioned in the Introduction, studies have been attempted on binary mixtures of alcohols or water with aprotic hydrocarbons^{40,41} or ethers.^{39,43,44} However these were not ideal combinations since they formed very inhomogeneous mixtures on the microscopic scale. This resulted in aggregates of the polar hydroxylic solvent acting as scavenging centers for electrons which would otherwise have been lost through geminate recombination in the aprotic component. Consequently, both the yield and optical properties of the solvated electrons were dominated by the polar component.

DMSO would appear to be a model hydrocarbon-like solvent for studying such binary mixtures. Unlike the aprotic solvents mentioned above it has a high free ion yield, comparable to that of the hydroxylic solvents. As a result, the scavenging of geminate ions by polar aggregates should not be a dominant factor. Furthermore, DMSO is completely miscible with water in all proportions; in fact DMSO-water mixtures show more intermolecular structure than is present in either of the pure liquids.⁸⁴⁻⁹²

1. Solvated Electrons

In DMSO-water binary mixtures two easily resolvable bands were observed for wavelengths > 400 nm. As in pure DMSO, the longer-lived band ($\tau_{1/2} \sim 2$ μ sec) was attributed to the DMSO positive ion and was centered at 550 nm for all mixtures. The other band was assigned to the solvated electron and was very short-lived ($\tau_{1/2} < 25$ nsec). The λ_{\max} of the electron band shifted from that in pure water ($\lambda_{\max} = 720$ nm) to that in pure DMSO ($\lambda_{\max} > 1500$ nm) with increasing DMSO concentration. In each mixture only a single electron band was observed. The lack of "shoulders" or broadening in the bands suggest that these spectra are not the result of a simple combination or overlap of the e_{aq}^- and e_{DMSO}^- absorbances. To prove this a series of representative spectra at various concentrations were constructed based on simple band overlap but the resultant spectra did not agree at all with the observed spectra. Furthermore, simple combination of the two spectra would require free "icebergs" of DMSO and water molecules in the milieu which is unlikely in view of the strong intermolecular interactions exhibited by the two components.

Figure 48 shows the spectra for the solvated electron in mixtures consisting of 0, 0.20, 0.28, 0.43, 0.72, 0.93 and 1.0 mole fraction DMSO. The spectra were all taken using 40 nsec pulses. They have not been corrected for decay during the pulse nor for the response time of the detection apparatus; but the contributions from the DMSO positive ions were deduced by extrapolation to the end of the pulse from times > 100 nsec when the electron band had fully decayed, and these have been subtracted. The absorption band of the hydrated electron, with $G\epsilon = 4.3 \times 10^4$ mols. $(100 \text{ eV})^{-1} \text{M}^{-1} \text{cm}^{-1}$ at λ_{max} (720 nm), corresponds closely to the published spectrum of e_{aq}^- .⁹³ The solvated electron decay followed good first-order kinetics in all binary mixtures. In pure water the kinetics were a mixture of first- and second-order and were not analyzed further although the mean lifetime was $> 10^{-6}$ sec. Decay plots for e_{s}^- were obtained using 10 nsec pulses and followed at $\lambda > 1000$ nm where the contribution of the positive ion was negligible for all mixtures. As in pure DMSO, the solvated electron is thought to decay by reacting with DMSO. The pseudo first-order rate constants thus obtained are expressed as half-lives (column 6) in Table IV. This table also records the observed λ_{max} , the width-at-half-height in energy units, ΔW , and the observed end of pulse absorbance, $G\epsilon_{\text{max}}$ (obs) of the solvated electron band for each of the mixtures. A second-order rate constant was calculated for each mixture by combining the observed first-order rate constant with the bulk concentration of DMSO. These are given in column 7 of Table IV and are observed to be fairly constant at $4.5 \times 10^6 \text{ M}^{-1} \text{sec}^{-1}$. This is somewhat higher than that for pure DMSO and for the dilute

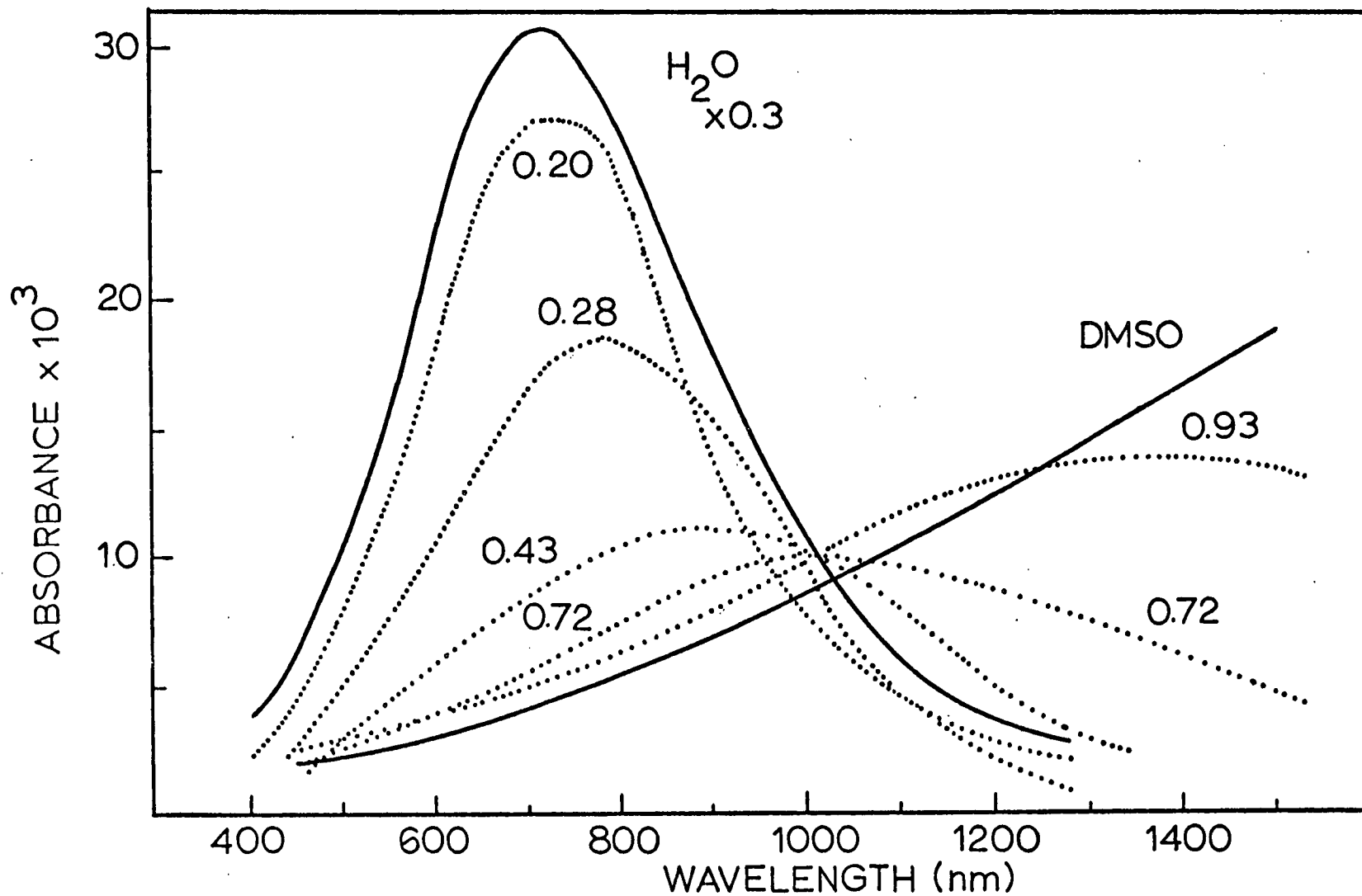


Figure 48. Absorption spectra of solvated electrons in DMSO-H₂O mixtures; 0, 0.20, 0.28, 0.43, 0.72, 0.93 and 1.0 mole fraction DMSO. Data points were obtained at 50 nm intervals. The data for pure water have been multiplied by a factor of 0.3 relative to the others.

TABLE IV. Summary of data obtained from studies on pulse irradiated DMSO-water mixtures at room temperature.

Mole Fraction							
DMSO	D_s^a	λ_{\max} (nm)	ΔW (eV)	$G\epsilon_{\max}(\text{obs})$ ($\times 10^{-3}$)	$t_{1/2}$ (nsec)	$k_2(\text{calc})^b$ ($M^{-1}\text{sec}^{-1}$)	$G\epsilon_{\max}(\text{corr})^c$ ($\times 10^{-3}$)
0	78	720	0.88	43.7	$>10^3$	--	43.7
0.017	78	--	--	--	340	2.9×10^6	--
0.20	75	750	0.76	11.0	22	4.5×10^6	20.5
0.28	73	800	0.83	7.22	19	4.4×10^6	14.8
0.43	67	900	0.97	4.24	15	4.5×10^6	10.2
0.72	57	1000	0.86	3.85	12	4.6×10^6	11.2
0.93	48	1350	>0.65	5.85	--	--	--
1.00	46	>1500	--	>7.44	14.5	3.4×10^6	>18.9

^a Data taken from references (84,85) for mixture temperature of 25°C.

^b Calculated from the observed pseudo-first order rate constant using bulk concentration of DMSO.

^c Corrected for decay during the pulse and response time of the detection system.

solution, 0.017 mole fraction DMSO (0.7 M in DMSO). The rate constant in this latter mixture, $2.9 \times 10^6 \text{ M}^{-1} \text{ sec}^{-1}$, is higher than the published values for the reaction of DMSO with hydrated electrons at concentrations up to and including 0.7 M DMSO in water ($k = 1.6 \times 10^6 \text{ M}^{-1} \text{ sec}^{-1}$).^{69,94}

The observed values, $G\epsilon_{\text{max}}$ (obs), were corrected for decay during the pulse and response time of the optical detection system using the same computational procedures mentioned previously. The values of $G\epsilon_{\text{max}}$ (obs) and $G\epsilon_{\text{max}}$ (corr) for e_s^- are plotted as a function of the mole fraction DMSO in Figure 49 and both are seen to pass through a minimum, the corrected one being more pronounced. This minimum may arise from a change in G, ϵ or a combination of both. It is believed that the minimum arises from a G value effect for two reasons. Firstly, the value of ϵ_{max} was estimated in the previous chapter to be $\sim 17,000 \text{ M}^{-1} \text{ cm}^{-1}$ which is similar to $\epsilon_{\text{max}} = 18,500 \text{ M}^{-1} \text{ cm}^{-1}$ for e_{aq}^- at 720 nm.⁹⁵ Consequently the pure components have very similar coefficients so that it seems unlikely that the mixture will show the sort of minimum given in Figure 49. This is further supported by the fact that ΔW is fairly constant for all mixtures. The oscillator strength of an absorption band, f_{mn} , is related to the integrated molar extinction coefficient ϵ by the relationship⁹⁶

$$f_{\text{mn}} = 4.32 \times 10^{-9} F \int_{\omega_1}^{\omega_2} \epsilon \, d\omega \quad (4.1)$$

where the integration extends over the entire band related to the transition from the state $n \leftarrow m$ and F is a correction factor near unity

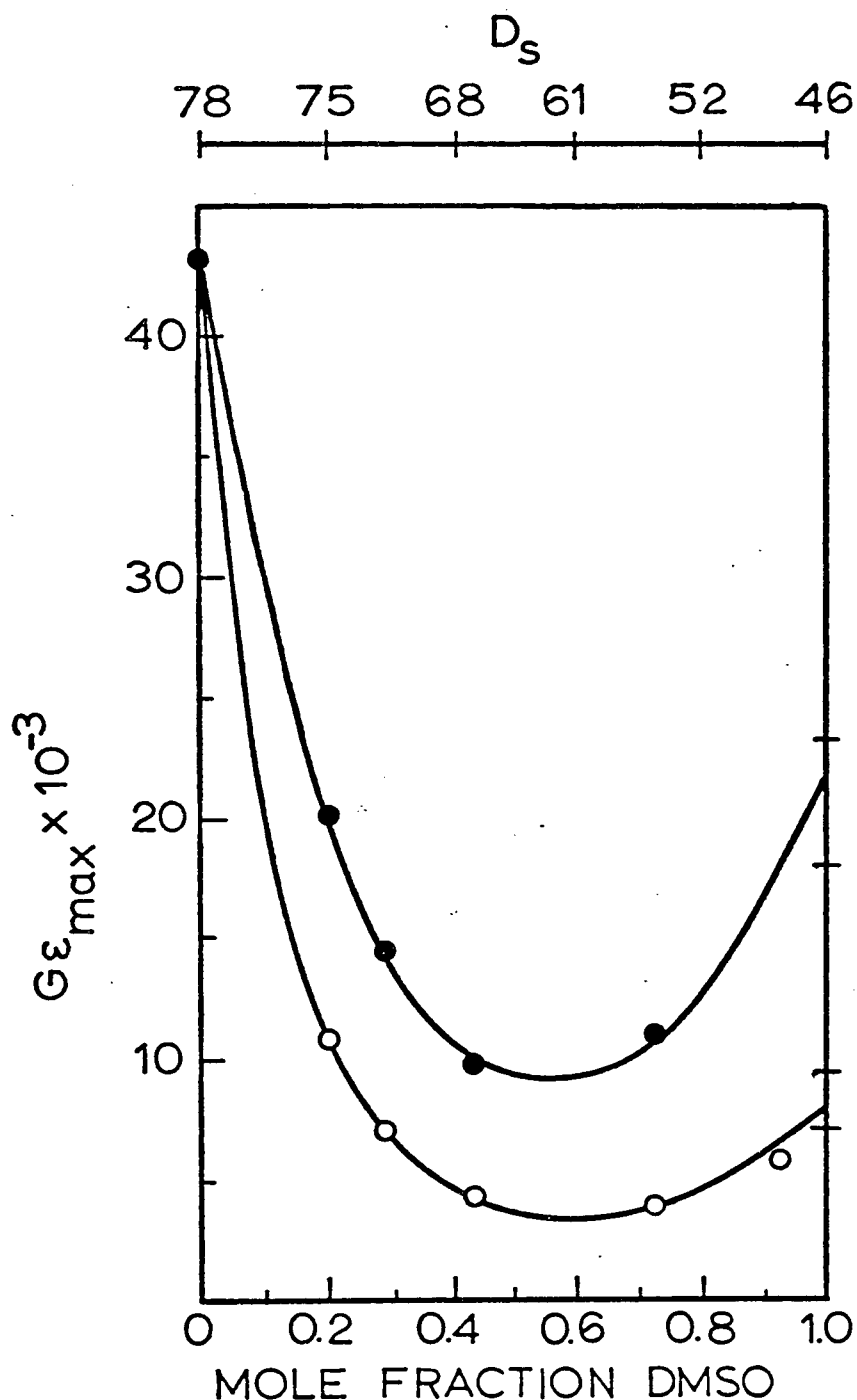


Figure 49. Plot of the values of $G\epsilon_{\max}$ for the solvated electron absorption bands presented in Figure 48 as a function of the mole fraction DMSO for the DMSO-H₂O mixtures. The non-linear axis showing the change as a function of static dielectric constant of the bulk mixture is shown on the top abscissa. ○, actual observed absorbance peak heights. ●, corrected for decay during the pulse and response time of the detector.

related to the refractive index of the medium which contains the absorbing species. For a single electron

$$\sum f_i = 1 \quad (4.2)$$

where the summation extends over all absorptions involving the electron. For most solvated electron bands the oscillator strength is $\sim 0.7 \pm 0.2$ which implies that transitions other than ($2p \leftarrow 1s$) must be very weak if they occur at all. Assuming a Gaussian shaped absorption band for the electron,

$$\int_{\omega_1}^{\omega_2} \epsilon \, d\omega \approx \epsilon_{\max} \Delta W \quad (4.3)$$

so that (4.1) becomes

$$f_{mn} \approx (\text{constant}) \epsilon_{\max} \Delta W \quad (4.4)$$

By analogy with other solvated electron bands the oscillator strength is not expected to change appreciably for the mixtures, ΔW is observed to be constant and hence the ϵ_{\max} should remain reasonably constant. Unfortunately suitable electron scavengers, such as anthracene, are not soluble enough in these binary mixtures to give an electron yield measurable by pulse radiolysis so that this inference could not be verified.

It should be noted that the observed minimum may also arise from an experimental artifact. One of the parameters used in the procedure for correcting the observed absorbance is the electron half-life. Since this minimum also coincides approximately with the fastest

decaying electrons (see Table IV) it is possible that the measured decay rate may have over-estimated the half-life slightly, producing a more pronounced minimum. However, the second order rate constants are all reasonably constant in this region which would suggest that this cannot be the reason for the minimum.

It is suggested that this minimum in the solvated electron yield, if it is a real effect, arises not from a decrease in the free ion yield but rather from an enhanced reaction of the thermal electrons prior to solvation. There are several reasons for this conclusion. The bulk dielectric constant for the mixtures changes monotonically with composition, from $D_s = 78$ (water) to $D_s = 46$ (DMSO), exhibiting no minimum. Consequently one would not expect the free ion yield to pass through a minimum. Furthermore, if the minimum arose from a free ion yield effect, then the yield of DMSO positive ions should have shown a similar effect in these mixtures. In fact they did not, as will be shown later, so that if this minimum is to be attributed to a change in the free ion yield it must arise solely from the contribution of water to the total free ion yield of e_s^- in the mixtures. However, it is unreasonable to suppose that water could affect the yield so markedly at > 0.8 mole fraction DMSO where less than 10% of the primary ionization events involve water molecules.

It is observed that the lifetime of the solvated electron in these mixtures passes through a similar minimum to the G_e values and this suggests that e_s^- react faster with DMSO in the mixtures than in pure DMSO. If the precursor electrons of e_s^- are also more reactive in these mixtures, then this would account for the minimum in the

solvated electron yield. Recently Koulkes-Pujo et al.⁹⁴ reported the effect of dilute solutions of DMSO on the hydrated electron up to 3.5 M in DMSO (0.077 mole fraction DMSO) and observed an increasing value of k/G with increasing DMSO concentration. In this expression k is the rate constant for the reaction of $e_{aq}^- + \text{DMSO}$ ($1.6 \times 10^6 \text{ M}^{-1} \text{ sec}^{-1}$) and G is the apparent yield of e_{aq}^- . The rate constant is treated as a constant in this study so that the increase in k/G corresponds to a decrease in G . This behavior was contrary to what the authors observed with other electron scavengers, such as N_2O , H^+ and CH_3Cl , in which the G value increased due to spur penetration. This phenomena in DMSO was attributed to the unhydrated electrons being scavenged before they could become solvated, thereby causing a decrease in G . These results are entirely consistent with the observations in this study. A decreased solvated electron yield (G) and/or an increased decay rate (k) as the concentration of DMSO is increased in this mole fraction region would give an increased k/G .

It is interesting that this region of minimum absorbance due to e_s^- occurs where these DMSO-water mixtures show maximum intermolecular structure as signified by a large viscosity increase, negative heat of mixing and considerable volume contraction.⁸⁴⁻⁹² Furthermore, measurements on the spin-lattice (T_1) and transverse (T_2) relaxation times indicate a minimum in molecular mobility around 0.35 mole fraction DMSO.⁸⁹ Perhaps this increased molecular structure provides for a lower activation energy for the reaction of the electron, both quasi-free and solvated, with DMSO. The lifetimes of these quasi-free electrons may be further reduced by the increased molecular

relaxation time. Those electrons which are initially trapped in less than optimum voids may react with the medium before they become fully solvated.

In Figure 50, the values of the photon energy (in cm^{-1}) at the absorption band maxima of the mixtures, $E_{\lambda_{\text{max}}}$, are plotted against their respective bulk dielectric constant. The dielectric constant data for the DMSO-water binary mixtures was obtained from the literature.^{84,85} It is interesting, but perhaps fortuitous, that this plot is approximately linear, within experimental error, out to 0.9 mole fraction DMSO. The absorption band width-at-half-height, ΔW , is fairly constant despite the widely different solvation energies provided by DMSO and water separately. This behavior is consistent with the continuum or semi-continuum model in which the electron can sample the environment of the mixture. If the electron was trapped by solvation with only a small number of molecules then the absorption bands could be expected to be much broader. The shift in absorption from the near infrared (pure DMSO) to the visible (pure water) with increasing water content may be due to either a decrease in the cavity radius or to an increase in electron-dipole interaction or a combination of both. Figure 51 shows a plot of $E_{\lambda_{\text{max}}}$ against the mole fraction of water in the mixture. From this correlation curve and Figure 50 it can be seen that neither DMSO nor water dominate the optical properties of the absorption band and suggests that electron solvation occurs by a combination of strong (water) and weak (DMSO) ion-dipole interactions, the extent of which is governed largely by the cavity radius through the composition of the mixtures.

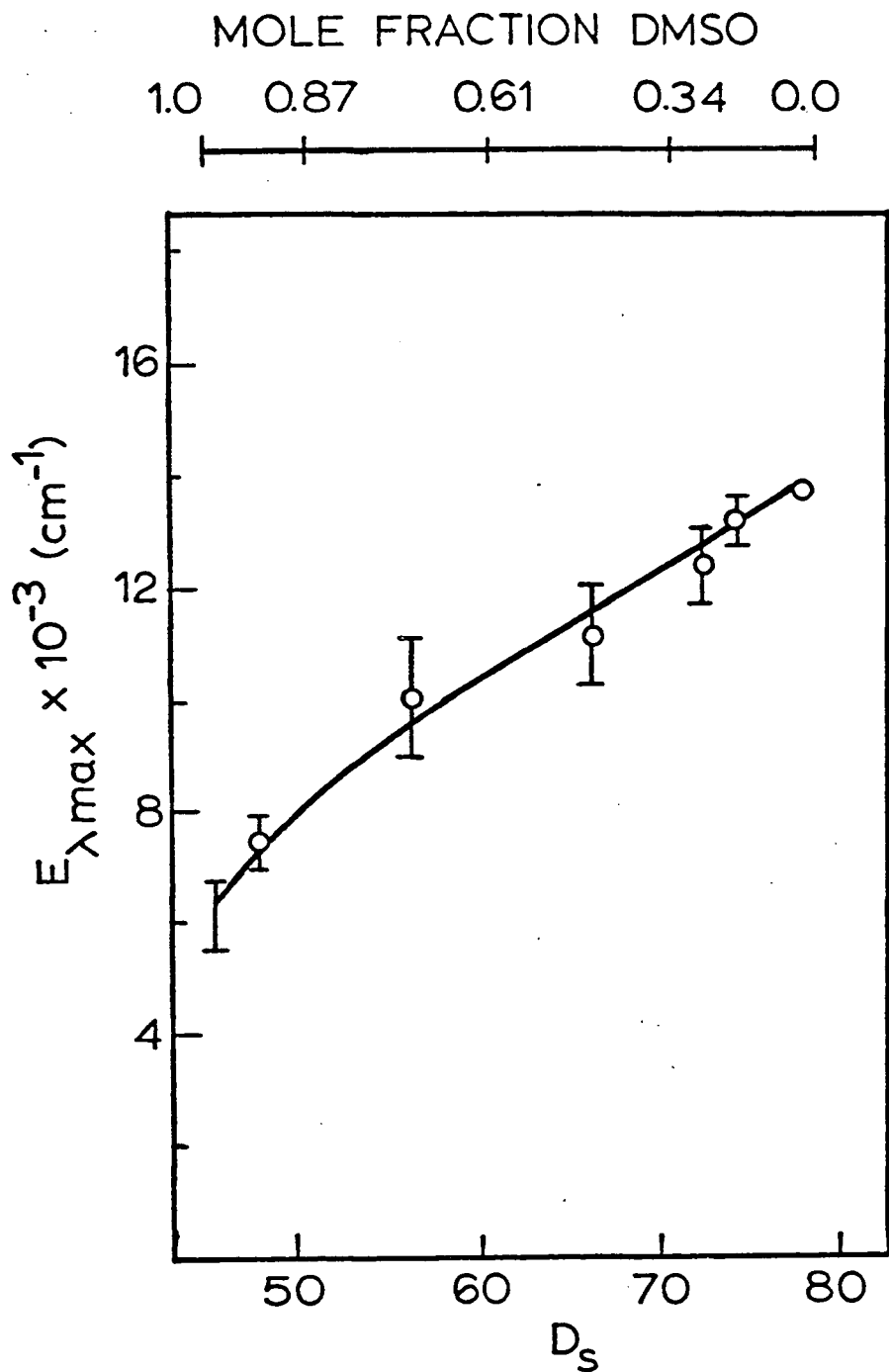


Figure 50. Plot of the photon energy of the absorption band maximum for the solvated electron in the DMSO-H₂O mixtures against the bulk static dielectric constant of the mixtures (at 25°C). The non-linear axis showing the corresponding mole fraction DMSO is shown in the upper abscissa.

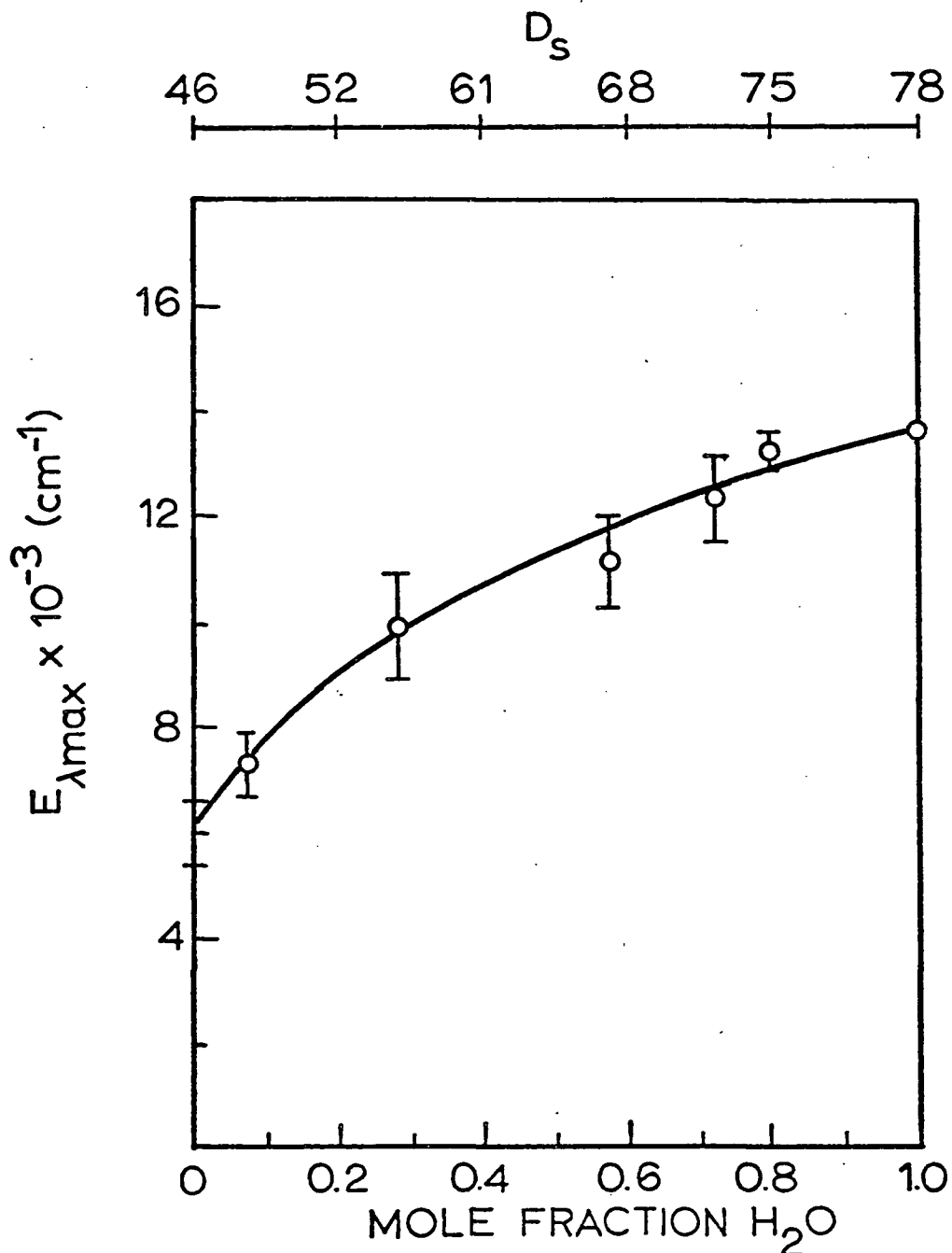


Figure 51. Plot of the photon energy of the absorption band maximum for the solvated electron in the DMSO- H_2O mixtures against the mole fraction of water. The non-linear axis showing the corresponding bulk dielectric constants of the mixtures is shown in the upper abscissa.

Thus the data are compatible with that of aqueous binary mixtures of ammonia,³⁸ ethylenediamine³⁸ and alcohols^{37,47,48} in which the stabilized electrons have absorption band maxima and half-widths intermediate between those of the pure liquids. In these mixtures the electrons see a polarized medium in which the interaction energy is dependent upon the properties of the continuum. However the results in DMSO-water mixtures are at variance with mixtures of other hydroxylic media and aprotic non-polar hydrocarbons^{40,41} or slightly polar ethers.^{39,43,44} The reason for this is that the thermal electrons do not see a dielectric continuum but rather a random distribution of strongly and weakly polarizable aggregates; consequently the optical properties of the stabilized electrons are dominated by the polar component.

It would appear then that for media which are completely miscible in all proportions the yield and optical properties of stabilized electrons depend upon the mean bulk properties of the mixture, regardless of the solvation power either component has for the electrons.

2. DMSO Positive Ions

The absorption band centered at 550 nm, and attributed to the DMSO positive ion, did not change in position or shape but did increase in magnitude as the DMSO concentration was increased. Figure 52(a) shows this absorbance change over the composition range 0.20 to 1.00 mole fraction DMSO. These spectra were obtained after the absorption due to the solvated electron had decayed (lifetime < 100 nsec) and were corrected to zero time by extrapolation back to the end of the pulse (the half-

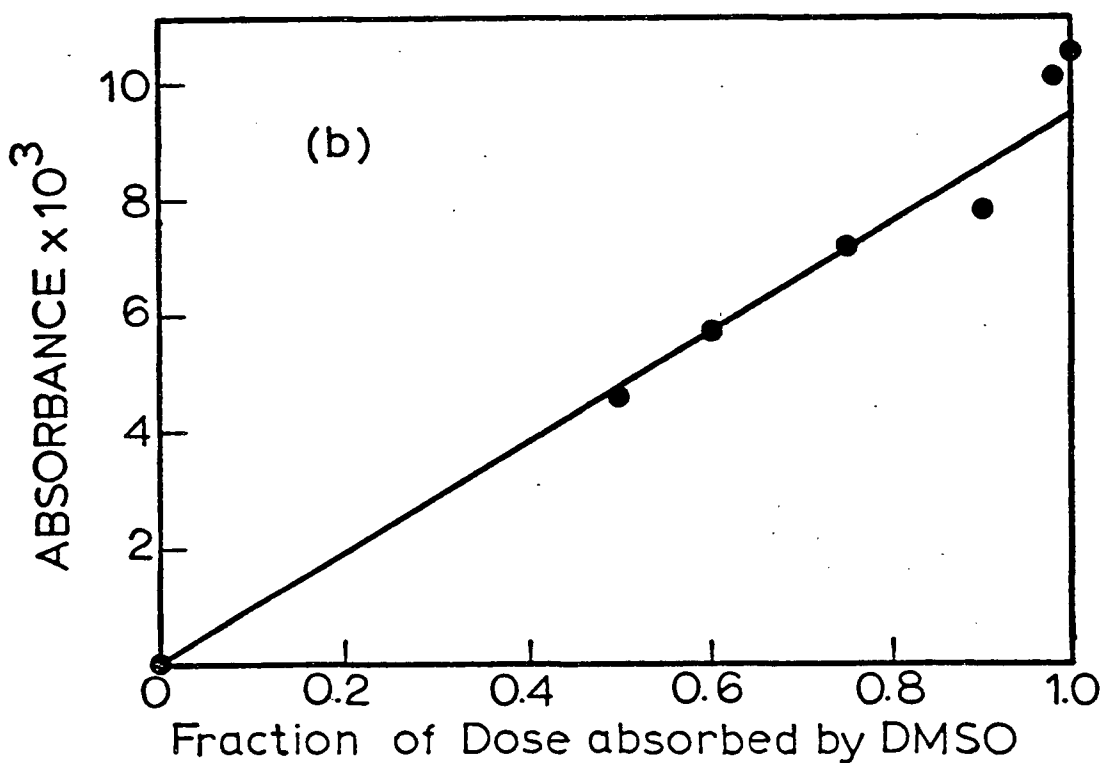
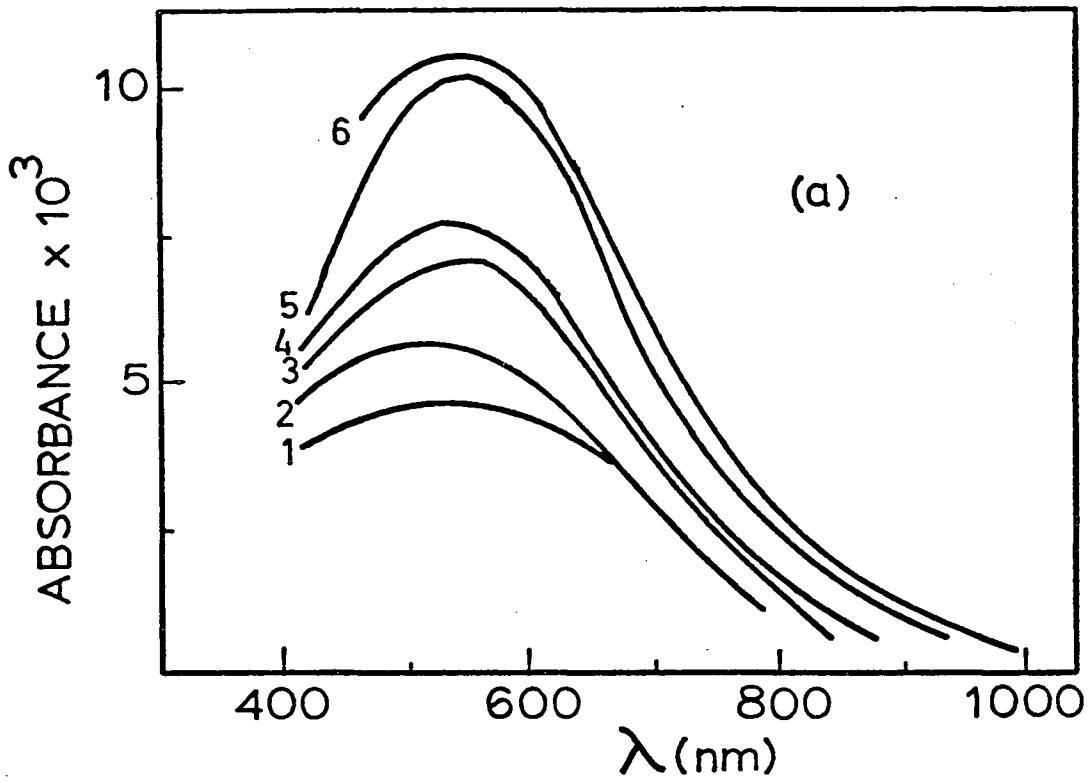
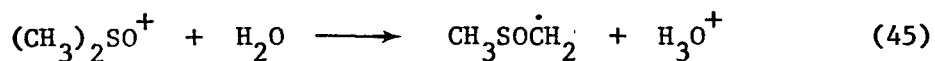


Figure 52. (a) Absorption spectra attributed to the DMSO positive ion produced in DMSO-H₂O mixtures. Curve 6 is pure DMSO; 5, 0.93; 4, 0.72; 3, 0.43; 2, 0.28; and 1, 0.20 mole fraction DMSO. (b) Peak absorbance (at 550 nm) of the bands shown in (a) plotted against the fraction of dose absorbed initially by DMSO.

life for the positive ion $\sim 2 \mu\text{sec}$ for all mixtures). The change in absorbance of the band at 550 nm as a function of the dose initially absorbed by the DMSO in the mixture (as given by its electron fraction and approximately equal to its volume %) is shown in Figure 52(b). It can be seen to be reasonably linear over the range studied.

The data given in Figure 52, when coupled with the fact that the lifetime of DMSO^+ is unaltered, strongly indicates that the cation is unaffected by the water content, even at 0.80 mole fraction water. This implies that the DMSO positive ion does not undergo proton or charge transfer with the water molecules nor is there any exchange of primary oxidizing species between the two components. It should be noted that various proton acceptors, such as ammonia⁹⁷ and ethanol,⁹⁸ have been used in nonpolar aprotic media as scavengers of positive ions; but the above data suggest that reaction (45) does not occur in DMSO-water binary mixtures.



However there is an important difference between nonpolar aprotic media, such as cyclohexane, and DMSO. In DMSO cations are strongly solvated whereas they are extremely unstable in the nonpolar aprotic solvents and hence will readily undergo proton transfer. Since both DMSO and water readily solvate cations, there is no "driving force" for the ionized species to undergo charge or proton transfer.

In view of the fairly large difference in ionization potential of DMSO (8.85 eV)⁹⁹ and water (12.6 eV),¹⁰⁰ it is surprising that the

yield of DMSO positive ions is independent of the water content. One would have expected charge or intermolecular energy transfer to occur from the water to the DMSO molecules. The initial deposition of energy by the high-energy electrons results in highly excited molecules, either through direct electronic excitation or excitation produced by ion neutralization (geminate recombination). Since these solutions are completely homogeneous, excitation transfer between the excited water molecules and neighbouring DMSO molecules could have resulted in the latter being ionized. Nevertheless, the linearity of Figure 52(b) suggests that the yield of DMSO positive ions in the mixture is simply proportional to its electron fraction. It would also appear that the yield of free ions (those electrons which escape geminate recombination) is independent of the bulk dielectric constant of the medium. Dilution of DMSO by water (up to 50% by volume) causes the bulk dielectric constant to change from 46 to 75 (at 25°C), yet the free ion yield of DMSO, as given by the yield of DMSO positive ions, is not appreciably changed. Perhaps the thermalization path of the low energy electron is shortened by the "tighter" DMSO-water structure but the increased coulombic attraction energy is compensated for by the higher dielectric constant.

It should be mentioned that in a mixture consisting of 0.72 mole fraction DMSO, the absorption at 550 nm was increased approximately 90% by the presence of 0.5 M Ag^+ and the electron band completely eliminated. As in the case of pure DMSO, this increase is attributed to scavenging of those electrons which were otherwise doomed to geminate recombination with their concomitant partner.

3. Transient Intermediates at 77°K

The pulse radiolysis of a DMSO-water glass at 77°K was undertaken for two reasons. Firstly, electron spin resonance studies on γ -irradiated aqueous DMSO glasses did not indicate the presence of trapped electrons (to be discussed in the next chapter). However their natural lifetime may have been very short (less than a few minutes) so that they would have decayed completely before esr measurements could be taken. It was hoped that the pulse radiolysis of a glassy mixture would show whether or not trapped electrons are formed and if so, to measure their decay rate. Secondly, a purple-coloured intermediate was observed upon γ -irradiation of the glasses. It was suspected that this transient was the DMSO positive ion but only by recording its optical spectrum could this supposition be verified.

An aqueous glass containing 0.39 mole fraction DMSO was prepared by rapidly plunging the optical cell containing the mixture into a dewar with optical windows filled with liquid nitrogen. The mixture had been previously deoxygenated by bubbling with high purity argon. At the end of the experiment both the DMSO-water glass and the cell were cracked. It is not known whether the cell cracked upon cooling down, warming up or during the experiment. However the "splinter crack" would probably prevent contamination by air (oxygen) since the cell was immersed in liquid nitrogen. The optical path length was 2 mm. The rest of the optical detection system was the same as described previously. An electron pulse width of 500 nsec was used which gave an approximate dose of 10^4 rads per pulse. Dosimetry was performed using an aqueous KCNS solution as previously described except the solution

was saturated with air rather than nitrous oxide. As a result, $G(\text{CNS})_2^-$ was taken as 2.9. The dosimetry was only approximate because the dewar did not contain an appropriate medium (such as methanol) to take account of the scattering of the high energy electron beam by the liquid nitrogen. The reason for this was that the cell was cracked and contamination of the dosimeter solution would have resulted. The actual dose absorbed by the glassy sample was probably higher for a given SEM reading than that calculated from the dosimeter results because the cell in liquid nitrogen would be in electronic equilibrium (electrons scattered out of the cell compensated by those scattered into the cell in dense surroundings). Consequently the absorbance readings, when expressed as $G\epsilon$, are probably an upper limit. The glassy sample was photobleached between pulses and the total absorbed dose was $< 3.5 \times 10^5$ rads.

The spectrum observed at the end of the 500 nsec pulse is shown in Figure 53. Only two distinct bands were observed, one centered at 550-600 nm and the other at $\lambda_{\text{max}} < 400$ nm. The absorption band of the DMSO positive ion in liquid DMSO was normalized to the spectrum of the glassy sample at 600 nm and is shown as the dotted line in Figure 53. It can be seen that the observed spectrum deviates from the positive ion band at $\lambda > 700$ nm suggesting that another intermediate is absorbing in this region. This is probably due to the transient absorption by the silica windows (Supracil) of the cell due to electron bombardment at 77°K. It is not believed to be due to the trapped electron for two reasons. Firstly, the trapped electron should have an absorption maximum at ~ 800 nm on the basis of the spectra given in Figure 48 for

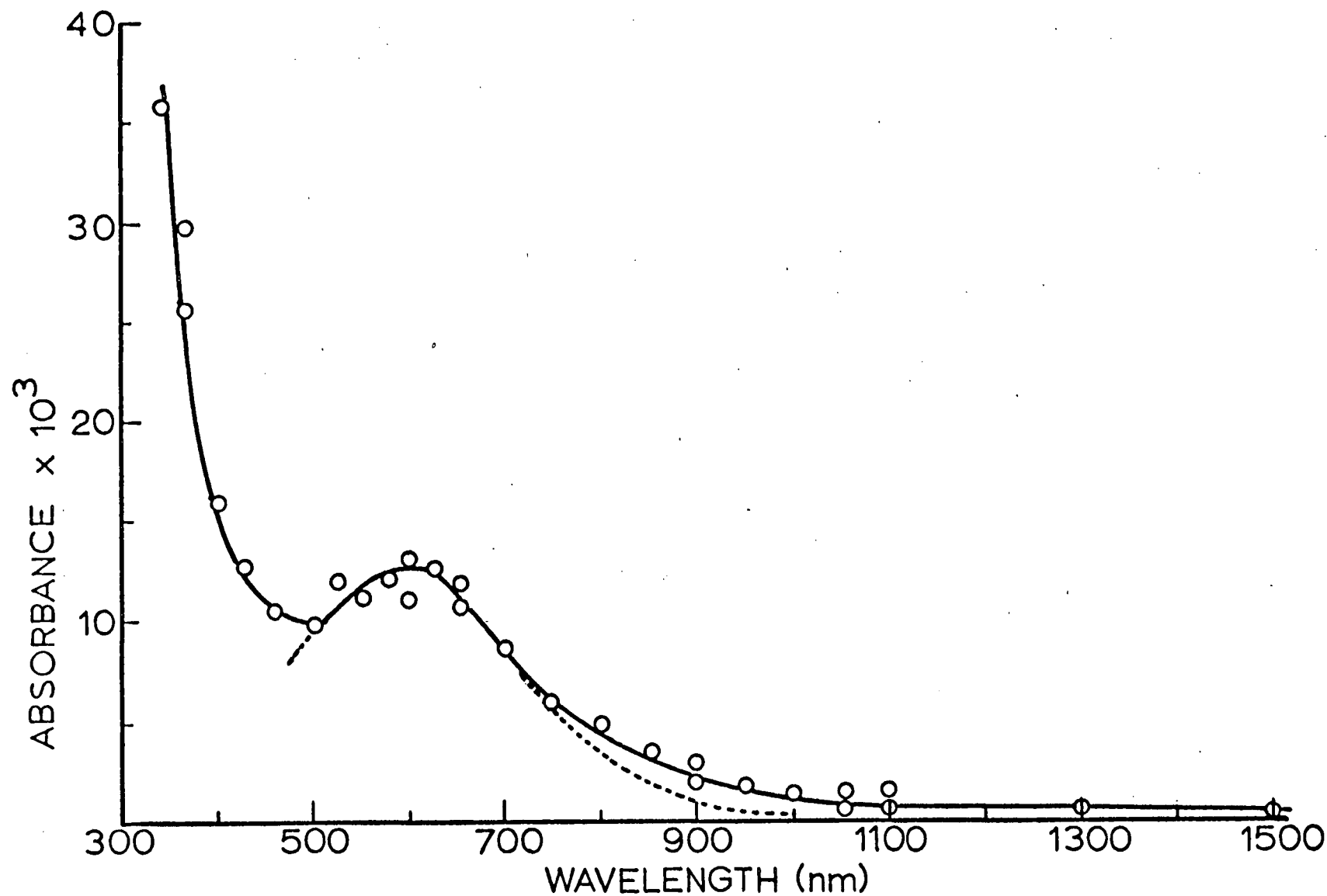


Figure 53. Absorption spectrum of transients produced by the pulse radiolysis of a DMSO-H₂O glass (39 mole % DMSO) at 77°K. The pulse width was 500 nsec, the dose per pulse being ~ 10 krad. The dotted curve is that of the DMSO positive ion in pure DMSO normalized at 600 nm.

the liquid mixtures (assuming no spectral shift) whereas the observed absorption in the region 600-1100 nm showed a very broad continuous tail with no discontinuity or the presence of any "shoulders". Secondly, the absorption maximum at 500-600 nm was calculated to be $G_{\epsilon} < 6000 \text{ mols. (100 eV)}^{-1} \text{M}^{-1} \text{cm}^{-1}$ which seems to be too small for a stable trapped electron.

The end of pulse oscilloscope traces showed no change in absorbance with time suggesting that any trapped or solvated electrons had reacted by the end of the pulse and hence that their lifetime was less than 10^{-6} sec. This is consistent with the esr studies on γ -irradiated glassy DMSO-water mixtures at 77°K in which no trapped electron signal could be detected. Even when the electrons were generated in the glass at 77°K in the spectrometer cavity by the ultraviolet photolysis of $\text{K}_4\text{Fe}(\text{CN})_6$, the electrons were unstable and decayed immediately, producing the same esr spectrum as the γ -irradiated glass. This will be discussed more fully in the next chapter.

It is worth noting that in many other polar and nonpolar low temperature glasses electrons can be trapped and stabilized indefinitely. It is suggested then that the activation energy is very low for the reaction of the electron with a DMSO molecule forming a part of its solvent cage so that reaction readily proceeds even at 77°K.

CHAPTER V
ELECTRON SPIN RESONANCE STUDIES ON
DMSO AND DMSO-H₂O MATRICES AT 77°K

A. INTRODUCTION

1. Basic Principles of ESR*

Use of the technique of electron spin resonance (esr) is restricted to those molecules or atomic species containing unpaired electrons. Because of its charge and intrinsic angular momentum, or spin, the electron has a magnetic moment associated with it. According to quantum theory, a single electron can spin in either of two directions as given by the quantum numbers $M_s = +1/2$ (α spin) or $M_s = -1/2$ (β spin). In the absence of any external magnetic field the electron has no preference for an α or β spin since they are of equal energy. When an external magnetic field is applied to the paramagnetic system, this degeneracy is removed. The electron will have lower energy if its spin magnetic moment is aligned so as to be in the direction of the applied field rather than against it, which is the only other allowed orientation. The energy separation between the two spin states is proportional to the product of a constant, β , (the electronic Bohr magneton) and the strength of the

* Prepared from references 59 and 104.

external magnetic field, H. The proportionality constant, g, is referred to as the spectroscopic splitting factor, or g-factor, and represents the rate of divergence of the magnetic energy levels with the magnetic field. If the paramagnetic species is irradiated with electromagnetic radiation possessing energy, $h\nu$, equal to the separation between the two energy levels, the unpaired electron will absorb energy and "flip over" to the state of higher energy in which its spin magnetic moment is aligned anti-parallel to the magnetic field. This resonance condition is described by equation (5.1).

$$h\nu = g\beta H \quad (5.1)$$

For a free electron $g = 2.0023$ (the deviation from the integral number being a relativistic correction for the orbital velocity of the electron). The term free electron or free spin refers to an unpaired electron having spin angular momentum but no orbital angular momentum (such as that possessed by an electron in an s orbital). Although this condition is rarely realized for organic free radicals, the orbital angular momentum associated with a p or d orbital electron is usually quenched so that the g-factors are near that of free electrons.

In principle electron spin resonance absorptions may be produced by varying the magnetic field (H), the radiation frequency (ν) or a combination of both. In practice, however, the frequency is usually fixed and the field slowly varied since the klystron oscillator which generates the microwave radiation is tunable only over a very narrow range. For the X-band spectrometer used in this study the microwave frequency was about 9.1 GHz so that the required magnetic field for the resonance

condition of a free electron occurred around 3200 gauss.

Thus studies in esr depend upon the absorption of microwave energy between non-degenerate spin states of a paramagnetic species. However the probabilities of upward (stimulated absorption) and downward (stimulated emission) transitions are equal; consequently the condition of resonance is dependent upon there being a difference in population between these two states. The ratio of paramagnetic species with their spins aligned in the direction of the applied magnetic field (N^-) to those aligned against it (N^+) at temperature T is given by the Boltzman distribution.

$$N^+/N^- = \exp(-g\beta H/kT) \quad (5.2)$$

Since $g\beta H \ll kT$ for temperatures above a few degrees absolute, the exponential factor is close to unity so that the excess population in the ground state is very small ($\sim 0.07\%$ for $g = 2$, $T = 300^\circ\text{K}$ and $H = 3000$ gauss). If the radiation field at resonance is appreciably increased, the upper and lower spin states will become equally populated so that there will be no net energy absorption and therefore no resonance signal. The spin system is then said to be power saturated. This saturation is counterbalanced by relaxation processes, as characterized by the spin-lattice relaxation time (T_1) and spin-spin relaxation time (T_2), which tend to restore thermal equilibrium. In the former process the spin system interacts with the medium or lattice by donating its excess energy to the vibrational and rotational modes of the surrounding molecules. Rapid dissipation of this excess

spin energy (short T_1) is essential if the population difference of the spin states is to be maintained. Although this population difference is greatest at low temperatures, therefore allowing a stronger absorption, the spin-lattice relaxation process is less efficient. Consequently free radicals are often easily power saturated at low temperatures.

Spin-spin relaxation involves magnetic interactions between the unpaired electrons and surrounding magnetic dipoles, such as other unpaired electrons or magnetic nuclei native to the lattice. These interactions are not energy dissipating and therefore do not contribute directly in returning the spin system to equilibrium. However the spin-lattice transitions described above may be enhanced if the spin-spin process brings the excess energy to a position for a propitious transition to the lattice.

These spin-spin transitions are important in another sense in that they cause broadening of the absorption lines. The total magnetic field experienced by a particular spin system will include contributions from its neighbours as well as the applied magnetic field; consequently the resonance transitions will occur over a range of frequencies corresponding to the variations in local field. In liquid media molecules undergo rapid random motion so that these induced dipolar fields are subjected to extensive time averaging. As a result the lines are narrower than those in the corresponding solid state where the paramagnetic species are prevented from rotational or translational motion.

A special case of spin-spin interaction may occur between the

unpaired electron and nuclear spins within the same atom or molecule. This interaction results, not in line broadening, but rather in resolved hyperfine structure. Just like the electron spin, the nuclear spin is quantized having $2I + 1$ states of equal energy for a nucleus of spin I . When a magnetic field is applied, these degenerate states are split and the nuclear magnetic moment forms the $2I + 1$ allowed orientations with respect to the field direction. Under the conditions of an esr experiment ($H \sim 3000$ gauss, $\nu \sim 9.0$ GHz) all $2I + 1$ nuclear moment orientations may be considered as equally probable since the difference in population of the nuclear sub-levels is several orders of magnitude less than the corresponding electron spin states. This results in each of the electron spin states being further split into $2I + 1$ sub-levels of equal separation. Since the nuclear spins are unaffected by the oscillating microwave field which causes the electronic transitions (the resonance frequency of a proton, for example, in a field of 3000 gauss is about 14 MHz), the selection rules for the esr transitions are $\Delta M_S = \pm 1$ and $\Delta M_I = 0$. The esr spectrum will therefore consist of $2I + 1$ lines. Often there are groups of nuclei in chemically and magnetically equivalent positions, in which case they act together to give a splitting characterized by their total spin $n_i I_i$. Here n_i is the number of equivalent nuclei with nuclear spin I_i . The combined interaction produces $2n_i I_i + 1$ lines of equal separation, the intensities of which can be identified with the coefficients of the appropriate multinomial expansion. The resulting line separation is called the hyperfine splitting. A much more complicated situation arises when the electron interacts with

more than one non-equivalent magnetic nuclei.

In solids and highly viscous media, in which the paramagnetic centres are not free to tumble, the hyperfine splittings will depend upon the relative orientation of the lattice and applied magnetic field. The magnetic dipole-dipole interactions between the unpaired electron and nuclear moments have a directional character associated with them so that the effective magnetic field felt by the electron will be anisotropic. This is accounted for by expressing the splittings in terms of a hyperfine tensor \bar{A} . If the paramagnetic species is rapidly reorienting, the anisotropic part will average to zero and the splittings will arise solely from the isotropic coupling (Fermi contact interaction).

The g-factor may similarly show anisotropic behaviour. If the unpaired electron possesses orbital angular momentum it will couple with the spin angular momentum. Because of the orientational dependence of this spin-orbit coupling, it will be easier to make the electron reverse its spin when the magnetic field is applied in certain directions as compared to others. This anisotropy results in the paramagnetic system resonating at different magnetic fields. For this reason the g-factor is often expressed as a tensor in which the principal values are g_{xx} , g_{yy} and g_{zz} . In most cases the off-diagonal elements are small and may be neglected so that, to a good approximation, $g_{xx} = g_x$, $g_{yy} = g_y$ and $g_{zz} = g_z$. Here x, y, and z refer to the laboratory fixed axes and are related to the crystal or molecular fixed axes by a suitable coordinate transformation matrix (not necessarily the same for the g and A tensors). In a liquid or slightly

viscous solid the observed g-values may be considered isotropic since the molecules will be tumbling rapidly and randomly; hence $g = 1/3(g_{xx} + g_{yy} + g_{zz})$.

2. Amorphous and Polycrystalline Media

In amorphous or polycrystalline solids the paramagnetic species are oriented randomly in the matrix. If the medium temperature is sufficiently low, rotational and translational motions will be hindered so that the time averaging properties of fluid systems are lost. Thus the observed resonance will be a sum of the individual resonances of the randomly oriented paramagnetic centres. In this case the spectrum will be governed by the anisotropy of the g-factor and hyperfine splitting as well as any broadening due to dipole-dipole interactions. This results in a less detailed picture of the structure and electronic distribution of the radical than if it was present in a single crystal or solution. However, since the primary objective of this and other studies in radiation chemistry is simply to identify the paramagnetic species involved in the chemical processes, studies on the amorphous or polycrystalline state are usually performed since the experimental procedure and mathematical analysis are less complicated.

Spectral line shapes have been computed for paramagnetic species randomly trapped in solid matrices.^{104,105} Two of the most commonly occurring line shapes are shown in Figure 54 for radicals exhibiting

no hyperfine structure. Figure 54(a) shows the resonance absorption for a radical possessing an axially symmetric g-tensor where $g_{xx} = g_{yy} = g_{\perp}$ and $g_{zz} = g_{\parallel}$ whereas Figure 54(b) refers to a completely asymmetric g-tensor where $g_1 < g_2 < g_3$. The applied magnetic field is taken as being aligned along the z axis. An example of a paramagnetic system having an axially symmetric \bar{g} and \bar{A} tensor with the same axis of symmetry for a single nucleus with nuclear spin $I = 1/2$ is shown in Figure 55. In this spectrum the anisotropic hyperfine splitting constants A_{\parallel} and A_{\perp} are $\gg \beta H(g_{\parallel} - g_{\perp})$. The central dotted portion is the theoretical spectrum in the absence of the hyperfine coupling.

These three cases represent the optimum conditions to be expected when dealing with polycrystalline and amorphous solids. In some matrices the specific features corresponding to the tensor components of A and g are lost due to excessive line broadening. This is especially true for radicals trapped in hydrocarbon matrices at low temperatures where the dipolar broadening due to the protons is often greater than $\beta H(g_{\parallel} - g_{\perp})$ and $(A_{\parallel} - A_{\perp})$. The broadening results in lines approximately Gaussian in shape with the peak-to-peak separation corresponding fairly closely to the isotropic component of the hyperfine splitting constant. Generally the line widths for the aliphatic radicals at 77°K are about 10-15 gauss but can be narrower if the radical is free to rotate or tumble within the trapping site and thereby average out the dipolar interactions. Often the broadening can be reduced significantly by using deuterated molecules. Since the nuclear moment of deuterium is smaller than that of hydrogen, the hyperfine

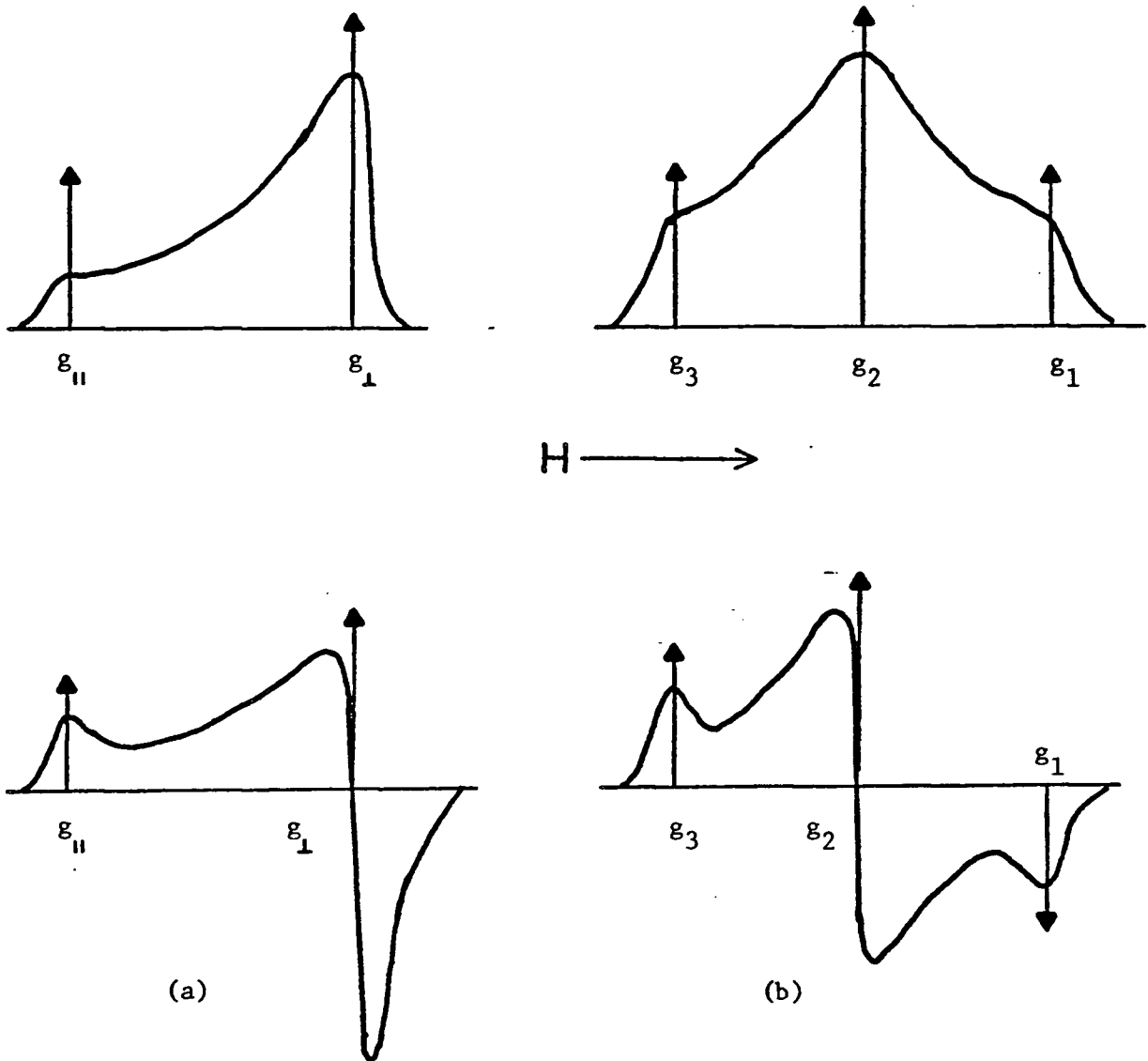


Figure 54. Theoretical esr line shapes for (a) axially symmetric and (b) completely asymmetric g tensors. The upper curves refer to absorption spectra of the paramagnetic species. The lower curves refer to the experimentally observed first derivative spectra. (Adapted from Figures 9.3 and 9.4, pages 324-325, reference 104).

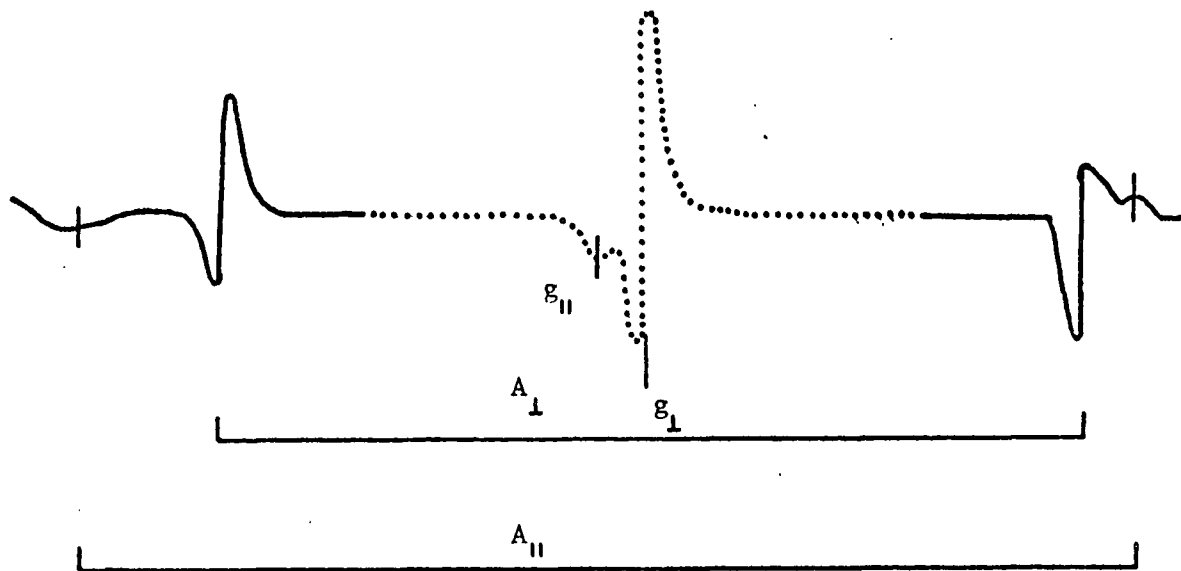


Figure 55. Theoretical first derivative esr spectrum for a paramagnetic species with $S = 1/2$, $I = 1/2$ and with axially asymmetric g and A tensors. The central dotted portion is the theoretical spectrum in the absence of the hyperfine interactions. (Adapted from Figure 9.7, page 327, reference 104).

interactions and line widths will be reduced compared to the unsubstituted medium.

In the preceding discussion it has been assumed that the resonance absorption is due to a single paramagnetic species randomly oriented in the matrix. Generally this is not the case. Often the spectrum is further complicated by the appearance of other radicals resonating in the same region so that identification is not always possible. This is particularly true if the medium has been exposed to ionizing radiation, such as X- or γ -rays, which are not selective in the types of radicals they produce. In many systems spectral analysis may be simplified by using a Hg lamp as the radiation source. Since ultraviolet photolysis is more selective in cleaving molecular bonds, only certain radicals will be produced.

B. RESULTS AND DISCUSSION

1. Pure DMSO

1.1 Ultraviolet Irradiated

The radicals produced when polycrystalline DMSO is photolyzed at 77°K with ultraviolet light exhibit a broad, asymmetric spectrum consisting of seven resolvable lines centered near $g = 2.004$ as shown in Figure 56. Since the Vycor envelope is opaque below 220 nm, the emitted light from the low-pressure mercury resonance arc is chiefly 253.7 nm corresponding to an energy of $\approx 110 \text{ kcal mole}^{-1}$. DMSO absorbs strongly below 260 nm suggesting that the first electronically excited state is comparable to the energy of this mercury line. If dissociation occurs by internal conversion from the lowest electronically

excited state, then the probability of radical formation will favour the weakest bond. In DMSO the C-S bond has a mean dissociation energy D of ~ 50 kcal/mole⁻¹ as compared to $D(S-O)$ and $D(C-H)$ which are 86 and 90-100 kcal mole⁻¹ respectively.¹⁰⁶ Since the C-S bond is appreciably weaker than the rest one would expect $CH_3\dot{S}O$ and $\cdot CH_3$ radicals to predominate in the primary photolytic process. The spectrum shown in Figure 56 tends to confirm this supposition.

The quartet, centered at $g = 2.003$ and having a hyperfine splitting of 22 ± 1 gauss (as measured from the derivative maxima), is that expected for an unpaired electron interacting with three equivalent α protons. The line width, ΔH , as measured between the peaks of the derivative maximum and minimum, is approximately 6 to 7 gauss indicating that the methyl radical is tumbling freely in the DMSO matrix at 77°K. The intensity distribution of the resonance lines of the quartet, as measured by the peak-to-peak amplitudes, agrees with the theoretical ratio of 1:3:3:1.

The asymmetric three line spectrum ascribed to the $CH_3\dot{S}O$ radicals is indicative of the resonance pattern observed for other sulfur radicals in ultraviolet and γ -irradiated thiols, sulfides, disulfides and sulfones where the anisotropy in the g -factor is attributed to the strong spin-orbit coupling of the unpaired electron localized on the sulfur atoms.¹⁰⁷⁻¹¹⁴ Since the sulfur resonance shows seven points of inflection, the three principle g -factors will correspond to the maximum, zero and minimum points in the derivative curve (see Figure 54(b)). The g -factors obtained in this manner are as follows: $g_1 = 1.988$, $g_2 = 2.004$ and $g_3 = 2.017$. No residual hyperfine splitting was

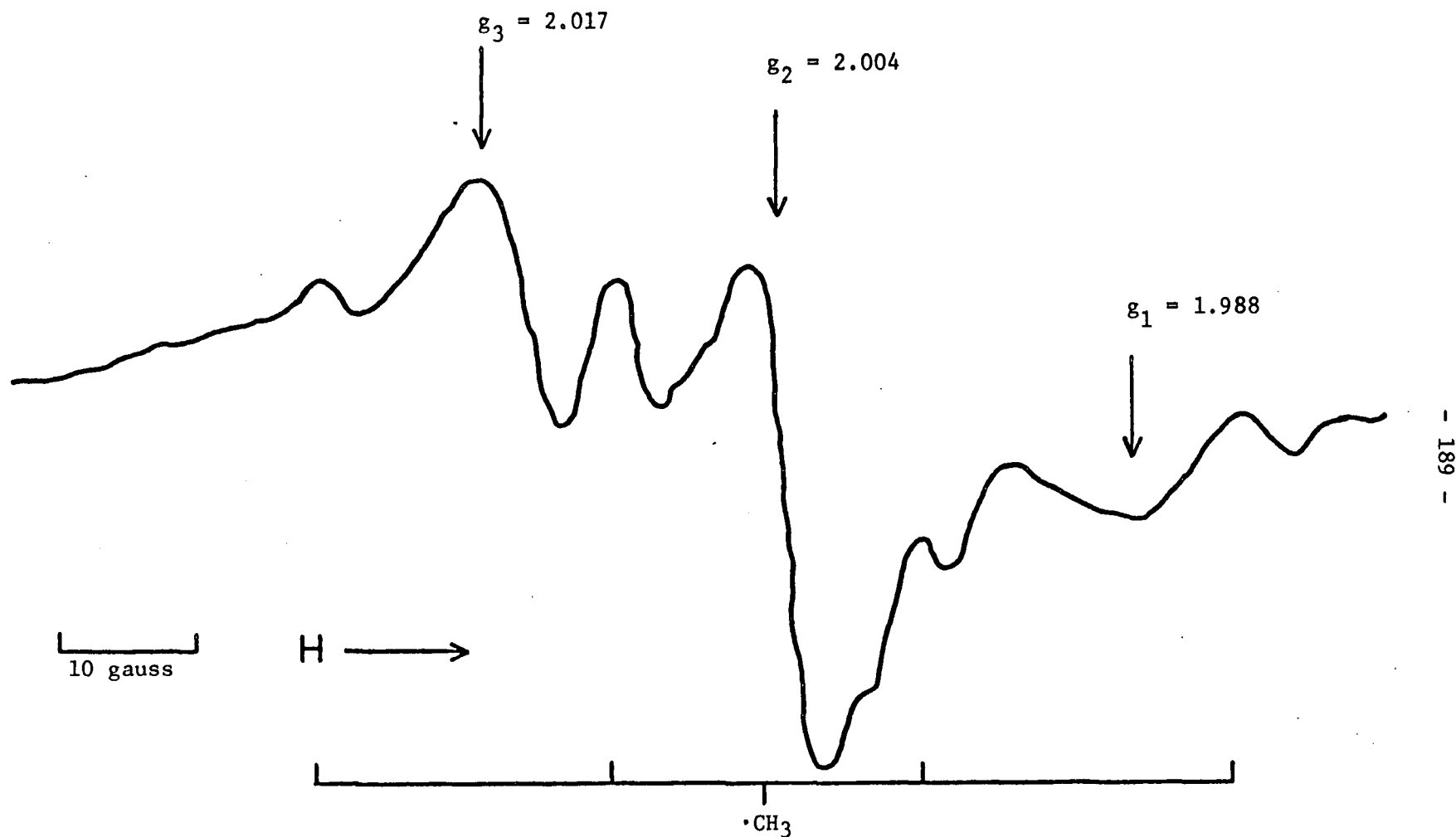


Figure 56. Electron spin resonance spectrum obtained after the ultraviolet photolysis of polycrystalline DMSO at 77°K. The arrows correspond to the asymmetric g -factors of the sulfur radical $\text{CH}_3\dot{\text{S}}\text{O}$. The methyl radical quartet is indicated by the stick plot.

observed suggesting that the unpaired electron is localized mainly on the sulfur atom and is not interacting with the β protons of the methyl group. It is possible, however, that the splitting is too small to be resolved due to the dipolar broadening.

1.2 γ -Irradiated

Figure 57 shows the esr spectrum obtained when the polycrystalline DMSO balls were γ -irradiated in the dark at 77°K. Unlike the photolyzed sample (Figure 56), the resonance spectra of the radicals produced were poorly resolved. The two derivative peaks on the high and low field portion of the spectrum correspond to the resonance positions of the outer lines of the methyl radical quartet. However the asymmetric sulfur pattern observed in the photolyzed sample cannot be positively assigned because of the overlapping resonance of other paramagnetic species.

When the microwave power was increased above 1.0 mW, one or more different paramagnetic species present in the γ -irradiated sample and centered near $g = 2.006$ began to saturate. This is evident from Figure 57(b) for which the microwave power is 10 mW. Superimposed upon the resonance pattern shown in Figure 57 is a broad asymmetric singlet centered at $g = 2.007$ with a line width of ~ 20 gauss. This singlet is not due to trapped electrons because the absorption is not saturated at high power (160 mW) and its g -factor is greater than the free spin value.

It is worth noting that the radicals produced in the samples by γ -irradiation and ultraviolet photolysis were stable and showed no signs of decay when the irradiated samples were kept in the dark in liquid nitrogen. Even after several days the resonance patterns and

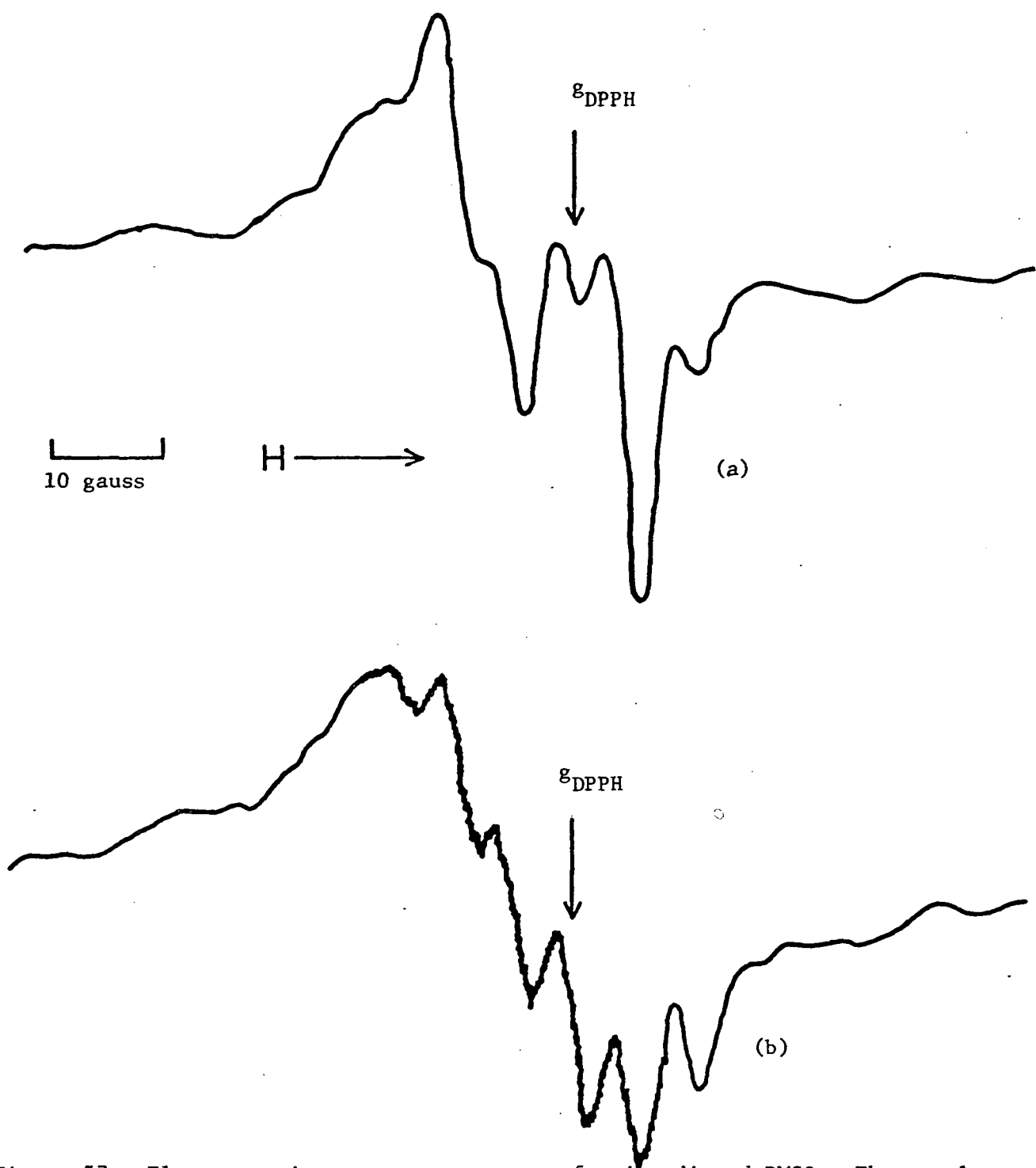


Figure 57. Electron spin resonance spectra of γ -irradiated DMSO. The sample was irradiated in the dark at 77°K to a total absorbed dose of 0.72 Mrad. (a) microwave power 0.44 mW; (b) microwave power 10 mW. $g_{\text{DPPH}} = 2.0036$.

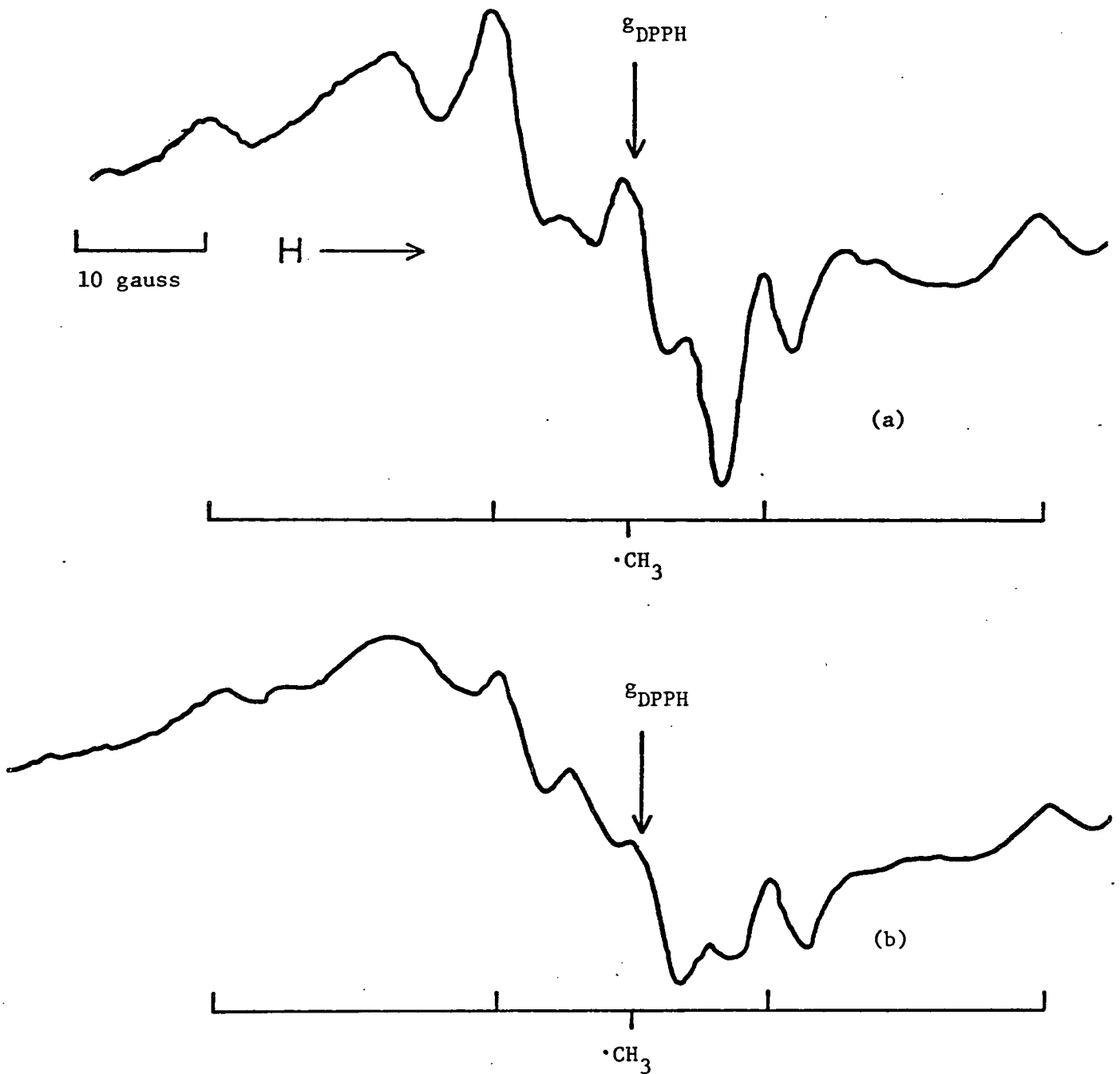


Figure 58. Electron spin resonance spectra of γ -irradiated DMSO after bleaching irradiated sample with ultraviolet light for forty minutes (in spectrometer cavity). Sample γ -irradiated at 77°K in the dark to a total absorbed dose of 0.72 Mrad. (a) microwave power 0.52 mW; (b) microwave power 10 mW.

intensities were unchanged. When the γ -irradiated sample was photobleached with ultraviolet light, the spectrum shown in Figure 58 was observed and is comparable to that found for direct ultraviolet photolysis and given in Figure 56. The spectral change did not arise from simple photolysis of the DMSO molecules since the methyl radical concentration was unchanged (as measured by the outer peaks of the quartet). Furthermore, the sample was photobleached in the esr cavity for only 40 minutes which, on the gain setting used, would not have caused any observable change in the spectrum due to the direct photolysis of DMSO. On the other hand, the broad singlet was reduced in intensity and the saturation effects at high microwave power (> 1.0 mW) were less pronounced suggesting that the observed resonance change was due to the partial bleaching of these two paramagnetic species.

2. DMSO-Water Matrices

2.1 γ -Irradiated Polycrystalline H_2O

In order to analyze the esr spectra of binary mixtures, it is essential to have a detailed knowledge of the type and stability of the resonance pattern induced in each of the pure components. The resonance spectrum of γ -irradiated polycrystalline water has been extensively studied and the line assignments are reasonably well understood.¹¹⁵ The spectrum observed in the present study is shown in Figure 59 and agrees with that observed by other authors. The "water resonance" is characterized by a distinct doublet split by about 40 gauss (line width ~ 12 gauss) and centered around $g = 2.008$. The broad "hump" to

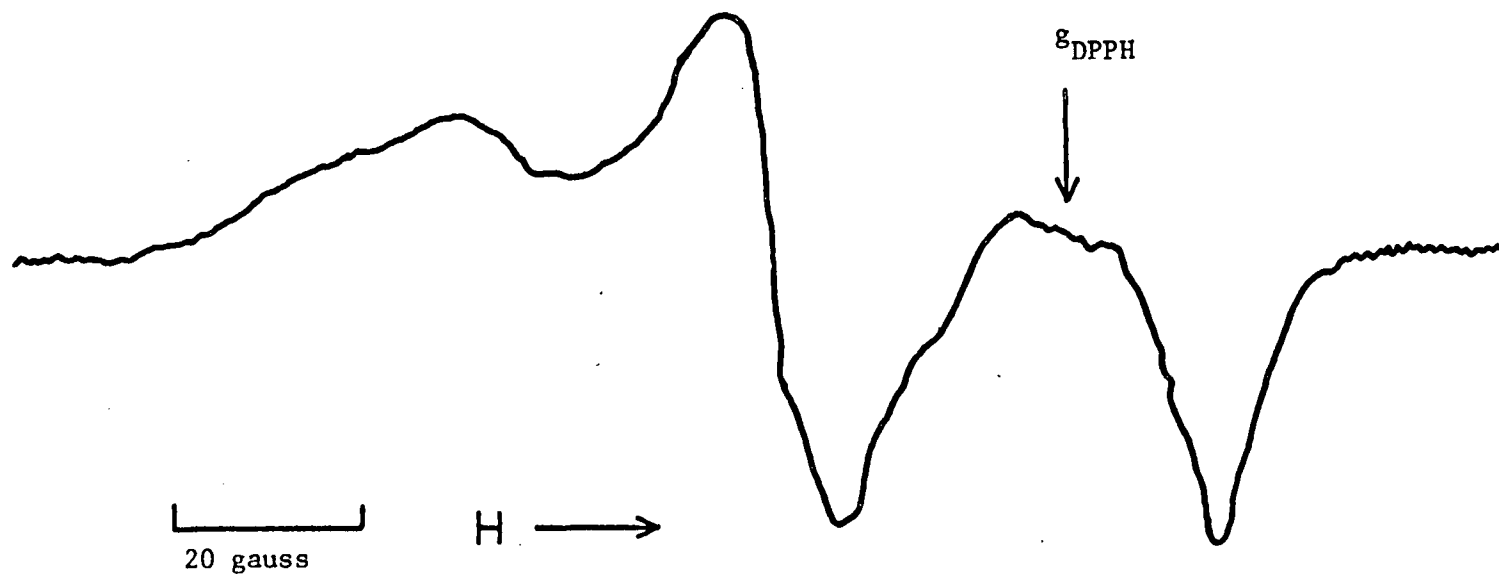


Figure 59. Electron spin resonance spectrum of γ -irradiated polycrystalline ice at 77°K. Resonance pattern corresponds to that of the $\cdot\text{OH}$ radical.

the low field side of the doublet had previously been attributed to such paramagnetic species as H_2O^+ , H_2O^- or $\text{HO}_2\cdot$. However subsequent investigations have shown that the entire esr spectrum may be assigned to an anisotropic $\cdot\text{OH}$ radical.¹¹⁵

Only the hydroxyl radical is observed by esr in γ -irradiated ice at 77°C. Other paramagnetic species produced in the radiolysis are either too unstable and immediately react with the matrix ($\text{H}\cdot$ atoms) or their yield is too low to be observed (e_t^- , $\text{HO}_2\cdot$).

2.2 γ -Irradiated DMSO- H_2O Mixtures

Electron spin resonance studies were made on a series of ten mixtures ranging from 0.01 to 0.89 mole fraction DMSO. Table V gives the mixtures studied and the type of matrix (amorphous or polycrystalline) formed in each system when "shock cooled" in liquid nitrogen by the "ball technique". Only two mixtures corresponding to 0.20 and 0.39 mole fraction DMSO formed glassy (amorphous) balls. The sample balls were γ -irradiated in the dark to a total absorbed dose of 0.96 Mrad. All photolysis or photobleaching experiments were performed with the dewar in the spectrometer cavity. When using the ultraviolet light source (Hg lamp), the bleaching time was always less than 20 minutes; consequently the observed changes in the spectrum were not due to the photolytic decomposition of the DMSO molecules.

Two distinct resonance patterns were observed for the composition range studied and were not a simple combination of the pure components. At high DMSO concentrations (0.89, 0.80, 0.69 and 0.67 mole fraction DMSO) the γ -irradiated matrices produced resonance spectra similar to

TABLE V. Summary of data obtained from studies on γ -irradiated DMSO-water matrices at 77°K.

Mole Fraction DMSO	Volume fraction ^a DMSO	Matrix at 77°K	Sample colour ^b after γ -irradiation	Radicals ^c observed
1.0	1.0	polycrystalline	yellow tinge	$\cdot X, \cdot SX, \cdot CH_3, (DMSO)^+$
0.89	0.97	polycrystalline	yellow tinge	$\cdot X, \cdot SX, \cdot CH_3, (DMSO)^+$
0.80	0.94	polycrystalline	yellow tinge	$\cdot X, \cdot SX, \cdot CH_3, (DMSO)^+$
0.69	0.90	polycrystalline	purple tinge	$\cdot X, \cdot SX, \cdot CH_3, (DMSO)^+$
0.67	0.89	polycrystalline	purple tinge	$\cdot X, \cdot SX, \cdot CH_3, (DMSO)^+$
0.39	0.71	amorphous	purple	$\cdot SX, \cdot CH_3, (DMSO)^+$
0.20	0.50	amorphous	purple	$\cdot SX, \cdot CH_3, (DMSO)^+$
0.11	0.33	polycrystalline	purple tinge	$\cdot SX, \cdot CH_3, (DMSO)^+$
0.06	0.20	polycrystalline	purple tinge	$\cdot SX, \cdot CH_3, (DMSO)^+$
0.03	0.10	polycrystalline	colourless	$\cdot SX, \cdot CH_3, (DMSO)^+, \cdot OH$
0.01	0.04	polycrystalline	colourless	$\cdot SX, \cdot CH_3, (DMSO)^+, \cdot OH$

^a Volume fraction approximately equal to fraction dose absorbed initially by DMSO in mixture.

^b Purple centre turned yellow upon bleaching with ultraviolet and visible light.

^c $\cdot X$ = paramagnetic species centered at $g = 2.006$, readily power saturated above 1.0 mW and photobleached with ultraviolet light.

$\cdot SX$ = asymmetric sulfur radical with $g_1 = 1.988$, $g_2 = 2.004$ and $g_3 = 2.017$.

those observed for pure DMSO. The first two mixtures had a yellow tinge after γ -irradiation whereas the latter two had a purple tinge. The paramagnetic species responsible for the saturation effects at low microwave power (hereafter called $\cdot X$ for brevity) were still present although their contribution to the overall spectrum diminished as the water content increased. This is indicated in Figure 60 in which the region of the spectrum where $\cdot X$ resonates shows the same behaviour upon power saturation (pure DMSO) as with addition of water (DMSO-water mixtures). The remaining part of the esr spectra of these four mixtures are compatible with Figure 57 (pure DMSO). When the irradiated samples were photobleached for 20 minutes with ultraviolet light, the broad asymmetric singlet and $\cdot X$ disappeared completely and the purple colour was replaced by a yellow tinge. The bleaching was accompanied by a slight increase ($\sim 20\%$) in the methyl radical yield. These features are shown in Figure 61 for 0.80 mole fraction DMSO and are representative of the other three mixtures. The methyl radical quartet and the asymmetric "sulfur pattern" are clearly evident after photobleaching (Figures 61(b) and (c)).

The remaining γ -irradiated mixtures (0.39, 0.20, 0.11, 0.06, 0.03 and 0.01 mole fraction DMSO) gave well-resolved esr spectra showing the broad asymmetric singlet, the characteristic "sulfur pattern" and the methyl radical quartet. However there was no evidence of $\cdot X$ as indicated by the power saturation behaviour of the spectra. Typical esr spectra of these mixtures are given in Figure 62 for 0.20 mole fraction DMSO. Traces of the hydroxyl radical were observed in the least concentrated DMSO mixtures (0.03 and 0.01 mole fraction DMSO),

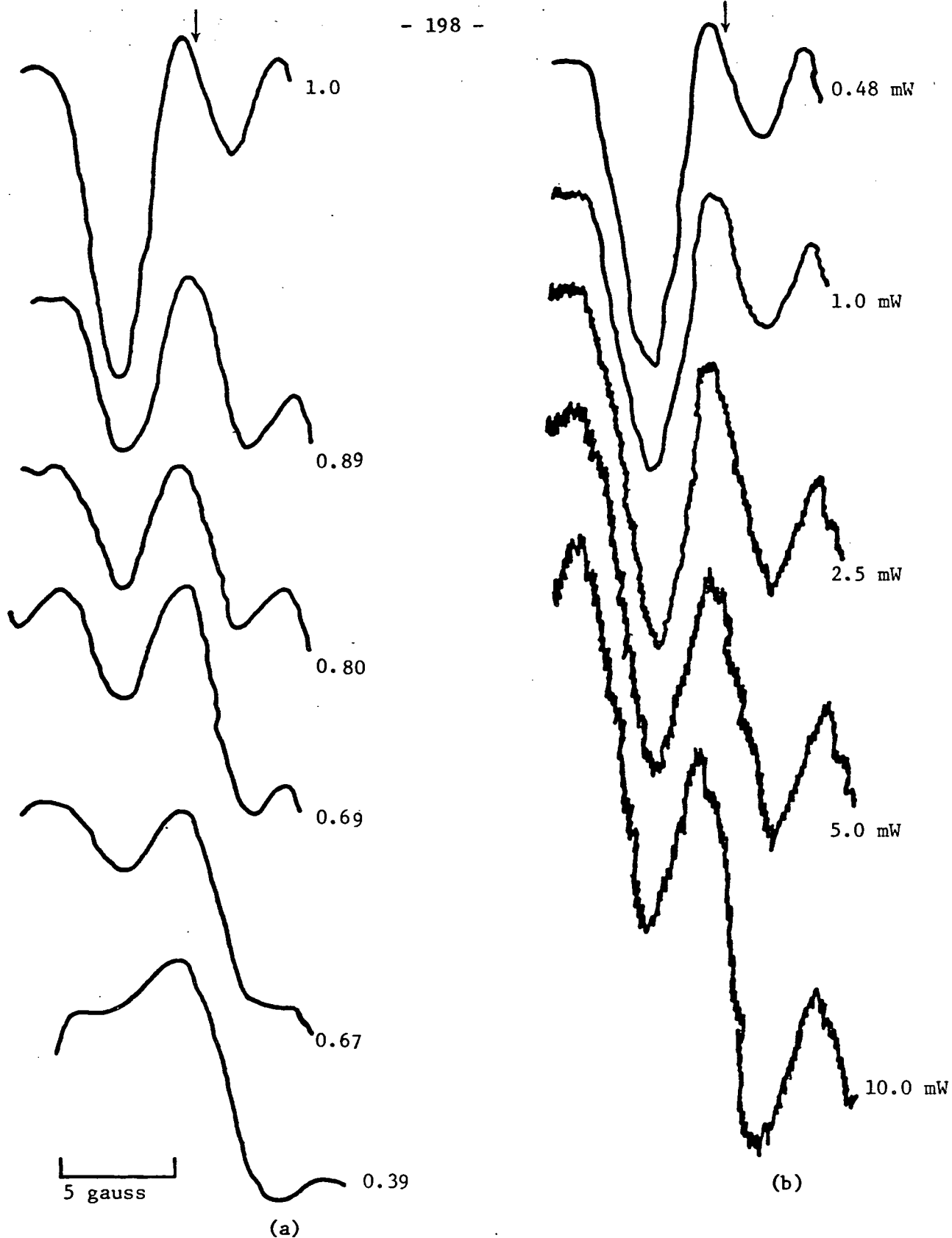


Figure 60. Resonance pattern showing behaviour of $\cdot X$ with (a) increasing water composition (microwave power 0.42 mW) and (b) increasing microwave power (pure DMSO). Numbers corresponding to spectra on left refer to mole fraction DMSO. The arrows refer to g_{DPPH} .

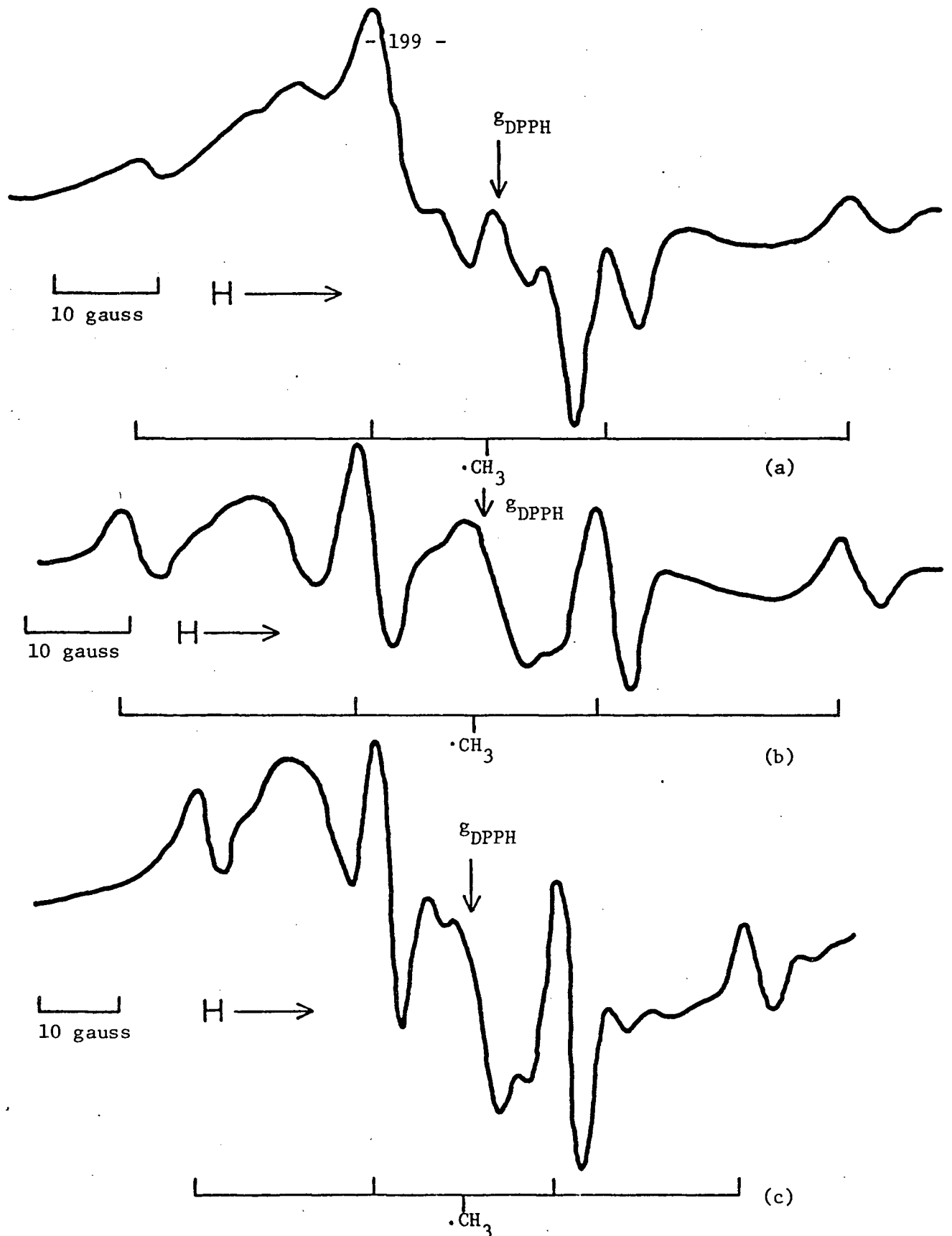


Figure 61. Electron resonance spectra of polycrystalline γ -irradiated DMSO-water mixture (0.80 mole fraction DMSO) at 77°K. (a) microwave power 0.42 mW; (b) after bleaching with ultraviolet light for 20 minutes, microwave power 0.42 mW; (c) same as (b), microwave power

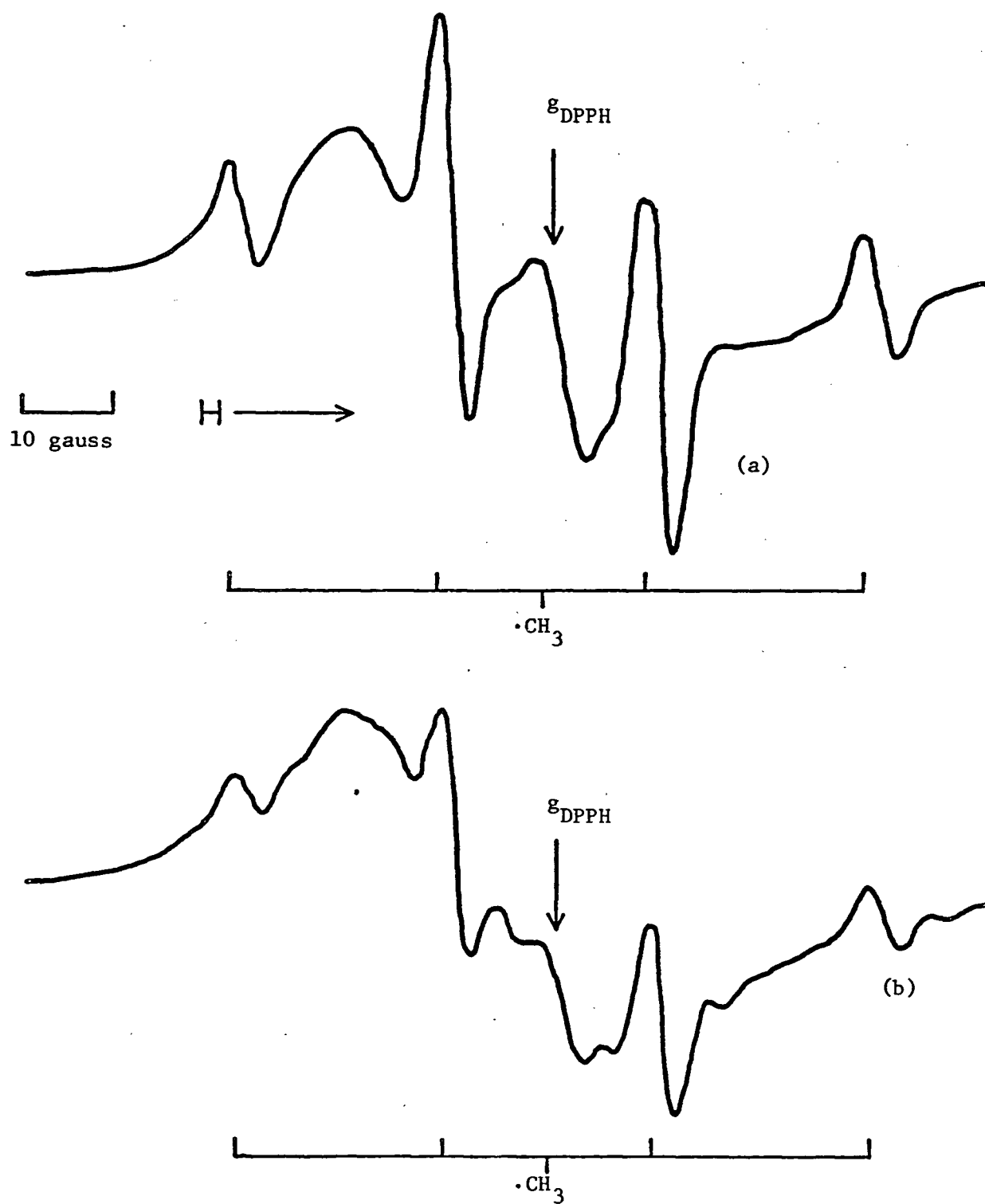
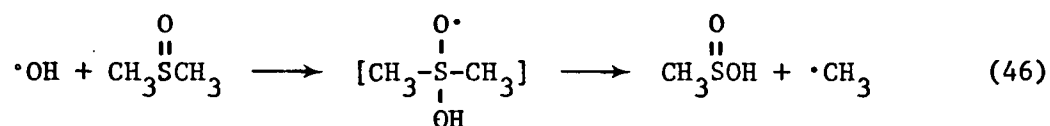


Figure 62. Electron spin resonance spectra of γ -irradiated DMSO-water glass (0.20 mole fraction DMSO) at 77°K. The "sulfur pattern" and methyl radical quartet are readily observed. (a) microwave power 0.42 mW; (b) microwave power 10 mW.

especially at high power, and the asymmetric singlet was not as pronounced (see Figure 63). The irradiated sample balls of these latter two mixtures were colourless whereas the other four samples were slightly purple. The purple colour and broad asymmetric singlet were readily photobleached with ultraviolet and visible light and the resulting spectra were identical to that shown in Figure 61(b). The methyl radical concentration showed a similar increase upon bleaching and the balls had a yellow tinge.

It is interesting that the hydroxyl radicals were only observed at the highest water concentrations (0.97 and 0.99 mole fraction water) despite the fact that their yield in γ -irradiated ice at 77°K is fairly high ($G(\cdot\text{OH}) = 0.8$).¹¹⁵ Electron spin resonance studies on the liquid state have shown that $\cdot\text{OH}$ radicals react at a diffusion-controlled rate with DMSO to produce methyl radicals by cleavage of the C-S bond.¹¹⁶⁻¹¹⁸ The mechanism proposed is given by equation (46).



It is suggested here that $\cdot\text{OH}$ radicals formed in the radiolysis of the DMSO-water mixtures react with DMSO even at 77°K. This inference is supported by the observation that hydroxyl radicals generated by the photodecomposition of hydrogen peroxide reacted with DMSO to give an esr spectrum composed of a methyl radical quartet and a broad, unidentified singlet ($\Delta H \sim 40$ gauss) centered near $g = 2.008$. The glassy sample was prepared from equal parts (by volume) DMSO and 15% hydrogen peroxide and photolysed at 77°K with ultraviolet

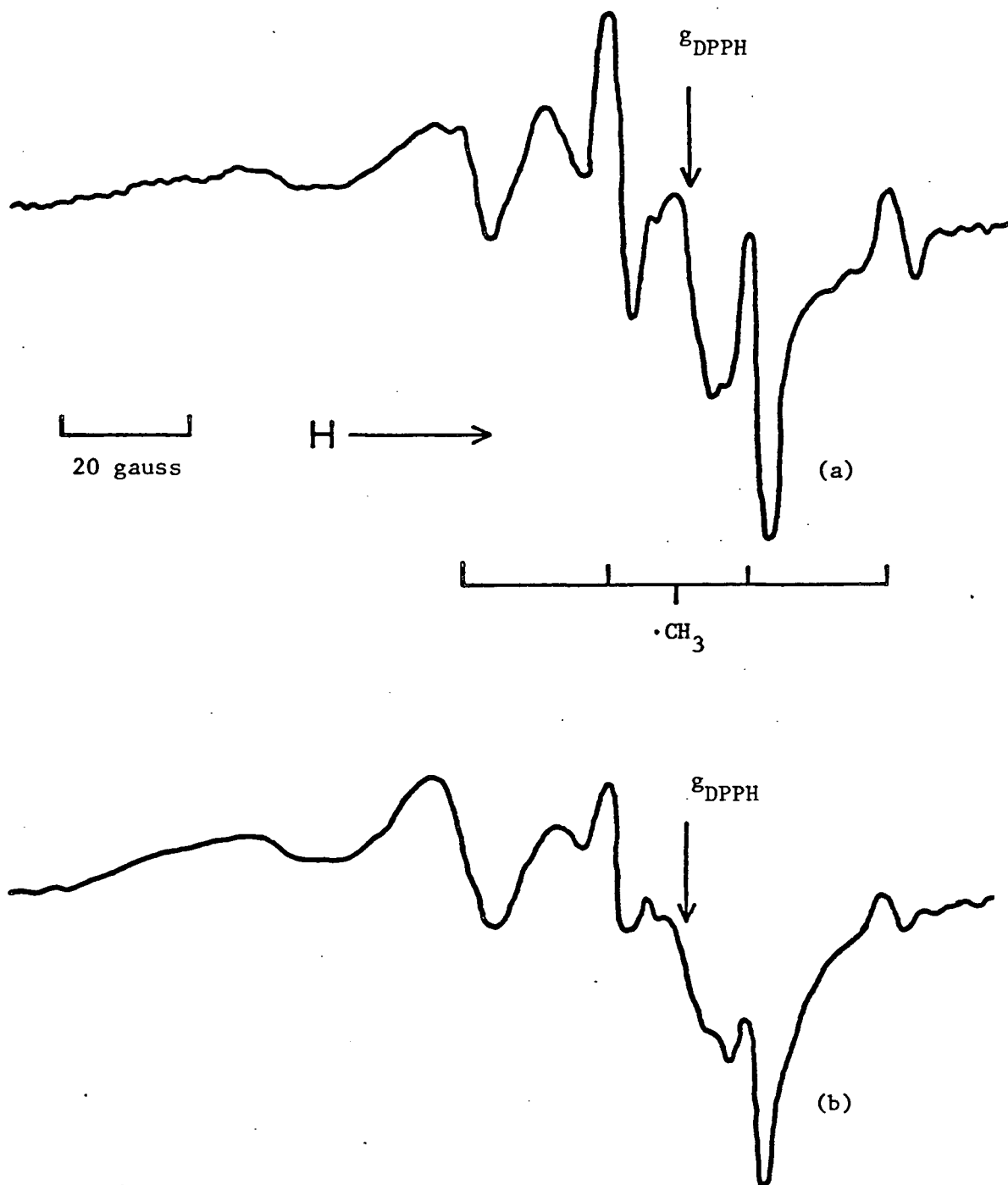


Figure 63. Electron spin resonance spectra of γ -irradiated polycrystalline DMSO-water mixture (0.01 mole fraction DMSO) at 77°K. (a) microwave power 0.42 mW; (b) microwave power 10 mW. The low field "hump" and doublet of the $\cdot\text{OH}$ radicals are evident at 10 mW power (see Figure 59).

light. Another possibility is that energy and charge transfer from the water to the DMSO molecules might be occurring in these mixtures at 77°K. Although these processes in the liquid state were discounted on the basis of the pulse radiolysis data discussed earlier, these transfer processes may be quite efficient in the solid state at low temperature.

The esr spectra indicate there are at least four distinct paramagnetic species (in addition to the $\cdot\text{OH}$ radical) produced by the γ -irradiation of DMSO-water mixtures and trapped in the matrices at 77°K. The methyl and asymmetric sulfur radicals are readily identified by their characteristic spectra and, as will be shown in the next section, are formed primarily by the reaction of electrons with DMSO. The identities of the other two paramagnetic entities are less certain.

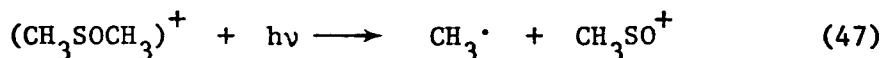
As mentioned already $\cdot\text{X}$ is only present in the polycrystalline media of high DMSO composition and its contribution to the resonance pattern decreases as the water content increases (see Figure 60). The radical is easily power saturated, photobleached with visible or ultraviolet light and is centered at $g = 2.006$. Since all known trapped electrons have isotropic g -values less than the free spin value ($g = 2.0023$),²² it is unlikely that $\cdot\text{X}$ is a trapped electron. However this cannot be taken as distinct evidence for the absence of trapped electrons. Theoretical studies indicate that electrons may be bound in the field of a stationary dipole moment provided the strength of the dipole moment is greater than 1.6 D.¹¹⁹ DMSO has a fairly large dipole moment (4.3 D) so that it is theoretically possible for electrons to be trapped in crystalline DMSO at low temperatures

where the dipoles are not free to rotate. The crystal structure of DMSO has been reported and the data indicate a strong coupling between a pair of DMSO molecules in which their dipoles are aligned in opposite directions.¹²⁰ Perhaps electrons are initially trapped in these strong dipolar fields but immediately form DMSO radical anions due to the presence of vacant low-lying d orbitals present on the sulfur atoms. Thus the DMSO radical anion or its decomposition product could be responsible for the resonance characteristics of $\cdot X$. If the stability of these radical anions is governed by the dipolar interactions associated with the DMSO molecules, then the addition of water may lower the radicals activation energy for reaction by breaking up these strong dipolar fields. This could explain why $\cdot X$ decreases as the water concentration increases.

The broad asymmetric singlet observed in pure DMSO and in all binary mixtures is attributed to DMSO positive ions for two reasons. Firstly, the esr spectrum obtained when electrons were generated in a DMSO-water glass (0.20 mole fraction DMSO) by the photoionization of $K_4Fe(CN)_6$ (see below) is comparable to that of the corresponding γ -irradiated glass (Figure 62) except for the absence of the broad asymmetric singlet and purple colour. This absence suggests that the singlet is due to an oxidized paramagnetic species produced by the ionizing radiation. Secondly, the purple centre and singlet show the same behaviour towards photobleaching inferring they correspond to the same species. It was shown in the previous chapter that the absorption spectrum of a purple centre is due to the DMSO positive ions. The absence of a distinct purple tinge at the highest DMSO compositions (1.0, 0.89 and 0.80 mole fraction DMSO) may be a yield effect. If the reactivity of the thermalized electrons is enhanced by the presence of water, as suggested by studies on the liquid mixtures, then the

fraction of DMSO positive ions escaping recombination in the polycrystalline state is expected to increase with increasing water composition.

The increase in methyl radicals upon photobleaching the γ -irradiated samples could be attributed to the photodecomposition of the DMSO positive ion according to equation (47).



Unfortunately the esr spectra corresponding to the positive ions and methyl radicals are not well-resolved so that it is impossible to see if the decay and build up of the respective radicals are comparable.

2.3 Photoionization of $\text{K}_4\text{Fe}(\text{CN})_6$ in Aqueous Glasses

Electrons may be generated in a system by exposing the sample to ionizing radiation but they can also be formed by photolysis of several solutes at wavelengths within their charge-transfer-to-solvent bands. The latter process is particularly useful when studying the reactions of electrons in solid matrices at low temperatures by esr since resonance interference by other radicals produced by ionizing radiation may be eliminated. Ferrocyanide ions are often used as a reducing solute since they are easily photoionized by ultraviolet light at 254 nm according to equation (48).¹²¹



In this study, electrons were generated at 77°K by photolysing with a low pressure mercury resonance lamp glassy samples containing 0.01 M

potassium ferrocyanide in the spectrometer cavity.

Two different glassy systems were investigated. One consisted of an aqueous DMSO glass (0.20 mole fraction DMSO) and the other an aqueous alkaline glass (8 M sodium hydroxide) to which DMSO was added as a scavenger (1.0 M DMSO). Electrons stabilized in aqueous alkaline glasses at 77°K have been shown previously to exhibit an intense blue colour ($\lambda_{\text{max}} = 580 \text{ nm}$) and narrow esr singlet ($\Delta H \sim 16 \text{ gauss}$) centered at $g = 2.0006$.¹¹⁵ Figure 65(a) shows the esr singlet obtained in the present study by the ultraviolet photolysis of the ferrocyanide ion in an aqueous 8 M sodium hydroxide glass at 77°K. The sample balls after photolysis were bright blue in colour. However trapped electrons were not observed in either the DMSO-water glass (Figure 64) or the alkaline glass containing 1.0 M DMSO (Figure 65(b)) upon photolysis, as indicated by the total absence of an esr singlet or colour centre in these samples. The esr spectrum of the DMSO-water glass is identical to the γ -irradiated sample (Figure 62) except for the absence of the broad singlet attributed to DMSO^+ . The resonance pattern of the alkaline glass (Figure 65(b)) is similar to Figures 62 and 64 except that the "sulfur pattern" appears to be more prominent. Similar spectra were obtained when an alkaline 8 M sodium hydroxide glass containing 1.0 M DMSO was γ -irradiated at 77°K to an absorbed dose of 0.2 Mrad (Figure 66(b)). In this case not all the electrons were scavenged, as indicated by the blue tinge of the irradiated sample. Subsequent photobleaching with ultraviolet light eliminated the blue colour and caused a slight ($\sim 10\text{-}20\%$) increase in the methyl radical resonance (Figure 66(c)). It was not possible to discern if the "sulfur pattern" changed in intensity with bleaching because of the

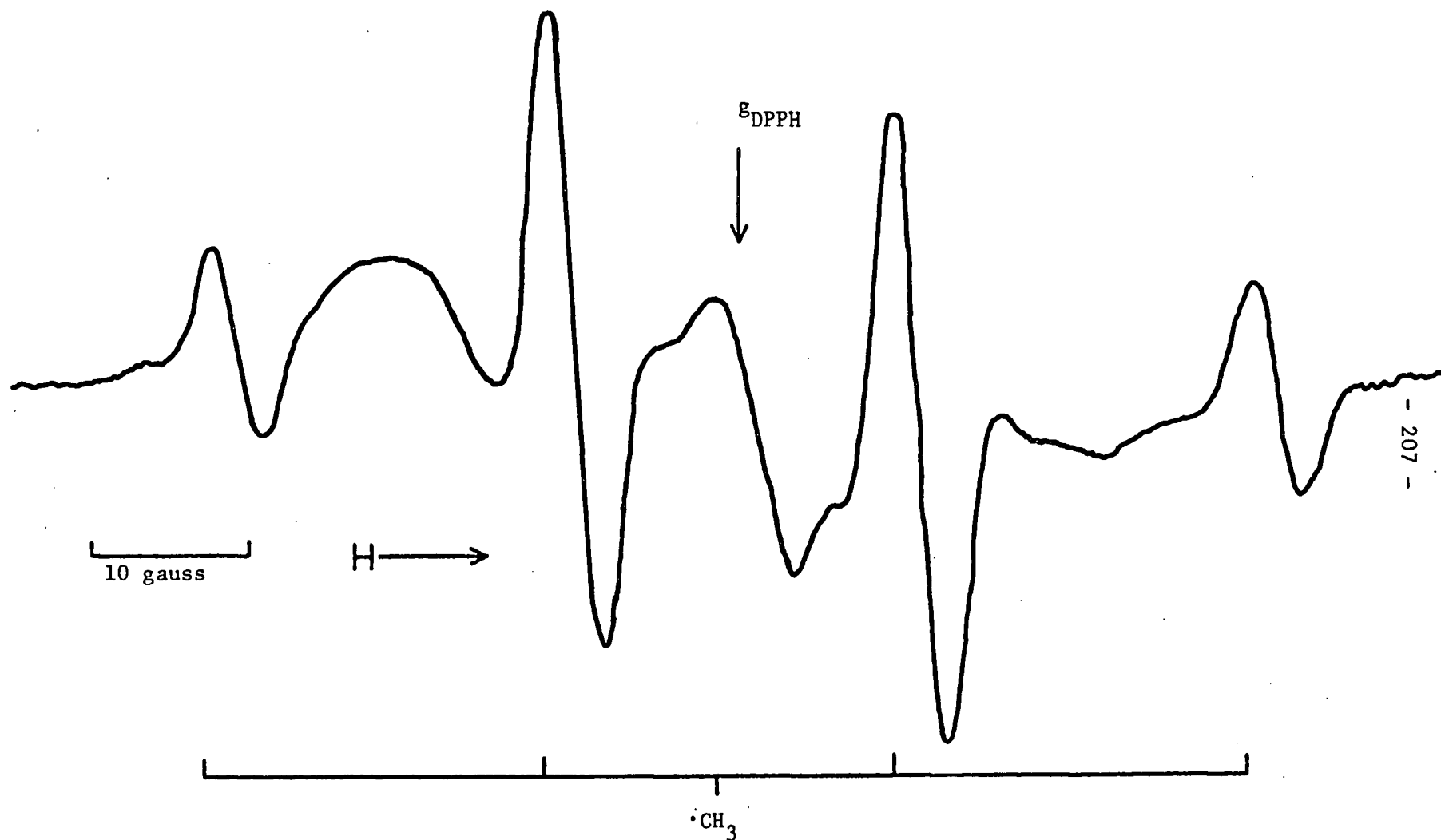


Figure 64. Electron spin resonance spectrum obtained after photoionization at 77°K of 0.01 M $K_4Fe(CN)_6$ in 0.20 mole fraction DMSO-water glass (compare to Figure 62(a)).

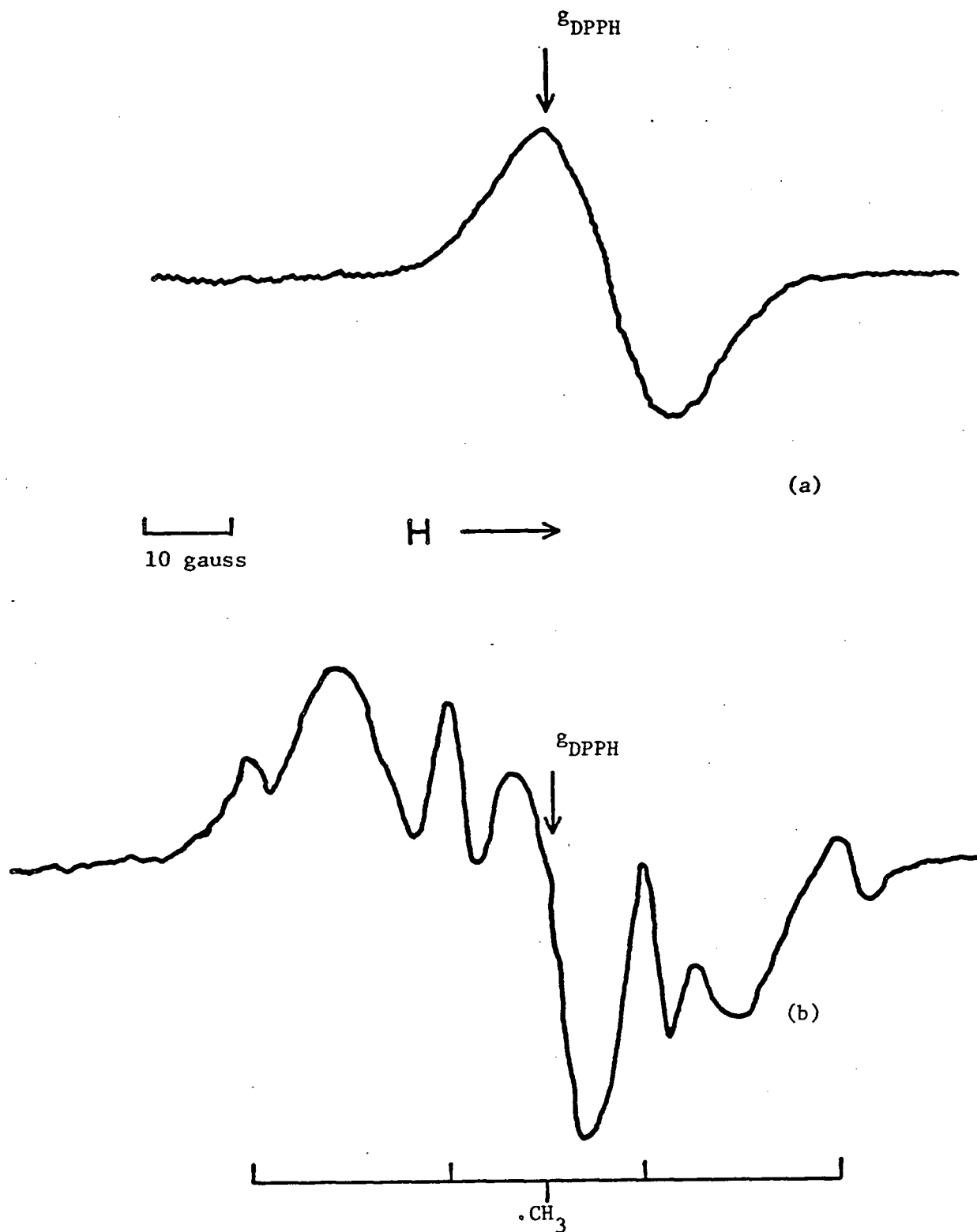


Figure 65. Electron spin resonance spectra obtained for the photoionization of $0.01 \text{ M K}_4\text{Fe}(\text{CN})_6$ in 8 M NaOH glass at 77°K . (a) no DMSO added; (b) 1.0 M DMSO present in glass.

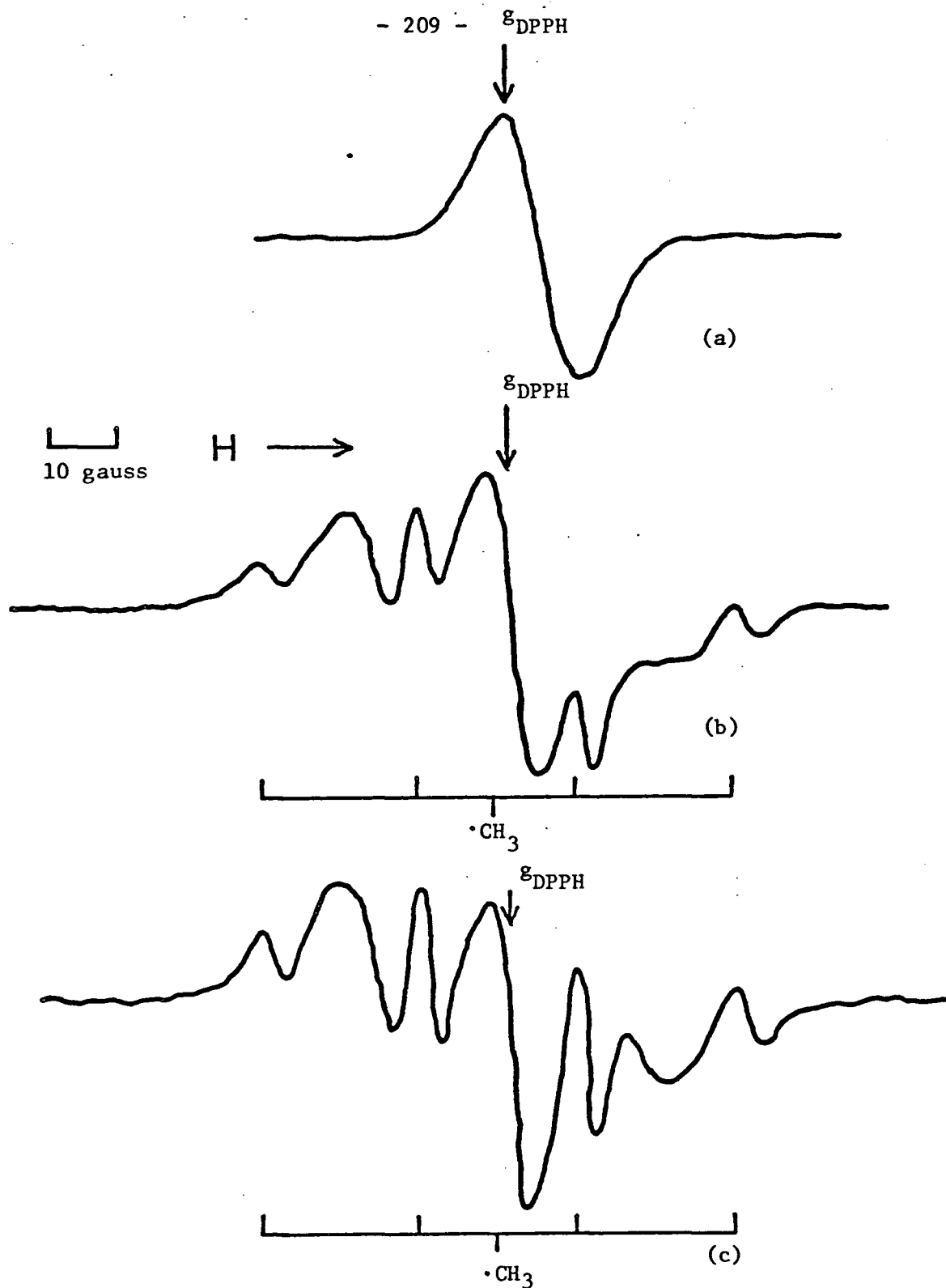


Figure 66. Electron spin resonance spectra obtained for γ -irradiation (0.24 Mrad) of 8 M NaOH glass at 77°K. (a) no DMSO added; (b) 1.0 M DMSO added; (c) after photobleaching (b) with ultraviolet light for 20 minutes.

decay of the underlying electron singlet.

The esr data shown in Figures 64, 65 and 66 thus strongly suggest that electrons react with DMSO in glassy solids at 77°K, and that the reaction produces methyl and sulfur radicals.

It is not known if the unidentified sulfur radical is produced in the same dissociation process as the methyl radicals or by another competing process. Although the asymmetric "sulfur pattern" and g-factors observed in the γ -irradiated DMSO and DMSO-water matrices are identical to those obtained in the photolysed DMSO sample (Figure 56), this similarity does not necessarily imply the sulfur resonance is due to $\text{CH}_3\dot{\text{S}}\text{O}$. Other sulfur radicals may be responsible for the observed resonance. For example, when polycrystalline balls of dimethyl sulfide at 77°K were similarly photolysed by ultraviolet light the $\text{CH}_3\text{S}\cdot$ radicals so produced gave almost identical "sulfur patterns".

REFERENCES

1. J.W.T. Spinks and R.J. Woods, An Introduction to Radiation Chemistry, John Wiley and Son, Inc., New York, N.Y., 1964, pages 39-77.
2. E.J. Henley and E.R. Johnson, The Chemistry and Physics of High Energy Reactions, Washington University Press, Washington, D.C., 1969, page 34.
3. Reference (1), page 41.
4. J.V. Jelly, Cerenkov Radiation, Pergamon Press, New York, N.Y., 1958, pages 1-78.
5. I.M. Frank and I. Tamm, Dokl. Acad. Nauk. SSSR 14, 109 (1937).
6. A. Mozumder and J.L. Magee, Radiation Res. 28, 203 (1966).
7. L.M. Dorfman and M.S. Matheson, in Progress in Reaction Kinetics, Vol. 3, G. Porter, editor, Pergamon Press, New York, N.Y., 1965, page 237.
8. M. Ebert, J.P. Keene, A.J. Swallow and J.H. Baxendale, Pulse Radiolysis, Academic Press, Inc., New York, N.Y. 1965.
9. L.M. Dorfman and M.S. Matheson, Pulse Radiolysis, M.I.T. Press, Cambridge, Mass., 1969.
10. E.J. Hart and J.W. Boag, J. Amer. Chem. Soc. 84, 4090 (1962).
11. For recent reviews on the solvated electron see the following:
 - (a) J.L. Dye, Scientific American, February, 1967, page 77
 - (b) D.C. Walker, Quart. Rev. 21, 79 (1967)
 - (c) F.S. Dainton, Ber. Bunsenges. Physik. Chem. 75, 608 (1971)
 - (d) American Chemical Society Publication, Solvated Electron, Advances Chem. Ser. 50, (1965).
 - (e) K. Eiben, Angew. Chem. Internat. Edit. 9, 619 (1970)

- (f) U. Schindewolf, *Angew. Chem.* 80, 165 (1968).
- (g) S.R. Logan, *J. Chem. Educ.* 44, 344 (1967)
- (h) A. Ekstrom, *Radiation Res. Rev.* 2, 381 (1970).
12. J.T. Richards and J.K. Thomas, *J. Chem. Phys.* 53, 218 (1970).
13. L. Kevan, *J. Chem. Phys.* 56, 838 (1972).
14. (a) M.J. Bronskill, R.K. Wolff and J.W. Hunt, *J. Phys. Chem.* 73, 1175 (1969)
- (b) M.J. Bronskill, W.B. Taylor, R.K. Wolff and J.W. Hunt, *Rev. Sci. Instr.* 41, 333 (1970)
- (c) M.J. Bronskill, R.K. Wolff and J.W. Hunt, *J. Chem. Phys.* 53, 4201 (1970)
- (d) R.K. Wolff, M.J. Bronskill and J.W. Hunt, *J. Chem. Phys.* 53, 4211 (1970).
15. F.S. Dainton, G.A. Salmon and U.F. Zucker, *Chem. Comm.* 1172 (1968).
16. B.G. Ershov and A.K. Pikaev, *Radiation Res. Rev.* 2, 1 (1969).
17. I. Eisele and L. Kevan, *J. Chem. Phys.* 53, 1867 (1970).
18. K.F. Baverstock and P.J. Dyne, *Can. J. Chem.* 48, 2182 (1970).
19. J.E. Bennett, B. Milne and A. Thomas, *J. Chem. Soc. A*, 1393 (1967).
20. W. Cronenweld and M.C.R. Symons, *J. Chem. Soc. A*, 2991 (1968).
21. (a) M.A. Bonin, K. Takeda, K. Tsuji and F. Williams, *Chem. Phys. Letters* 2, 363 (1968).
- (b) K. Takeda and F. Williams, *Mol. Phys.* 17, 677 (1969).
22. R.J. Eglund and M.C.R. Symons, *J. Chem. Soc. A*, 1326 (1970).
23. E.D. Sprague, K. Takeda and F. Williams, *Chem. Phys. Letters* 10, 299 (1971).
24. J. Jortner, *Radiation Res., Suppl.* 4, 24 (1964).

25. J. Jortner in Radiation Chemistry of Aqueous Systems, G. Stein, editor, Wiley-Interscience, New York, N.Y., 1968, page 91.
26. S. Noda, K. Fueki and Z. Kuri, Bull. Chem. Soc. Japan 42, 16 (1969).
27. (a) M. Natori and T. Watanabe, J. Phys. Soc. Japan 21, 1573 (1966)
(b) M. Natori, J. Phys. Soc. Japan 24, 913 (1968).
28. K. Iguchi, J. Chem. Phys. 48, 1735 (1968).
29. D.A. Copeland, N.R. Kestner and J. Jortner, J. Chem. Phys. 53, 1189 (1970).
30. (a) K. Fueki, D.F. Feng and L. Kevan, J. Phys. Chem. 74, 1976 (1970).
(b) K. Fueki, D.F. Feng, L. Kevan and R.E. Christofferson, J. Phys. Chem. 75, 2297 (1971).
31. K. Fueki, D.F. Feng and L. Kevan, Chem. Phys. Letters 10, 504 (1971).
32. R.A. Holroyd in Fundamental Processes in Radiation Chemistry, P. Ausloos, editor, Interscience Publishers, New York, N.Y., 1968, page 413.
33. G.R. Freeman and J.M. Fayadh, J. Chem. Phys. 43, 86 (1965).
34. E. Hayon, J. Chem. Phys. 53, 2353 (1970).
35. A. Mozumder, J. Chem. Phys. 50, 3153 (1969).
36. S.M. Silverman and E.N. Lassette, J. Chem. Phys. 44, 2219 (1966).
37. S. Arai and M.C. Sauer, Jr., J. Chem. Phys. 44, 2297 (1966).
38. J.L. Dye, M.G. Debacker and L.M. Dorfman, J. Chem. Phys. 52, 6251 (1970).
39. T.J. Kemp, G.A. Salmon and P. Wardman, reference (8) page 247.
40. L.B. Magnusson, J.T. Richards and J.K. Thomas, Int. J. Radiat. Phys. Chem. 3, 295 (1971).
41. B.J. Brown, N.T. Barker and D.F. Sangster, J. Phys. Chem. 75, 3639 (1971).

42. G.R. Freeman, J. Phys. Chem. 76, 944 (1972).
43. L.M. Dorfman, F.Y. Jou and R. Wageman, Ber. Bunsenges. Physik. Chem. 75, 681 (1971).
44. J.H. Baxendale and M.A.J. Rodgers, J. Phys. Chem. 72, 3849 (1968).
45. D.C. Walker and S.C. Wallace, Can. J. Chem. 49, 3398 (1971).
46. (a) D.A. Head, Ph.D. Thesis, University of British Columbia, 1969
(b) D.A. Head and D.C. Walker, Can. J. Chem. 48, 1657 (1970).
47. A. Ekstrom and J.E. Willard, J. Phys. Chem. 72, 4599 (1968).
48. B.G. Ershov, I.E. Makarov and A.K. Pikaev, High Energy Chem. 1, 414 (1967).
49. L. Shields, J. Phys. Chem. 69, 3186 (1965).
50. L.M. Dorfman in reference (11d), page 36.
51. A.J. Parker, Chemical Reviews 69, 1 (1969).
52. L.P. Hammett, Physical Organic Chemistry, McGraw-Hill, New York, N.Y., 1970, Chapter 8.
53. Reference (1), pages 106-112.
54. G.J. Flynn, This laboratory, private communication.
55. N.V. Klassen, H.A. Gillis and D.C. Walker, J. Chem. Phys. 55, 1979 (1971).
56. S.M. Sze, Physics of Semiconductor Devices, Wiley-Interscience, New York, N.Y., 1969, Chapter 12.
57. G.E. Adams, J.W. Boag, J. Curren and B.D. Michael, reference (8), page 117.
58. D.C. Walker, N.V. Klassen and H.A. Gillis, Chem. Phys. Letters 10, 636 (1971).
59. R.S. Alger, Electron Paramagnetic Resonance - Techniques and Applications, Interscience, New York, N.Y., 1969.

60. A.M. Koulkes-Pujo and M. Berthou, *J. Chim. Phys.* 66, 1178 (1969).
61. J.C. Machado, C. Ronneau, J. Cara, D.J. Apers and P.C. Capron, *Radiochem. Radioanal. Letters* 8, 33 (1971).
62. J.J.J. Myron and W.W. Parkinson, ORNL-4373 (1969).
63. D.E. O'Conner and W.I. Lyness, *J. Org. Chem.* 30, 1620 (1965).
64. A.M. Koulkes-Pujo, L. Gilles, B. Lesigne and J. Sutton, *Chem. Comm.* 749 (1971).
65. N.V. Klassen, private communication.
66. E.A. Shaede, private communication.
67. D.M. Brown, F.S. Dainton, J.P. Keene and D.C. Walker, *Proc. Chem. Soc.* 266 (1964).
68. E.M. Fielden and E.J. Hart, *Rad. Res.* 33, 426 (1968).
69. G. Meissner, A. Henglein and G. Beck, *Z. Naturforsch.* 22b, 13 (1967).
70. S. Arai, H. Ueda, R.F. Firestone and L.M. Dorfman, *J. Chem. Phys.* 50, 1072 (1969).
71. S. Arai, A. Kira and M. Imamura, *J. Chem. Phys.* 54, 5073 (1971).
72. L.I. Grossweiner and M.S. Matheson, *J. Chem. Phys.* 23, 2443 (1955).
73. B. Cerek, M. Ebert, J.P. Keene and A.J. Swallow, *Science* 145, 919 (1964).
74. H.C. Sutton, G.E. Adams, J.W. Boag and B.D. Michael, in reference (8), page 61.
75. M.C. Matheson, W.A. Mulac, J.L. Weeks and J. Rabani, *J. Phys. Chem.* 70, 2092 (1966).
76. D. Zehavi and J. Rabani, *J. Phys. Chem.* 76, 312 (1972).

77. T.J. Kemp, J.P. Roberts, G.A. Salmon and G.F. Thompson, J. Phys. Chem. 72, 1464 (1968).
78. L. Dogliotti and E. Hayon, J. Phys. Chem. 71, 2511 (1967).
79. E. Heckel, A. Henglein and G. Beck, Ber. Bunsenges. Physik. Chem. 70, 149 (1966).
80. W. Roebke, M. Renz and A. Henglein, Int. J. Radiat. Phys. Chem. 1, 39 (1969).
81. J.H. Baxendale, E.M. Fielden and J.P. Keene, in reference (8), page 207.
82. D.M. Brown and F.S. Dainton, Trans. Far. Soc. 62, 139 (1966).
83. J. Pukies, W. Roebke and A. Henglein, Ber. Bunsenges. Physik. Chem. 72, 842 (1968).
84. E. Tommila and A. Pajunen, Suomen Kemistilehti B 41, 172 (1968).
85. R.K. Wolford, J. Phys. Chem. 68, 3392 (1964).
86. J.R. Jezorek and H.B. Mark, Jr., J. Phys. Chem. 74, 1627 (1970).
87. S.A. Schichman and R.L. Amey, J. Phys. Chem. 75, 98 (1971).
88. J.M.G. Cowie and P.M. Toporowski, Can. J. Chem. 39, 2240 (1961).
89. K.J. Packer and D.J. Tomlinson, Trans. Far. Soc. 67, 1302 (1971).
90. R.G. LeBel and D.A.I. Goring, J. Chem. and Engineering Data 7, 100 (1962).
91. G.J. Safford, P.C. Schaffer, P.S. Leung, G.F. Doebbler, G.W. Brady and E.F.X. Lyden, J. Chem. Phys. 50, 2140 (1969).
92. E.A. Symons, Can. J. Chem. 49, 3940 (1971).
93. J.P. Keene, Radiation Res. 22, 1 (1964).
94. A.M. Koulkes-Pujo, B.D. Michael and E.J. Hart, Int. J. Radiat. Phys. Chem. 3, 333 (1971).

95. E.M. Fielden and E.J. Hart, *Radiation Res.* 32, 564 (1967).
96. J.G. Calvert and J.N. Pitts, *Photochemistry*, John Wiley and Sons, New York, 1967, pages 170-2.
97. F. Williams, *J. Amer. Chem. Soc.* 86, 3954 (1964).
98. J.W. Buchanan and F. Williams, *J. Chem. Phys.* 44, 4377 (1966).
99. F.I. Vilesov and B.L. Kurbatov, *Dokl. Akad. Nauk. SSSR* 140, 1364 (1961).
100. Reference (1), page 149.
101. E.A. Shaede, Ph.D. Thesis, University of British Columbia, 1971.
102. M.C. Sauer, S. Arai and L.M. Dorfman, *J. Chem. Phys.* 42, 708 (1965).
103. J.H. Baxendale, C. Bell and P. Wardman, *Chem. Phys. Letters* 12, 347 (1971).
104. P.A. Ayscough, *Electron Spin Resonance in Chemistry*, Methuen and Company, London, 1967.
105. F.K. Kneubuhl, *J. Chem. Phys.* 33, 1074 (1960).
106. H. Mackle, *Tetrahedron* 19, 1159 (1963).
107. T. Henriksen, *J. Chem. Phys.* 36, 1258 (1962).
108. T. Henriksen, *J. Chem. Phys.* 37, 2189 (1962).
109. F.K. Truby, *J. Chem. Phys.* 40, 2768 (1964).
110. J.J. Windle, A.K. Wiersema and A.L. Tappel, *J. Chem. Phys.* 41, 1996 (1964).
111. P.B. Ayscough, K.J. Ivin and J.H. O'Donnell, *Trans. Far. Soc.* 61, 1110 (1965).
112. D.H. Volman, J. Wolstenholme and S.G. Hadley, *J. Phys. Chem.* 71, 1798 (1967).
113. P.S.H. Bolman, I. Safarik, D.A. Stiles, W.J.R. Tyerman and O.P. Strausz, *Can. J. Chem.* 48, 3872 (1970).

114. J. Skelton and F.C. Adam, *Can. J. Chem.* 49, 3536 (1971).
115. For recent review see L. Kevan in Radiation Chemistry of Aqueous Systems, G. Stein, Editor, Interscience Publishers, New York, 1968, page 21.
116. C. Lagercrantz and S. Forshult, *Acta. Chem. Scand.* 23, 811 (1969).
117. B.M. Bertilsson, B. Gustafsson, I. Kuhn and K. Torssell, *Acta. Chem. Scand.* 24, 3590 (1970).
118. H. Taniguchi, H. Takagi and H. Hatano, *J. Phys. Chem.* 76, 135 (1972).
119. M.A. Bonin, Ph.D. Thesis, The University of Tennessee, 1969.
120. R. Thomas, C.B. Shoemaker and K. Eriks, *Acta. Cryst.* 21, 12 (1966).
121. P.B. Ayscough, R.G. Collins and F.S. Dainton, *Nature* 205, 965 (1965).